Dipl. Ing. Josip Matić BSc

Modeling and Analysis of Pharmaceutical Hot Melt Extrusion

DOCTORAL THESIS

to achieve the university degree of
Doktor der technischen Wissenschaften

submitted to
Graz University of Technology

Supervisor
Univ.-Prof. Dipl.-Ing. Dr.techn. Johannes Khinast
Institute of Process and Particle Engineering
Research Center Pharmaceutical Engineering GmbH

Graz, February 2021

AFFIDAVIT

I declare that I have authored this thesis independently, that I have not used other than the declared sources/resources, and that I have explicitly indicated all material which has been quoted either literally or by content from the sources used. The text document uploaded to TUGRAZonline is identical to the present doctoral thesis.

Date, Signature

Josip Matić

Modeling and Analysis of Pharmaceutical
Hot Melt Extrusion

Dissertation

First assessor

Univ.-Prof. Dipl.-Ing. Dr.techn. Johannes Khinast
Institute of Process and Particle Engineering
Research Center Pharmaceutical Engineering GmbH
Graz University of Technology

Second assessor

Univ.-Prof. Mag.pharm. Dr.rer.nat. Roblegg Eva
Institute of Pharmaceutical Sciences
University Graz

“The happiness of your life depends upon the quality of your thoughts. “

(Marcus Aurelius)

Preface

My first contact with the topic of pharmaceutical Hot Melt Extrusion happened during my Master Thesis, under the joint supervision of the Faculty of Mechanical Engineering at the University of Sarajevo, the Institute of Process and Particle Engineering (IPPE) at the Technical University Graz and the Research Center of Pharmaceutical Engineering (RCPE) in Graz. The thesis was centered on the simulations of screw elements (conveying, mixing and kneading screw element pairs) found in twin screw extruders. As part of the Master thesis I was introduced to Smoothed Particle Hydrodynamics (SPH), a Lagrangian fluid dynamics simulation method, and applied it for the characterization of individual twin screw extruder element pairs. Following the work on my Master thesis and after some consultations with Prof. Johannes Khinast, I´ve decided to stay in Graz, and in the cooperation with the IPPE and RCPE, focus on process understanding, setup and scale-up of pharmaceutical Hot Melt Extrusion. By doing so I was exposed to a number of industrially driven projects with companies that are global leaders in equipment manufacturing, such as Leistritz, Coperion and Thermo Fisher Scientific, as well as leading pharmaceutical companies like Bayer Technology Services, Debiopharm, Pozlab, Applied Manufacturing Science, Zentiva, Abbott Laboratories, AbbVie Inc., Lyndra Therapeutics and many more. This helped me to understand the everyday issues pharmaceutical companies face during formulation development, process setup, scale-up and transfer from a non-GMP to a GMP facility. Inspired by this experience, I´ve focused by PhD on the industrially relevant issues concerning the product development, process setup and scale-up of HME based formulations. To do so, I´ve performed a number of simulations using the previously mentioned SPH method, the in-house developed reduced order model for extrusion (1D HME) and a number of experiments for validation purposes and product quality analysis, presented here. The hope is that the performed work will lead to quick, waste free and reliable HME based product and process development by helping the industry move from a trial-and-error approach towards a Quality by Design (QbD) approach.

Acknowledgement

The presented work could not have been possible without the help and close collaboration with different institutions, companies and colleagues. It takes a whole village to get a PhD.

First of all, my sincere thanks go to my fiancé Martina Trogrlić, my parents Vinko and Ružica Matić and my brother Marko Matić. Without their love and support, it would not have been possible to do any work, let alone finish this PhD with ease of mind and purpose.

Thanks go to Prof. Johannes Khinast who gave me the opportunity to work on this topic even thought I was just starting in the field of pharmaceutical hot melt extrusion. With his help, I was able to work in a systematic way on the complex topic of HME process setup and scale-up, and providing a platform for future development and cooperation. Only with the help and infrastructure provided by Johannes it was possible to work on this topic in such an interdisciplinary way on the edge between university and industry.

Further, thanks go to all members of the Institute of Process and Particle Engineering (IPPE) at the Technical University Graz and to the Research Center Pharmaceutical Engineering (RCPE). I was lucky enough to have worked in both institutions during my PhD and to benefit from both, university and industry driven problem solving. Without their help, projects and infrastructure if would have not been possible to even define a PhD idea, let alone run thousands of simulations, experiments, material and analytical measurements and cooperate with the leading institutions in the field. One major advantage I had working at IPPE and RCPE, in comparison to all of my other colleagues working on this topic from around the world, is the possibility to work interdisciplinary with simulation experts, formulation experts, analytical experts and process development experts with different backgrounds and skills, which I´m extremely thankful and proud on.

My special gratitude goes to all of my colleagues who help me with scientific and life advices throughout all of the thought and joyful times we spent together. Special thanks go to Andreas Eitzlmayr who introduced me to HME simulations and guided me thought my Master thesis which served as an introduction to my PhD. To all of the IPPE staff an especially my former office mates Theresa Hörmann-Kincses, Daniel Treffer, Sara Zellnitz and Otto Scheibelhofer. Special thanks go to my Master students Hannes Bauer and Carolina Alva, who helped me the development and execution of the different simulation approaches and in the experimental setup

and analysis of the various extrusions. All of my (former and current) colleagues at RCPE: Amrit Paudel, Simone Pival-Marko, Gerold Koscher, Phillip Clarke, Hsiao Wen Kai, Massimo Bresciani, Dalibor Jajčević, Sulaiman Mohsenzada the whole Pilot plant, Material Science and Analytical lab team and Areas 1, 2 and 3 at RCPE.

Moreover, I would like to thank all of our industrial partners, Leistritz Extrusionstechnik, Coperion GmbH, Bayer Technology Service, Pozlab, Applied manufacturing Science, Zentiva, Debiopharm, Abbott Laboratories, AbbVie Inc., Lyndra Therapeutics and many more.

Kurzfassung

Die Schmelzextrusion ist ein kontinuierliches Herstellungsverfahren, das in der pharmazeutischen Industrie zunehmend zur Herstellung verschiedener Zwischen- oder Enddosierungsformen eingesetzt wird. Es wird typischerweise als Werkzeug zur Verbesserung der Löslichkeit von schwerlöslicher pharmazeutischer Wirkstoffe benutzt. Diese Verbesserung wird typischerweise durch die Erzeugung von amorphen festen Dispersionen in der Formulierung erreicht. Die Schmelzextrusion kann auch als effizientes Mischverfahren verwendet werden, bei dem verschiedene pharmazeutische Wirkstoffe in einen oder mehrere polyedrische Träger eingebaut werden, die die Freisetzungsgeschwindigkeit *in vivo* (und *in vitro*) steuern. Für den Prozess werden meistens gleichläufige Doppelschneckenextruder benutzt. Diese Prozessplattform ist durch ihre Flexibilität und hochmodulare aufbauweise bekannt und ist für die Verarbeitung von verschiedenen Formulierungen sehr gut geeignet. Diese hohe Prozessflexibilität kann jedoch auch eine erhebliche Herausforderung führen wenn es darum geht neue Formulierungen effizient und schnell zu verarbeiten. Und genau da versucht diese Arbeit anzusetzen.

Aufbauend auf den Fortschritten in der Hochauflösenden Simulationen von einzelnen Schneckenelementen und den mechanistischen Simulationen vom ganzen Prozess, wurden verschiedene Extruder, Schneckenelemente und Formulierungen untersucht. Zunächst wurde der Einfluss der Querschnittgeometrie auf die Leistung einzelner Schneckenelemente mit Hilfe detaillierten Smoothed Particle Hydordynamics Simulationen ermittelt. Nach der theoretischen Analyse von einzelnen Schneckenelementen, wurde eine Reihe von Experimentelenversuchen mit zwei verschiedenen Formulierungen untersucht, mit dem Ziel die mechanistischen Simulationen vom ganzen Prozess zu validieren. Nach der Validierung wurde eine *in silico* Prozessübertragung für Extruder mit unterschiedlichen Querschnittsgeometrien vorgeschlagen. Im Anschluss an diese Studie wurde der Schwerpunkt auf die Skalierbarkeit des pharmazeutischen Schmelzextrusion Prozesses gelegt, mit der Annahme, dass zur Aufrechterhaltung der Produktqualität die thermomechanische Belastungshistorie der Formulierung über verschiedene Extruder großen hinweg konstant gehalten werden muss. Unterschiedliche Konfigurationen Analysiert mit Hilfe von Prozesssimulationen zeigten, dass die in der Literatur verwendeten traditionellen Scale-up Regeln, die aus der Lebensmittel- oder Polymerverarbeitung Industrie übernommen wurden, nicht die gleiche thermomechanische Belastungshistorie über verschiedene Skalen hinweg garantieren und in Folge

höchstwahrscheinlich auch nicht zu einem gleichwertigen Produkt führen. Darauf folgte eine groß angelegte experimentelle Kampagne mit dem Ziel, die resultierende Produktqualität mit dem vorherrschenden Prozesszustand in Beziehung zu setzen und die Skalierbarkeit des Prozesses experimentell zu testen. Es wurde gezeigt, wie die Produktqualität mit den verschiedenen Prozesseinstellungen und den thermomechanischen Belastungen im Prozess zusammenhängt. Darüber hinaus wurde bestätigt, dass die traditionellen Scale-up Regeln nicht zu einer Äquivalenz des Prozesszustands in verschiedener Extruder Skalen führen und daher die Produktqualität des ursprünglichen Aufbaus nicht erhalten. Schließlich wurde der Simulationsansatz mit einer modernen, qualitätsorientierten Produktentwicklungsplattform für Extrusion Basierte pharmazeutische Produkte verbunden.

Abstract

Hot melt extrusion is a continuous manufacturing process increasingly used in the pharmaceutical industry for the production of various intermediate or final dosage forms. It is typically used as a tool for enhancing the solubility of poorly soluble active pharmaceutical ingredients by creating amorphous solid dispersions. It can also be used as an efficient mixing process that incorporates different active pharmaceutical ingredients into one or more polymeric carriers that control the release velocity *in vivo* (and *in vitro*). Closely intermeshing co-rotating twin screw extruders are usually used as the equipment of choice to facilitate the process. The use of twin screw extruders allows the process to be tailored to the processed formulation and expected product by adjusting the highly modular screw configuration and by finding the right process settings. The process flexibility allows for a wide variety of different formulations that can be processed but can pose a significant challenge when efficient process setup and scale-up is needed, especially for novel formulations. Here is where this work tries to address and solve some of the product development issues.

Building on the advances in high fidelity simulations of individual screw elements and mechanistic reduced order process simulations; different extruders, extruder screw elements and formulations were investigated. First, the impact the screw cross section geometry has on the performance of individual screw element was investigated using detailed smoothed particle hydrodynamics simulations. Following the theoretical investigation, a number of experimental setups was investigated with two different formulations, validating the *in house* developed reduced order code for pharmaceutical extrusion. Following the validation, an *in silico* process transfer was proposed for extruders with different cross section geometries. Following this study, the focus was laid on the scalability of the HME process, under the assumption that to transfer the product quality, the thermomechanical load history of the formulation has also to be kept constant across different extruder scales. Different *in silico* setups showed that the traditional scale-up rules found in literature, translated from food or polymer processing industries, do not guarantee the same thermomechanical load history across different scale and will most likely not result in an equivalent product. This was followed up with a large scale experimental campaign with the goal of relating the resulting product quality with the prevailing process state and to experimentally test the process scalability. The connection between the product quality and different process settings and the thermomechanical loads in the process was analyzed in detail. In addition, it was confirmed that the traditional scale-up rules do not

result in the equivalence of process state along different extruder scales and hence do not preserve the product quality of the original setup. Finally, the *in silico* approach was connected to a modern, quality by design driven product development platform for extrusion based pharmaceutical products.

Table of Contents

List of Figures

List of Tables

1

Introduction

Hot Melt Extrusion (HME) is still searching for its place in the secondary drug production cycle in the pharmaceutical industry. It is a continuous manufacturing process that utilizes closely intermeshing co-rotating twin-screw extruders (TSE) for processing of powders or liquids into a continuous strand that can be further pelletized and processed into the final dosage form. The process itself is borrowed from the food and polymer processing industries and requires a specific design approach that will be discussed in detail in the upcoming chapters. HME is a highly flexible process and can be tailored to any formulation or product in mind, under the condition that a certain thermal stability of the active pharmaceutical ingredient (API) is given. This makes it difficult to setup the process efficiently for a yet unknown formulation without extensive experimental efforts that often require prohibitively high amounts of API. Usually, in early stage development of a new drug product, the amounts of material available for process setup investigations is measured in grams rather than kilograms, which is typically needed for a reliable HME setup. To address this issue we studied the process extensively, analyzed how it responds to different settings and formulations, how it changes during scale-up and how the product quality is linked to the prevailing process state using in-house developed simulation tools and extensive experimental efforts. A short introduction into the topic outlining the main ideas and concepts needed for better understanding of the work will be given in this chapter.

1.1 Pharmaceutical Hot Melt Extrusion Decomposed

As mentioned above, HME was developed in the food and polymer industries as a potent mixer of highly viscous products with a continuous manufacturing nature [1]–[4]. It is a one-step solidification process that mixes and solidifies various powders and liquids into strands and pellets that can be used as an intermediate or even final dosage form. In the context of the pharmaceutical industry, HME is viewed as a solvent free continuous manufacturing process capable of addressing the solubility problem of new APIs [5]–[12]. The solubility problem is reflected in the low solubility of new API compounds, classified as BCS2 or BCS4 class in the Biopharmaceutical Classification System [13]–[16]. HME provides the possibility of creating amorphous solid dispersions (ASDs) of poorly soluble crystalize APIs that are embedded, solubilized and stabilized in a polymer matrix. ASDs are known to exhibit instability and tend to recrystallize over time, losing the solubility enhancement. Yet by embedding them into a polymer matrix not only can the API be kept amorphous for an extended period of time, oversaturation can also be achieved, reducing the amount of drug that has to be administered to the patient. In addition to the usual oral immediate release ASDs, formulations with an extended release over day, week or months can also be prepared and manufactured [17]–[23]. Besides creating ASDs, it is also possible to control the particle size distribution (PSD) of crystalline APIs and embed them into a polymer carrier. The production of nanopharmaceuticals is also documented where HME was used as a one-step solidification process transforming nano-suspensions or solutions into a solid dosage form [24]–[28]. Some of HME based pharmaceuticals are listed in Table 1.1.

Table 1.1. Pharmaceutical products based on Hot Melt Extrusion

Pharmaceutical Company	Commercial Name	Pharmaceutical Company	Commercial Name
Abbott Laboratories	Norvir® Kaletra®	Pfizer Janssen	Zithromax® Nucynta®
Merz	Onmel®	Reckitt Benckiser Healthcare	Nurofen Meltlets Lemon®
Merck	Noxafil®	AstraZeneca	Zoladex®
Purdue Pharma	Palladone®	Valeant Pharmaceuticals	Lacrisert®
AbbVie	Viekirax® Venclyxto® Mavyret®	Sanofi Aventis Allergan Merck US	Depo-Profact® Ozudrex® Implanon®
Novartis	Eucreas®		

At different stages of the product development cycle, different extruder scales, usually from different vendors, are used, Table 1.2. During the formulation development and screening phase the goal is to test different excipients and API loadings. Since in this stage usually the amount of API available is limited, low throughput screening is preferred. Here, extruders from 5mm to 12mm screw diameter are often used, with throughputs starting from a couple of grams per hour up to 100g/h. Moving to the pilot plant scale where the goal is to test the processability of the formulation, asses the downstream processing, the long term process stability and to produce the first clinical batches. Typically extruders in the size from 12mm to 18mm are used here, with throughputs starting from 100g/h to 5kg/h, depending on the formulation. Depending on the formulation and product in question, the pilot plant scale can also be the final production scale. If higher throughputs are needed than the move to bigger pharma grade extruders can be made. The extruder size ranges from 18mm to 55mm, with throughputs from 2kg/h to 20kg/h, depending on the formulation.

Table 1.2. Extruder manufacturers for pharmaceutical HME processes; overview of extruder scales.

	Three Tec	Thermo Fisher	Leistritz	Coperion
Table Top Extrusion (formulation screening)	5mm 9mm 12mm	Mini HME* 11mm	12mm	
Pilot Plant Scale (Process Setup)	16mm 18mm	16mm	16mm** 18mm	18mm
Production Scale (Production)	24mm 32mm 55mm	24mm	27mm	40mm

*Conical Extruder
**Triple Flighted NANO16

The process scalability and transferability is a significant challenge and will be discussed in detail in the upcoming chapters.

1.1.1 Individual Screw Elements

To facilitate a variety of products in one production process, HME utilizes closely intermeshing co-rotating twin screw extruders (TSEs) as the technological platform of choice [1], [3]. TSEs have a highly modular screw configuration that allow to closely tailor the HME process to the processed formulation. With the careful arrangement of the screw elements it is possible to create various processing zones along the screw configuration. The most often found HME zones are: the powder conveying and densification zone, melting zone, various mixing zones

with different distributive and dispersive mixing actions, degassing zone and a pressure build-up and strand shaping zone through the extruder die. The different screw element types usually associated with pharmaceutical HME can be broadly classified in three main groups: conveying, kneading and mixing elements. Each of the three different screw types has an allocated task in the screw configuration and is characterized by a specific design dimension. Conveying elements have the simplest geometry and are usually utilized for powder and melt conveying, densification, pressure build-up and degassing process steps. They are characterized by their screw pitch, i.e. the length of one full rotation of the cross section. As it will be shown in the coming chapters, the screw pitch primarily determines the conveying and pressure build-up characteristics of the conveying screws. For example, a low screw pitch generally favors good pressure build-up capabilities of the conveying screw, but lacks in terms of melt conveying. The opposite is true for higher pitched screw elements. They tend to have a relatively low pressure build-up capacity, but very good melt conveying capabilities, i.e. they transport more melt per screw rotation in the axial direction, in comparison to their lower pitch counterparts. The next screw element type is the mixing element. Its geometry is similar to that of standard conveying elements, with additional axial cut-outs. Those cut-outs can differ in their number, base geometry and angle with regards to the screw axis. Nevertheless, all mixing elements have the basic task of redistributing, folding and stretching the melt flow in order to achieve a high distributive mixing action while simultaneously limiting the dissipative power input. Kneading elements have a similar task to mixing elements in that they are designed to further mix the polymer API mixture. They differ in the mixing mechanism. Whereas mixing elements primarily provide a distributive mixing action, kneading elements are also know for high dispersive mixing, i.e. they are effective in dispersing agglomerates. Whether a kneading element will have a primarily dispersive of distributive mixing action is determined by the thickness of the individual kneading discs. Thicker kneading discs favor a more dispersive mixing and thinner discs favor more distributive mixing [2]. Regardless of the mixing action, kneading elements are known to introduce a significant amount of dissipation into the processed melt in comparison to the gentler mixing elements. In addition to the kneading block thickness, a defining feature of kneading elements is the angle between the kneading discs. Usually kneading elements have an angle between the kneading discs starting from 30°, 45°, 60° and ending with 90° kneading elements. As shown in the following chapters, every increase in the angle between the kneading discs, for a constant kneading block thickness, tends to decrease the melt conveying and pressure build-up capacities of the screw. An extreme example are the kneading blocks that have a conveying neutral screw geometry. In the case of traditional double

flighted screw elements, such kneading elements have a 90° angle between the kneading discs, and a 60° angle in the case of triple flighted kneading elements. The number of flights in the cross section geometry of the screw does not only determine the kneading element angle at which the screw is conveying neutral, but also determines the free cross section, the extruder throughput range, the number and location of high shear gap regions and the shear rate distribution across the screw cross section. Most of the extruder screw elements are designed with a double flighted screw cross section, which can be regarded as the standard cross section type. Single flighted screw geometry cross sections are used for specific tasks of high pressure generation and high conveying capacity in single or twin screw extruders. They have a significant drawback as the single flighted screw geometry cross section also results in a comparatively large screw-barrel gap region, which is characterized with high dissipative energy and high melt temperature peaks. Consequently, the single flighted screw geometry cross section is not often used in the pharmaceutical industry, as the processed APIs tend to be temperature sensitive. On the other hand, triple flighted screw geometry cross sections are also characterized in comparatively high pressure build-up capacities but, due to the reduction in the free cross section, have a significantly lower throughput range in comparison to similarly sized double flighted screw elements. A combination of double- and triple flighted screw elements can be seen in some screw configurations where triple flighted kneading element are used. The use of triple flighted kneading elements in an otherwise double flighted screw configuration can be justified by the inherently higher number of kneading block flights that enhance the distributive and dispersive mixing action.

1.1.2 Screw Configurations and Processing Zones

Combining the above mentioned characteristic of the individual screw element types, a screw configuration can be tailored to the specific needs of processing the formulations. Different assemblies of the individual screw elements result in different processing zones with different process tasks in mind, Figure 1.1. A typical screw configuration used in pharmaceutical HME is assembled as follows:

- The screw configuration starts with a **powder intake zone**. Typically a previously mixed physical mixture of the formulation (also called premix) is feeded by a gravimetrically or volumetrically controlled feeder into the extruder intake. The powder intake can be facilitated with high pitched conveying elements that ensure a high free

volume for the powder. This is important as the powder density and flowability can be a limitation in terms of throughput. The high pitched conveying screws are often followed by a pitch reduction that results in a powder densification, elimination of air pockets and as a preparation for the next processing zone.

- After the powder intake and densification, the **powder melting** process is facilitated. This is typically performed by a combination of different kneading elements. A typical kneading element array for this purpose (for double flighted screw cross section geometries) can be assembled from a combination of 30° and 60° kneading elements. Such a combination allows for sufficient mixing of the powder-melt mixture and a creation of a soft conveying deficit due to the difference in the conveying capacities of the 30° and 60° kneading elements (this is discussed in more detail in the upcoming chapters). This conveying deficit results in a higher degree of fill in the 60° element zone, in comparison to the 30° element zone, and results in a sufficient local residence time of the processed formulation in order to get it fully molten at the end the melting zone.
- Following the powder melting zone is one, or a series of, dedicated **mixing zones**. The main task of the mixing zone is, as the name suggest, to facilitate sufficient distributive and dispersive mixing of the different phases, solid or liquid, and the incorporation of the API into the polymer matrix. This can be facilitated by a series of kneading elements or by a use of dedicated mixing elements in combination with back conveying elements. Both approaches have their advantages and disadvantages. A series of kneading elements is typically very good when it comes to the distributive and dispersive mixing action, but tends to drastically increase the viscous dissipation (consequently also the melt temperature), increasing the mechanical and thermal load on the formulation. Especially when conveying neutral kneading elements are used. In contrast, mixing elements tend to have a good distributive mixing with a comparatively low viscous dissipation, but typically lack in dispersive mixing action. Both variants are significant points along the screw configuration where changes in the formulation can occur. If not managed well issues in the final product can arise, be it in the form of not sufficiently mixed components, residual crystallinity, unwanted agglomerates or degradation, as discussed in detail in the following chapters.
- Depending on the final product and the chosen feeding strategy, multiple mixing zones can be facilitated with dedicated **feeding ports**. The screw design found in secondary feeding points consists of high pitched conveying elements, with similar reasoning

behind as in the case of the powder intake zone. The high pitched conveying elements have a high free volume that allows for higher side feeding rates. A special case is the secondary feeding of liquids, nano-suspensions or nano-solutions. Here, to counteract potential leakage of the liquids, fully filled zones before and after the secondary feeding ports have to be arranged. A fully filled zone is a zone where the processed formulation takes up all of the available free volume. In this particular instance, this is achieved by the use of conveying neutral elements (conveying neutral kneading elements, mixing elements, kneading blocks and some kind of barriers) or back conveying elements. Both options are valuable and the decision is made depending on the formulation used and the characteristics of the final product.

- Following the mixing zone(s), a **degassing zone** is typically facilitated. The degassing zone is used to expel unwanted moisture from the processed formulations, coming from the excipients or the secondary liquid phase added to the process in one of the previous feeding ports. From the screw configuration stand point, again high pitched conveying elements are the screws of choice, as they provide a low filling degree (due to the high available free volume) and a high free surface area from which the moisture can be degassed. The degassing itself is can be done either at atmospheric pressure or under vacuum. Regardless of the choice of the degassing, it is advisable to have fully filled section before and after the degassing zone.
- Following the degassing zone the **material discharge (die section) and pressure build-up zones** are facilitated. Depending on the downstream, the die setup, number of die holes, the cylindrical length of the die and die cross section geometry are chosen to make the downstream processing as simple as possible. To provide the pressure needed for overcoming the die assembly and to provide a stable flow with a minimum of unwanted flow pulsation, a series of conveying elements with the pitch reduction towards the die is used. The pitch reduction has two main purposes: (1) it increases the local filling degree creating a seal for the degassing zone and (2) increases the pressure build-up efficiency of the used screws. It should be noted that twin screw extruders (especially with a double flighted screw cross section geometry) tend to produce pulsations in the flow exiting the die, caused by the periodic fluctuations in the location of the maximal axial velocity peaks in the screw cross section. Here, single screw extruders are significantly better and provide a stable flow exiting the die that guaranties a constant cross section geometry of the produced strand.

- A special case in the downstream of twin-screw extruders can be the use of a special melt pump and die assembly facilitating **co-extrusion**. Here, the strengths of twin screw extrusion and single screw extrusion can be combined producing a co-extrudate with a twin screw extruder core and single screw extruded skin. The core can be a multi component formulation whereas the co-extrudate skin is typically a simple, dissolution rate controlling polymer. Special care has to be dedicated to proper cross section geometry of the core and to the control of the skin thickness and cross section distribution.

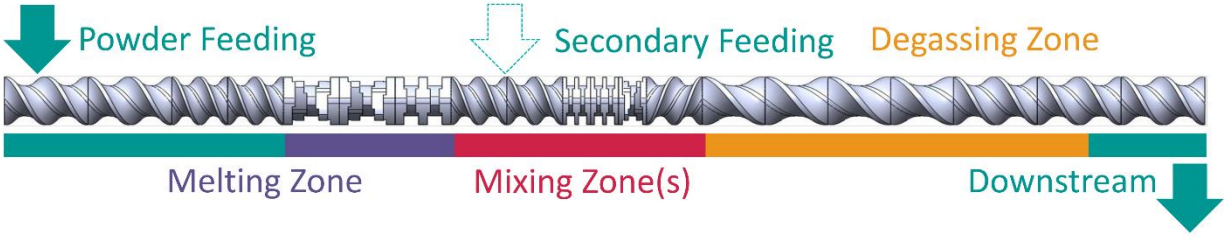

Figure 1.1. A typical screw configuration found in pharmaceutical HME.

1.1.3 Independent and Dependent Process Variables

In addition to the importance of the individual screw elements, their geometry and the fully assembled screw configuration, understanding the process independent (process settings) and the process dependent (process response) process settings is one more important step towards process understanding. The independent process variables are the process settings that can be set during the process execution. In addition the screw element type, the screw geometry, screw configuration, number and location of secondary feeding ports, degassing pressure and die assembly discussed in the previous chapter; the screw speed, throughput(s) and barrel temperature are regarded as the most important process independent variables. It should be noted that the screw speed, throughput and barrel temperature are the simplest to adjust process settings and are therefore also often a part of most Design of Experiment (DoE) studies performed during the process setup. On the other hand, the dependent process variables are a direct process response to the independent process variables and the formulation properties. They can be divided into:

- Process dependent variables that can be monitored or measured directly at the extruder, like the process torque, specific mechanical energy consumption (SMEC), melt pressure and temperature at the die and residence time distribution (RTD);
- Process dependent variables that can be computed using various *in silico* tools, like the axial distributions of the filling degree of the extruders, axial melt temperature, pressure and SMEC distributions, local and overall residence time distributions and many more.

DoE studies aim to establish a (functional or non-functional) link between the process independent and process dependent variables that are easily measured during the process execution, and the resulting product quality. Typically a set of carefully chosen process setup changes is performed by adjusting the process independent variables and the effect of those changes on the process dependent variables and the product quality is observed. Then a link between the input and output variables can be established via some sort of statistical data analysis. This knowledge is than used to define the process space confined by the independent process variables. For process settings outside the defined process space only limited recommendation can be made with this method, especially when significant changes in the screw configuration or equipment type or scale are made. This is also the main drawback of DoE studies, besides the waste and costs generally associated with experimental studies.

To overcome shortcomings of a pure DoE based approach it is critical to understand and establish the link between the different process variables and the resulting product quality. A first step is to establish a link between the independent and dependent process variables. The link between the independent and dependent process variables is established by taking into account the formulation properties relevant for processability. In the case of HME process development the most important formulation properties are the specific volume, formulation viscosity, heat capacity and thermal conductivity. Each of the listed formulation properties together with the process independent process variables is responsible for a certain process response that can be quantified with help of the process dependent variables.

The specific volume is a formulation property that quantifies the amount of volume the formulation occupies under predefined temperature and pressure conditions. The inverse quantity of the specific volume is the formulation density. Naturally, the specific volume is the formulation property responsible for the filling degree along the screw configuration. For formulations with a higher specific volume the filling degree is also going to be higher for the same process settings, and vice versa. Combining the specific volume with the screw speed, configuration and throughput yields the axial filling degree distribution. The chosen screw

configuration already defines the possible fully filled regions along the screws. They are typically located in zones with lower conveying capacities, i.e. in the regions of kneading elements, conveying neutral elements, back conveying elements and in the die zone. The amount of partial filling is then decided as a function of the screw speed, throughput and specific volume of the formulation. Here, a higher screw speed will result in a lower filling degree in the partially filled sections and higher throughput in a higher fill of the partially filled sections, for the same formulation. It is also important to note that the filling degree along the screw is one of the main factors influencing the local and overall RTD of the processed formulations.

The formulation viscosity defines the resistance the formulation has to deformation. This is a crucial property for understanding the amount of torque needed for the processing and the temperature rise resulting from the viscous dissipation. Higher viscosity formulation have a higher resistance to deformation, hence require higher torque for the rotation of the screw and processing, in comparison to lower viscosity formulations. The specific mechanical energy consumption is also indirectly influenced by the torque needed for the processing of the formulation, as it is calculated form the process torque, throughput and screw speed. In addition, higher viscosity formulation naturally also result in higher viscous dissipation, which is a result of the shear rates coming from the screw (mainly determined by the screw geometry and screw speed) and the formulation viscosity. Viscous dissipation tends to raise the temperature of the processed formulation. Exactly by how much the temperature is raised is determined by the heat capacity and thermal conductivity of the formulation. The heat capacity dictates how much dissipative (or other) energy is needed to increase the temperature of the processed formulation by one degree. On the other hand, the thermal conductivity of the formulation quantifies the ability of the processed formulation to be distribute a certain temperature and be cooled (or heated) by the surrounding.

The formulation properties, together with the process dependent and independent variables define a unique process state that results in a certain product quality. The process state represents the cycle of shear rate, temperature and exposure time (residence time) the formulation is exposed to during the processing. Following the new QbD guidelines, the goal is to connect the process state uniquely to the resulting product quality and to ensure repeatability, process stability and scalability [29]–[35].

1.2 Pharmaceutical Hot Melt Extrusion Process Simulations

Describing the process state as a function of the used screw configuration, process parameters and processed formulation is of great importance for understanding the process, effectively setting up and scaling up the process. The *in situ* process setup allows limited insights into the process state. Depending on the scale of the extruder, only limited information can be extracted from the process using standard control tools. Besides the throughput, screw speed and barrel temperature control, which should be a basic prerequisite for process setup, typically only the process torque (and SMEC), melt pressure and temperature at the die are measured. It should be noted that the torque and SMEC values coming from the extruder software are integral process values, i.e. they do not show the individual SMEC or temperature peaks along the screw that might significantly affect the resulting product. Similar, the melt temperature and pressure and the die only show a snapshot at one location. This means that it is theoretically possible to setup different processes (for example with different screw configurations) that would result in the same integral process parameters but in different product qualities. This is insufficient to capture the complexity of the different processing zones along the screw and to unambiguously describe the prevailing process state. To do so, different simulation tools are indispensable.
The approach presented in this work heavily relies on two main simulation approaches:

1. 3D Smoothed Particle Hydrodynamics (SPH) based simulations of individual screw element pairs [36]–[39]; and
2. 1D HME reduced order full process simulations [40], [41].

It is important to mention that SPH simulations are often used to characterize a certain screw geometry and to use the results as an input for the reduced order 1D HME simulations. To do this, the results are presented in a dimensionless way, as proposed by Pawlowksi and Kohlgrüber [1], [42].

1.2.1 Dimensionless Theory for Twin Screw Extruders

The dimensionless theory presented by Pawlowski for single- and Kohlgrüber twin-screw extruder separates the screw performance in two groups: the pressure and the power characteristics. The pressure characteristics shows the relation between the dimensionless

throughput and the dimensionless pressure build-up. The dimensionless throughput is calculated as:

$$\dot{V}^* = \frac{\dot{V}}{nD^3} \tag{1}$$

And the dimensionless pressure build-up as:

$$p^* = \frac{\Delta pD}{\eta nL} \tag{2}$$

Where $\dot{V}$ is the volumetric throughput rate, n is the screw speed, D is the nominal barrel diameter, p is the pressure drop, η is the melt viscosity and L is the screw length. On the other hand, the power characteristics shows the relation between the dimensionless throughput, similar to the pressure characteristics, with the dimensionless power consumption of the investigated screw. The dimensionless power consumption is calculated as:

$$P^* = \frac{P}{\eta n^2 D^2 L} \tag{3}$$

Where P is the consumed power. Both, the pressure and power characteristics are linear and independent of the fluid viscosity, screw speed and element size (dimeter and length) in the case of Newtonian fluids in the creeping flow regime ($Re \ll 1$). This means that, under these special conditions, the results are only a function of the screw geometry, which makes this approach convenient for the parametrization of the screw elements. A schematic of the pressure and power characteristics is shown in Figure 1.2. The axial intersects of the pressure and power characteristics are enough to capture the performance of the investigated screw, under these conditions. The A1 axial intercept in the pressure characteristics represents the inherent conveying capacity of the screw, and the A2 intercept represents the pressure build-up capacity of the investigated screw. The conveying ratio Λ is defined as the ration between the current dimensionless throughput and the conveying capacity of the screw:

$$\Lambda = \frac{\dot{V} \cdot A1}{nD^3} \tag{4}$$

For $\Lambda < 0$, the screw is in a backwards conveying state. This means that the melt is going against the conveying direction of the screw, i.e. the pressure gradient at the beginning of the screw is higher than the pressure build-up capacity of the screw. This is the case in back conveying element that are used in the screw configuration to enhance the mixing and increase the residence time distribution of the melt.

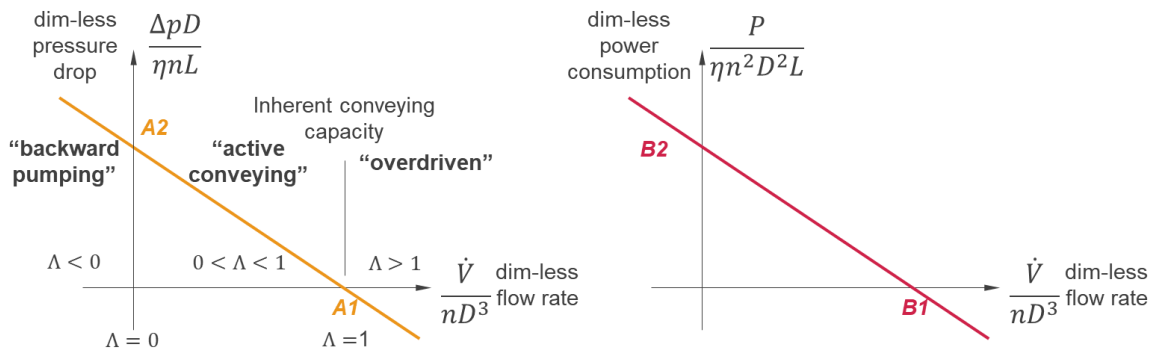

Figure 1.2. A schematic of the pressure and power characteristics for Newtonian fluids under creeping flow conditions.

In the case the conveying ratio lying between 0 and 1 ($0 < \Lambda < 1$), the screw is in its normal operating space. In the case the conveying ratio is above 1 ($\Lambda > 1$), the screw is overdriven by the melt, i.e. the melt moves quicker in the conveying direction then (due to some pressure drop upstream) it typically would if only conveying by the screw. This scenario can theoretically occur if screw elements with extremely low conveying capacity are paired with screw elements with high conveying capacity and are hence overdriven by the screw with the significantly higher conveying capacity. In a similar way, the intercepts B1 and B2 are characteristic points in the power consumption of the screw.

Using a dimensionless approach for analyzing the screw performance makes it easier to compare the performance of difference screw designs independent of the formulation, different extruder screw scales and, most importantly, a great way of reducing the complex flow data from the 3D SPH simulations into a reduced order 1D HME simulation model. More details on the dimensionless analysis can be found here [1], [42], on SPH in general here [43]–[46], on the use of SPH in characterizing individual screw element pairs here [36]–[38], [47] and on creating a reduced order model and using it for HME process analysis here [40], [41], [47].

1.3 Abbreviations

1D	one-dimensional
API	active pharmaceutical ingredient
CFD	computational fluid dynamics
RTD	residence time distribution
SPH	smoothed particle hydrodynamics
HME	hot melt extrusion
TSE	co-rotating twin-screw extruder

1.4 Nomenclature

Latin symbols

A1, A2, B1, B2 [-]	Axial intercepts of the dimensionless pressure and power curves
D $[mm]$	Nominal barrel diameter
L $[mm]$	Screw length
n $[rpm]$	Screw speed
p $[bar]$	Pressure
P $[W]$	Screw power
Re $[-]$	Reynolds number
$\dot{V}$ $[\frac{m^3}{h}]$	Volumetric throughput
$\dot{V}^*, p^*, P^*$ $[-]$	Dimensionless volumetric throughput, pressure and power, respectively

Greek symbols

η $[Pas]$	Melt viscosity
Λ $[-]$	Conveying ratio

1.5 References

[1] K. Kohlgrüber *et al.*, *Co-Rotating Twin-Screw Extruder*. München: Carl Hanser Verlag GmbH & Co. KG, 2007.

[2] K. Kolter, M. Karl, and A. Gryczke, *Hot-Melt Extrusion with BASF polymers*, no. 2nd Revised and Enlarged. BASF, 2012.

[3] C. Rauwendaal and Dr. Chris Rauwendaal, *Polymer Extrusion*, Fifth Edit. München: Carl Hanser Verlag GmbH & Co. KG, 2014.

[4] J. G. Khinast and J. Rantanen, *Continuous Manufacturing of Pharmaceuticals*. Chichester, UK: John Wiley & Sons, Ltd, 2017.

[5] M. A. Repka *et al.*, "Melt extrusion with poorly soluble drugs – An integrated review," *Int. J. Pharm.*, vol. 535, no. 1–2, pp. 68–85, 2018.

[6] M. M. Crowley *et al.*, "Pharmaceutical Applications of Hot-Melt Extrusion: Part I," *Drug Dev. Ind. Pharm.*, vol. 33, no. 9, pp. 909–926, Jan. 2007.

[7] M. A. Repka *et al.*, "Pharmaceutical Applications of Hot-Melt Extrusion: Part II," *Drug Dev. Ind. Pharm.*, vol. 33, no. 10, pp. 1043–1057, Jan. 2007.

[8] M. Monschke, K. Kayser, and K. G. Wagner, "Processing of Polyvinyl Acetate Phthalate in Hot-Melt Extrusion—Preparation of Amorphous Solid Dispersions," *Pharmaceutics*, vol. 12, no. 4, p. 337, Apr. 2020.

[9] J. M. Vasoya *et al.*, "Development of Solid Dispersion by Hot Melt Extrusion Using Mixtures of Polyoxylglycerides With Polymers as Carriers for Increasing Dissolution Rate of a Poorly Soluble Drug Model," *J. Pharm. Sci.*, vol. 108, no. 2, pp. 888–896, Feb. 2019.

[10] J. Breitenbach, "Melt extrusion: from process to drug delivery technology," *Eur. J. Pharm. Biopharm.*, vol. 54, no. 2, pp. 107–117, Sep. 2002.

[11] H. Patil *et al.*, "Hot-Melt Extrusion: from Theory to Application in Pharmaceutical Formulation," *AAPS PharmSciTech*, vol. 17, no. 1, pp. 20–42, Sep. 2015.

[12] M. F. Simões, R. M. A. Pinto, and S. Simões, "Hot-melt extrusion in the pharmaceutical industry: toward filing a new drug application," *Drug Discov. Today*, vol. 24, no. 9, pp. 1749–1768, Sep. 2019.

[13] G. L. Amidon, H. Lennernäs, V. P. Shah, and J. R. Crison, "A Theoretical Basis for a Biopharmaceutic Drug Classification: The Correlation of in Vitro Drug Product Dissolution and in Vivo Bioavailability," *Pharm. Res.*, vol. 12, no. 3, pp. 413–420, Mar. 1995.

[14] J. M. Butler and J. B. Dressman, "The Developability Classification System: Application of Biopharmaceutics Concepts to Formulation Development," *J. Pharm. Sci.*, vol. 99, no. 12, pp. 4940–4954, Dec. 2010.

[15] H. D. Williams *et al.*, "Strategies to Address Low Drug Solubility in Discovery and Development," *Pharmacol. Rev.*, vol. 65, no. 1, pp. 315–499, Jan. 2013.

[16] J. Matić, A. Paudel, H. Bauer, R. A. L. Garcia, K. Biedrzycka, and J. G. Khinast, "Developing HME-Based Drug Products Using Emerging Science: a Fast-Track Roadmap from Concept to Clinical Batch," *AAPS PharmSciTech*, vol. 21, no. 5, p. 176, Jul. 2020.

[17] I. Koutsamanis, A. Paudel, K. Nickisch, K. Eggenreich, E. Roblegg, and S. Eder, "Controlled-Release from High-Loaded Reservoir-Type Systems—A Case Study of Ethylene-Vinyl Acetate and Progesterone," *Pharmaceutics*, vol. 12, no. 2, p. 103, Jan. 2020.

[18] Y. Zhu, N. H. Shah, A. Waseem Malick, M. H. Infeld, and J. W. McGinity, "Controlled Release of a Poorly Water-Soluble Drug from Hot-Melt Extrudates Containing Acrylic Polymers," *Drug Dev. Ind. Pharm.*, vol. 32, no. 5, pp. 569–583, Jan. 2006.

[19] A. Q. Vo *et al.*, "A novel floating controlled release drug delivery system prepared by hot-melt extrusion," *Eur. J. Pharm. Biopharm.*, vol. 98, pp. 108–121, Jan. 2016.

[20] M. Fukuda, N. A. Peppas, and J. W. McGinity, "Floating hot-melt extruded tablets for gastroretentive controlled drug release system," *J. Control. Release*, vol. 115, no. 2, pp. 121–129, Oct. 2006.

[21] M. Stanković *et al.*, "Low temperature extruded implants based on novel hydrophilic multiblock copolymer for long-term protein delivery," *Eur. J. Pharm. Sci.*, vol. 49, no. 4, pp. 578–587, Jul. 2013.

[22] M. Stanković, H. W. Frijlink, and W. L. J. Hinrichs, "Polymeric formulations for drug release prepared by hot melt extrusion: application and characterization," *Drug Discov. Today*, vol. 20, no. 7, pp. 812–823, Jul. 2015.

[23] M. Stanković, J. Tomar, C. Hiemstra, R. Steendam, H. W. Frijlink, and W. L. J. Hinrichs, "Tailored protein release from biodegradable poly(ε-caprolactone-PEG)-b-poly(ε-caprolactone) multiblock-copolymer implants," *Eur. J. Pharm. Biopharm.*, vol. 87, no. 2, pp. 329–337, Jul. 2014.

[24] R. Baumgartner, A. Eitzlmayr, N. Matsko, C. Tetyczka, J. G. Khinast, and E. Roblegg, "Nano-extrusion: A promising tool for continuous manufacturing of solid nano-formulations," *Int. J. Pharm.*, vol. 477, no. 1–2, pp. 1–11, Dec. 2014.

[25] R. Baumgartner, J. Matić, S. Schrank, S. Laske, J. G. J. Khinast, and E. Roblegg, "NANEX: Process design and optimization," *Int. J. Pharm.*, vol. 506, no. 1–2, pp. 35–45, Jun. 2016.

[26] A. M. Bhagurkar, M. A. Repka, and S. N. Murthy, "A Novel Approach for the Development of a Nanostructured Lipid Carrier Formulation by Hot-Melt Extrusion Technology," *J. Pharm. Sci.*, vol. 106, no. 4, pp. 1085–1091, Apr. 2017.

[27] H. Patil, X. Feng, X. Ye, S. Majumdar, and M. A. Repka, "Continuous Production of Fenofibrate Solid Lipid Nanoparticles by Hot-Melt Extrusion Technology: a Systematic Study Based on a Quality by Design Approach," *AAPS J.*, vol. 17, no. 1, pp. 194–205, Jan. 2015.

[28] L. A. D. Silva *et al.*, "Preparation of a solid self-microemulsifying drug delivery system by hot-melt extrusion," *Int. J. Pharm.*, vol. 541, no. 1–2, pp. 1–10, Apr. 2018.

[29] V. P. Kumar and N. V. Gupta, "A Review on quality by design (QBD) for Pharmaceuticals," *Int. J. Drug Dev. Res.*, vol. 7, no. 1, pp. 35–44, 2015.

[30] L. X. Yu *et al.*, "Understanding Pharmaceutical Quality by Design," *AAPS J.*, vol. 16, no. 4, pp. 771–783, Jul. 2014.

[31] V. Mishra, S. Thakur, A. Patil, and A. Shukla, "Quality by design (QbD) approaches in current pharmaceutical set-up," *Expert Opin. Drug Deliv.*, vol. 15, no. 8, pp. 737–758, Aug. 2018.

[32] A. Gupta and M. A. Khan, "Hot-Melt Extrusion: An FDA Perspective on Product and Process Understanding," in *Hot-Melt Extrusion: Pharmaceutical Applications*, Chichester, UK: John Wiley & Sons, Ltd, 2012, pp. 323–331.

[33] ICH Q8, "EMEA/CHMP, 2009, ICH Topic Q 8 (R2) Pharmaceutical Development, Step 5: Note for Guidance on Pharmaceutical Development," vol. 8, no. June, 2017.

[34] ICH Q9, "INTERNATIONAL CONFERENCE ON HARMONISATION OF TECHNICAL REQUIREMENTS FOR REGISTRATION OF PHARMACEUTICALS FOR HUMAN USE ICH HARMONISED TRIPARTITE GUIDELINE QUALITY RISK MANAGEMENT Q9," 2005.

[35] ICH Q10, "INTERNATIONAL CONFERENCE ON HARMONISATION OF TECHNICAL REQUIREMENTS FOR REGISTRATION OF PHARMACEUTICALS FOR HUMAN USE PHARMACEUTICAL QUALITY SYSTEM Q10," 2009.

[36] A. Eitzlmayr and J. Khinast, "Co-rotating twin-screw extruders: Detailed analysis of conveying elements based on smoothed particle hydrodynamics. Part 2: Mixing," *Chem. Eng. Sci.*, vol. 134, pp. 880–886, Sep. 2015.

[37] A. Eitzlmayr, J. Matić, and J. G. Khinast, “Analysis of flow and mixing in screw elements of corotating twin-screw extruders via SPH,” *AIChE J.*, vol. 63, no. 6, pp. 2451–2463, Jun. 2017.

[38] A. Eitzlmayr and J. G. Khinast, “Co-rotating twin-screw extruders: Detailed analysis of conveying elements based on smoothed particle hydrodynamics. Part 1: Hydrodynamics,” *Chem. Eng. Sci.*, vol. 134, pp. 861–879, Sep. 2015.

[39] H. Bauer, J. Matić, and J. Khinast, “Characteristic parameters and process maps for fully-filled twin-screw extruder elements,” *Chem. Eng. Sci.*, p. 116202, Oct. 2020.

[40] A. Eitzlmayr *et al.*, “Mechanistic modeling of modular co-rotating twin-screw extruders,” *Int. J. Pharm.*, vol. 474, no. 1–2, pp. 157–176, Oct. 2014.

[41] A. Eitzlmayr *et al.*, “Experimental characterization and modeling of twin-screw extruder elements for pharmaceutical hot melt extrusion,” *AIChE J.*, vol. 59, no. 11, pp. 4440–4450, Nov. 2013.

[42] J. Pawlowski, *Die Ähnlichkeitstheorie in der physikalisch-technischen Forschung*. Berlin, Heidelberg: Springer Berlin Heidelberg, 1971.

[43] J. J. Monaghan, “SPH without a Tensile Instability,” *J. Comput. Phys.*, vol. 159, pp. 290–311, Apr. 2000.

[44] J. P. Morris, P. J. Fox, and Y. Zhu, “Modeling Low Reynolds Number Incompressible Flows Using SPH,” *J. Comput. Phys.*, vol. 136, no. 1, pp. 214–226, Sep. 1997.

[45] J. J. Monaghan, “Smoothed particle hydrodynamics,” *Reports Prog. Phys.*, vol. 68, no. 8, pp. 1703–1759, Aug. 2005.

[46] G. R. Liu and M. B. Liu, *Smoothed Particle Hydrodynamics a mesfree particle method*. Singapore: World Scientific Publishing Co. Pte. Ltd., 2003.

[47] J. Matić, A. Witschnigg, M. Zagler, S. Eder, and J. Khinast, “A novel in silico scale-up approach for hot melt extrusion processes,” *Chem. Eng. Sci.*, vol. 204, pp. 257–269, Aug. 2019.

2

Goals and Content

Providing a platform for process understanding, setup, scale-up and product development is the main goal of this work. Understandably, this will always be a work in progress, where every simulation and experiment represent an incremental step towards final goal. For now, it is important to understand the bigger picture, show the boundaries of the current approaches, fill in some gaps with our work and prepare the path for future development.

2.1 Goals

In order to provide a holistic approach for product development, significant effort have to be made in understanding the different production stages. Hot melt extrusion (HME) based product development can be divided into different phases, that include but are not limited to:

- Product definition, i.e. amorphous solid dispersion or solution, crystalline dispersion, nano-crystalline dispersion, immediate or extended release, tablet, capsule or implant;
- Formulation development, i.e. choosing the appropriate excipient(s), testing out different active pharmaceutical ingredients (API) and loadings, release testing;
- Process selection and development, i.e. definition of a possible production route, small scale formulation processability and compatibility testing, stable process development and scale-up.

The mentioned phases are all part of the preclinical process development and usually have limited amounts of API available for testing (measured in grams). The lack of API represents a significant difficulty for the process development of HME based products, due to the nature of the process, significant amounts of premix are used (measured in kilograms) for the process development. To overcome this issue it is possible to apply different simulation tools in order to create an *in silico* process surrogate that will be used for testing of different formulations and process settings.

The basis for the *in silico* process surrogate was created by Dr. Andreas Eitzlmayr in his work on 1D HME process simulations and Smoother Particle Hydrodynamics (SPH) simulation of individual HME screw elements [1]–[6]. This work is a direct continuation and aims to apply the different simulation tools in industry relevant applications during process setup and scale-up.

2.2 Content

Chapters 1 and 2 provide a basing introduction into the presented topic and overview of the goal and content of the thesis, respectively.

The thesis consists of five Chapters (Chapters 3 to 7) summarizing the research done on HME process setup and scale-up. Chapters 4, 5 and 7 were already published in different journal, whereas Chapters 3 and 6 are indented for publishing and will be submitted soon.

Chapter 3 is focused on two extruders of different size and cross section design. The Leistritz NANO16 is a 16mm triple-flighted co-rotating twin screw extruder and the Leistritz ZSE18 is an 18mm double flighted co rotation twin screw extruder. The different screw elements of both extruders were analyzed using high fidelity SPH simulations, showing the impact of the cross section design on the screw performance. Furthermore, two different formulations were extruded using the NANO16 extruder, generating data for the validation of the 1D HME simulation software and creating an *in silico* process transfer from the NANO16 to the ZSE18 extruder.

Chapter 4 focuses on investigating the individual screw elements of two double flighted extruders, the Coperion ZSK18 and the Leistritz MIC27. SPH simulations were made showing the scalability between the differently designed and sized screw elements. In addition, experiments on the ZSK18 extruder were analyzed using the 1D HME simulations, creating an *in silico* process surrogate. Furthermore, different scale-up approaches were tested *in silico*, showing the issues in traditional process transfer from the ZSK18 to the MIC27 extruders and proposing a scale-up approach based on thermomechanical load the formulation experiences during processing.

Moving beyond SPH and 1D HME *in silico* process mirroring, Chapter 5 shows the first attempts at connecting the product quality with the process state. Here, the Leistritz ZSE12 extruder was used for a number of experimental setups analyzing the impact the process setup has on the resulting product quality. As a measure of the product quality the API degradation in the extrudates was used. It was possible to show the correlation between the API degradation to the thermomechanical load the formulation experiences during processing, i.e. the API degradation was directly correlated to the local melt temperature and local mean residence time (exposure time) at certain position along the screw configuration.

Continuing the research from Chapter 5, Chapter 6 analyzed the same formulation and different scale-up approaches when moving from the Leistritz ZSE12 to the Leistritz ZSE18 extruder. Using the same simulation approach shown in Chapter 5 it was again possible to correlate the resulting product quality (API degradation in the extrudate) to the thermomechanical load the formulation was experiencing (local melt temperature and local mean residence time). This shown that the approach is valid across different extruder scales.

Chapter 7 gives a more holistic overview of the whole HME product development path starting from QbD based principles to basic formulation development for HME based products and *in silico* based process setup, scale-up and GMP transfer.

Chapter 8 and 9 provide a conclusion and outlook for future development, and a summary of journal and conference contributions respectively.

2.3 Abbreviations

1D	one-dimensional
API	active pharmaceutical ingredient
GMP	good manufacturing practice
SPH	smoothed particle hydrodynamics
HME	hot melt extrusion
QbD	quality by design

2.4 References

[1] A. Eitzlmayr *et al.*, "Experimental characterization and modeling of twin-screw extruder elements for pharmaceutical hot melt extrusion," *AIChE J.*, vol. 59, no. 11, pp. 4440–4450, Nov. 2013.

[2] A. Eitzlmayr *et al.*, "Mechanistic modeling of modular co-rotating twin-screw extruders," *Int. J. Pharm.*, vol. 474, no. 1–2, pp. 157–176, Oct. 2014.

[3] A. Eitzlmayr, G. Koscher, and J. G. Khinast, "A novel method for modeling of complex wall geometries in smoothed particle hydrodynamics," *Comput. Phys. Commun.*, vol. 185, no. 10, pp. 2436–2448, Oct. 2014.

[4] A. Eitzlmayr and J. Khinast, "Co-rotating twin-screw extruders: Detailed analysis of conveying elements based on smoothed particle hydrodynamics. Part 2: Mixing," *Chem. Eng. Sci.*, vol. 134, pp. 880–886, Sep. 2015.

[5] A. Eitzlmayr and J. G. Khinast, "Co-rotating twin-screw extruders: Detailed analysis of conveying elements based on smoothed particle hydrodynamics. Part 1: Hydrodynamics," *Chem. Eng. Sci.*, vol. 134, pp. 861–879, Sep. 2015.

[6] A. Eitzlmayr, J. Matić, and J. G. Khinast, "Analysis of flow and mixing in screw elements of corotating twin-screw extruders via SPH," *AIChE J.*, vol. 63, no. 6, pp. 2451–2463, Jun. 2017.

3

A Case Study in Pharmaceutical HME Process Development: Influence of the Screw Cross Section*

In this work we analyzed in detail the impact the screw cross section geometry has on the performance of screw elements in co-rotating twin screw extruders. For this purpose we analyzes screw elements from the triple flighted NANO16 and double flighted ZSE18 twin screw extruders from Leistritz. To directly compare the influence the cross section geometry has on the screw performance we used our Smoothed Particle Hydrodynamics simulation approach and computed the dimensionless throughput, pressure build-up and power consumption values of the various screws. In addition to the high fidelity simulations, we also performed a number of experimental process setups on the NANO16 extruder with two different formulations, representing the usual amorphous solid dispersions formulations often used in pharmaceutical hot-melt extrusions. To analyze the process setups on the NANO16 extruder and understand the impact the screw configuration and formulation have on the internal process state we performed 1D HME simulations. The simulations were validated with the torque, specific mechanical energy consumption, mean residence time and melt temperature measurements performed during processing. In addition, a virtual process transfer from the NANO16 to the ZSE18 extruder was performed for both formulations, under the assumption of keeping the temperature and exposure time cycle constant on both extruder scales as a guaranty of equivalent product quality.

* This chapter is based on: J. Matić, M. Stanković-Brandl, H. Bauer, A. Paudel and J. Khinast, "A Case Study in Pharmaceutical HME Process Development: Influence of the Screw Cross Section" *In preparation*

3.1 Introduction

The pharmaceutical industry is experiencing a move from batch towards continuous manufacturing and product development supported by a Quality by Design (QbD) approach [1]–[7]. One of the prominent continuous manufacturing technologies gaining traction in the pharmaceutical industry is hot melt extrusion (HME). It is a flexible process that ensures high mixing of highly viscous fluids and is a one-step solidification process most notably used for the solubilization of poorly soluble active pharmaceutical ingredients [8]–[10] (APIs) for immediate or controlled release formulation [11]–[13]. Moreover, the process was also shown to be suitable for nano-formulations [14]–[21], or for the manufacturing of specific drug delivery devices [22]–[25]. The move towards a QbD development approach and the recent needs for quick and robust drug development calls for a reliable and inexpensive product and process development [26]–[32]. For this to be achieved, a significant knowledge about the formulation and process understanding is inevitable and still has to be amended. It is still a challenge to identify and link the critical material attributes (CMAs) of the formulation, the critical process parameters (CPPs) with the resulting critical quality attributes (CQA) of the product. Moreover, the movement towards more rapid, reliable and cost effective product development is only possible if the critical CMA-CPP-CQA connections can be made even before the first experimental runs. Hence, significant developments in this field are expected.

The equipment of choice for the HME process is typically a closely intermeshing co-rotating twin-screw extruder (TSE). TSE's are characterized by excellent mixing capabilities and high process modularity, making them suitable for a wide variety of formulations and final products. The high process flexibility comes primarily from the modular screw configurations, utilizing different conveying, mixing, kneading or special screw elements in order to perform the specific processing tasks in mind. By carefully arranging the screw elements in the screw configuration, different processing zones can be established. The processing zones usually found in HME are the powder conveying and densification zone, melting zone, various mixing zones (depending on the formulation and the number of additional feeding ports), degassing zone, pressure build-up and strand shaping zone. Hence, understanding the screw geometry and the impact it has on the melt flow and mixing is crucial for proper screw configuration assembly. In addition to the differences in geometry between the different screws elements (pitch, number of kneading blocks, their angle and thickness or the specific geometry of the mixing elements) the screw cross section geometry has to be taken into account too. Usually, screw elements for HME have

a double flighted screw geometry with the ratio between the outer and inner screw diameter being a characteristic value for process transfer and scale-up. Single flighted and triple flighted screw elements can be found as special elements in an otherwise double flighted screw configuration. As an example kneading elements with a triple flighted cross section geometry or single flighted discharge elements in an otherwise double flighted screw configuration can be found. The intended tasks behind the change in the cross section geometry for these elements is high dispersive mixing in the case of triple flighted kneading elements and high pressure build up generation in the case of single flighted discharge elements. Relatively recently, Leistritz introduced the NANO16, a 16mm twin screw extruder with a triple flighted screw cross section geometry. Understanding how the geometry of the screw cross section impact the process setup and how to transfer such a process to another screw cross section geometry is a significant challenge.

To date, our group has worked intensively on sample preparation for quick formulation screening [24], [33] and on development of a high-fidelity simulation environment that is based on Smoothed Particle Hydrodynamics (SPH) and 1D mechanistic modelling, as tools for HME process understanding, design, scale-up and cleaning [1], [34]–[40]. In this framework, SPH is used for detailed screw characterization of individual screw element pairs commonly found in twin screw extruders. The focus is on determining and isolating the effect the screw geometry has on the melt flow field and distributive mixing action. The knowledge gained by such an approach is then applied in our in-house developed 1D HME simulation code to accurately compute axial distributions of filling degree, pressure, melt temperature, specific mechanical energy consumption (SMEC), and local and overall residence time distributions (RTD) [15], [38], [39]. Using this approach, it is possible to evaluate different screw geometries in terms of their conveying capacity, pressure build-up capacity, power consumption and distributive mixing action, with the goal of choosing the adequate elements for the tasks allocated in the screw configuration and to help during screw transfer from one size or extruder vendor to another. In addition, the use of the 1D HME simulation approach allows for an *in silico* process development, evaluation and scale-up, by testing different formulations, screw configurations and process settings. This approach is particularly important during early process development, process transfer and scale-up.

In this work we´ll investigate the influence of the screw geometry cross section on the screw performance by comparing the screw elements of double flighted ZSE18 Leistritz with the screw elements of the triple flighted NANO16 Leistritz. Moreover, process setup of the two

formulations on the NANO16 extruder was evaluated in detail using experiments and 1D HME simulations, followed by a virtual process transfer to the ZSE18 extruder.

3.2 Materials and Methods

3.2.1 Equipment and Screw Elements

Both extruders are closely intermeshing co-rotating twin screw extruder, but differ significantly in their size, intended throughput range and screw geometry. The Leistritz NANO16 can be compared to a small size table top extruder in terms of throughput range (up to 1kg/h, depending on the formulation), despite its nominal diameter of 16mm. The reason for this can be found in the comparably low free volume due to the triple flighted cross section geometry of the screw elements. In the other hand, the Leistritz ZSE18 is a twin screw extruder with a traditional double flighted screw cross section geometry. In the context of pharmaceutical extrusion, it is a full size pilot plant or even production size extruder, with throughputs up to 5kg/h, depending on the formulation. Here, the influence of the screw cross section design can be clearly observed. Although the nominal screw diameters differ only by 2mm (12.5%), the free cross section area differs by a factor of around 2.4. Consequently, the difference in the throughput range of the two extruders is understandable.

The nominal screw geometry values are summarized in Table 3.1 and shown in Figure 3.1. The investigated screw elements are a typical combination of conveying, kneading and mixing elements usually found in a screw configurations for pharmaceutical production. The nomenclature used is as follows. The nominal screw diameter is denoted at the beginning of the screw name with 16 for the NANO16 screw elements and 18 for the ZSE18 screw elements. Next, the type of the element is denoted with a capital letter C for conveying, K for kneading and M for mixing elements, followed by the pitch (in mm) or kneading angle (in °) for kneading elements. In the case of the NANO16 extruder, three different conveying elements were investigated with pitches of 10mm, 15mm and 20mm (16C10, 16C15, 16C20 respectively), two kneading elements with a kneading block angle of 30° and 60° (16K30 and 16K60 respectively) and one mixing elements with a pitch of 15mm (16M15). The kneading elements have a kneading block thickness of 1.6mm in the case of the investigated NANO16 elements. In the case of the ZSE18 extruder four different conveying elements were investigated with pitches of 10mm, 15mm, 20mm and 30mm (18C10, 18C15, 18C20 and 18C30 respectively), three kneading elements with a kneading block angle of 30°, 60° and 90° (18K30, 18K60, 18K90)

and one mixing element with a pitch of 15mm (18M15). The kneading elements have a kneading block thickness of 4mm in the case of the investigated ZSE18 elements.

Table 3.1. Nominal cross section geometry dimensions for NANO16 and ZSE18.

		NANO16	ZSE18
D	Barrel diameter [mm]	16	18
D_o	Outer screw diameter [mm]	15.9	17.8
D_i	Inner screw diameter [mm]	13.8	11.8
Cl	Centreline distance [mm]	15	15

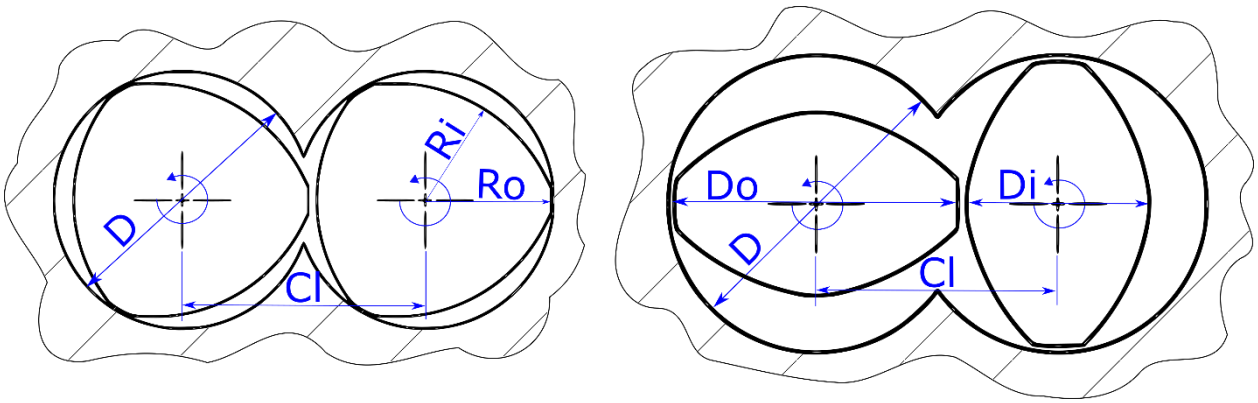

Figure 3.1. Nominal cross section geometries of the triple flighted NANO16 (left) and double flighted ZSE18 (right). In the case of NANO16, Ro and Ri are the outer screw and inner screw radii.

3.2.2 Formulation Properties

Two formulations were used in the experimental and simulation setups, a physical blend of 85 wt% Kollidon VA64 and 15 wt% Itraconazole, and a physical blend of 80 wt% Soluplus and 20 wt% Ibuprofen. The formulations were parametrized in order to be used as input for the 1D HME simulation code. For this purpose, the melt rheology, specific volume, heat capacity and thermal conductivity of the formulations were measured and fitted with suitable material models. The specific volume of the formulation was measured using a PVT100 device in accordance with the ISO 17744 guidelines. The measurements were performed within ranges of 40°C-220°C and 200bar-1200bar, using isobaric cooling mode with a linear cooling rate of 6°C/min. The Schmidt model [41] was fitted to the experimentally obtained data, in order to be used in the 1D HME simulations for the calculation of the specific volume v $[cm^3/g]$:

$$v_{(p,T)} = \frac{K_1}{p+K_4} + \frac{K_2 \cdot T}{p+K_3} \quad (1)$$

Two sets of K_1 to K_4 parameters were used, one for the solid phase (if the temperature T was below the transition temperature) and one for the liquid phase (if the temperature T was above the transition temperature). The transition temperature T_{tr} $[°C]$ is a function of pressure p and is calculated as:

$$T_{tr(p)} = K_8 + K_9 \cdot p \quad (2)$$

The relevant K_1 to K_9 parameters can be found in
Table 3.2.

Table 3.2 K parameters used for the calculation of the specific volume according to the Schmidt model for the Itraconazole-Kollidon VA64 and Ibuprofen-Soluplus mixtures.

		Formulation A 15 wt% Itraconazole in 85 wt% Kollidon VA64		Formulation B 20 wt% Ibuprofen in 80 wt% Soluplus	
		Solid state	Melt state	Solid state	Melt state
K1	[bar cm³/g]	12112	11623	14325	15058
K2	[bar cm³/(g°C)]	1.0293	1.9013	1.7925	1.7142
K3	[bar]	2493.5	2971	2506.5	2294
K4	[bar]	14954	14731	15838	16707
K8	[°C]	99.113		98.418	
K9	[°C/bar]	0.012642		0.012902	

Rheology of the formulation was measured via a standard plate-plate rheometer (MCR 301 from Anton-Paar). The sample preparation for the rheology measurements was performed using the in house developed vacuum compression molding tool [33]. The measured frequency ranged between $0.1s^{-1}$ to $628s^{-1}$ for three probe temperatures of 120°C, 140°C and 160°C for the Ibuprofen-Soluplus mixture and 150°C, 160°C and 170°C for the Itraconazole-Kollidon VA64 mixture. The obtained data points were then fitted to a simplified variant of the Carreau-Yassuda model for non-Newtonian fluids:

$$\eta(\dot{\gamma}, T) = \frac{\eta_0 a_T}{\left(1+\frac{|\dot{\gamma}|a_T}{\dot{\gamma}_{crit}}\right)^{\overline{m}}} \quad (3)$$

where η ist the viscosity in $[Pa \cdot s]$, $T[°C]$ is the melt temperature, $\dot{\gamma}[s^{-1}]$ is the shear rate, $\dot{\gamma}_{crit}[s^{-1}]$ is the critical shear rate, $\eta_0[Pa \cdot s]$ the zero-shear-rate viscosity and a_T is the Williams-Landel-Ferry temperature shift factor calculated as:

$$a_T[-] = exp\left[-\frac{C_1(T-T_r)}{C_2+T-T_r}\right] \quad (4)$$

with $T_r[°C]$ being the reference temperature. The viscosity parameters used for the fit are shown in Table 3.3.

Table 3.3. Parameters for the Carreau-Yassuda viscosity fits for the investigated formulations.

		Formulation A 15 wt% Itraconazole in 85 wt% Kollidon VA64	Formulation B 20 wt% Ibuprofen in 80 wt% Soluplus
η_0	[Pas]	1200	136
$\dot{\gamma}_{crit}$	[s^{-1}]	32.93	32.25
m	[-]	0.3951	0.3509
T_r	[°C]	170	160
C_1	[-]	15.14	22.87
C_2	[°C]	134.82	277.13

The heat capacity and thermal conductivity were approximated via linear temperature-dependent fits, and were measured via modulated differential scanning calorimetry (mDSC) using the DSC 2014 F1 Phoenix® with an automated sampling unit (NETZSCH-Geraetebau GmbH, Selb, Germany). Two linear temperature-dependent fits were used to describe the heat capacity data of the formulations, one below the T_g of the formulation and one above. The linear temperature-dependent fits have the general form as:

$$c_p = D_1 + D_2 \cdot T \quad (5)$$

Where $c_p\ [J/kgK]$ is the heat capacity, $T[°K]$ is the melt temperature and D_1 and D_2 are the formulation specific coefficients summarized in Table 3.4.

Table 3.4. Formulation specific coefficients used for the modelling of the heat capacity.

		Formulation A 15% Itraconazole in 85% Kollidon VA64		Formulation B 20% Ibuprofen in 80% Soluplus	
		Solid state	Melt state	Solid state	Melt state
D_1	[J/kgK]	1152.789	1514.139	1228.991	1509.999
D_2	[J/kgK²]	3.433	2.847	8.116	3.703
T_g	[°C]	98.6		40	

The thermal conductivity $\lambda\ [W/mK]$ was modeled is a similar way with a linear temperature-dependent function in the form:

$$\lambda = E_1 + E_2 \cdot 10^{-4} \cdot T \quad (7)$$

where $T[K]$ is again the melt temperature and E_1 and E_2 are the formulation specific coefficients summarized in Table 3.5.

Table 3.5. Formulation specific coefficients used for the modelling of the thermal conductivity.

		Formulation A 15% Itraconazole in 85% Kollidon VA64	Formulation B 20% Ibuprofen in 80% Soluplus
E_1	[W/mK]	0.1579	0.1535
E_2	[W/mK²]	1.861	1.626

3.2.3 HME Process Setup

HME experiments were performed on the Leistritz NANO16 extruder. The screw configuration consisted of a combination of the screw elements that were investigated as part of the SPH screw characterization. The screw configuration starts with the highest pitch conveying element available, 16C20, to allow a high powder intake. The 16C20 conveying element is followed by a 16C15 conveying element with a lower pitch before the first kneading zone. The reason for the reduction of the screw pitch is twofold: (1) a reduced pitch will help in compacting the powder and eliminating any air pockets that might have formed, and (2) a reduction in pitch will help to build-up sufficient pressure to overcome the following kneading section. The first kneading section is assembled of a combination of 16K30 and 16K60 kneading elements and was used to fully melt the premix. The first kneading section is followed by series of conveying elements, 16C20, 16C15 and 16C10, with a pitch reduction towards the second kneading section. The second kneading section is comprised of two 16K60 kneading elements and is followed by the degassing and extrudate discharge zones, which were again assembled from conveying elements with a stepwise pitch reduction, 16C20, 16C15 and 16C10. The extrudate discharge was facilitated with a die with a diameter of 2mm and a cylindrical length of 12mm. The presented screw configuration can be considered a typical screw configuration for two component mixtures, where achieving an amorphous solid dispersion is the final goal. The details are summarized in Table 3.6.

Table 3.6 The screw configuration used for the NANO16 and ZSE18 extrusion trials (NANO16) and 1D HME simulations (both screws).

NANO16					ZSE18				
Screw	**Pitch/Angle [mm/°]**	**Length [mm]**	**Dim. L. [-]**	**Sections [-]**	**Screw**	**Pitch/Angle [mm/°]**	**Length [mm]**	**Dim. L. [-]**	**Sections [-]**
16C15	15	10							
16C20	20	90	8.1	1	18C30	30	120	8.3	1
16C15	15	30			18C15	15	30		
16K30	30°	15	1.9	2	18K60	60°	15	1.7	2
16K60	60°	15			18K90	90°	15		
16C20	20	30			18C30	30	60		
16C15	15	30	5.6	3	18C20	20	30	6.7	3
16C10	10	30			18C15	15	30		
16K60	60°	15	1.9	4	18K90	90°	15	1.7	4
16K60	60°	15			18K90	90°	15		
16C15	15	30			18C30	30	60		
16C20	20	30	7.5	5	18C20	20	30	6.7	5
16C10	10	60			18C10	10	30		
	Total:	400	25			Total:	450	25	

A variety of process settings was tested with the two formulations. For the Itraconazole-Kollidon VA64 formulation (Formulation A from now on), in total five different process settings were investigated with two different throughputs (0.2kg/h and 0.4kg/h), four different screw speeds (50rpm, 150rpm, 300rpm and 400rpm) and two barrel temperature settings (with temperatures in the processing zone (130°C to 160° and 140°C to 160°C). Similarly, for the Ibuprofen-Soluplus formulation (Formulation B from now on), five different process settings were investigated with two different throughput states (0.2kg/h and 0.4kg/h), four screw speeds (50rpm, 150rpm, 300rpm and 400rpm) and one barrel temperature setting (barrel process unit settings of 120°C). The used process settings are listed in Table 3.7 and Table 3.8.

Table 3.7. Process settings used for the extrusion and 1D HME process simulation of the two investigated formulations on the NANO 16 extruder.

Formulation	$\dot{m}\ [kg/h]$	$n\ [rpm]$	Barrel temp.
A1 & B1	0.2	50	1 & 3
A2 & B2	0.2	150	1 & 3
A3 & B3	0.2	300	1 & 3
A4 & B4	0.2	400	1 & 3
A5	0.4	300	2
B5	0.4	150	3

Table 3.8. Barrel temperature settings used for the extrusion and 1D HME process simulation of the two investigated formulations on the NANO 16 extruder.

Barrel temp.	Z [°C]	Z0 [°C]	Z1 [°C]	Z2 [°C]	Z3 [°C]	Z4 [°C]	Z5 [°C]	Z6 [°C]
1	70	-*	130	130	150	150	150	160
2	70	-*	140	140	150	150	150	160
3	70	-*	120	120	120	120	120	120

*Powder intake zone, ambient temperature

3.2.4 Computational Approach

The investigation of the NANO16 extrusions was done in two steps. In the first step, all six available screw elements were investigated in detail using the high fidelity Smoothed Particle Hydrodynamics (SPH) simulation approach. In or previous works we presented this approach as a potent platform for the detailed investigation of the flow field and distributive mixing action of individual screw element pairs used in pharmaceutical HME [1], [35], [36], [39], [42]. In the second step, the resulting flow fields from the SPH simulation are converted to the so-called dimensionless pressure and power characteristics and used as descriptors of the screw geometry performance for the reduced order 1D HME simulations software [26], [38], [43]. By combining the screw performance descriptors from the SPH simulations and the material data measurements in the 1D HME reduced order code, it is possible to fully represent the HME process and calculate the axial distributions of the filling degree, melt temperature, specific mechanical energy consumption (SMEC) and local and overall residence time distribution (RTD). The generated data will be used to fully describe the impact every screw element, as well as the whole process setup, have on the outcome of the HME processing.

3.3 Results and Discussion

3.3.1 SPH Screw Characterization and Comparison to Standard Screw Elements

The different screw elements available for the two extruders were characterized using the Smoothed Particle Hydrodynamics (SPH) simulation method and are presented in a dimensionless form. Such a representation allows to directly compare the conveying capacity, pressure build up capacity and power consumption of the different screw element pairs among

each other. Moreover, such an approach also excludes the impact the formulation has on the flow field, hence making the results only a function of the screw geometries, allowing for better understanding the impact the cross section geometry has on the flow field. The results are summarized in Figure 3.2 to Figure 3.5. The pressure characteristics (Figure 3.2 for the conveying elements and Figure 3.3 for the kneading and mixing elements) shows the dimensionless conveying capacity (x axis) versus the dimensionless pressure build-up (y axis) of the screw pairs. Looking at the results for the conveying elements it is clear that the NANO16 screw elements have a significantly higher pressure build-up capacity in comparison to the ZSE18 elements. As a trade of, the ZSE18 element have a significantly higher conveying capacity in comparison to the NANO16 elements. On the example of the 10mm pitched elements, to build-up the same amount of pressure, the ZSE18 18C10 conveying element will need roughly double the screw length in comparison to the NANO16 16C10 element. On the other hand, the ZSE18 18C10 will be able to convey roughly twice the amount of material in comparison to the NANO16 16C10 screw element, in the case where no back-pressure is present. Around the dimensionless throughput of 0.05 both element will have a similar performance in terms of their ability to build-up pressure. In the case of kneading and mixing elements, Figure 3.3, similar conclusions can be drawn. The kneading and mixing elements of the ZSE18 extruder generally have a higher conveying but lower pressure build-up capacity in comparison to their NANO16 counterparts. Due to the triple-flighted screw cross section the kneading element with the 60° angle between the kneading discs (16K60) is the neutral conveying kneading element in the case of the NANO16 extruder, in contrast to the 90° 18K90 in the case of the double-flighted screw geometry of the ZSE18 extruder. The higher angle of the pressure characteristic curve in the case of the 16K60, in comparison to the 18K90, results in a higher pressure gradient needed to overcome the NANO16 screw element.

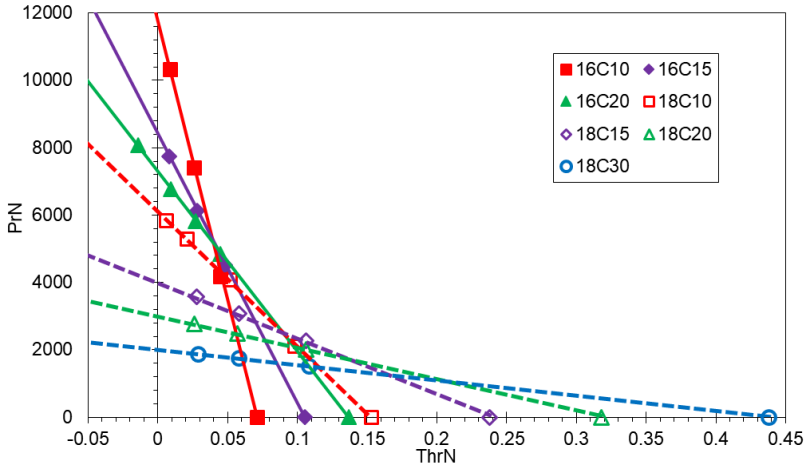

Figure 3.2 SPH results: Pressure characteristics of the NANO16 and ZSE18 Conveying elements.

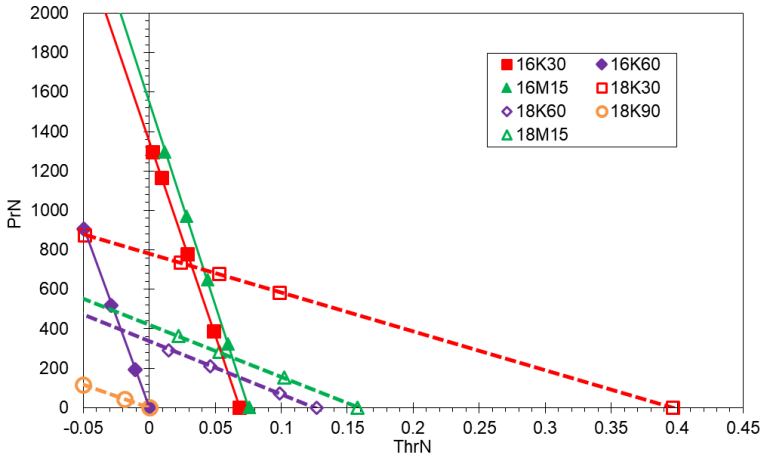

Figure 3.3. SPH results: Pressure characteristics of the NANO16 and ZSE18 Kneading and Mixing elements.

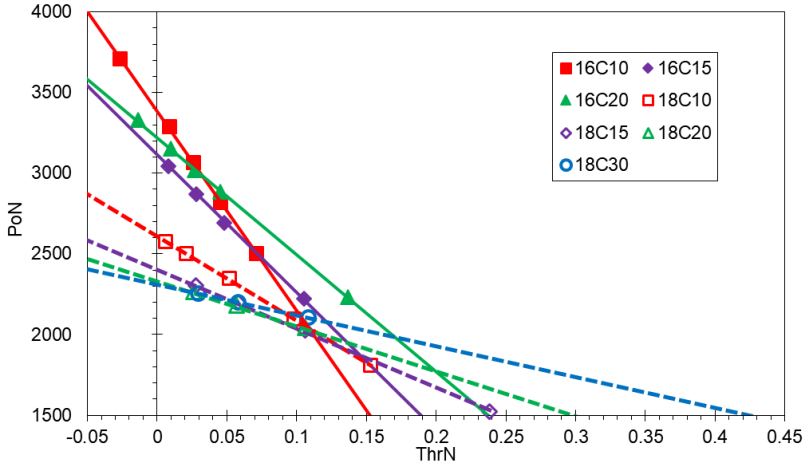

Figure 3.4. SPH results: Power characteristics of the NANO16 and ZSE18 Conveying elements.

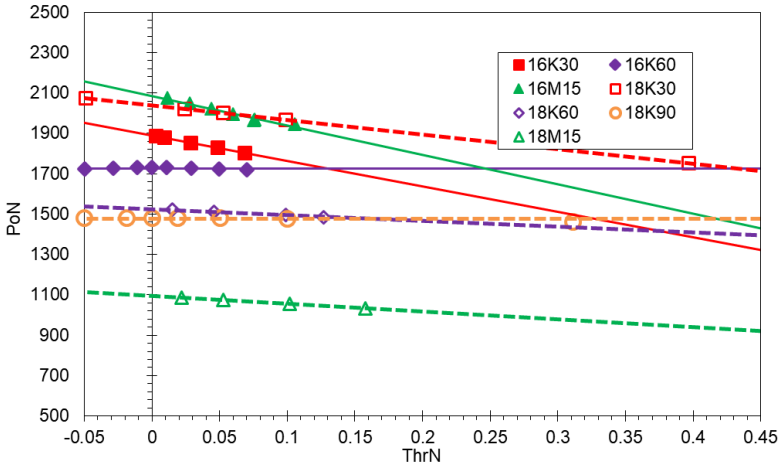

Figure 3.5. SPH results: Power characteristics of the NANO16 and ZSE18 Kneading and Mixing elements.

Besides the importance of the pressure characteristics in setting up a HME screw configuration, knowing the amount of power a certain screw geometry is going to introduce into the melt is also important during process setup and screw transfer during scale-up. The dimensionless power characteristic curves of the NANO16 and ZSE18 investigated screw element pairs are presented in Figure 3.4 in the case of conveying elements, and in Figure 3.5 in case of kneading and mixing elements. Similar to the results of the pressure characteristics, the NANO16 conveying elements have a higher power consumption in comparison to their counterparts in the ZSE18 extruder. This means that for a similar filling degree (the amount of material in the screws) the NANO16 conveying elements will lead to a higher power input into the melt in comparison to the ZSE18 conveying elements. The results are a little bit different in the case of mixing and kneading elements, Figure 3.5. In the case of the NANO16 extruder, we have only one actively conveying kneading element (16K30) which in terms of its power characteristics (Figure 3.5), sits between the 18K30 (higher power consumption) and 18K60 (lower power consumption). In the case of the two neutrally conveying kneading elements, the NANO16 16K60 has a higher power consumption in comparison to the ZSE18 18K90 screw element. Significantly higher differences in terms of power consumption can be seen in the case of mixing elements, where the 16M15 shows a significantly higher power consumption in comparison to the 18M15 mixing element. Providing that a satisfactory process setup was reached on the NANO16 extruder, a successful process transfer should be able to the ZSE18 extruder, given that in the case of the kneading and mixing elements the power consumption tend to be lower.

3.3.2 HME Process Setup on the NANO16

As part of the process execution, the torque, specific mechanical energy consumption (SMEC), mean residence time (mRT) and melt temperature were monitored during the execution of the experiments and compared to the *in silico* obtained values for code validation. The process torque and SMEC are shown in Figure 3.6 and Figure 3.7.

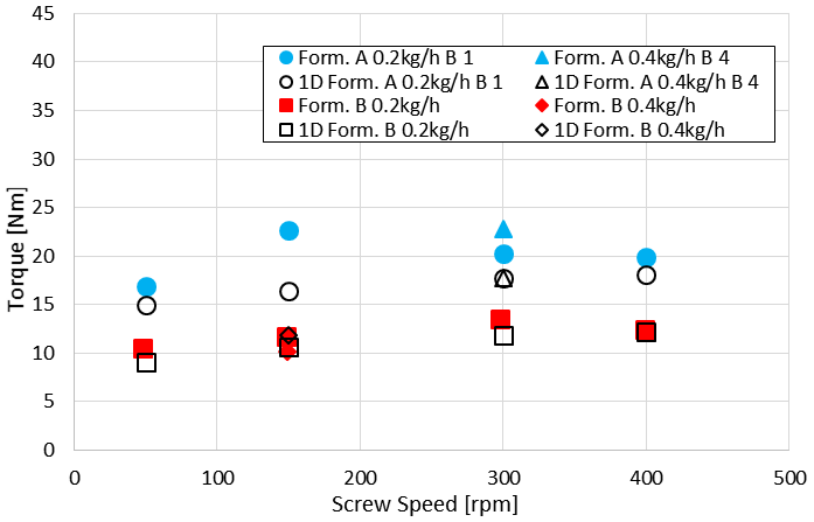

Figure 3.6 Torque values obtained experimentally and *in silico* for the extrusions on the NANO16 extruder for the 15% Itraconazole in 85% Kollidon VA64 (Form. A) and 20% Ibuprofen in 80% Soluplus (Form. B) formulations.

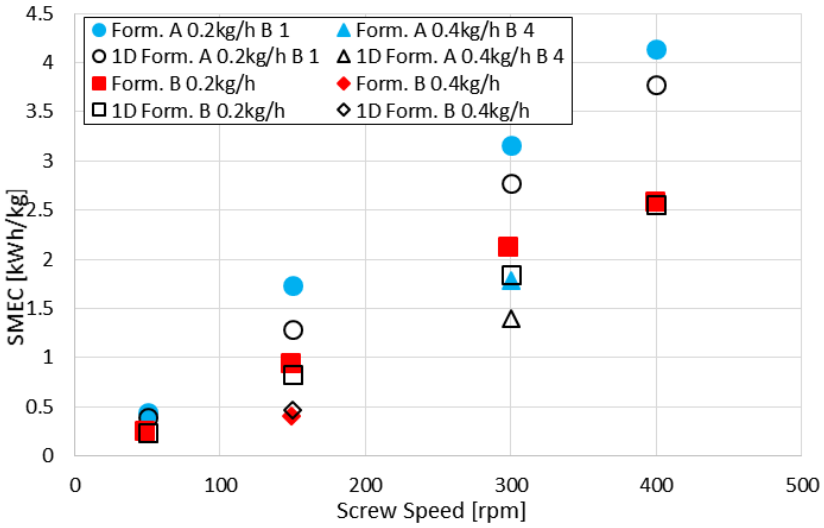

Figure 3.7. SMEC values obtained experimentally and *in silico* for the extrusions on the NANO16 extruder for the 15% Itraconazole in 85% Kollidon VA64 (Form. A) and 20% Ibuprofen in 80% Soluplus (Form. B) formulations.

The process torque values are a direct process response to the viscosity of the processed formulations. A higher melt viscosity represents a higher melt resistance to deformation, hence resulting in a higher process torque required for its processing. From the viscosity data presented in Table 3.3, it is clear that Formulation A has a higher viscosity in comparison to Formulation B. For a melt temperature of 140°C, Formulation A has a zero-shear-viscosity of two orders of magnitude higher in comparison to Formulation B. As a result, the torque required for the processing of the Formulation A is higher (roughly by a factor of 1.5 to 2) in comparison for the torque required for the processing of the Formulation B. It should also be noted that the barrel temperature settings needed for the processing differ by approximatelly 30°C between the two formulations, Table 3.8. Similar to the torque values, the SMEC values needed for the processing of the two formulations are shown in Figure 3.7. Although the barrel temperature settings are different for the two formulations, Formulation A still requires a higher SMEC input for the processing. The mean residence time (mRT) and the melt temperature were also measured during the process and compared to the *in silico* results. The result are shown in Figure 3.8 and Figure 3.9.

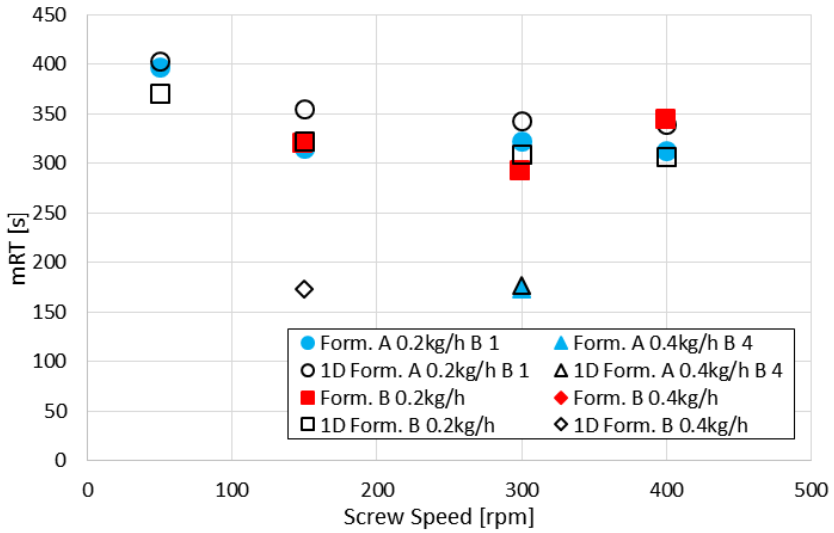

Figure 3.8. mRT values obtained experimentally and *in silico* for the extrusions on the NANO16 extruder for the 15% Itraconazole in 85% Kollidon VA64 (Form. A) and 20% Ibuprofen in 80% Soluplus (Form. B) formulations.

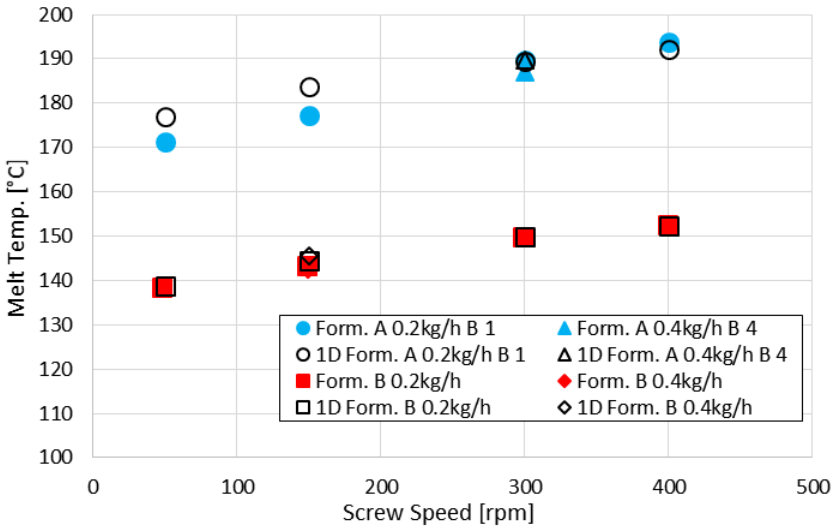

Figure 3.9. Melt temperature values obtained experimentally and *in silico* for the extrusions on the NANO16 extruder for the 15% Itraconazole in 85% Kollidon VA64 (Form. A) and 20% Ibuprofen in 80% Soluplus (Form. B) formulations.

The mRT was measured via a camera system that traced the color intensity of a tracer (2mg of tracer was introduced in the powder intake zone) exiting the extruder. The experimental and *in -silico* values are in good agreement and show the impact the formulation, screw speed and throughput have on the results. Surprisingly, the change of formulation did not drastically impact the mRT of the process. The screw speed and throughput have an inverse result on the mRT, i.e. an increase in the throughput or screw speed generally results in a reduction of the mRT. The throughput has a significantly higher impact on the mRT than the screw speed. The melt temperature was measured in the region of the degassing zone using an infrared thermometer. The *in silico* obtained melt temperature is a cross section averaged melt temperature, additionally averaged along the length of the degassing opening. The measured melt temperature values are in good agreement with the *in silico* obtained values. Similar to the torque and SMEC results, melt temperature results reflect the differences in viscosity between the two formulations. Formulation A has a significantly higher melt temperature in comparison to the Formulation B results, mainly due to the higher melt viscosity. The difference in the barrel temperature setting should also be acknowledged which is also a direct response to the differences in the formulation viscosities.

Figure 3.10 and Figure 3.11 show the impact of the formulation on the distribution of the filling degree, melt temperature and SMEC along the screw for one process setting. The filling degree does not seem to be significantly different for the two tested formulations, which was also

expected from the results of the mRT measurements. Differences can be observed in the partially filled section where Formulation A results in consistently lower filling degree in comparison to the Formulation B. As the screw configuration (i.e. available free volume), throughput and screw speed are the same for both formulations (0.2kg/h at 50rpm), the differences in the filling degree can be explained by the different density of the two formulations for two different formulation temperatures. In the case of Formulation A and an overall average melt temperature of around 170° is the resulting melt density higher by around 110kg/m³ in comparison to Formulation B at an average melt temperature of around 130°C. This explains the observed differences in the filling degree along the screw. Moving to the fully filled zones, it is clear that the two kneading sections and the extruder die will create the fully filled sections regardless of the formulation. This is expected as the used 16K60 element is conveying neutral as well as the die section. It the location of the two kneading sections, an increase in the melt temperature and SMEC input can be observed, seen in Figure 3.11. The higher energy inputs are due to (1) a more aggressive screw geometry of the kneading elements, in comparison to conveying elements, and (2) a relatively long mRT in the location of the fully filled section in comparison to the partially filled sections. A stepwise change of the axial SMEC input can also be observed with every change in the conveying section due to the change in screw pitch and filling degree. All of this has to be taken into account when designing the process and when transferring the process to another extruder and scale.

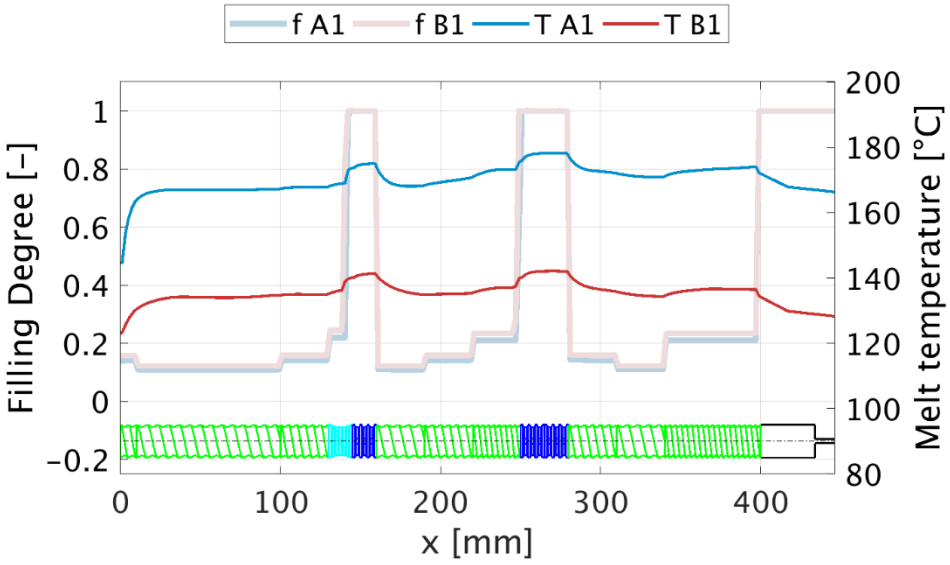

Figure 3.10. 1D HME results: Filling degree and Melt temperature distribution along the screw for both formulations at 0.2kg/h and 50rpm (Barrel temp. in the process section Formulation A at 150°C; Formulation B at 120°C).

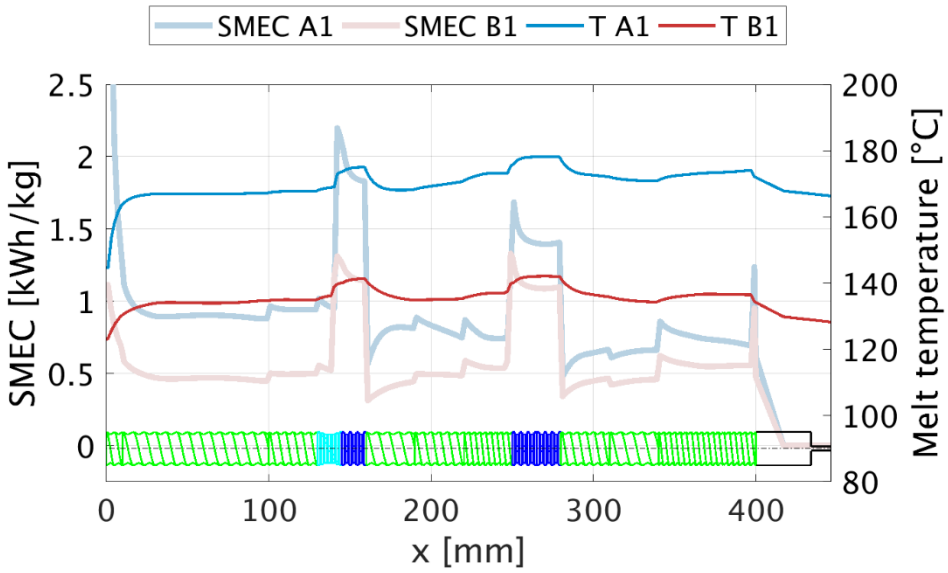

Figure 3.11. 1D HME results: Filling degree and Melt temperature distribution along the screw for both formulations at 0.2kg/h and 50rpm (Barrel temp. in the process section Formulation A at 150°C; Formulation B at 120°C).

3.3.3 Virtual Process Transfer

Following the process setup and analysis of the NANO16 extrusions, a virtual process transfer is attempted. The goal of the process transfer is to make sure the exposure time (overall mRT and local mRT) and the exposure temperature of the formulation is kept as similar as possible across the two extruder scales [1], [39]. The screw configuration plays a crucial role, hence the screw configuration transfer has been performed taking into consideration the dimensionless lengths of the different processing zones along the screw and the data from the SPH simulations, Table 3.6. The dimensionless length of both screw configurations (total screw length divided by the nominal screw diameter) is equal to 25. Usually the screw configurations for the ZSE18 extruder have a dimensionless screw length of 40. In this particular case this would also be possible by increasing the lengths of the partially filled conveying sections in the powder intake zone and directly after each of the two kneading section. This would not have a significant impact on the overall RTD or local mRT (fully filled sections mostly contribute to the RTD) or the axial melt temperature, hence should not impact the expected product significantly. The throughput moving to the ZSE18 extruder was increased by a factor of 2.5 (from 0.2kg/h to 0.5kg/h and from 0.4kg/h to 1kg/h for both formulations), the screw speed was kept constant (only a 2mm change in screw diameter) and barrel temperatures were directly transferred.

For the purpose of analysis, the axial melt temperature distribution, the local mRT (in the two kneading zones and in the die section) and the overall process RTD were computed and compared, Figure 3.12 and Figure 3.13 for Formulation A, and Figure 3.14 and Figure 3.15 for Formulation B. By comparing the axial melt temperature distributions for both formulations, it is clear that the proposed process settings on the ZSE18 extruder resulted with an overall lower melt temperature along the whole screw configuration. In addition to the melt temperature, local mRT in the three fully filled zones (first kneading section at around 0.4 dimensionless length, second kneading section at around 0.7 dimensionless length and the die section at the screw discharge) suggest that by transferring the two investigated formulations to the ZSE18 extruder, the local mRT is kept lower in comparison to the NANO16 process setup. This ensures that the processed formulation experiences a somewhat lower processing temperature and similar exposure time as the on the NANO16 extruder.

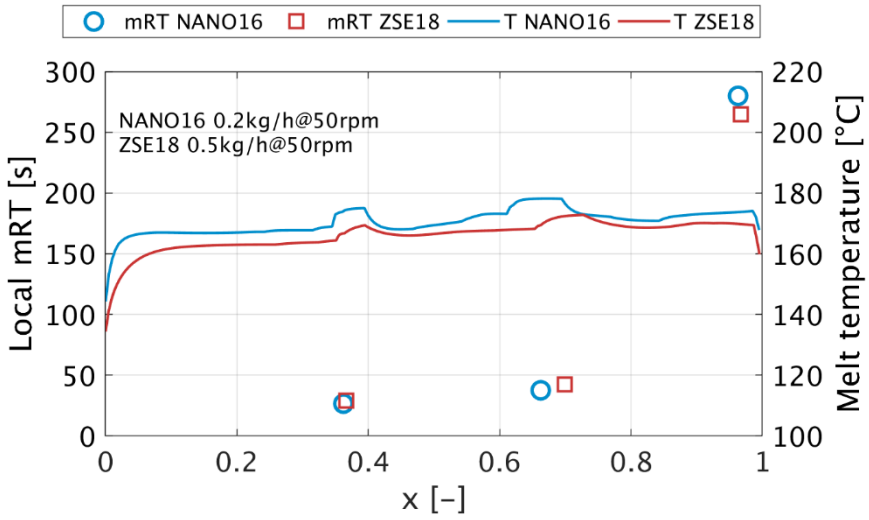

Figure 3.12 Axial melt temperature and local mRT. Process transfer from the 0.2kg/h at 50rpm NANO16 to 0.5kg/h 50rpm ZSE18; Formulation A.

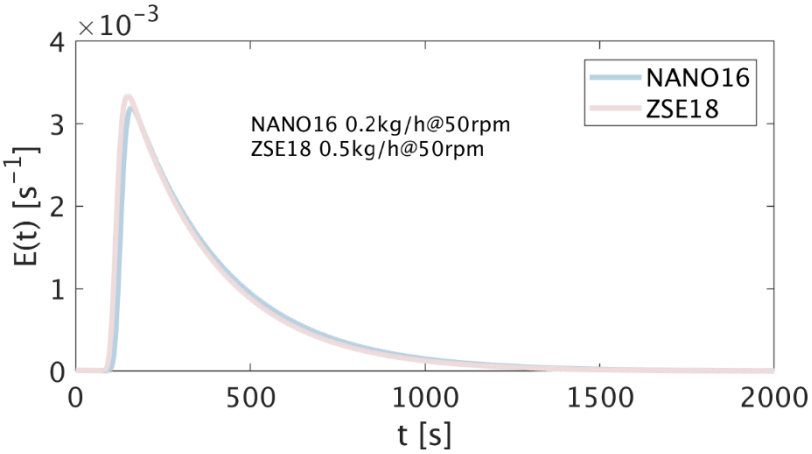

Figure 3.13. Residence time distribution. Process transfer from the 0.2kg/h at 50rpm NANO16 to 0.5kg/h 50rpm ZSE18; Formulation A.

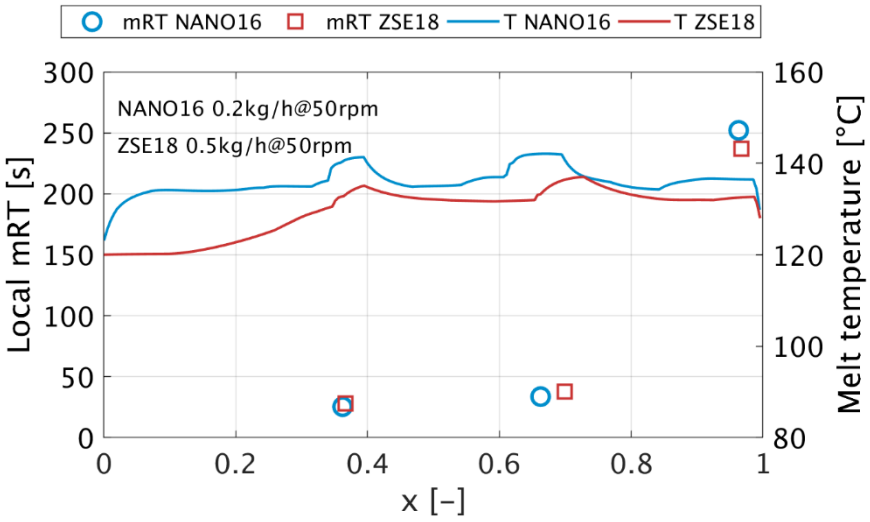

Figure 3.14. Axial melt temperature and local mRT. Process transfer from the 0.2kg/h at 50rpm NANO16 to 0.5kg/h 50rpm ZSE18; Formulation B.

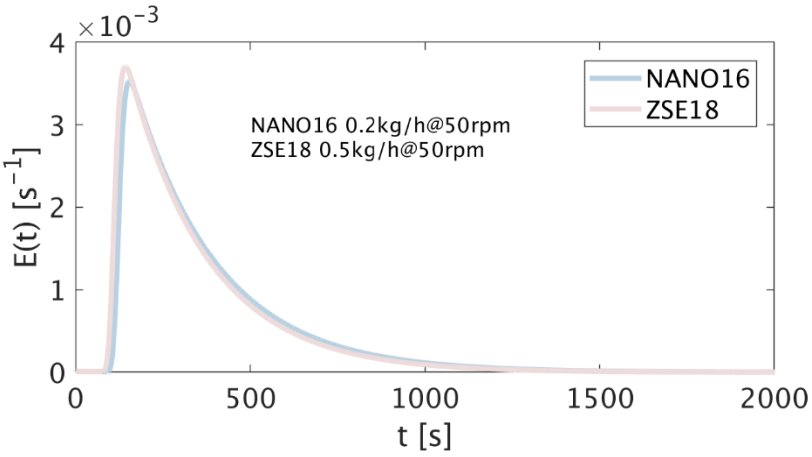

Figure 3.15. Residence time distribution. Process transfer from the 0.2kg/h at 50rpm NANO16 to 0.5kg/h 50rpm ZSE18; Formulation B.

Under the assumption that a certain product quality is the result of the temperature and mRT history, the formulation experiences during processing, it can be concluded that the same product quality will be reached for both setups. Similar temperature and mRT times have been achieved for both formulations, despite a significant differences in the SMEC values for the processes on the two different extruders, Figure 3.16 and Figure 3.17.

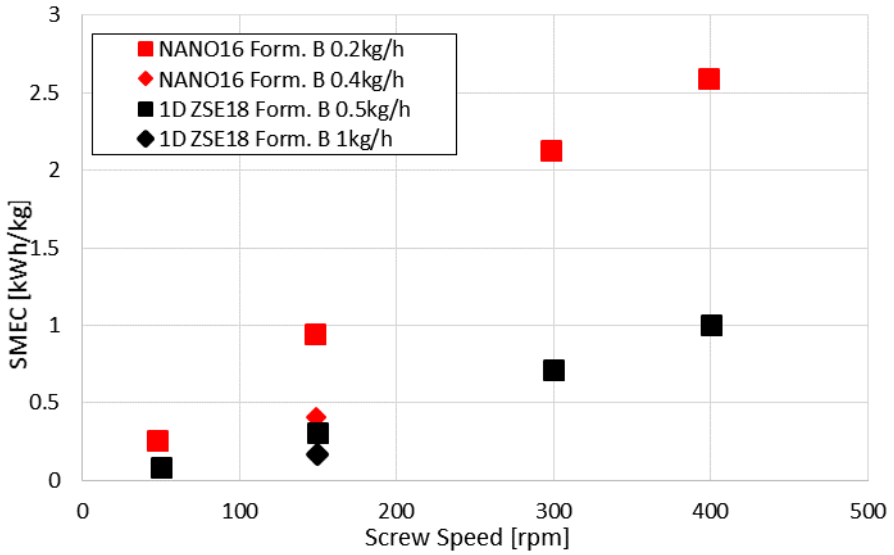

Figure 3.16. Process transfer from NANO16 to ZSE18. Comparison of experimentally achieved (NANO16) and *in silico* obtained (ZSE18) process SMEC values for Formulation B.

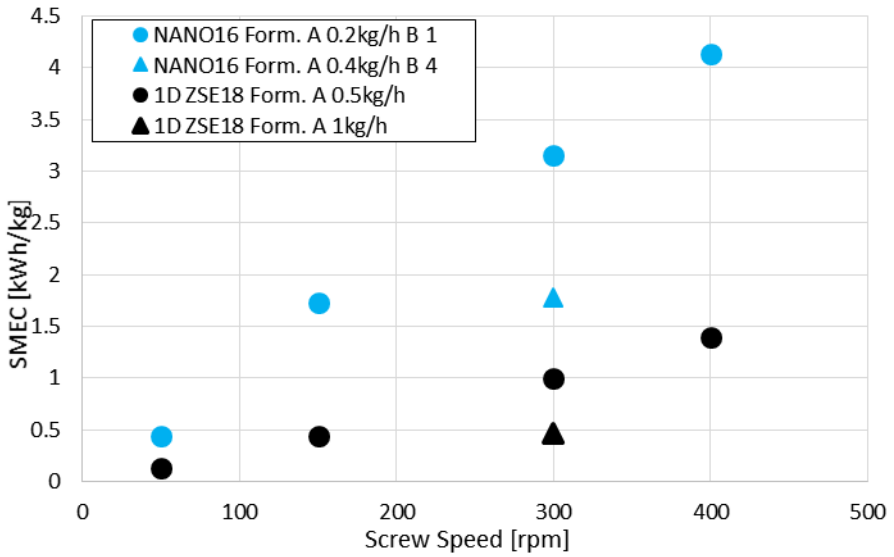

Figure 3.17. Process transfer from NANO16 to ZSE18. Comparison of experimentally achieved (NANO16) and *in silico* obtained (ZSE18) process SMEC values for Formulation A.

The difference between the experimentally obtained SMEC values (NANO16 extruder) and the SMEC values predicted for the process setup on the ZSE18 extruder differ by a factor 3 to 4. This significant difference implies once more that the assumption of constant SMEC is not valid process transfer and scale-up.

3.4 Summary and Conclusion

In this chapter we analyzed the impact of the design of the screw cross section on the screw performance of elements found in TSEs. For this purpose two extruders were analyzed, the triple flighted 16mm NANO16 and the double flighted 18mm ZSE18 extruders from Leistritz. By carefully analyzing the screw performance of the two extruders significant differences in the conveying capacity, pressure build-up capacity and energy consumption were found and discussed. In addition, a number of process setups, including two formulations, on the NANO16 extruder was analyzed and compared to the data obtained by the 1D HME simulations. For otherwise similar process setups (same screw configuration, screw speed, throughput but different barrel temperatures), differences in the axial distribution of SMEC, melt temperature and mRT coming from the formulation, were analyzed and discussed. Taking all the gained knowledge into account, a virtual process transfer, involving the transfer of the screw configuration and process settings, was attempted from the NANO16 to the ZSE18 extruder. Under the assumption that the same product quality can be expected if the formulation undergoes the same temperature and exposure time cycle (locally and globally) scale-up settings were found and presented. Despite a significant difference in the predicted SMEC between the setups on two extruders, the settings promise to result in similar axial melt temperature distributions, similar local mRT in the difference fully filled zones (i.e. kneading and die zones) and similar overall RTD. This further strengthens the need for integrated product development that takes into account the characteristics of the processed formulation, high fidelity simulations of the screw performance and *in silico* process development and transfer as a basis of QbD based pharmaceutical product development.

3.5 Abbreviations

1D	One dimensional
A1 to A5	Process settings with the Formulation A 15% Itaconazole 85% Kollidon VA64
API	Active Pharmaceutical Ingredients
B1 to B5	Process settings with the Formulation B 20% Ibuprofen 80% Soluplus
CMA	Critical Material Attributes
CPP	Critical Process Parameters
CQA	Critical Quality Attributes
f	Filling degree
HME	Hot Melt Extrusion
mDSC	modular Differential Scanning Calorimetry
mRT	mean Residence Time
NANO16	16mm triple flighted closely intermeshing twin screw extruder from Leistritz
QbD	Quality by Design
RTD	Residence Time Distribution
SMEC	Specific Mechanical Energy Consumption
SPH	Smoothed Particle Hydrodynamics
ThrN	Dimensionless Throughput number
PrN	Dimensionless Pressure number
PoN	Dimensionless Power number
TSE	Co-rotating Twin Screw Extruder
ZSE18	18mm double flighted closely intermeshing twin screw extruder from Leistritz

3.6 Nomenclature

Latin symbols

a_T $[-]$	Williams-Landel-Ferry temperature shift factor
C_1, C_2	Parameters for the Williams-Landel-Ferry temperature shift factor
c_p $[J/kgK]$	Specific volume
D_1, D_2	Parameters for the specific volume model
E_1, E_2	Parameters for the thermal conductivity model
K_1 to K_9	Parameters used to parametrize the Schmidt model for specific volume calculations
p $[bar]$	Pressure
m [-]	Viscosity exponent
T, T_r, T_g, T_{tr} $[°C]$	Temperature, Representative Temperature, Glass Transition Temperature and Transition Temperature, respectively
Z_0 to Z_6 [°C]	Barrel temperature control points

Greek symbols

v $[cm^3/g]$	Specific Volume
η, η_0 $[Pas]$	Viscosity and zero viscosity, respectively
$\dot{\gamma}, \dot{\gamma}_{crit}[s^{-1}]$	Shear rate and critical shear rate, respectively
λ $[W/mK]$	Thermal conductivity

3.7 References

[1] J. Matić, A. Paudel, H. Bauer, R. A. L. Garcia, K. Biedrzycka, and J. G. Khinast, "Developing HME-Based Drug Products Using Emerging Science: a Fast-Track Roadmap from Concept to Clinical Batch," *AAPS PharmSciTech*, vol. 21, no. 5, p. 176, Jul. 2020.

[2] L. X. Yu *et al.*, "Understanding Pharmaceutical Quality by Design," *AAPS J.*, vol. 16, no. 4, pp. 771–783, Jul. 2014.

[3] V. P. Kumar and N. V. Gupta, "A Review on quality by design (QBD) for Pharmaceuticals," *Int. J. Drug Dev. Res.*, vol. 7, no. 1, pp. 35–44, 2015.

[4] V. Mishra, S. Thakur, A. Patil, and A. Shukla, "Quality by design (QbD) approaches in current pharmaceutical set-up," *Expert Opin. Drug Deliv.*, vol. 15, no. 8, pp. 737–758, Aug. 2018.

[5] A. Gupta and M. A. Khan, "Hot-Melt Extrusion: An FDA Perspective on Product and Process Understanding," in *Hot-Melt Extrusion: Pharmaceutical Applications*, Chichester, UK: John Wiley & Sons, Ltd, 2012, pp. 323–331.

[6] ICH Q8, "EMEA/CHMP, 2009, ICH Topic Q 8 (R2) Pharmaceutical Development, Step 5: Note for Guidance on Pharmaceutical Development," vol. 8, no. June, 2017.

[7] M. T. Islam, M. Maniruzzaman, S. A. Halsey, B. Z. Chowdhry, and D. Douroumis, "Development of sustained-release formulations processed by hot-melt extrusion by using a quality-by-design approach," *Drug Deliv. Transl. Res.*, vol. 4, no. 4, pp. 377–387, Aug. 2014.

[8] H. McFall *et al.*, "Formulation of aripiprazole-loaded pH-modulated solid dispersions via hot-melt extrusion technology: In vitro and in vivo studies," *Int. J. Pharm.*, vol. 554, pp. 302–311, Jan. 2019.

[9] J. M. Vasoya *et al.*, "Development of Solid Dispersion by Hot Melt Extrusion Using Mixtures of Polyoxylglycerides With Polymers as Carriers for Increasing Dissolution Rate of a Poorly Soluble Drug Model," *J. Pharm. Sci.*, vol. 108, no. 2, pp. 888–896, Feb. 2019.

[10] A. Schittny, H. Ogawa, J. Huwyler, and M. Puchkov, "A combined mathematical model linking the formation of amorphous solid dispersions with hot-melt-extrusion process parameters," *Eur. J. Pharm. Biopharm.*, vol. 132, pp. 127–145, Nov. 2018.

[11] Y. Zhu, N. H. Shah, A. Waseem Malick, M. H. Infeld, and J. W. McGinity, "Controlled

Release of a Poorly Water-Soluble Drug from Hot-Melt Extrudates Containing Acrylic Polymers," *Drug Dev. Ind. Pharm.*, vol. 32, no. 5, pp. 569–583, Jan. 2006.

[12] A. Q. Vo *et al.*, "A novel floating controlled release drug delivery system prepared by hot-melt extrusion," *Eur. J. Pharm. Biopharm.*, vol. 98, pp. 108–121, Jan. 2016.

[13] M. Fukuda, N. A. Peppas, and J. W. McGinity, "Floating hot-melt extruded tablets for gastroretentive controlled drug release system," *J. Control. Release*, vol. 115, no. 2, pp. 121–129, Oct. 2006.

[14] R. Baumgartner, A. Eitzlmayr, N. Matsko, C. Tetyczka, J. G. Khinast, and E. Roblegg, "Nano-extrusion: A promising tool for continuous manufacturing of solid nano-formulations," *Int. J. Pharm.*, vol. 477, no. 1–2, pp. 1–11, Dec. 2014.

[15] R. Baumgartner, J. Matić, S. Schrank, S. Laske, J. G. J. Khinast, and E. Roblegg, "NANEX: Process design and optimization," *Int. J. Pharm.*, vol. 506, no. 1–2, pp. 35–45, Jun. 2016.

[16] A. M. Bhagurkar, M. A. Repka, and S. N. Murthy, "A Novel Approach for the Development of a Nanostructured Lipid Carrier Formulation by Hot-Melt Extrusion Technology," *J. Pharm. Sci.*, vol. 106, no. 4, pp. 1085–1091, Apr. 2017.

[17] L. A. D. Silva *et al.*, "Preparation of a solid self-microemulsifying drug delivery system by hot-melt extrusion," *Int. J. Pharm.*, vol. 541, no. 1–2, pp. 1–10, Apr. 2018.

[18] H. Patil, X. Feng, X. Ye, S. Majumdar, and M. A. Repka, "Continuous Production of Fenofibrate Solid Lipid Nanoparticles by Hot-Melt Extrusion Technology: a Systematic Study Based on a Quality by Design Approach," *AAPS J.*, vol. 17, no. 1, pp. 194–205, Jan. 2015.

[19] M. Stanković, J. Tomar, C. Hiemstra, R. Steendam, H. W. Frijlink, and W. L. J. Hinrichs, "Tailored protein release from biodegradable poly(ε-caprolactone-PEG)-b-poly(ε-caprolactone) multiblock-copolymer implants," *Eur. J. Pharm. Biopharm.*, vol. 87, no. 2, pp. 329–337, Jul. 2014.

[20] M. Stanković *et al.*, "Low temperature extruded implants based on novel hydrophilic multiblock copolymer for long-term protein delivery," *Eur. J. Pharm. Sci.*, vol. 49, no. 4, pp. 578–587, Jul. 2013.

[21] M. Stanković, H. W. Frijlink, and W. L. J. Hinrichs, "Polymeric formulations for drug release prepared by hot melt extrusion: application and characterization," *Drug Discov. Today*, vol. 20, no. 7, pp. 812–823, Jul. 2015.

[22] C. Bode, H. Kranz, A. Fivez, F. Siepmann, and J. Siepmann, "Often neglected:

PLGA/PLA swelling orchestrates drug release: HME implants," *J. Control. Release*, vol. 306, no. May, pp. 97–107, Jul. 2019.

[23] A. Cossé, C. König, A. Lamprecht, and K. G. Wagner, "Hot Melt Extrusion for Sustained Protein Release: Matrix Erosion and In Vitro Release of PLGA-Based Implants," *AAPS PharmSciTech*, vol. 18, no. 1, pp. 15–26, Jan. 2017.

[24] S. Eder *et al.*, "Establishment of a Molding Procedure to Facilitate Formulation Development for Co-extrudates," *AAPS PharmSciTech*, vol. 18, no. 8, pp. 2971–2976, Nov. 2017.

[25] I. Koutsamanis *et al.*, "Formulation and processability screening for the rational design of ethylene-vinyl acetate based intra-vaginal rings," *Int. J. Pharm.*, vol. 564, no. April, pp. 90–97, Jun. 2019.

[26] K. Kohlgrüber, *Co-Rotating Twin-Screw Extruder*. München: Carl Hanser Verlag GmbH & Co. KG, 2007.

[27] C. Rauwendaal, *Polymer extrusion: Fifth edition*, Fifth Edit. München: Carl Hanser Verlag GmbH & Co. KG, 2014.

[28] J. Breitenbach, "Melt extrusion: from process to drug delivery technology," *Eur. J. Pharm. Biopharm.*, vol. 54, no. 2, pp. 107–117, Sep. 2002.

[29] M. M. Crowley *et al.*, "Pharmaceutical Applications of Hot-Melt Extrusion: Part I," *Drug Dev. Ind. Pharm.*, vol. 33, no. 9, pp. 909–926, Jan. 2007.

[30] M. A. Repka *et al.*, "Pharmaceutical Applications of Hot-Melt Extrusion: Part II," *Drug Dev. Ind. Pharm.*, vol. 33, no. 10, pp. 1043–1057, Jan. 2007.

[31] H. Patil, R. V. Tiwari, and M. A. Repka, "Hot-Melt Extrusion: from Theory to Application in Pharmaceutical Formulation," *AAPS PharmSciTech*, vol. 17, no. 1, pp. 20–42, Feb. 2016.

[32] R. C. Evans, S. O. Kyerematen, L. Asmus, M. Degenhardt, J. Rosenberg, and K. G. Wagner, "Development and Performance of a Highly Sensitive Model Formulation Based on Torasemide to Enhance Hot-Melt Extrusion Process Understanding and Process Development," *AAPS PharmSciTech*, vol. 19, no. 4, pp. 1592–1605, May 2018.

[33] D. Treffer, A. Troiss, and J. G. Khinast, "A novel tool to standardize rheology testing of molten polymers for pharmaceutical applications," *Int. J. Pharm.*, vol. 495, no. 1, pp. 474–481, Nov. 2015.

[34] A. Eitzlmayr *et al.*, "Experimental characterization and modeling of twin-screw extruder elements for pharmaceutical hot melt extrusion," *AIChE J.*, vol. 59, no. 11, pp. 4440–

4450, Nov. 2013.

[35] A. Eitzlmayr, J. Matić, and J. G. Khinast, "Analysis of flow and mixing in screw elements of corotating twin-screw extruders via SPH," *AIChE J.*, vol. 63, no. 6, pp. 2451–2463, Jun. 2017.

[36] A. Eitzlmayr and J. G. Khinast, "Co-rotating twin-screw extruders: Detailed analysis of conveying elements based on smoothed particle hydrodynamics. Part 1: Hydrodynamics," *Chem. Eng. Sci.*, vol. 134, pp. 861–879, Sep. 2015.

[37] A. Eitzlmayr and J. G. Khinast, "Co-rotating twin-screw extruders: Detailed analysis of conveying elements based on smoothed particle hydrodynamics. Part 1: Hydrodynamics," *Chem. Eng. Sci.*, vol. 134, pp. 861–879, Sep. 2015.

[38] A. Eitzlmayr *et al.*, "Mechanistic modeling of modular co-rotating twin-screw extruders," *Int. J. Pharm.*, vol. 474, no. 1–2, pp. 157–176, Oct. 2014.

[39] J. Matić, A. Witschnigg, M. Zagler, S. Eder, and J. Khinast, "A novel in silico scale-up approach for hot melt extrusion processes," *Chem. Eng. Sci.*, vol. 204, pp. 257–269, Aug. 2019.

[40] M. Spoerk *et al.*, "Novel Cleaning-in-Place Strategies for Pharmaceutical Hot Melt Extrusion," *Pharmaceutics*, vol. 12, no. 6, p. 588, Jun. 2020.

[41] T. W. Schmidt, "Zur Abschätzung der Schwindung," Aachen, 1986.

[42] A. Eitzlmayr and J. Khinast, "Co-rotating twin-screw extruders: Detailed analysis of conveying elements based on smoothed particle hydrodynamics. Part 2: Mixing," *Chem. Eng. Sci.*, vol. 134, pp. 880–886, Sep. 2015.

[43] J. Pawlowski, *Die Ähnlichkeitstheorie in der physikalisch-technischen Forschung*. Berlin, Heidelberg: Springer Berlin Heidelberg, 1971.

4

A Novel *In Silico* Scale-Up Approach for Hot Melt Extrusion Processes*

The goal of our study was to develop a rational *in silico* scale-up and process transfer approach for hot melt extrusion processes occurring in the pharmaceutical and other industries. To that end, we performed high-fidelity simulations of individual twin-screw extruder elements via the Lagrangian-based Smoothed Particle Hydrodynamics (SPH) method. To parametrize a mechanistic 1D hot-melt extrusion (HME) model, the data generated by the SPH simulations was used together with the material properties. Two co-rotating twin-screw extruder setups were compared: the Coperion ZSK18 and the Leistritz MIC27 extruders. The pressure and power characteristics of the two extruders with different screw elements and geometries were obtained and compared. The impact of the HME process parameters (throughput, screw speed and barrel temperature) on the filling degree, melt temperature, axial specific mechanical energy consumption (SMEC) and residence time distribution in the two extruders was established. The torque and SMEC values obtained *in silico* were then compared to experiments to ensure that the 1D HME simulations were set up correctly.

Next, scale-up methods from the literature were evaluated, yielding an unsatisfactory set of process parameters that might lead to material degradation. Finally, a rational scale-up approach was proposed. Based on this novel method alternative parameter settings on the MIC27 extruder were established, assuring equivalent thermo-mechanical load on the product compared to the process using the ZSK18 extruder.

---

* This chapter is based on: J. Matić, C. Alva, A. Witschnigg, S. Eder, K. Nickel, A. Paudel and J. Khinast, "Towards Predicting Product Quality in Hot Melt Extrusion: ZSE12" *Chem. Eng. Sci.*, vol. 204, pp. 257–269, Aug. 2019.

4.1 Introduction

Hot melt extrusion (HME) is a continuous manufacturing method increasingly applied in the pharmaceutical industry, mainly to produce amorphous forms of otherwise poorly-soluble active pharmaceutical ingredients (APIs). Alternatively, a previously amorphous or crystalline API could be distributed in the polymer matrix, without changing the state of the API. Typically, intermeshing co-rotating twin-screw extruders (TSE) with highly-adaptable screw configurations are used, making it possible to customize and adjust the HME process depending on the formulation. In addition, adaptable screw elements offer effective melt conveying, pressure build-up and degassing (conveying screw elements). Depending on the screw geometry, low energy distributive mixing and flow folding (classic mixing elements), as well as high shear melt-up and dispersive mixing (kneading elements)[1]–[8], can be achieved.

Due to the many possibilities and combinations of screw elements and process parameters, designing an HME process for a specific formulation is a challenge. Even more, process development is generally performed on the lab scale and requires scale-up to the production scale. The available screw speed ranges vary between extruders. So do the geometries of the individual screw elements, the screw-barrel and screw-screw gap thicknesses, the ratios between the outer and inner screw diameters and the ability of the extruder to cool down or heat up the melt. This significantly affects the residence time distributions (RTD) of the melt, which - in addition to the temperature distribution - has a major impact on the quality and performance of the intermediate product.

As such, good process understanding is essential for safer, faster and less expensive drug development, manufacturing and market supply. Typically, in the engineering literature process understanding is synonymous for the ability to model a process via mechanistic models. Thus, in our previous work we presented a comprehensive modeling method, based on a 1D HME simulation approach [9]–[11] and a detailed 3D screw characterization method via a smoothed particle hydrodynamics (SPH) method [12]–[15]. This framework allows a detailed understanding of the processes in a HME system, including temperature and pressure profiles, fill levels and residence time distribution. Thus, our approach decreases the number of experiments required, enabling at last *in silico* design and scale up to establish a manufacturing approach based on Quality by Design (QbD) principles.

In this work we examine the scale-up (or process transfer) problem often encountered in industry. Specifically, we investigated two scale-up methods proposed by Menges and Rauwendaal [16]–[18] via our SPH screw analysis and 1D HME framework. Furthermore, we examined under which conditions these scale-up methods are valid, and if our method gives more accurate results. Then an alternative scale-up setup is proposed based on the results of the 1D HME simulations. The extruders studied were a Coperion ZSK18 and a Leistritz MIC27 twin-screw co-rotating machines. Two types of simulations are described in this paper:

- SPH simulations, determining the pressure and power characteristics of individual screw elements, and
- 1D mechanistic simulation, determining the axial hold-up, temperature, pressure and shear-fields profiles in the extruders.

The latter was compared to experimental data.

4.2 Extruder and Screw Elements

The geometry parameters and the cross section geometry of the two investigated extruders are shown in Table 4.1 and Figure 4.1, respectively. The available screw elements can generally be divided into three categories:

- *Conveying screw elements* with various pitches (hereinafter termed C), with a number indicating the screw pitch, i.e., C16 is a double-flighted conveying element with a pitch of 16mm
- *Mixing elements* with various pitches and axial cutouts geometry (hereinafter termed M), with a number indicating the screw pitch, i.e., M12 is a double-flighted mixing element with a pitch of 12mm
- *Kneading elements* with various stagger angles between the individual kneading blocks and various kneading block thicknesses (hereinafter termed K), with a number indicating the stagger angle, i.e., K90 is a double-flighted kneading element with a stagger angle of 90°.

Table 4.1. Screw geometry parameters of the ZSK18 and MIC27 extruders.

	$ZSK18_{SPH,real}$	$MIC27_{SPH}$	$MIC27_{real}$
D [mm]	18.3	27.6	27.2
D_o [mm]	18	27	27
D_i [mm]	11.6	18.3	18.4
D_o/D_i	1.55	1.48	1.47
Cl [mm]	15	23.5	23
Δx [mm]	0.15	0.3	0.1

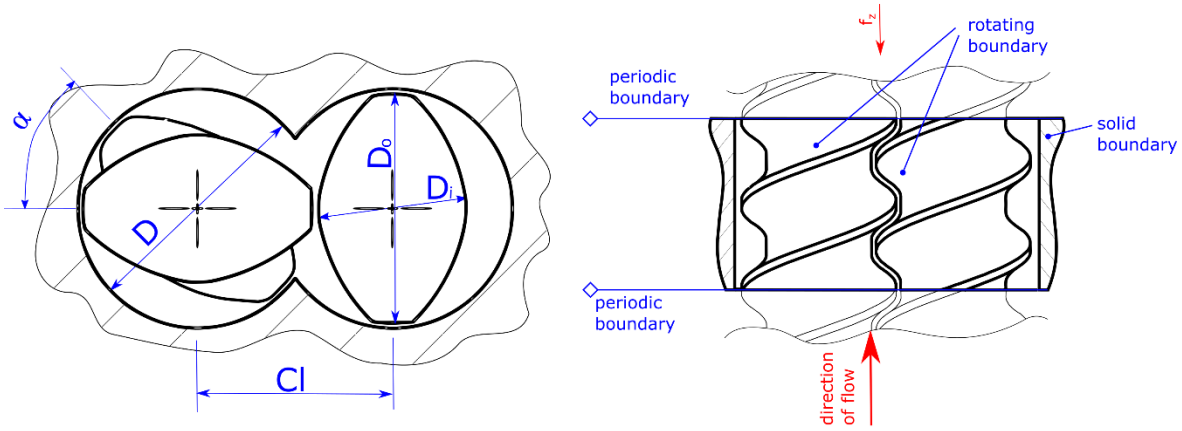

Figure 4.1. Screw cross section (left) and SPH simulation setup (right)

In our study, eight screw elements of the ZSK18 extruder were investigated: four conveying elements ($C8_{18}$, $C12_{18}$, $C16_{18}$ and $C24_{18}$), one mixing element ($M12_{18}$) and three kneading elements ($K45_{18}$, $K45L_{18}$ and $K90_{18}$) with a predefined number of kneading blocks. Two of the investigated kneading elements had the same kneading block thickness of $\Delta z = 2.55mm$ ($K45_{18}$ and $K90_{18}$) and the third one had a kneading block thickness of $\Delta z = 4mm$ ($K45L_{18}$). Seven screw elements of the MIC27 extruder were studied: three conveying elements ($C15_{27}$, $C20_{27}$ and $C30_{27}$), one mixing element ($M15_{27}$) and three kneading elements ($K90_{27}$, $K60_{27}$ and $K30_{27}$), with the same kneading block thickness of $\Delta z = 5mm$. The barrel diameter and the centerline distance of the MIC27 extruder were adjusted in order to keep the number of computational SPH particles feasible, as described in Eitzlmayr et al. [15]. The adjustments impact the absolute values of the pressure and power characteristics but not the ratios between the individual screw elements, hence can be used to investigate and parametrize the screw elements.

The screw elements of the two investigated extruders vary in terms of their D_o/D_i ratio and their smallest gap clearance Δx (Table 4.1). Higher D_o/D_i ratios lead to higher free cross-section surfaces and broader shear rate distributions in the cross section, whereas smaller gap clearances result in highly localized shear peaks. This creates differences in the mechanical and thermal loads exerted on the processed material. In addition, the two extruders differ with respect to the available screw speed range ($n_{ZSK18} = 120 - 1200rpm$ and $n_{MIC27} = 100 - 400rpm$) and the maximal available torque ($\tau_{max}^{ZSK18} = 75Nm$ and $\tau_{max}^{MIC27} = 200Nm$).

4.3 Extruder Modeling

4.3.1 Computational Approach

Singe- and twin-screw extruders were theoretically and experimentally analyzed by Pawlowski and Kohlgrüber [4], [19], who established the dimensionless relations between the throughput and pressure drop (pressure characteristics) and between the throughput and power consumption (power characteristics). The dimensionless representation of the throughput$\left(\dot{V}/nD^3\right)$, the pressure drop $(\Delta pD/\eta nL)$ and the power consumption $(P/\eta n^2 D^2 L)$ are determined based on $\dot{V}$ (volumetric throughput), Δp (pressure drop), n (screw speed), D (screw nominal diameter), L (screw length) and η (fluid viscosity).Using these dimensionless groups for the pressure and power characteristics of individual screw elements, it is possible to describe the flow in fully- and partially-filled, Newtonian and non-Newtonian, and single-, twin- and multiple-screw extruder elements. With regard to the special conditions under the creeping flow regime $(Re \to 0)$ occurring in the HME process (due to high fluid viscosities) and a temperature-independent Newtonian fluid, these correlations are linear and independent of the length scale, viscosity and screw speed. As such, the pressure and power characteristics can be represented using the axis intercepts A_1, A_2 and B_1, B_2:

$$\frac{\Delta pD}{\eta nL} = A_2 \cdot \left(1 - \frac{1}{A_1}\frac{\dot{V}}{nD^3}\right) \quad (1)$$

$$\frac{P}{\eta n^2 D^2 L} = B_2 \cdot \left(1 - \frac{1}{B_1}\frac{\dot{V}}{nD^3}\right) \quad (2)$$

The A_1 parameter, generally termed *inherent conveying capacity*, is the dimensionless flow rate of a fully-filled screw element when conveying without back-pressure. B_1 is the dimensionless flow rate at zero dimensionless driving power. A_2 and B_2 are the dimensionless pressure drop and the driving power, respectively.

In order to computationally determine the pressure and power characteristics of individual HME screw elements, a Lagrangian-based simulation method for fluid dynamics, the smoothed particle hydrodynamics method (SPH) [20]–[25], was applied. Spatial discretization was performed by introducing moving fluid particles, making this approach suitable for simulating complex moving geometries, high fluid domain deformation and free surface flow, which cannot be achieved using the standard mesh-based CFD approaches.

The method proposed by Eitzlmayr et. al [9], [10] was used for developing our mechanistic 1D model. The flow in the extruder was represented as a series of pressure- and shear-driven mass flow rates. The geometry of the screw elements and their ability to convey and build up pressure were reflected by their inherent conveying capacity (A_1) and pressure build-up capacity (A_2), previously determined via the SPH simulations. The material's data were applied to correctly represent the processed material *in silico*. Finally, the data obtained in the 1D simulation were compared to the experiments that validated the results.

The screw elements of the investigated MIC27 extruder were characterized via the SPH method and presented in our previous work [15], except the $C20_{27}$, $K60_{27}$ and all screw elements of the ZSK18 extruder.

4.3.2 SPH Simulation Set-Up

Figure 4.1 shows the simulation setup consisting of a two screw elements with melt inside the barrel. The z-axis is the direction of the axial melt flow. Since the pressure and power characteristics are invariant to the element's screw length, periodic boundary conditions can be used in the z-plane. The prerequisite for the use of the periodic boundaries is the angular position (tilt; α in Figure 4.1) of the cross-section at beginning and the end of the screw element, which has to be equal. With this in mind, the representative screw length of the conveying elements is equal to half of their pitch, or a multiple of the half-pitch length. The representative length of the kneading elements is a function of the stagger angle and the kneading block thickness. The representative length of the simulated kneading elements of the ZSK18 extruder had to be adjusted to the real screw geometry in order to satisfy the condition of identical cross-section tilt. Consequently, all of the simulated ZKS18 kneading elements had four kneading blocks, as opposed to five in the real screw geometry. Including one kneading block more in the screw geometry does not impact the investigated pressure and power characteristics, as it represents a natural continuation of the geometry, just like the periodic boundaries do. The first

and the last kneading blocks were set to half the block thickness, since the periodic boundaries infinitely replicate the screw element in the axial direction. The kneading element of the MIC27 extruder were assembled as described in our previous publication [15], also using an adapted screw length compared to the real geometry. The length of the mixing elements was the same as in the real geometry, as the cut-outs pattern is not repeating itself across the whole screw length.

The number of the fluid SPH particles required for the simulation depends on the free available volume $V_{free} = A_{free} \cdot L$ and the particle resolution. Selecting the smallest possible screw length (i.e., half of the screw pitch) thus decreases the computational costs. The particle resolution was chosen to be equal to the smallest gap clearance Δx, i.e., $\Delta x_{SPH,18} = 0.15mm$ and $\Delta x_{SPH,27} = 0.3mm$. The particle number was calculated as $N_{total} = V_{free}/\Delta x$. The particle number required for the different screw element simulations is shown in Table 4.2 and Table 4.3. The particles were initiated into the simulation domain into a regular cubic grid, which was not sufficient to fully fill the simulation domain (i.e., the particle number was lower than the predicted one) due to the geometry's curvature, causing inconsistencies in the continuity equation. To address this issue, we selected the initial particle spacing that was smaller than the resolution, ensuring a higher initial fluid density and a particle expansion that filled the entire simulation domain in the first time steps. To account for a higher initial fluid density, the density time correction was applied as proposed by Eitzlmayr et al. [13]. The smoothing length was set to $h = 1.2 \cdot \Delta x_{SPH}$, as used in the literature[15], [20], [24]. To ensure the correct representation of the flow through tight clearances with only one particle layer, the clearance model described in [13] was used.

Generally, polymer systems processed via HME are highly viscous (10^2-10^3Pas) and shear rates applied to the material are between $20s^{-1}$ and $2000s^{-1}$. As such, the Reynolds number is low ($Re \ll 1$), leading to creeping-flow conditions inside the extruder. The Reynolds number was calculated as $Re = n \cdot D^2 \rho/\eta$, where n is the screw speed, D is the barrel diameter, ρ is the melt density and η *is* the viscosity, as proposed by Kohlgrüber [26]. In Newtonian fluids under the creeping flow conditions, the dimensionless flow rate, pressure drop and power consumption are not affected by the melt viscosity. In our previous work, we confirmed this assumption [15] and showed that the creeping flow conditions in co-rotating twin-screw extruders occur at $Re \ll 10$. Thus, the screw speed was set to $n = 2.5s^{-1}$ and the viscosities were $\eta_{18} = 0.1Pas$ and $\eta_{27} = 0.2Pas$ for the ZSK18 and MIC27 screw elements, respectively.

The melt density was maintained at $\rho = 1000\,kg/m^3$, resulting in a Reynolds numbers of $Re_{18} = 8.1$ and $Re_{27} = 9.5$. The operation states (different flow rates) were varied via an axial acceleration a_z. At $a_z = 0\,m/s^2$, the inherent conveying capacity (A_1 point) was calculated. By increasing the applied axial acceleration, the relevant process operation points were simulated.

Table 4.2. SPH simulation parameters for the ZSK18 extruder.

Element	a_z	C	Δt	V	N_{total}	L	ρ_{init}	p_0	C_{rep}	η
	[m/s²]	[m/s]	[µs]	[mm³]	[10³]	[mm]	[kg/m³]	[Pa]	[N]	[Pas]
$C8_{ZSK18}$	0-120	24	0.2	786.424	233	4	1100	800	0.001	0.1
$C12_{ZSK18}$	0-100	22	0.4	1179.635	350	6	1150	600	0.001	0.1
$C16_{ZSK18}$	0-80	22	0.4	1572.847	466	8	1030	1000	0.001	0.1
$C24_{ZSK18}$	0-40	22	0.4	2359.271	699	12	1040	800	0.001	0.1
$M12_{ZSK18}$	0-6.67	20	0.4	2765.731	819	12	1150	300	0.001	0.1
$K45_{ZSK18}$	0-30	22	0.5	2673.256	792	12.8	1030	1200	0.001	0.1
$K45L_{ZSK18}$	0-30	22	0.5	3977.293	1178	19.2	1100	800	0.0005	0.1
$K90_{ZSK18}$	0-10	22	0.4	2731.216	809	12.8	1100	500	0.001	0.1

Table 4.3. SPH simulation parameters for the MIC27 extruder.

Element	a_z	c	Δt	V	N_{total}	L	ρ_{init}	p_0	C_{rep}	η
	[m/s²]	[m/s]	[µs]	[mm³]	[10³]	[mm]	[kg/m³]	[Pa]	[N]	[Pas]
$C20_{MIC27}$	0-100	10	1	4175.905	154	10	1100	1000	0.002	0.2
$K60_{MIC27}$	0-30	10	1	10910.564	404	21	1100	1000	0.002	0.2

The speed of sound, which is relevant to the Tait equation of state, was determined according to the theoretical criteria proposed by Morris et. all [27]:

$$c^2 \geq \frac{1}{\delta} max\left(V_0^2, \frac{\nu V_0}{L_0}, a_z L_0\right) \tag{3}$$

The speed of sound limits the maximal allowed relative density variation, defined as $\delta = \Delta\rho/\rho_0$, and is typically assumed to be $\delta = 0.01$. In the equation 3, V_0 is the maximum expected fluid velocity, ν is the kinematic fluid viscosity and L_0 is the relevant length scale. The first, second and third criteria limit the speed of sound based on the particle speeds, the viscous forces and the axial particle acceleration, respectively. To predict the required time step, four time step criteria were used:

$$\Delta t \leq min\left(0.25\frac{h}{c}, 0.125\frac{h^2}{\nu}, 0.25\sqrt{\frac{h}{a}}, \frac{0.3h}{c(1+1.2\beta)}\right) \tag{4}$$

where $\beta = 10\,\nu/hc$ is the artificial viscosity calculated using the kinematic viscosity, smoothing length and speed of sound. The first criteria is the standard Courant-Friedrich-Lewy (CFL) condition, the second and third ones are due to viscous and body forces, respectively. The last one takes into account the combined CFL and viscous limitations. The chosen parameters are listed in Table 4.2 und Table 4.3.

4.3.3 Screw Configuration Geometry – 1D Simulation Set-Up

The screw configuration used during the experiments and 1D simulations on the small scale extruder, the ZSK18, is shown in Figure 4.2. The screw configuration was chosen based on experience from various other extrusions of different formulations, with the goal to have a sufficiently complex, non-trivial design (one kneading zone and one mixing zone with a back-conveying element).

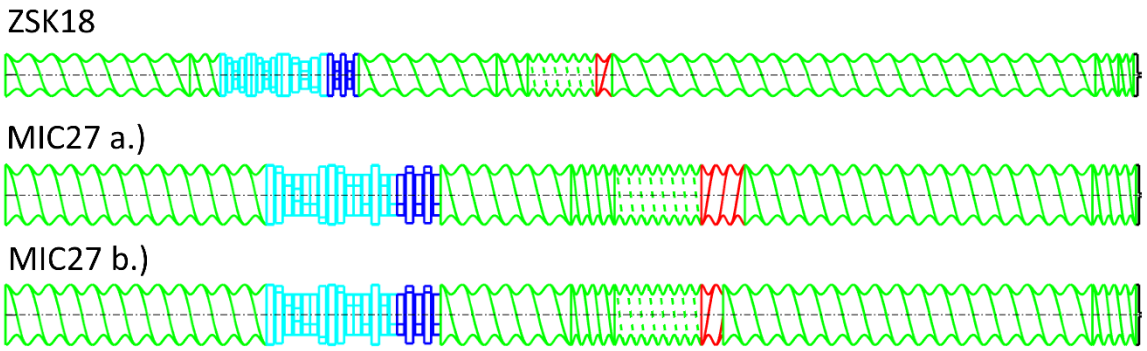

Figure 4.2. The used screw configuration, utilizing various conveying elements (green), mixing elements (dashed green), back conveying elements (red) and kneading elements (dark blue for K90 and light blue for all others).

Three distinct processing zones can be identified in the screw configuration. The first zone is the high-shear kneading section consisting of three kneading blocks, $K45_{18}$, $K45L_{18}$ and $K90_{18}$. The second one is a mixing section consisting of the mixing element $M12_{18}$ and the back conveying element $C16_{18}$, where the back conveying element ensures a significant melt residence time in the location of the mixing element. The third zone consists of a series of conveying elements, $C16_{18}$ and $C8_{18}$, creating the pressure necessary for conveying the melt through the die. The axial discretization in the simulations was $\Delta x_{1D,18} = 2mm$. The process parameters in the experiments and 1D simulations are presented in Table 4.4.

Table 4.4. 1D simulation and experimental process setup for the ZSK18 extruder.

Exp.	n	ṁ	Barrel temperature profile
	[rpm]	[kg/h]	[°C]
e_1	120	2	60/80/100/100/100/110/110/110/110/120
e_2	200		
e_3	120	2	60/80/115/115/115/125/125/125/125/135
e_4	200		
e_5	120	2	60/80/130/130/130/140/140/140/140/150
e_6	200		

The scale-up from the ZKS18 to the MIC27 extruder was performed via the Menges and Rauwendaal scaling laws presented in detail in Appendix of this paper. The transfer of screw configuration to the MIC27 extruder was done taking into account the starting configuration and available screw elements on the MIC27 extruder. The resulting screw configurations and process parameters are provided in Figure 4.2 and Table 4.5, respectively.

Table 4.5. 1D simulation and experimental process setup for the MIC27 extruder

Exp.	n	ṁ	Barrel temperature profile
	[rpm]	[kg/h]	[°C]
1M	107	3.15	60/80/100/100/100/110/110/110/110/120
1R	110	4.93	
2M	178	3.15	
2R	183	4.93	
3M	107	3.15	60/80/115/115/115/125/125/125/125/135
3R	110	4.93	
4M	178	3.15	
4R	183	4.93	
5M	107	3.15	60/80/130/130/130/140/140/140/140/150
5R	110	4.93	
6M	178	3.15	
6R	183	4.93	
E1	100	7	60/80/100/100/80/110/80/110/110/120
E2	150	7	

The MIC27a screw configuration is the result of the available screw elements and the screw transfer, whereas the MIC27b is the adjusted screw configuration, with a shorter back-conveying element (which was not available to us in the experiments). The MIC27b screw configuration was used only in silico for the E1 and E2 theoretical scale-up setups, explained

in detail in the discussion section. The axial discretization in the simulations was also done with a resolution of $\Delta x_{1D,27} = 2mm$.

4.4 Materials

In the experiments and 1D simulations, a pharmaceutical formulation of 90% Soluplus® and 10% Fenofibrate was considered. Soluplus® is an acetic acid ethenyl ester polymer with 1-ethenylhexahydro-2H-azepin-2-one and α-hydro-ω-hydroxypoly(oxy-1,2-ethanediyl) grafts. The amphiphilic chemical structure of Soluplus® (PEG: hydrophilic backbone; PVCL, PVAc: lipophilic side chains) leads to a good interaction with drugs, forming solid dispersions and significantly improving the solubility of solid dosage forms in aqueous media. As an API we selected a poorly water-soluble lipid-regulating drug, i.e., fenofibrate. This API increases the high-density lipoprotein levels by reducing the expression of cholesteryl ester transfer protein, ultimately minimizing the risk of heart diseases and preventing strokes[28].

For an accurate *in silico* description of the premix, suitable material models are required. The melt's viscosity was described using the temperature- and shear-dependent Carreau-Yasuda model:

$$\eta(\dot{\gamma}, T) = \frac{\eta_0 a_T}{\left(1+\frac{|\dot{\gamma}|a_T}{\dot{\gamma}_{crit}}\right)^m} \tag{5}$$

where T is the melt temperature, $\dot{\gamma}$ is the shear rate, $\dot{\gamma}_{crit}$ is the critical shear rate, η_0 the zero-shear-rate viscosity and a_T is the Williams-Landel-Ferry temperature shift factor calculated as:

$$a_T = exp\left[-\frac{C_1(T-T_r)}{C_2+T-T_r}\right] \tag{6}$$

Here T_r is the reference temperature. The viscosity parameters of the Soluplus-Fenofibrate (90%-10%) formulation are listed in Table 4.6 and shown in Figure 4.3.

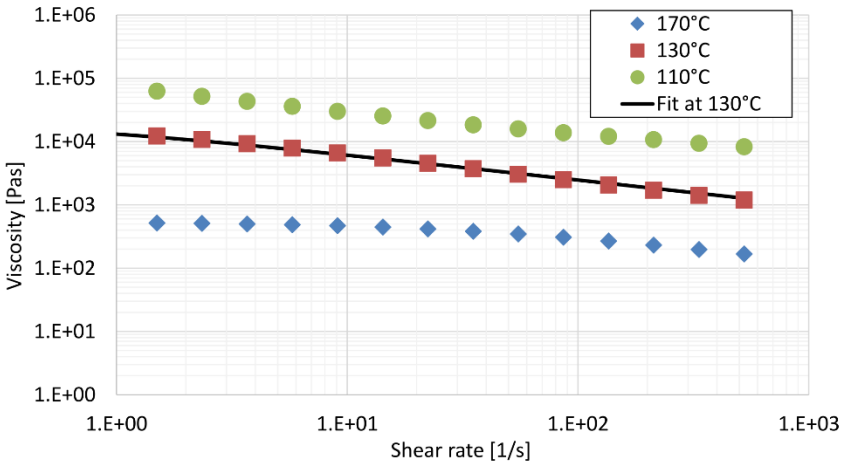

Figure 4.3. Measured viscosity and Carrueau-Yassuda viscosity fit.

Table 4.6. Carreau-Yassuda viscosity fits.

η_0 [Pa·s]	550
$\dot{\gamma}_{crit}$ [s^{-1}]	26.401
m [-]	0.4007
T_r [°C]	170
C_1 [-]	22.1978
C_2 [°C]	268.9598

In order to calculate density ρ, the Menges model was used, which describes the density as a function of pressure p and temperature T, i.e.,

$$\rho = \left(\frac{K_1}{p+K_4} + \frac{K_2 T}{p+K_3}\right)^{-1} \tag{7}$$

The glass transition temperature between is described as:

$$T_g = K_8 + K_9 p \tag{8}$$

The parameters used to fit the Menges density model are listed in Table 4.7.

Table 4.7. Menges specific volume parameters.

	Solid	Liquid
K_1 [bar cm³/g]	29716	29519
K_2 [bar cm³/g°C]	0.35526	1.1618
K_3 [bar]	1671.5	2614.4
K_4 [bar]	34326	34783
	Transition temperature	
K_8 [°C]	72.729	
K_9 [°C/bar]	0.020912	

The heat capacity and thermal conductivity of the melt were modeled using linear temperature-dependent fits. The thermal capacity for temperatures below the glass transition temperature of $T_g = 76.33\,^{\circ}\,C$, was modeled as:

$$c_{p,s} = 172.98 + 36.48 \cdot T \tag{9}$$

and above the glass transition temperature as:

$$c_{p,m} = 1600 + 3.83 \cdot T \tag{10}$$

The thermal conductivity was modeled as:

$$\lambda = 0.1615 + 10^{-4}T \tag{11}$$

To evaluate the solid state of the HME pellets, differential scanning calorimetry (DSC) was used. The experiments were performed using a DSC 204 F1 Phoenix® equipped with an automated sampling unit (NETZSCH-Geraetebau GmbH, Selb, Germany). The pellets were ground and transferred into aluminium pans that were closed with a pierced lid via cold welding. The samples were heated from 0°C to 200°C with a heating rate of 10°K/min followed by cooling to room temperature with a cooling rate of -10 K/min. Nitrogen served as analytical gas (flow rate: 50.0 ml/min) and every sample was investigated in triplicate.

4.5 Results and Discussion

4.5.1 SPH Results – ZSK18 and MIC27

The flow rate $\dot{V}$ of the simulated screw elements was evaluated in accordance with the method presented in [15]. Various throughput conditions were simulated using an axial mass-specific body force, a_z, against the conveying direction. The resulting data are the pressure and power characteristics for the ZSK18 and MIC27 extruders (Figure 4.4 and Figure 4.5, respectively) and the values of the A_1, A_2, B_1 and B_2 points (Table 4.8 and Table 4.9, respectively). The linearity of the pressure and power characteristics curves reflects the linearity of the Stokes equations for Newtonian fluids under the creeping flow conditions, experimentally confirmed by Pawlowski [19] for single-screw extruders.

The pressure gradient is strongly influenced by the screw pitch or the stagger angle. Comparing the ZSK18 and MIC27 conveying elements, it is apparent that a higher screw pitch results in a higher inherent conveying capacity (A_1 point) and a lower pressure build-up capacity (A_2 point). The relation between the A_1 and A_2 points and the screw pitch is nearly linear. The A_1 value of the $C8_{18}$ screw element is nearly half the A_1 value of the $C16_{18}$ conveying element. The A_2

value of the $C16_{18}$ element is nearly half the A_2 level of the $C8_{18}$ conveying element. The same pattern can be observed for the $C12_{18}$ and $C24_{18}$ conveying screw elements.

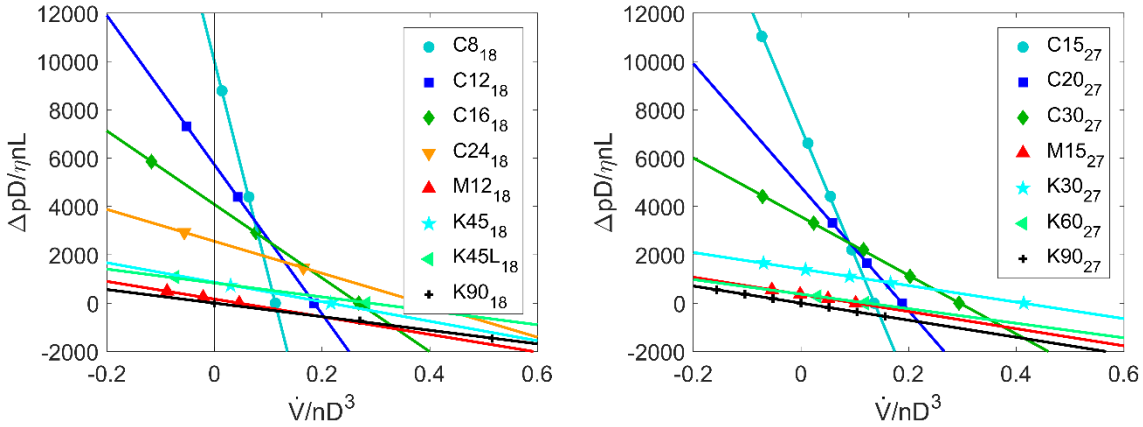

Figure 4.4. Pressure characteristics of the ZSK18 (left) and MIC27 (right) extruders.

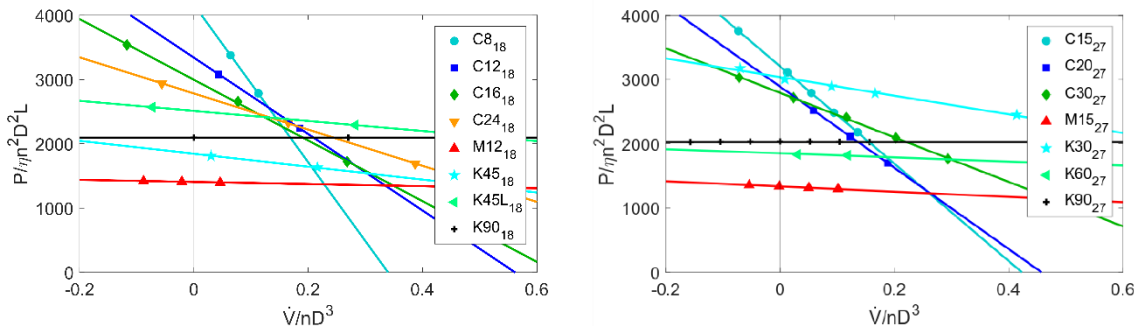

Figure 4.5. Power characteristics of the ZSK18 (left) and MIC27 (right) extruders.

The mixing elements $M12_{18}$ and $M15_{27}$ have a significantly lower pressure build-up capacity and similar conveying capacity, compared to their conveying element counterparts, $C12_{18}$ and $C15_{27}$ respectively. The drop in the pressure build-up capacity can be attributed to the axial cut-outs in the mixing elements geometry, creating an excessive melt backflow once an axial pressure gradient is introduced.

The same effect is observed for the kneading elements, with the stagger angle between the individual kneading blocks dictating the pressure drop. The figures indicates that a higher stagger angle leads to a lower pressure build-up capacity ($K45_{18}$, $K90_{18}$ and $K30_{27}$, $K60_{27}$, $K90_{27}$) and a higher conveying capacity. The extreme cases are the $K90_{18}$ and the $K90_{27}$ kneading elements: the pressure characteristics curve passes through the origin, suggesting a non-conveying behavior. In order to establish a flow in non-conveying elements, axial pressure is required. The thickness of kneading blocks influences the angle of pressure characteristics

curves. The kneading elements of the same disc thickness ($K45_{18}$, $K90_{18}$ and $K30_{27}$, $K60_{27}$, $K90_{27}$) have parallel pressure characteristics curves.

Table 4.8. SPH pressure and power characteristics results for the ZSK18 extruder.

Element	A_1	A_2	B_1	B_2
$C8_{ZSK18}$	0.113	9999.5	0.340	4164
$C12_{ZSK18}$	0.185	5726.9	0.562	3339.9
$C16_{ZSK18}$	0.268	4082.1	0.634	2995.9
$C24_{ZSK18}$	0.387	2557.3	0.989	2782.8
$M12_{ZSK18}$	0.046	167.3	8.681	1406.4
$K45_{ZSK18}$	0.214	864.2	1.834	1845.2
$K45L_{ZSK18}$	0.288	831.2	3.204	2511.9
$K90_{ZSK18}$	A_0=2810		B_0=2094.9	

Table 4.9. SPH pressure and power characteristics results for the MIC27 extruder.

Element	A_1	A_2	B_1	B_2
$C15_{MIC27}$	0.137	7228	0.424	3205
$C20_{MIC27}$	0.188	4803	0.457	2890
$C30_{MIC27}$	0.295	3583	0.807	2795
$M15_{MIC27}$	0.102	354	3.02	1309
$K30_{MIC27}$	0.416	1378	2.22	2970
$K60_{MIC27}$	0.123	373	5.79	1853
$K90_{MIC27}$	A_0=3535		B_0=2032	

Comparing conveying elements with a similar pitch but different extruder size, the $C16_{18}$ and the $C15_{27}$ conveying elements, the pressure characteristics shows that the $C15_{27}$ conveying element has a lower A_1. The reasons are the increased gap distance in the MIC27 extruder and the difference in the D_o/D_i geometry parameters (Table 4.1), with $(D_o/D_i)_{18} > (D_o/D_i)_{27}$ creating a smaller relative free surface area in the MIC27 screw elements and a lower conveying capacity. However, the pressure build-up capacity of the $C15_{27}$ conveying element is higher than that of the $C16_{18}$ element, regardless of a bigger gap in the MIC27 extruder.

In addition, differences in the pitch of the conveying elements affect the power characteristics (Figure 4.5). The conveying screw elements have high driving power consumption (B_2 point) (Table 4.8 and Table 4.9) and a steep power-consumption gradient due to their high-pressure build-up capacities. The $C15_{27}$ conveying element has higher driving power consumption than $C16_{18}$ due to its higher pressure build-up capacity. However, due to the reduced pressure generation and melt back-flow, the mixing and kneading elements have a lower driving power consumption. For all investigated elements, the lower gap volume fraction and the low pressure

build-up capacity result in the lowest driving power consumption of the $M12_{18}$ and $M15_{27}$ mixing elements. The $K90_{18,27}$ kneading element has a constant power characteristic due to its non-conveying screw nature, as attested by the pressure characteristics.

4.5.2 1D Simulation Results and Comparison to Experiments

As described in the previous sections, the 1D HME simulations allow studying of the process state variables (filling degree, axial melt-temperature and pressure gradients, torque, SMEC and RTD) as a function of the process input parameters (throughput, screw speed, barrel temperature settings, die and screw configuration setup), for different processed materials. The process conditions studied *in silico* are equal to the experimental setup, shown in Table 4.4 for the ZSK18 extruder, and Table 4.5 for the MIC27 extruder. The exceptions are the E1 and E2 settings on the MIC27 extruder, which were obtained from the *in silico* investigation and will be discussed later.

For a first comparison between the experimental and *in silico* obtained results, the output torque values were compared. Table 4.10 and Figure 4.6 show the comparison for the smaller ZSK18 extruder (in the range from e1 to e6) and Table 4.11 and Figure 4.7 the comparison for the bigger MIC27 extruder (in the range1M/1R to 6M/6R). Comparing simulations with the experimental results, it can be seen that the *in silico* predictions are quite good, given the complexity of the process and the simplifications made in the 1D HME model. The maximum difference is about 30% for the case of the ZSK18 and experiments e1 and e2. For the other cases the difference is close to 10% and below. The main difference can be attributed to the location of the melt zone, as our model does not resolve the powder intake and melting zones, and to the measurement inaccuracy, as the torque values are indirectly estimated as part of the extruder control software, based on the electric motor current consumption.

Table 4.10. ZSK18 1D vs experiments.

Exp.	n	$\dot{m}$	$Torque_{exp}$	$Torque_{1D}$	Torque difference	$SMEC_{exp}$	$SMEC_{1D}$
	[rpm]	[kg/h]	[Nm]	[Nm]	[%]	[kWh/kg]	[kWh/kg]
e_1	120	2	29.3	22.3	9.2	0.184	0.140
e_2	200		27.2	23.0	5.6	0.285	0.241
e_3	120	2	19.1	19.3	-0.3	0.120	0.121
e_4	200		20.4	19.9	0.7	0.214	0.208
e_5	120	2	12.1	16.3	-5.6	0.076	0.103
e_6	200		14.4	16.8	-3.2	0.150	0.176

Table 4.11. MIC27 1D vs experiments.

Exp.	n	ṁ	$Torque_{exp}$	$Torque_{1D}$	Torque difference	$SMEC_{exp}$	$SMEC_{1D}$
	[rpm]	[kg/h]	[Nm]	[Nm]	[%]	[kWh/kg]	[kWh/kg]
1M	107	3.15	93.6	72.0	11.4	0.333	0.256
1R	110	4.93	96.1	77.9	9.6	0.224	0.182
2M	178	3.15	83.8	75.5	4.4	0.496	0.447
2R	183	4.93	82.2	79.2	1.5	0.319	0.308
3M	107	3.15	70.2	62.1	4.2	0.250	0.221
3R	110	4.93	73.6	67.6	3.1	0.172	0.158
4M	178	3.15	66.7	65.1	0.9	0.395	0.385
4R	183	4.93	68.4	68.7	-0.1	0.266	0.267
5M	107	3.15	52.5	52.0	0.3	0.187	0.185
5R	110	4.93	56.7	56.9	-0.1	0.132	0.133
6M	178	3.15	54.9	54.8	0.1	0.325	0.324
6R	183	4.93	55.1	58.1	-1.6	0.214	0.226
E1	100	7	-	91.0	-	-	0.136
E2	150	7	-	94.1	-	-	0.211

Looking at Figure 4.6, it is obvious that the barrel temperature settings have a significant impact on torque. Higher barrel temperature settings result in a higher melt temperature (for all other settings kept constant), effectively lowering the melt viscosity. The decrease in viscosity in general results in a lower viscous dissipation, which is in turn reflected in a lower overall SMEC and torque needed. The same trend can be observed in the bigger extruder. By calculating the torque, and in turn the viscous dissipation (contained in the SMEC value), it can be expected that the locations of the fully filled zones and the melt temperature are also predicted correctly, as most of the SMEC is consumed in the fully filled zones and the melt temperature is the result of a balance between the viscous dissipation and barrel cooling power, for a given formulation (rheology, heat capacity, temperature conductivity and so on).

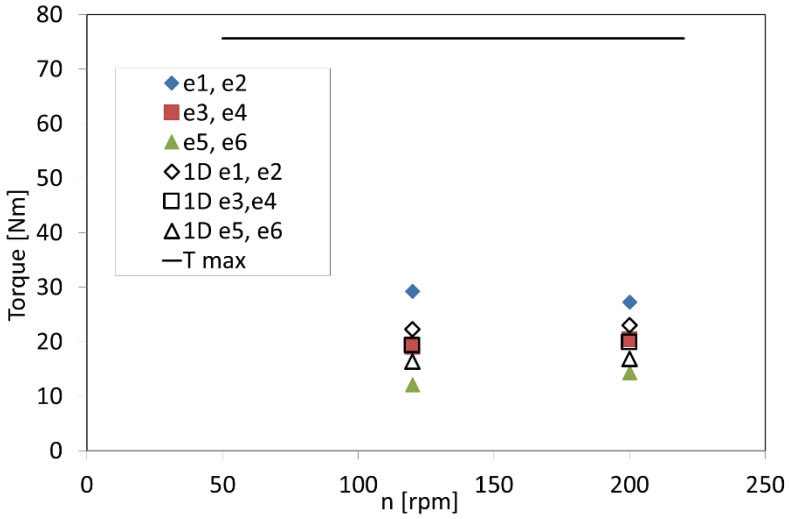

Figure 4.6. Torque: 1D simulations vs experiments – ZSK18.

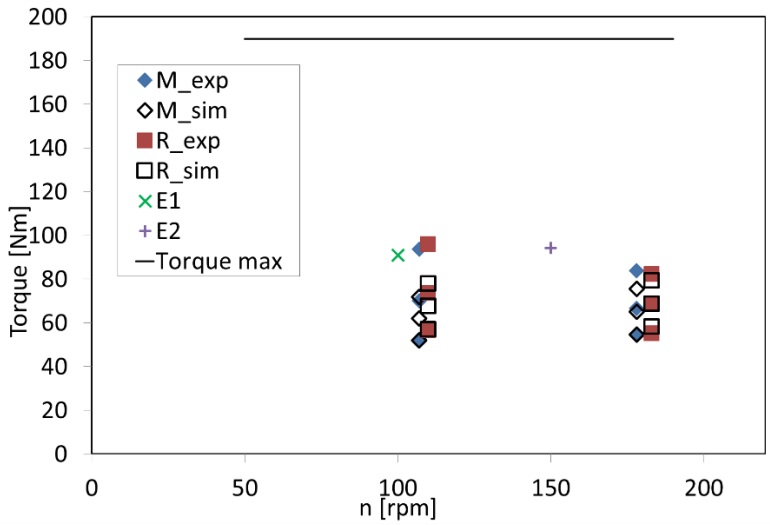

Figure 4.7. Torque: 1D simulation vs experiments – MIC27.

Influence of the screw speed and barrel temperature settings on the process state variables will for simplicity only be discussed for the example of the smaller ZSK18 extruder. However, all the observations and conclusions are also valid for other extruder scales and process setting variants. The filling degree is a function of the specific volume of the processed material and the free screw volume, shown in Figure 4.8 for constant screw speeds (for ZSK18: top figure - 120rpm, lower figure - 200rpm). Three things can be observed: (1) the barrel temperature settings do not influence the filling degree, (2) the location of the fully filled zones is not a function of the screw speed and (3) the filling degree decreases with an increase of screw speed.

A decrease in the filling degree (for a constant throughput) at a higher screw speed is expected since the filling degree (f) is inversely proportional to the screw speed:

$$f = \frac{\dot{m}}{\rho V_{free} n} \tag{12}$$

The position of the fully-filled zones is not influenced by the screw speed, but rather by the difference in the individual conveying capacities of the screw elements. As such, it is a function of the screw configuration. The first fully-filled zone is established due to the non-existent conveying capacity of K90 kneading elements. The second one is caused by the back-conveying action of the left-handed elements before the mixing elements, and the third one is due to a build-up before the die section.

The location, number and size of the fully filled zones directly influence the residence time distribution, as well as the local SMEC and melt temperature peaks. Figure 4.9 shows the axial SMEC distribution and melt temperature distribution for the e1 (120rpm, low temp.) and e2 (200rpm, low temp.) cases of the ZSK18 process settings. The location of the SMEC and melt temperature peaks coincide with the location of the fully filled zones. It can also be seen that there is a difference between the amount of energy dissipated by the kneading element sequence (first fully filled zone), the mixing element sequence (second fully filled zone) and by the conveying element in the discharge zone (third fully filled zone). At the entrance into all three zones, a high SMEC peak can be observed, resulting in a sharp melt temperature increase and decrease of viscosity. Apparently, the kneading blocks (first zone) and the conveying elements at the discharge (third zone) cause considerably higher energy dissipation compared to the mixing element (second zone). The explanation for the comparably lower energy input by the mixing element is the existence of the axial cutouts in the mixing screw geometry, which is also observed in the power characteristics of the screw elements. In contrast, the back-conveying element after the mixing element causes a sharp increase in the dissipated energy, resulting in the highest melt temperature peak. The residence time distribution is a direct function of the filling state in the extruder. A higher overall filling (high throughput, low screw speed) will lead to a wider and longer RTD compared to a low overall filling (low throughput and high screw speed).

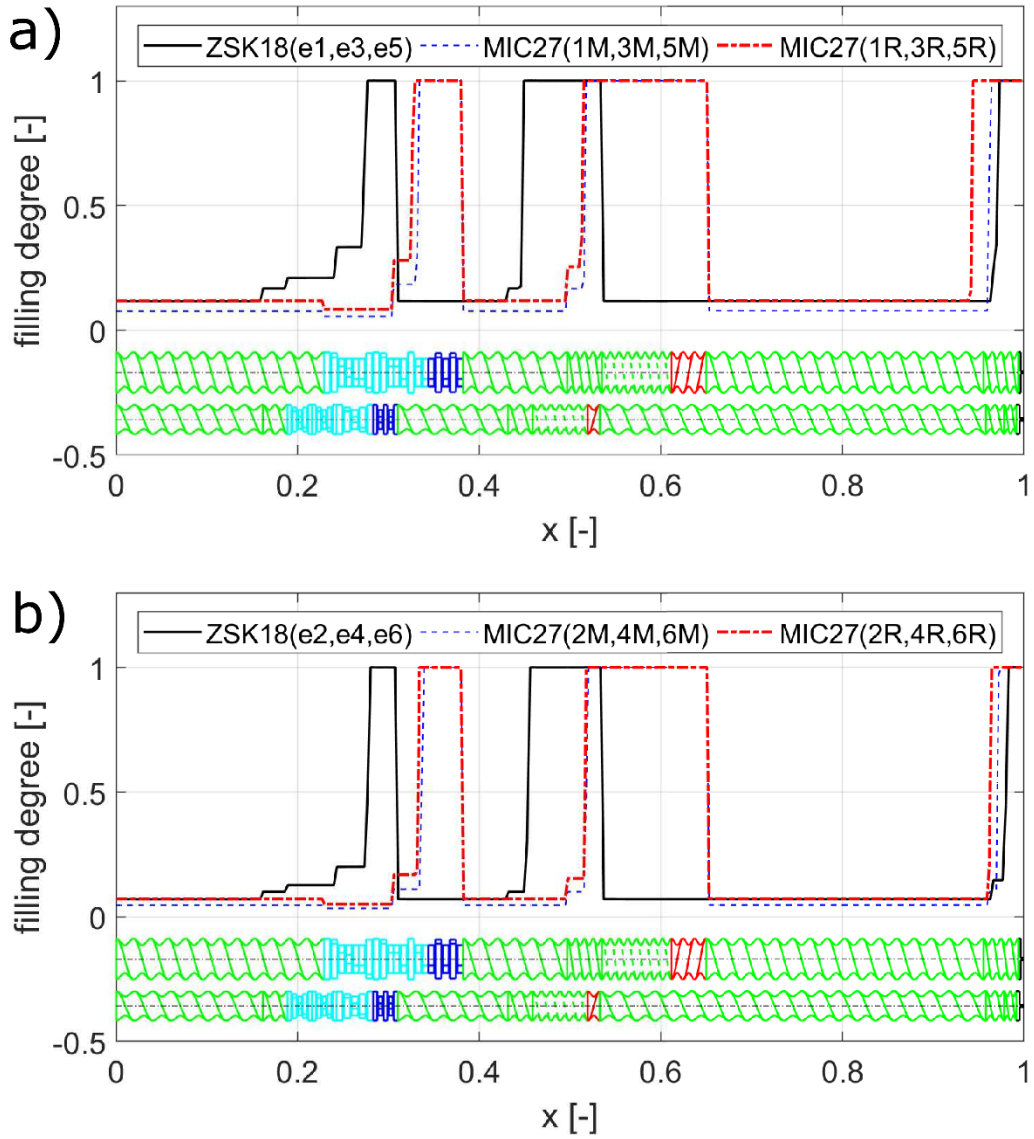

Figure 4.8. Filling degree: scale-up comparison between ZSK18 (bottom screw) and MIC27 (top screw).

Figure 4.10 shows the RTD (not including the transport times) for two different screw speeds (e1 and e2 settings). As the barrel temperature (and melt temperature) does not decisively influence the filling degree, the RTD is also not impacted (i.e., there is no significant different between e1 and e3 for example). However, screw speed has an important impact, with higher speeds shortening and narrowing the RTD. Based on the knowledge of the location of the fully filled zones a mean residence time (mRTD) for the individual fully filled zones can be calculated. Then, based on the filling degree distribution, melt temperature trajectory, SMEC distribution and the individual residence times, a history of the thermo-mechanical stress

exerted on the processed material can be determined and used for the process setup and scale-up.

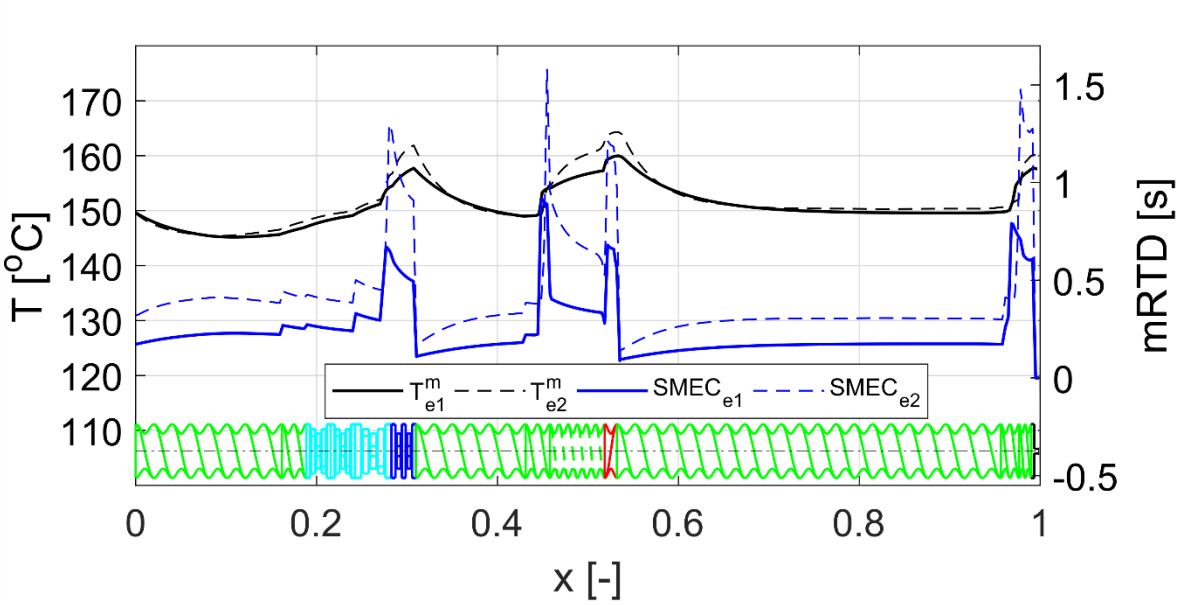

Figure 4.9. Axial melt temperature and SMEC distribution for two settings on the ZSK18 extruder.

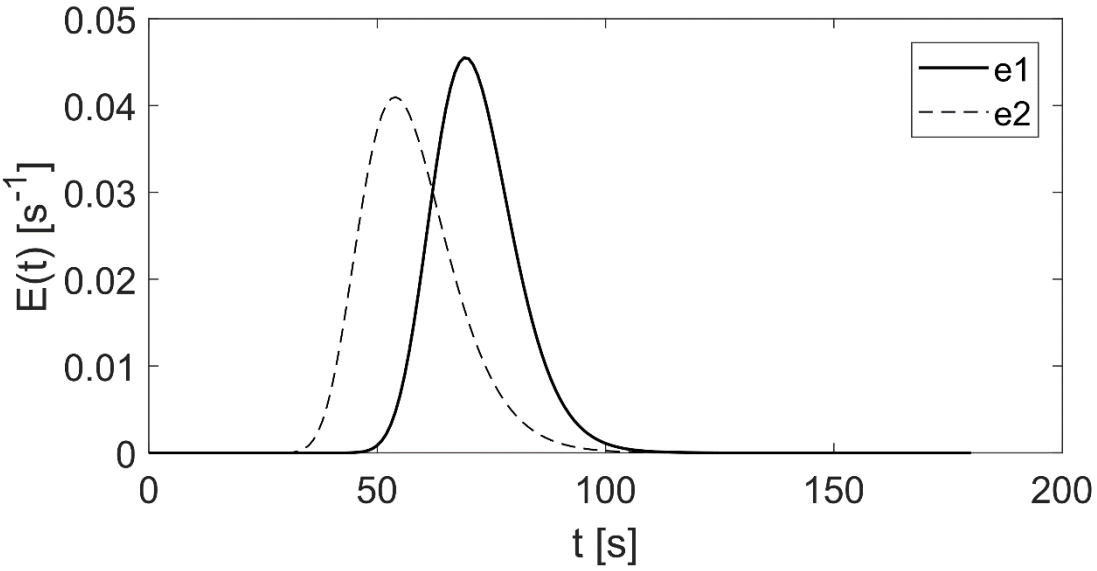

Figure 4.10. RTD for two settings on the ZSK18 extruder.

4.5.3 Scale-up from ZSK18 to MIC27

Scale-up from the ZSK18 to the MIC 27 has been done (computationally) by the methods proposed by Menges and Rauwendaal. Both approaches are described in the Appendix. A comparison between the original process (on the ZSK18 extruder) and the scaled-up process on

the MIC27 extruder is performed by comparing the filling degrees, RTD and melt temperature distributions. Looking at Figure 4.8, clear differences in the filling level profiles can be observed. The length of the first filling zone is similar in both extruders, whereas the second and third filling zone sections are considerably longer in the MIC27 processes. This can be attributed to the differences in the screw configuration and the inadequate scale-up of the screw speed and throughput. This leads to a longer and wider RTD, compared to the original process, as shown in Figure 4.11.

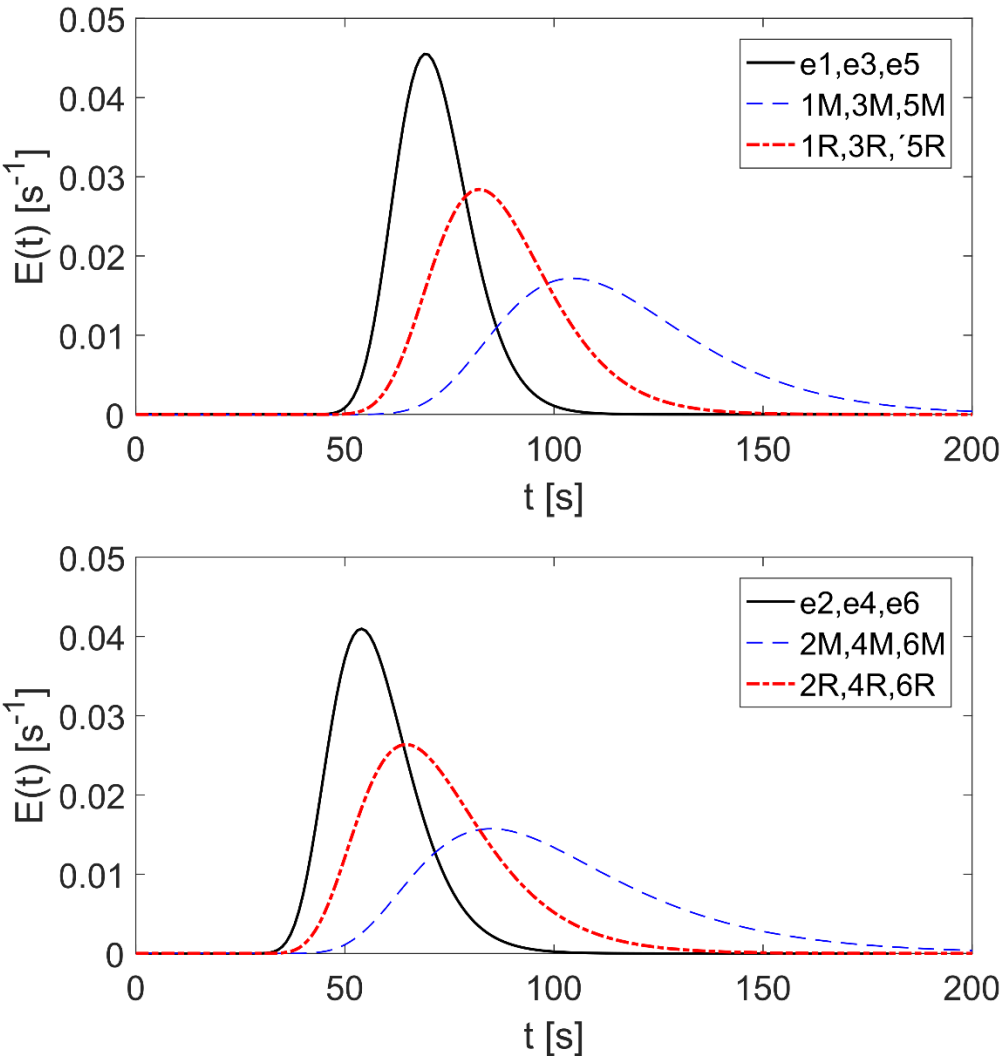

Figure 4.11. RTD: scale-up comparison between ZSK18 and MIC27.

A wider RTD indicates better axial mixing inside the extruder. Yet, a longer RTD (higher mean residence time) indicates that the processed material is experiencing a high shear and temperature load for a longer time period. As we know the location and the amount of material in the fully filled zones, we can calculate a mean residence time distribution (mRTD) for the

different processing zones and investigate the problem in more detail. For that, we plotted the mRTD together with the axial melt temperature distribution for the e1 and e2 settings on the ZSK18 extruder, and the 1M, 1R and 2M, 2R settings for the MIC27 extruder in Figure 4.12.

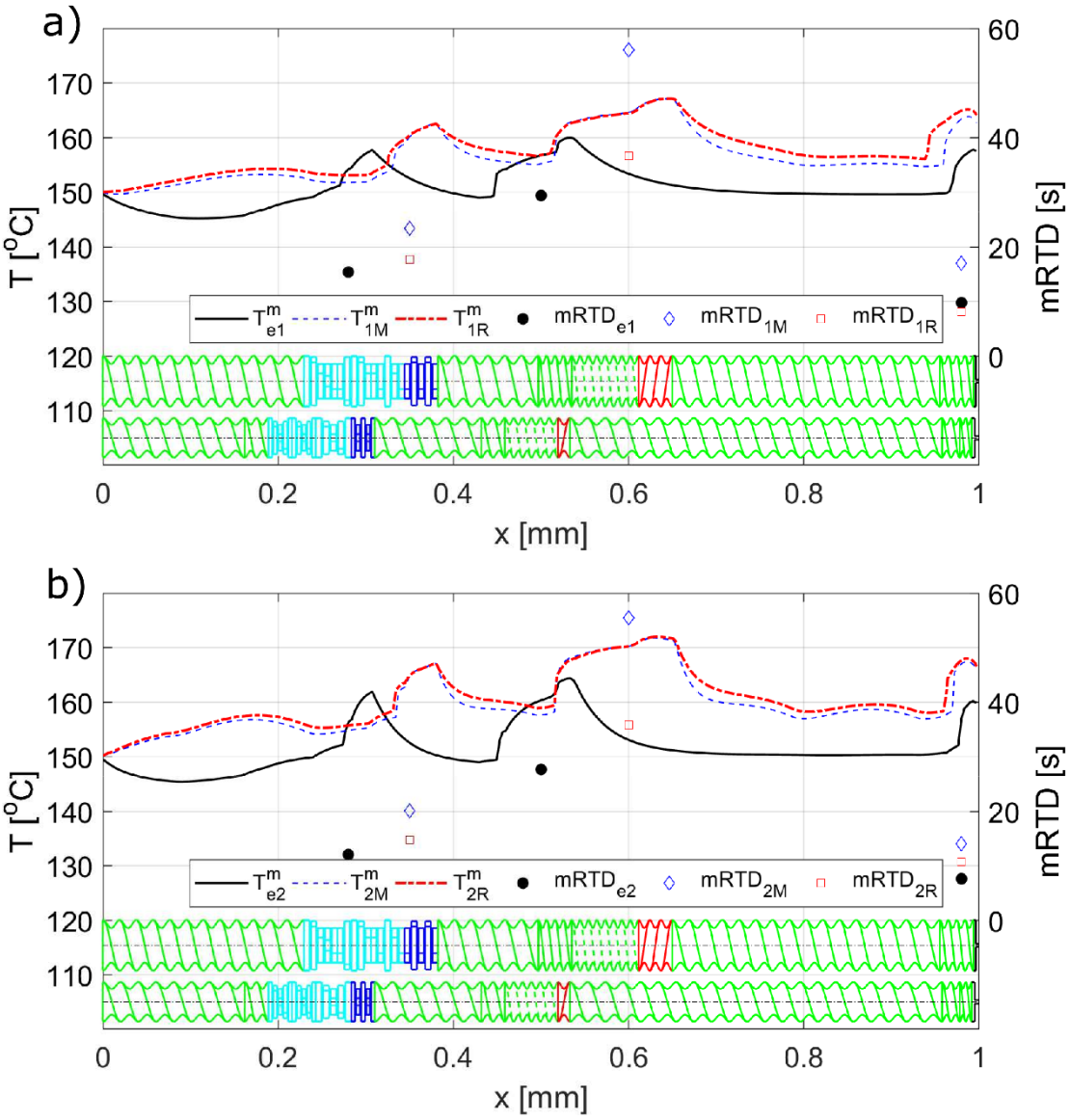

Figure 4.12. Melt temperature and local mRTD: scale-up comparison between ZSK18 (e1 and e2 settings) and the corresponding MIC27 (1M, 1R and 2M, 2R) settings.

Both the Menges and the Rauwendaal scale-ups lead to a considerably higher melt temperature inside the extruder when compared to the original process and to a higher mRTD for all three fully -filled zones. The highest differences can be seen in the second fully-filled zone, where the temperature difference is around 10°C and the mRTD difference around 10s for the Rauwendaal scale-up and up to 30s for the Menges scale-up approach. As a result, the processed material undergoes a significantly higher thermal exposure, for a longer time period, possibly

leading to API and/or polymer matrix degradation. Although both scale-up methods seek to achieve an integral SMEC that is as similar as possible to the original process, the melt temperature is much higher in the scaled-up process. Part of the reason that this fails is that it is not possible to accurately scale for constant SMEC while not taking into account the actual screw configuration and screw geometry, as can be seen when comparing the SMECs from the two scales in Table 4.10 and Table 4.11. The usefulness of the integral values of SMEC and RTD, as well as the melt temperature measurements before and/or after the die, shown by some authors, becomes doubtful, as these methods do not reflect the gradients and temperature maxima in the whole process. Hence, it can be argued that the SMEC alone is not a reliable scale-up guideline since it merely reflects the energy that is dissipated in the melt due to the screws, neglecting local phenomena, melt cooling and the RTD.

Knowing this, an in silico DoE can be started with the goal of ensuring an as-similar-as-possible thermo-mechanical history of the processed material at different scales. For example, by rationally adjusting the screw configuration, i.e., using half of the length of the back-conveying element in the mixing zone as shown in Figure 4.2 for MIC27b), screw speed, throughput and the barrel temperature (Table 4.5 and Table 4.11, E1 and E2 cases) much better scale-up results can be obtained, as shown in Figure 4.13. The E1 and E2 cases shown on the MIC27 extruder, compare well with the e1 and e2 settings on the ZSK18 extruder. The melt temperature and local mRTD comparison is shown in Figure 4.13, and the full RTD in Figure 4.14. When comparing the axial melt temperatures of the two setups (e1 vs. E1 and e2 vs. E2) it is apparent that the change in the process settings resulted in more similar melt temperatures. Especially when comparing the melt temperature peaks (first and second fully filled zones), where there was a difference of up to ~10°C in the Menges and Rauwendaal setups, now there is a difference of ~2°C. The melt temperature in the partially filled zones is also lower, compared to the Menges and Rauwendaal setups. The local mRTD in the fully filled (shear-relevant) zones is also much more similar in the *in silico* scaled case.

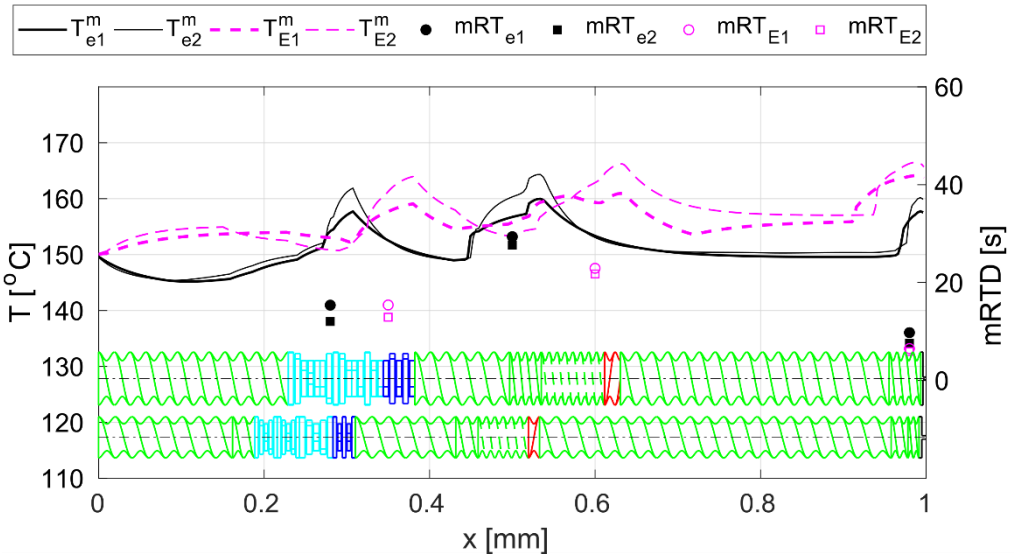

Figure 4.13. Melt temperature and mRTD distribution: *in silico* scale-up of the e1 and e2 ZSK18 HME processes.

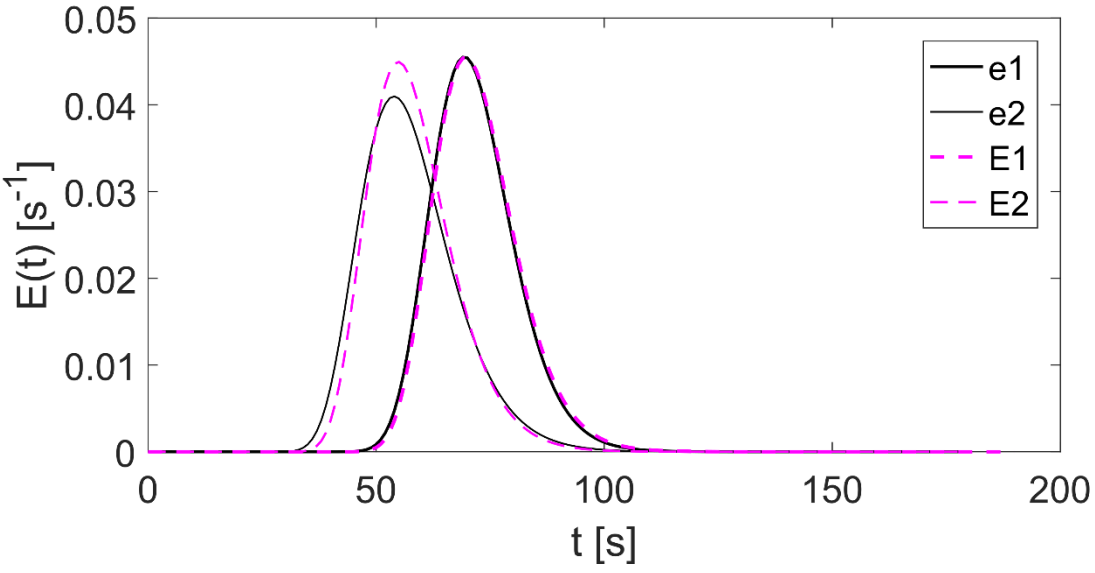

Figure 4.14. RTD via *in silico* scale-up of the e1 and e2 ZSK18 HME processes.

In the second zone, the change of the length of the left-handed element allowed for an even shorter mRTD compared to the original process. As a result, the overall RTD is virtually the same for the e1 and E1 processes, with a slight difference between the e2 and E2 processes. The similarity between temperature peaks of the fully filled zones, the local mRTDs of the individual fully filled zones and the overall RTD, suggest a similar thermo-mechanical history of the product and, ultimately, a similar product quality. Lastly, the throughput was increased

by 55% in comparison to the Menges suggestion, 30% in comparison to the Rauwendaal suggestion and 71% when compared to the original process. Thus, a successful scale-up is achieved without the (common) problem of obtaining undesired decomposition products upon scale-up.

Concerning the solid state of the produced pellets, all pellets showed a single T_g around 50°C upon heating, which is in accordance with theoretical considerations applying the Fox equation [29]. An endothermic peak attributed to the fenofibrate melting was not observed. Since the T_g was below the T_g of the polymer and the endothermic fenofibrate melting event was not evident, it can be assumed that an amorphous single-phase system was obtained via HME [30]. Soluplus® itself exhibits a glass transition around 72°C and fenofibrate shows an endothermic peak at 84°C corresponding to the drug´s melting. TGA studies showed that Soluplus® degrades at 293 °C [31]. In this study it was also shown that when the polymer was kept at 130 °C for 20 minutes no degradation was evident.

4.6 Summary and Conclusions

In this work we presented a new direction for pharmaceutical HME process understanding and scale-up, based on an *in silico* approaches. Building on our previous work, the screw elements of the two extruders were fully characterized using the SPH approach, and analyzed. Effects of the screw-barrel gap size and differences in the D_o/D_i ratio on the pressure on power characteristics of the elements were noted and discussed. Furthermore, different HME setups on the Coperion ZSK18 and the Leistritz MI27 extruders were investigated *in silico* and the obtained torque and SMEC results were compared to experimental results, showing good agreement. The impact of the screw speed, throughput and barrel temperature on the melt temperature, RTD, torque and SMEC was discussed.

Next, two common scale-up methods used in the polymer industry were investigated and compared to the original process. It was shown that this methodology is not adequate for pharmaceutical applications, as the resulting SMEC, melt temperature and RTD are not equal to the original and would most likely lead to product degradation, given the small processing windows that pharmaceutical product typically have. As this was not apparent without the use of detailed modeling (melt temperatures and local mRTD), it was not possible to directly compare scale-up approaches in such detail before. Using the proposed *in silico* approach,

scale-up can be easily automated and the process settings can be computed for a given RTD, SMEC and melt temperature on one scale.

Nevertheless, the presented *in silico* approach does not replace experiments yet, as we are not able to predict the product quality based on the state variables reliably. Hence, more work is required for understanding the effect of mechanical and thermal loads on the product performance, enabling a full HME process setup *in silico*. The thermal and mechanical loads on the premix during HME could be described via unique markers (the input and output energy, especially in combination with the local residence times) to predict the performance of the product. Furthermore, work is needed to experimentally validate the melt temperature and RTD calculated *in silico*.

4.7 Appendix (theoretical HME scale-up procedure)

4.7.1 Menges and Feistkorn Scale-up Approach

In general, a process transfer encompasses either scale-up or scale-down, or a transfer between similarly-sized extruders with different screw configurations. Scale-up (i.e., a transfer from a small-scale laboratory device to an industrial production plant) is the most common and demanding task.

Since technical problems can, in general, be described via mathematical relations (even if they are not known), scaling is generally performed using a dimension analysis. This is done based on the assumption that every model of a process can be converted into a set of non-dimensional equations [32]. For a specific problem, all relevant parameters should be linearly-independent and target parameters have to be determined at first. Next, the relation between these parameters has to be formulated in a dimensionless manner according to the Π-theorem: “Every physical relation between n parameters can be reduced to a relation with only $m = n – r$ dimensionless groups (Π_i- quantities) that are independent of each other.” Here, r is the rank of the dimensional matrix [32], [33]. Following this procedure, the Π_i- quantities can be created.

Table 4.12. Π_i quantities in extrusion processes

Similarity	Π_i- *quantities*
Specific drive power	$\pi_1 = \frac{P}{\dot{m} \cdot c_v \cdot (T_m - T_r)}$
Specific heating capacity	$\pi_2 = \frac{H}{\dot{m} \cdot c_v \cdot (T_m - T_r)}$
Pressure build up	$\pi_3 = \frac{p}{\rho \cdot c_v \cdot (T_m - T_r)}$
Mixing effect	$\pi_4 = \frac{\dot{V}_D}{\dot{V}_S}$
Heat transfer	$\pi_5 = \frac{\alpha \cdot h}{\lambda}$
Thermal homogeneity	$\pi_6 = \frac{\lambda \cdot \Delta T_H \cdot D \cdot L}{\dot{m} \cdot c_p \cdot (T_m - T_r) \cdot h}$

First, the steady-state energy balance of the extruder is considered:

$$P \pm H = \dot{m} \cdot c_v \cdot (T_1 - T_0) + \Delta p \cdot \dot{V} \quad (13)$$

Here, P is the driving power and H is the heating or cooling contribution, c_v the specific heat capacity at constant volume and T_1 and T_0 temperatures at time 0 and 1. The first term on the right side of the equation describes the enthalpy change in the material and the second one represents the pump energy. By dividing the entire equation by the enthalpy term, the first three Π_i- quantities (Table 4.12) can be established.

Table 4.13. Menges and Feistkorn determined exponents[16].

A (variables)	Exponents
L	$1 + \omega$
(D – a)	ψ
h	ψ
n	$-x$
S	ε
$\dot{\gamma}$	$-(\psi + x - 1)$
$T_m - T_r$	$\xi(\psi + x - 1)$
p	$\xi(\psi + x - 1)$
$\dot{m}$	$\varepsilon + \psi - x + 1$
P	$\varepsilon + \psi - x + 1 + \xi(\psi + x - 1)$
H	$\varepsilon + \psi - x + 1 + \xi(\psi + x - 1)$
M_D	$\varepsilon + \psi - x + 1 + \xi(\psi + x - 1)$
$\bar{t}$	$\omega + x - \varepsilon + 1$
$\dot{q}$	$\psi + \varepsilon - x - \omega - 1 + \xi(\psi + x - 1)$
ΔT_H	$2\psi + \varepsilon - x - \omega - 1 + \xi(\psi + x - 1)$
i	0

Table 4.14. Geometry and process parameters of the model and target extruder according to the Menges and Feistkorn scale-up method

A (variables)	Exponent		D/D_0	A	A_0	A/A_0
L	$1+\omega$	$\omega = 0.22$	0.67	720	990	0.73
(D – a)	ψ	$\psi^* = 0.71$	0.67	3.0	4.0	0.75
h	ψ	$\psi = 0.76$	0.67	3.2	4.4	0.74
n	$-x$	$x = 0.29$	0.67	120 / 200	107 / 178	1.125
S	ε	$\varepsilon = -0.35$	0.67	1.2	1.1	1.15
$\dot{\gamma}$	$-(\psi + x - 1)$	0	0.67	–	–	–
ṁ	$\varepsilon + \psi - x + 1$	1.12	0.37	2	3.15	1.20

The fourth one is the mixing factor, which is basically the ratio between the drag flow and the pressure flow. The last two Π_i- quantities are linked to the thermal properties and reflect the heat transfer and the thermal homogeneity. This is critical since most APIs and excipients are thermally unstable. The shown Π_i were derived and presented in the paper of Menges and Feistkorn [16], [17], hence we call this method the Menges approach (marked with M in the paper) method throughout the paper. [17] Using the established Π_i quantities, model laws can be derived. These laws consist of the relationship between the ratio of the diameters (with some exponent) and the searched variables (geometry or process parameter), as shown in:

$$\frac{A}{A_0} = \left(\frac{D}{D_0}\right)^{exp} \tag{14}$$

Here, *A* and A_0 are the variables (where subscript *0* stands for the original/model extruder), and *D* and D_0 are the screw diameters of the target and original/model extruder, respectively [16], [17]. The main task then is to determine the exponents for the various process and geometry variables. As we are looking at the Menges scale-up approach, we adapted his results (they were looking at a counter-rotating extruder, whereas we are investigating co-rotation extruders) and presented them in Table 4.13. The exponents ω, ψ and ε are determined from equation 14. The exponent x has to be determined by setting a boundary condition for the screw speed and throughput, and the remaining once are calculated as:

$$\psi = \frac{3-\varepsilon-\kappa+\omega+\xi}{2-\kappa+\xi} - x \cdot \frac{\xi+1-\kappa}{2-\kappa+\xi} \tag{15}$$

$$\kappa = -\frac{\ln\frac{\eta}{\eta_0}}{\ln\frac{\dot{\gamma}}{\dot{\gamma}_0}}; at\ T = const. \tag{16}$$

$$\xi = -\frac{\ln\frac{T_m}{T_{m0}}}{\ln\frac{\dot{\gamma}}{\dot{\gamma}_0}}; at\ \eta = const. \tag{17}$$

As can be seen from equation 15 to 17, the exponents ψ, κ and ξ are a function of the material viscosity. Choosing the correct viscosity point (or correct shear rate) and temperature at which to evaluate exponents is challenging without *in silico* tools, as it is difficult or impossible to accurately measure these variables during the process.

The boundary condition used for determining the exponent x is the equal shear rate condition between the two extruders. Setting a constant shear rate constrain is reasonable as the pharmaceutical APIs are shear sensitive. This means that the exponent connected to the shear rate in Table 4.13, $-(\psi + x - 1)$, was set to zero Since the ψ exponent is double-determined, ψ^* was introduced. The rest of the calculated exponents are shown in Table 4.14.

4.7.2 Rauwendaal Scale-up Approach

There are some methods [4], [18], [34], [35] for the process transfer of twin-screw extruders which are not directly based on the Π_i- quantities, offering a more practical approach based on geometrically (e.g., identical D_o/D_i ratio) and energetic similarities (e.g., τ/Cl^3) [36].

Table 4.15. The transfer parameters used according to the Rauwendaal scale-up method.

K_1 [mm]	17.67
K_2 [mm]	19.28
V_{free1} [mm³]	143923
V_{free2} [mm³]	386810

Table 4.16. Technical details of the used extruders.

Specifications	Unit	Pharma-Extruder ZSK 18	MIC 27
Length to diameter ratio	L/D	40	37/1
Barrel length (L)	mm	720	972
Barrel bore diameter	mm	18.2	27.2
Screw diameter (D_o)	mm	18	27
Root diameter (D_i)	mm	11.6	18.3
Diameter ratio (D_o/D_i)	-	1.55	1.48
Channel depth (h)	mm	3.2	4.35
Center-line spacing (a)	mm	15	23
Maximum torque per screw	Nm	34.2	100
Power density	Nm/cm³	10.13	12.5
Maximum screw speed	rpm	1200	400

They all propose that certain quantities, such as the average shear rate, the mean residence time and/or the melt pressure, should be kept constant during the scale transfer. One of these methods is the approach described by Rauwendaal [18], which we used as the second scale-up method (marked with R in the paper). The screw speed n of the target extruder was calculated with the goal of keeping the average shear rate constant, as:

$$n = \frac{K_0 \cdot n_0}{K}; \text{ where } K = \frac{\pi \cdot D}{h_{ave}} \tag{18}$$

Here h_{ave} is the average screw channel depth. The throughput of the target extruder was calculated based on the condition for constant degree of fill:

$$\dot{m} = \frac{V_{free} \cdot n \cdot \dot{m}_0}{V_{free0} \cdot n_0} \tag{19}$$

Here, V_{free} is the free extruder volume. As discussed in the paper, this condition is not effective for assuring the same degree of filling, as it only takes into account the geometrical similarities between the extruders, but not the screw configuration, location and length of the different fully filled zones. The transfer parameters used for the scale-up and the used technical details are listed in Table 4.15 and Table 4.16, respectively.

4.8 Abbreviations

API	Active Pharmaceutical Ingredient
CFD	Computational Fluid Dynamics
CFL	Courant-Friedrich-Lewy condition
HME	Hot-Melt Extrusion
MIC27	Leistritz 27mm co-rotating twin-screw extruder
mRTD	mean Residence Time Distribution
QbD	Quality by Design
RTD	Residence Time Distribution
SMEC	Specific Mechanical Energy Consumption
SPH	Smoothed Particle Hydrodynamics
TSE	co-rotating Twin-Screw Extruder
WLF	Williams-Landel-Ferry
ZSK18	Coperion 18mm co-rotation twin-screw extruder

4.9 Nomenclature

Latin symbols

a_T [-]	Williams-Landel-Ferry temperature shift factor
A_1, A_2 [-]	Axial intercepts of the pressure characteristics
B_1, B_2 [-]	Axial intercepts of the power characteristics
A_{free} [m²]	Free available cross section
a_z [m/s²]	Axial acceleration
c [m/s]	Speed of sound
$c_{p,s}$, $c_{p,m}$ [J/kgK]	Heat capacity of solid and melt, respectively
c_v [J/m³K]	Specific heat capacity at constant volume
C_1 and C_2 [–,°C]	Fitting parameters for the WLF temperature shift factor
D [m]	Barrel diameter
D_i [m]	Inner screw diameter
D_o [m]	Outer screw diameter
f [-]	Filling degree
H [kW]	Heating and cooling contribution

h [m] SPH smoothing length

h_{ave} [m] Average screw channel depth

K_1, K_2, K_3, K_4, K_8, K_9 [bar cm³/g, bar cm³/g°C, bar, bar, °C, °C/bar] Menges density factors

L and L_0 [m] Screw length and relevant length scale, respectively

$\dot{m}$ [kg/h] Throughput

n [rpm] Screw speed

N_{total} [-] SPH particle number

P [kW] Driving power

p [bar] Pressure

Re [-] Reynolds number

T, T_r and T_g [°C] Melt temperature, reference melt temperature and transition temperature, respectively

$\dot{V}$ [m³/s] Volumetric throughput

V_0 [m/s] Maximal expected fluid velocity

V_{free} [m³] Free available volume

Δp [bar] Pressure drop

Δx [m] Smallest screw-barrel gap distance/SPH particle resolution

Δz [m] Kneading block thickness

Greek symbols

α [°] Cross section/kneading block tilt angle

β [-] Artificial viscosity

$\dot{\gamma}$, $\dot{\gamma}_{crit}$ [s^{-1}] Shear rate and critical shear rate, respectively

δ [-] Relative density variation

η and η_0 [Pas] Fluid viscosity and zero-shear-viscosity, respectively

λ [W/mK] Thermal conductivity

ν [m²/s] Kinematic fluid viscosity

ρ, ρ_0 [kg/m³] Fluid density and initial fluid density, respectively

τ [Nm] Extruder torque

$\omega, \psi, \varepsilon, \chi, \kappa, \xi$ [-] Exponents of the Menges and Feistkorn scale-up method

4.10 References

[1] J. Breitenbach, "Melt extrusion: from process to drug delivery technology," *Eur. J. Pharm. Biopharm.*, vol. 54, no. 2, pp. 107–117, Sep. 2002.

[2] H. Patil *et al.*, "Hot-Melt Extrusion: from Theory to Application in Pharmaceutical Formulation," *AAPS PharmSciTech*, vol. 17, no. 1, pp. 20–42, Sep. 2015.

[3] M. M. Crowley *et al.*, "Pharmaceutical Applications of Hot-Melt Extrusion: Part I," *Drug Dev. Ind. Pharm.*, vol. 33, no. 9, pp. 909–926, Jan. 2007.

[4] K. Kohlgrüber and W. Wiedmann, *Co-Rotating Twin Screw Extruder: Fundamental, Technologies and Applications*. Munich: Carl Hanser Publishers, 2008.

[5] Dr. Chris Rauwendaal, *Rauwendaal Polymer Extrusion*. Munich: Carl Hanser Verlag, 2014.

[6] H. Patil, R. V. Tiwari, and M. A. Repka, "Hot-Melt Extrusion: from Theory to Application in Pharmaceutical Formulation," *AAPS PharmSciTech*, vol. 17, no. 1, pp. 20–42, Feb. 2016.

[7] M. Maniruzzaman, J. S. Boateng, M. J. Snowden, and D. Douroumis, "A Review of Hot-Melt Extrusion: Process Technology to Pharmaceutical Products," *ISRN Pharm.*, vol. 2012, pp. 1–9, 2012.

[8] D. Douroumis, *Hot-Melt Extrusion: Pharmaceutical Applications*. Chichester, UK: John Wiley & Sons, Ltd, 2012.

[9] A. Eitzlmayr *et al.*, "Mechanistic modeling of modular co-rotating twin-screw extruders," *Int. J. Pharm.*, vol. 474, no. 1–2, pp. 157–176, Oct. 2014.

[10] A. Eitzlmayr *et al.*, "Experimental characterization and modeling of twin-screw extruder elements for pharmaceutical hot melt extrusion," *AIChE J.*, vol. 59, no. 11, pp. 4440–4450, Nov. 2013.

[11] R. Baumgartner, J. Matić, S. Schrank, S. Laske, J. G. Khinast, and E. Roblegg, "NANEX: Process Design and Optimization," *Internaitonal J. Pharm.*, vol. 506, pp. 35–45, 2016.

[12] A. Eitzlmayr, G. Koscher, and J. G. Khinast, "A novel method for modeling of complex wall geometries in smoothed particle hydrodynamics," *Comput. Phys. Commun.*, vol. 185, no. 10, pp. 2436–2448, Oct. 2014.

[13] A. Eitzlmayr and J. G. Khinast, "Co-rotating twin-screw extruders: Detailed analysis of

conveying elements based on smoothed particle hydrodynamics. Part 1: Hydrodynamics," *Chem. Eng. Sci.*, vol. 134, pp. 861–879, Sep. 2015.

[14] A. Eitzlmayr and J. Khinast, "Co-rotating twin-screw extruders: Detailed analysis of conveying elements based on smoothed particle hydrodynamics. Part 2: Mixing," *Chem. Eng. Sci.*, vol. 134, pp. 880–886, Sep. 2015.

[15] A. Eitzlmayr, J. Matić, and J. G. Khinast, "Analysis of flow and mixing in screw elements of corotating twin-screw extruders via SPH," *AIChE J.*, vol. 63, no. 6, pp. 2451–2463, Jun. 2017.

[16] G. Menges and W. Feistkorn, "Scale-Up of twin screw extruders application and verification with the example of PVC," *Adv. Polym. Technol.*, vol. 4, no. 2, pp. 123–129, 1984.

[17] G. Menges, J. Wortberg, and A. Mayer, "Model theory—an approach to design series of single-screw extruders," *Adv. Polym. Technol.*, vol. 3, no. 2, pp. 157–165, 1983.

[18] C. Rauwendaal, "Twin Screw Extruders," in *Polymer Extrusion (Fifth Edition)*, Fifth Edit., C. Rauwendaal, Ed. Hanser, 2014, pp. 697–761.

[19] J. Pawlowski, *Die Ähnlichkeitstheorie in der physikalisch-technischen Forschung*. Berlin, Heidelberg: Springer Berlin Heidelberg, 1971.

[20] M. B. Liu and G. R. Liu, "Smoothed Particle Hydrodynamics (SPH): an Overview and Recent Developments," *Arch. Comput. Methods Eng.*, vol. 17, no. 1, pp. 25–76, Feb. 2010.

[21] G. R. Liu and M. B. Liu, *Smoothed Particle Hydrodynamics a mesfree particle method*. Singapore: World Scientific Publishing Co. Pte. Ltd., 2003.

[22] G. R. Liu, *Mesh Free Methods*. CRC Press LLC, 2003.

[23] G. R. Liu and Y. T. Gu, *An Introduction to Meshfree Methods and Their Programming*. Berlin/Heidelberg: Springer-Verlag, 2005.

[24] J. J. Monaghan, "Smoothed particle hydrodynamics," *Reports Prog. Phys.*, vol. 68, no. 8, pp. 1703–1759, Aug. 2005.

[25] D. Violeau, *Fluid Mechanics and the SPH Method*. Oxford: Oxford University Press, 2012.

[26] K. Kohlgrüber, *Co-Rotating Twin Screw Extruder: Fundamental, Technologies and Applications*. Munich: Carl Hanser Publishers, 2008.

[27] J. ~.- Morris and P. ~J. Fox, "Modeling low Reynolds number incompressible flows using SPH," *J. Comput. Phys.*, vol. 136, no. 136, pp. 214–226, 1997.

[28] Singh S, R. J. Inamullah, N. Choudhary, and Sharma S, "An Official Publication of Association of Pharmacy Professionals STABILITY-INDICATING UV-VIS SPECTROPHOTOMETRIC METHOD FOR ESTIMATION OF ATORVASTATIN CALCIUM AND FENOFIBRATE IN TABLET DOSAGE FORM," *Bull. Pharm. Res.*, vol. 2, no. 3, pp. 159–66, 2012.

[29] D. R. Morgan, S. Kalachandra, H. K. Shobha, N. Gunduz, and E. O. Stejskal, "Analysis of a dimethacrylate copolymer (Bis-GMA and TEGDMA) network by DSC and 13C solution and solid-state NMR spectroscopy," *Biomaterials*, vol. 21, no. 18, pp. 1897–1903, 2000.

[30] K. Eggenreich *et al.*, "Injection molding as a one-step process for the direct production of pharmaceutical dosage forms from primary powders," *Int. J. Pharm.*, vol. 505, no. 1–2, pp. 341–351, May 2016.

[31] G. Terife, P. Wang, N. Faridi, and C. G. Gogos, "Hot Melt Mixing and Foaming of Soluplus and Indomethacin," *Polym. Eng. Sci.*, vol. 52, no. 8, pp. 1629–1639, 2012.

[32] M. Zlokarnik, "Dimensionsanalyse," in *Scale-up: Modelluebertragung in der Verfahrenstechnik*, Second Edi., Weinheim: Wiley-VCH Verlag GmbH & Co. KGaA, 2005, pp. 3–15.

[33] H. Herwig, *Strömungsmechanik*. Wiesbaden: Vieweg Teubner Verlag, 2008.

[34] J. Thiry, F. Krier, and B. Evrard, "A review of pharmaceutical extrusion: Critical process parameters and scaling-up," *Int. J. Pharm.*, vol. 479, no. 1, pp. 227–240, 2015.

[35] C. Rauwendaal, "Scale-up of single screw extruders," *Polym. Eng. Sci.*, vol. 27, no. 14, pp. 1059–1068, Aug. 1987.

[36] K. Kohlgrüber, *Co-Rotating Twin Screw Extruder: Fundamental, Technologies and Applications*. Carl Hanser Publishers, 2008.

5

Towards Predicting the Product Quality in Hot Melt Extrusion: Small Scale Extrusion*

In product development, it is crucial to choose the appropriate drug manufacturing route accurately and timely and to ensure that the technique selected is suitable for achieving the desired product quality. Guided by the QbD principles, the pharmaceutical industry is currently transitioning from batch to continuous manufacturing. In this context, process understanding and prediction are becoming even more important. With regard to hot melt extrusion, the process setup, optimization and scale-up in early stages of product development are particularly challenging due to poor process understanding, complex product-process relationship and a small amount of premix available for extensive experimental studies. Hence, automated, quick and reliable process setup and scale-up requires simulation tools that are accurate enough to capture the process and determine the product-process relationships. To this end, the effect of process settings on the degradation of the active pharmaceutical ingredient (API) in a lab-scale Leistritz ZSE12 extruder was investigated. As part of the presented study, the limitations of traditional process analysis using integral process values were investigated, together with the potential that simulations may have in predicting the process performance and the product quality. The results of our investigation indicate that the average melt temperatures and the exposure times in specific zones along the screw configuration correlate well with the API degradation values and can be used as potent process design criteria to simplify the process development.

---

* This chapter is based on: J. Matić, C. Alva, A. Witschnigg, S. Eder, K. Reusch, A. Paudel and J. Khinast, "Towards Predicting Product Quality in Hot Melt Extrusion: Small Scale Extrusion" *Int. J. Pharm. X*, vol. 2, p. 100062, Dec. 2020.

5.1 Introduction

Hot melt extrusion (HME) is increasingly applied in the pharmaceutical industry, mostly for solubilization of poorly soluble active pharmaceutical ingredients [1]–[5] (APIs) in immediate release, control release [6]–[8] and nano [9]–[13] formulations, as well as for the manufacturing of specific drug delivery devices [14]–[17]. This trend calls for fast, reliable and inexpensive product and process development [18]–[28]. Typically, formulation and process development are disconnected, i.e., during the formulation development the formulation's processability is not considered. If at all, the formulation is only tested in a table-top-scale extruder, making it extremely challenging to transfer the product to the pilot and production scales. With that regard, the flexibility of HME in terms of process settings and screw configurations (the significant width of processing window) is of advantage, since a variety of formulations can be processed and various product goals can be fulfilled (e.g., immediate or controlled release formulations).

However, defining the optimal setting within this wide process window is challenging, especially across different scales. Thus, many tests are conducted to optimize the process performance. In addition, there are no universally applicable scale-up laws and the screw designs are not necessarily directly transferable (especially when multiple extruder vendors are involved). The process windows can vary so significantly that certain formulations are simply not processable on a bigger extruder. Lastly, few people in the pharmaceutical industry are trained to design, scale and optimize HME processes. All of this contributes to a significant increase in the development costs and risks, making HME an unlikely production choice. In light of that, significant effort has been made to better understand the technology and the process-product relationships, which is in alignment with the FDA Quality by Design (QbD) guidelines for pharmaceutical processes [29]–[34].

In terms of process development and transfer, the HME process is still mostly viewed as a black-box, and subtle differences in the screw geometry, screw configuration and processing conditions between the various extruder scales are been neglected or disregarded. The reason is relatively simple: although crucial for process understanding, experimental methods cannot offer insights into the extruder operation since only global parameters can be determined (e.g., the overall specific mechanical energy (SMEC), residence time distribution (RTD) of the process and the melt pressure and temperature at the die) for a given screw configuration and process settings. Resolved and detailed information (local fill rates, temperature inhomogeneity in the melt, shear distributions, pressures, etc.) are generally not available and cannot be

obtained even using sophisticated PAT (Process Analytical Technology) equipment. Simulation methods can tackle these challenges and provide a much deeper process understanding. Considering the costs and complexity of process setup, it would be desirable to estimate the potential process windows and product quality ranges early on in the formulation phase, during which small amounts of API are typically available. This way, it would be possible to choose candidate formulations adequately and early on in the development stage.
Essentially, for a model-based process design for a specific formulation, three prerequisites exist:

- a small-scale measurement methodology sufficiently similar to HME that requires small amounts of the formulation, with the goal of testing the formulation's response to various mechanical stress conditions;
- a solid process understanding, i.e., a process model that predicts the process response (filling degree, melt temperature, RTD, SMEC, etc.) as a function of input parameters (screw configuration, screw speed, throughput, barrel temperature, etc.); and
- a link between the critical material attributes (CMAs), the critical process parameters (CPPs) and the formulation responses (i.e., critical quality attributes, CQAs), in order to map out regions where the in-spec quality product is obtained. This is also known as the Design Space (DS) according to the QbD terminology.

To date, our group has worked intensively on the first two issues, developing a vacuum compression molding tool for rapid sample preparation [16], [35] and creating a high-fidelity Lagrangian simulation environment that is based on a combination of Smoothed Particle Hydrodynamics (SPH) and 1D mechanistic modelling as a tool for the HME process understanding, design and scale-up [36]–[40]. In our framework, SPH was used for a detailed 3D characterization of individual screw element pairs commonly found in co-rotating intermeshing twin screw extruders. The focus was on determining the dimensionless pressure build-up and power consumption [18], [41] of the element pairs, as well as their distributive mixing action. The knowledge gained was subsequently applied for our 1D HME simulation code developed in-house, which accurately computes axial distributions of filling degree, pressure, melt temperature, SMEC, and local and overall RTDs. Details on the internals of the 1D HME code, the assumption, connections to the SPH simulation results, melt temperature calculation procedure, heat transfer coefficient calculations and so on, can be found in papers published earlier from our group [36], [40]. Unlike the commercially available 1D codes for extrusion, to calculate the melt flow 1D HME utilizes the dimensionless pressure and power

characteristics and the distributive mixing action as the descriptor of individual screw performance, rather than simplified screw geometries. This is particularly advantageous when using nonstandard, complex mixing and/or kneading elements with discontinuous screw geometries, where the pressure and power characters can easily be calculated by means of high-fidelity 3D SPH simulations.

The underlying assumption of our approach is that the product quality is the result of the formulation's thermo-mechanical exposure during the process. If the thermo-mechanical history can be mirrored on various scales, so can be the resulting quality. With that regard, considering the full complexity of the process is crucial, rather than treating the process as a black-box problem (i.e., analyzing it based on integral values of SMEC and RTD and, occasionally, die melt temperature and pressure). The influence of every screw element in the screw configuration has to be examined, and the screw setup has to be addressed adequately in order to reach appropriate states of thermo-mechanical load on the product on various extruder scales.

The present study addresses the third point on the list by examining the influence of process conditions on the API degradation in a lab scale 12mm (ZSE12) intermeshing co-rotation twin screw extruder from Leistritz. It included the process setup for the small-scale extruder (ZSE12), a comparison between the predicted (via 1D HME) and experimentally obtained process responses and an investigation of the product quality as a response to the process settings selected. First, the link between the product quality, the process settings and the readily available process variables, such as torque, SMEC and mean residence time distribution (mRTD) was investigated. This attempt resulted in limited success. However, the investigation was extended to include the possible correlations between the product quality and the process variables that are not easily available to an average process engineer, e.g., the melt temperature in a specific zone along the screw configuration and the mean residence time associated with that zone (local exposure time a certain local temperature peak). This is the novelty of the presented study and can be considered a step forward in extruder process setup, scale-up and design.

The overall goal of this study was to achieve a better understanding of the relation between the product quality attributes selected (i.e., degradation) and the HME settings in order to achieve a more reliable process setup and scale-up based on modeling.

5.2 Materials and Methods

5.2.1 Equipment and Process setup

As mentioned above, in this study the ZSE12 12 mm extruder from Leistritz was used. This choice is in line with the initial product development phase that generally begins with the formulation screening and involves a small-scale extruder to minimize the amount of material requested and keep the process uncomplicated. The general extruder dimensions and a cross section of the ZSE12 extruder are presented in Table 5.1 and Figure 5.1.

The used screw configuration was the only one available at the time since the equipment was still in its prototype state. Six screw elements make up the entire configuration, of which three are standard conveying elements with pitches of 10mm, 16mm and 20mm. The other three screw elements are kneading elements with angles (α in Figure 5.1) of 30°, 60° and 90° between the individual kneading blocks. The full screw configuration has a length of 480mm (standard 40L/D), as shown in Table 5.2 and Figure 5.2, and various processing zones. The powder intake zone consists of a series of conveying elements with a pitch of 20mm, ending with two 16mm pitcher elements before the melting zone. High-pitched conveying elements in the beginning of the powder intake zone are used for increasing the available free volume of the powder feed and achieving the maximum throughput for the extruder. Reducing the pitch before the kneading zone serves two purposes: (1) the powder is compacted, eliminating air pockets that might have formed; and (2) the lower pitch elements are more suitable for pressure build-up before the first kneading zone.

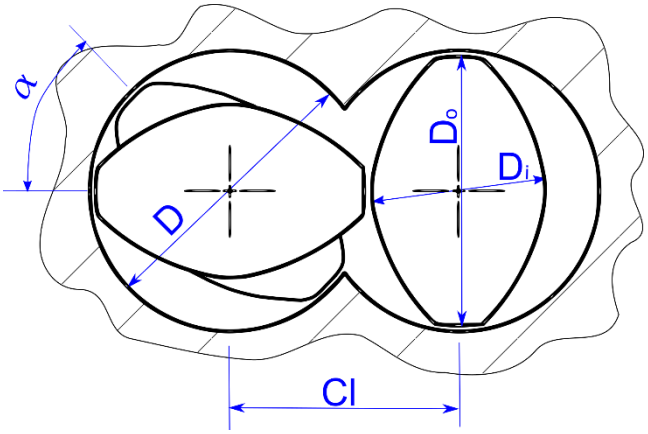

Figure 5.1. Details of the twin-screw extruder screw cross section showing the barrel diameter (D), screw outer and inner diameters (D_o and D_i, respectively), screw centerline distance (Cl) and the angle between the kneading discs for kneading elements (α).

Table 5.1. General characteristics of Leistritz lab-scale 12mm ZSE12 HP-PH extruders.

ZSE12 HP-PH	
D – Barrel diameter	12mm
D_o – Outer screw diameter	11.85mm
D_i – Inner screw diameter	7.85mm
Cl – centerline distance	10mm
τ_{max} – Maximal available torque	20Nm
Theoretical throughput range	0.05 – 1kg/h
n – Screw speed	up to 1000rpm

The first kneading zone (also melting zone) contains a combination of 30° and 60° kneading elements. Its process function is to fully melt the polymer-API mixture. The setup involving two angles of the kneading elements results in different inherent conveying capabilities, which creates a “soft” back-conveying zone. As a result, a small section with an increased fill degree can be expected. The kneading zones following the initial melting zone consist of three sections and ensuring the various stages of distributive and dispersive mixing action and increased mechanical energy input: the first one with a 90° kneading element, the second one with a combination of 30° and 60° kneading elements and the third one with a 60° kneading element. Note that the first and third kneading section have the same configuration (i.e., a combination of 30° kneading element followed by a 60° kneading element) but different process functions (i.e., melting and mixing, respectively). Three mixing zones are not required for the formulation examined and such a screw setup is normally used when liquid and/or secondary powder feeding in employed in the remaining conveying sections (which is not the case in this study). Before the die, a pressure build-up zone is set up by reducing the conveying element pitch: first, from 20 mm to 16 mm and then to 10 mm. The goal is to build up enough pressure to force the extrudate through the die. The die has a cylindrical length of 3.75 mm and a cylindrical diameter of 2 mm. The same screw configuration with the inherent conveying and pressure build-up numbers of the individual screw element pairs was also used as a basis for the screw discretization in the 1D HME simulations.

Table 5.2. The screw configuration for the trials on the ZSE12 prototype extruder, with the used A_1 and A_2 parameters for the 1D HME simulations.

Official Name	Short Name	Screw Length [mm]	Pitch/Angle [mm/°]
GFA-2-20-30-A	C20	30	20
GFA-2-20-30	C20	30	20
GFA-2-20-30	C20	30	20
GFA-2-20-10	C20	10	20
GFA-2-16-20	C16	20	16
GFA-2-16-20	C16	20	16
GFA-2-16-20	C16	20	16
KB4-2-10-30°-Re	K30	10	30°
KB4-2-10-60°-Re	K60	10	60°
GFA-2-16-10	C16	10	16
KB4-2-10-90°	K90	10	90°
GFA-2-16-20	C16	20	16
GFA-2-16-20	C16	20	16
KB4-2-10-30°-Re	K30	10	30°
KB4-2-10-60°-Re	K60	10	60°
GFA-2-16-20	C16	20	16
GFA-2-16-20	C16	20	16
GFA-2-16-20	C16	20	16
GFA-2-16-20	C16	20	16
KB4-2-10-60°-Re	K60	10	60°
GFA-2-16-20	C16	20	16
GFA-2-16-20	C16	20	16
GFA-2-16-20	C16	20	16
GFA-2-16-10	C16	10	16
GFA-2-10-20	C10	20	10
GFA-2-10-20	C10	20	10
GFA-2-10-20	C10	20	10
	Total length:	480mm	

Nomenclature: C-conveying element; K-kneading element.

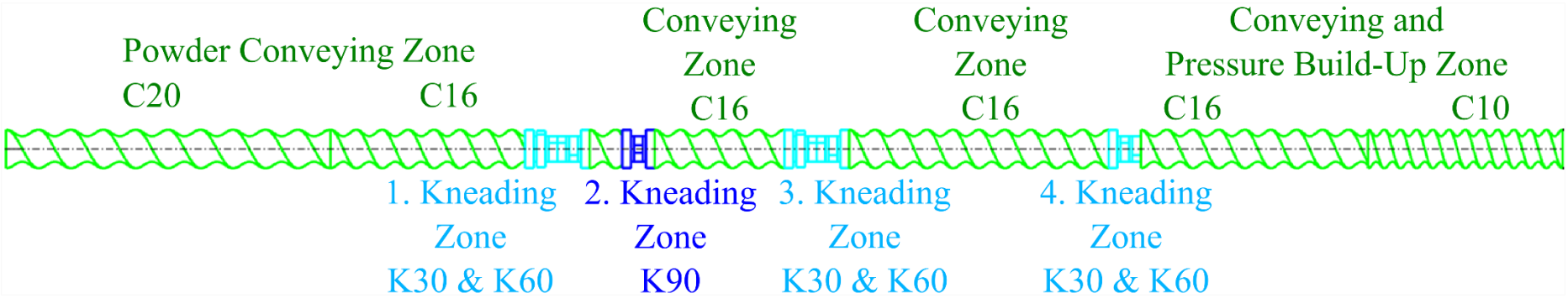

Figure 5.2. Prototype screw configuration used for the ZSE12 extruder experiments and 1D HME simulations. The screw configuration is assembled from three conveying elements with pitches for 20mm, 16mm and 10mm (C20, C16 and C10 respectively), and kneading elements with an angle between the discs of 30°, 60° and 90° (K30, K60 and K90 respectively).

The process settings (screw speed, throughput and barrel temperature) were chosen to cover the broadest processing window possible, disregarding the possible ramifications for the product quality. The goal of any formulation and process development step is the production of an in-spec product (in our case, amorphous API without any degradation). However, assuming that in-spec product can be achieved within a process window (i.e., the design space), it may be even more interesting to study under which process conditions the product fails and why (i.e., the envelope of failure). Hence, the process throughput was set from 0.1 kg/h to 0.4 kg/h; the screw speed was set to 100rpm, 300 rpm and 500rpm. The two barrel temperature settings were 120°C and 140°C, ensuring a broad process window for our study. Details of process settings are provided in Table 5.3 and Table 5.4.

Table 5.3. Throughputs, screw speeds and barrel temperature profiles used for the ZSE12 trials and 1D HME simulations.

Exp. Nr.	Throughput [kg/h]	Screw speed [rpm]	Barrel temperature profile
PN 1	0.1	100	I
PN 2	0.4		
PN 3	0.1	100	II
PN 4	0.4		
PN 5	0.1	300	I
PN 6	0.4		
PN 7	0.1	300	II
PN 8	0.4		
PN 9	0.1	500	I
PN 10	0.4		
PN 11	0.1	500	II
PN 12	0.4		

Table 5.4. Barrel temperature settings used for the ZSE12 trials and simulations.

Profile	Barrel 1	Barrel 2	Barrel 3	Barrel 4	Barrel 5	Barrel 6	Barrel 7	Barrel 8	Die
I	40°C	60°C	120°C	120°C	120°C	120°C	120°C	120°C	120°C
II	40°C	60°C	140°C	140°C	140°C	140°C	140°C	140°C	140°C

5.2.2 Formulation

The model formulation was a simple two-component system comprising Eudragit RL PO with a 20% mass loading of Famotidine. Famotidine is prone to thermal degradation. Eudragit RL PO is an established polymer applied in hot-melt-extruded formulations [42]–[44]. Famotidine commercially available as polymorph B (Haihang Industry Co., Ltd., China) and Eudragit RL PO (Evonik Industries, Germany) were the materials used in the extrusion experiments. Pre-blends with 20% of Famotidine content were prepared in 2L containers (1 kg) and mixed with the Turbula T2F (WAB-Group, Switzerland) for 10 min at 60 rpm.

Research shows that the two components do not interact with each other [45]. They are suitable candidates for the preparation of solid dispersions since the melting point of Famotidine (form B, 166°) and the expected extrusion temperature window of Eudragit RL (165-170°C) [46] are within a similar temperature range. Furthermore, Famotidine is a thermolabile drug, which begins to degrade shortly after melting [47], making degradation a probable event in the chosen process settings.

To model the process via our 1D HME simulation tool, the used formulation had to be parametrized. Heat capacity, thermal conductivity, specific volume and viscosity of the selected formulation were measured, analyzed and fitted with suitable models. The PVT behavior of the formulation was measured using a PVT100 device in accordance with the ISO 17744 guidelines. The measurements were performed at 40°C-220°C and 200bar-1200bar. The data obtained were fitted to the Schmidt model [48] in order to be used in the 1D HME simulations to calculate specific volume v $[cm^3/g]$:

$$v_{(p,T)} = \frac{K_1}{p+K_4} + \frac{K_2 \cdot T}{p+K_3} \quad (1)$$

Two sets of K_1 to K_4 parameters are used, one for the solid phase (if temperature T is below the transition temperature) and one for the liquid phase (if temperature T [°C] is above the transition temperature). The transition temperature T_{tr} $[°C]$ is a function of pressure p [bar] and is calculated as:

$$T_{tr(p)} = K_8 + K_9 \cdot p \quad (2)$$

The relevant K_1 to K_9 parameters can be found in Table 5.5.

Rheology of the formulation was measured with a standard plate-plate rheometer (MCR 301 from Anton-Paar). The sample preparation for the rheology measurements was performed using the vacuum compression molding tool, that was specifically developed for such purposes [35]. The frequency range measured spans between $0.1s^{-1}$ to $628s^{-1}$ for three probe temperatures of

100°C, 115°C and 130°C. The data points obtained were subsequently fitted via a simplified variant of the Carreau-Yassuda model for non-Newtonian fluids:

$$\eta(\dot{\gamma}, T) = \frac{\eta_0 a_T}{\left(1+\frac{|\dot{\gamma}|a_T}{\dot{\gamma}_{crit}}\right)^m} \quad (3)$$

where η ist the viscosity in $[Pa \cdot s]$, $T[°C]$ is the melt temperature, $\dot{\gamma}[s^{-1}]$ is the shear rate, $\dot{\gamma}_{crit}[s^{-1}]$ is the critical shear rate, $\eta_0[Pa \cdot s]$ the zero-shear-rate viscosity and a_T $[-]$ is the Williams-Landel-Ferry temperature shift factor calculated as:

$$a_T[-] = exp\left[-\frac{C_1(T-T_r)}{C_2+T-T_r}\right] \quad (4)$$

with $T_r[°C]$ being the reference temperature. The viscosity parameters used for the fit are shown in

Table 5.6.

Table 5.5. K parameters used for the calculating of the specific volume according to the Schmidt model.

	Solid state	Melt state
K1 [bar cm³/g]	28811	35221
K2 [bar cm³/(g°C)]	1.0731	1.2637
K3 [bar]	3050.1	2650.9
K4 [bar]	35556	44179
K8 [°C]	106.12	
K9 [°C/bar]	0.002816	

Table 5.6. Parameters for the Carreau-Yassuda viscosity fit.

η_0 [Pas]	50250
$\dot{\gamma}_{crit}$ [s^{-1}]	0.64
m [-]	0.5703
T_r [°C]	130
C_1 [-]	15.1378
C_2 [°C]	132.0361

The heat capacity and thermal conductivity were approximated via linear temperature-dependent fits. Both were measured via modulated differential scanning calorimetry (mDSC) using the DSC 2014 F1 Phoenix® with an automated sampling unit (NETZSCH-Geraetebau GmbH, Selb, Germany). The heat capacity $[J/m^3K]$ below glass transition temperature $T_g = 65°C$ is:

$$c_{p,s} = -273.04 + 38.22 \cdot T \quad (5)$$

and above the glass transition temperature as:

$$c_{p,m} = 2095.35 + 1.55 \cdot T \quad (6)$$

The thermal conductivity $\lambda[W/mK]$ was modeled as:

$$\lambda = 0.15633 + 4.704 \cdot 10^{-4} \cdot T \quad (7)$$

where T is the melt temperature.

5.2.3 Mean residence time measurements

In the course of the process, the residence time distribution (RTD) was measured, evaluated and compared to the results obtained via 1D HME. The measurements were executed after a steady state was reached and samples for product-quality measurements were obtained. A blue pigmented tracer pellet of approximately 10-20mg was inserted into the extruder's powder inlet. At the same time a camera (Fujifilm Fine Pix HS25EXR) began recording the die's strand outlet. The resulting videos were post-processed in Matlab® (Mathworks, Natick, MA, USA) using the script developed earlier [49]–[51]. Each video frame was analyzed to determine the average values assigned to the RGB color space within a specified mask, which deliberately included only the portion of strand where the color change was observed. For a better signal, the score of 1st Principal Components (PC1) of RGB values was computed and accessed. The PC1 signals obtained were fitted to an analytical solution of the Fokker-Planck equation for twin-screw extruders, where the exit age distribution $E(\tau)$ is a function of the Peclet number Pe and the dimensionless time $\tau = t/\theta$, with t being the actual time and θ being the mean residence time (mRT):

$$color\ values = k\ f(Pe, \tau) \quad (8)$$

$$\mathrm{E}(\tau) = \mathrm{f}(\mathrm{Pe}, \tau) = \sqrt{\frac{\mathrm{Pe}}{\pi\tau}} \exp\left(-\frac{\mathrm{Pe}}{4}\frac{(1-\tau)^2}{\tau}\right) - \frac{\mathrm{Pe}}{2}\exp(\mathrm{Pe})\,\mathrm{erfc}\left(\sqrt{\frac{\mathrm{Pe}}{4}}\frac{1+\tau}{\sqrt{\tau}}\right) \quad (9)$$

5.2.4 API degradation

The extrudate samples consisted of pellets from the strand granulator collected after reaching a steady process. Triplicates of randomly-sampled pellets were weighed in volumetric flasks and dissolved in methanol in an ultrasound bath for 10 min. The resulting solutions were transparent, ranging from colorless to red, correlating with the extrudate color. This suggests that the impurity responsible for the color may be soluble in methanol. The percent of degradation f was calculated based on the difference between initial pre-blend content C_0 and final extrudate content $C_{extrudate}$ from the UPLC measurements.

$$f = \frac{C_0 - C_{extrudate}}{C_0} \cdot 100\% \quad (10)$$

Table 5.7. HPLC method for the Famotidine detection.

Column	Waters Acquity UPLC T3 1.8µm x 100mm	
Calibration Range	50-700ppm	
Flow	0.400ml/min	
Wavelength	266nm	
Column Temperature	40°C	
Sample Temperature	20°C	
Injection Volume	1µl	
Duration	10min	
Mobile Phase Flow		
Time [min]	Volume [%]	
	0.03% TFA in Water	ACN
0.0	97	3
0.5	97	3
1.0	20	80
8.0	20	80
8.1	97	3
10.0	97	3

ACN = acentonitryl
TFA = trifluoroacetic acid

The content of Famotidine from the extrudates Famotidine solutions was obtained via UPLC using an Acquity UPLC™ HSS T3 (100 × 2.1 mm^2) 1.8-µm column at 40°C and a detection wavelength of 266 nm. Gradient elution was applied to separate FAM from its impurities, with a mobile phase of ACN (acetronytril) and TFA (trifluoroacetic acid) in water, a variable composition over time and a constant flow rate of 0.4 m**L**/min. Full specifications are provided in Table 5.7.

5.3 Results and Discussion

5.3.1 Effect of process settings on the extruder state

As part of the process control and simulation validation efforts, the process torque, SMEC and RTD were captured, analyzed and compared to the values obtained in the 1D HME simulations. A detailed analysis can provide valuable insights into the process, showing the effect of the process settings on the filling degree, the melt temperature and the pressure profile (see our earlier work [52]). A comparison between the experimental and *in silico* values is important for validating the simulations, including the A1 and A2 values used to parametrize the screws, and the parametrization of the formulation obtained via the material's measurements. Note that the A1 and A2 values represent the inherent conveying and pressure build-up capacities of individual screw element pairs, respectively. They are a dimensionless representation of the conveying and pumping action of the screw geometries and are discussed in more detail in our earlier work [37], [38] and the literature [18], [41]. The experimental and modelled torque and SMEC values are shown in Table 5.8, Figure 5.3 and Figure 5.4, respectively.

Table 5.8. Process and product response for the applied settings.

Trial Nr.	Throughput [kg/h]	Screw speed [rpm]	Barrel temp.	Torque [Nm]	SMEC [kWh/kg]	mRT_{1D} [s]	API Degradation
PN 1	0.1	100	I	3.91	0.410	530	7%
PN 2	0.4			4.25	0.112	164	3%
PN 3	0.1	100	II	2.82	0.295	527	18%
PN 4	0.4			3.30	0.087	163	7%
PN 5	0.1	300	I	3.72	1.170	503	27%
PN 6	0.4			4.42	0.347	136	9%
PN 7	0.1	300	II	3.01	0.947	499	44%
PN 8	0.4			3.73	0.292	135	19%
PN 9	0.1	500	I	3.60	1.884	498	61%
PN 10	0.4			4.29	0.562	131	24%
PN 11	0.1	500	II	2.82	1.477	494	81%
PN 12	0.4			3.39	0.444	130	36%

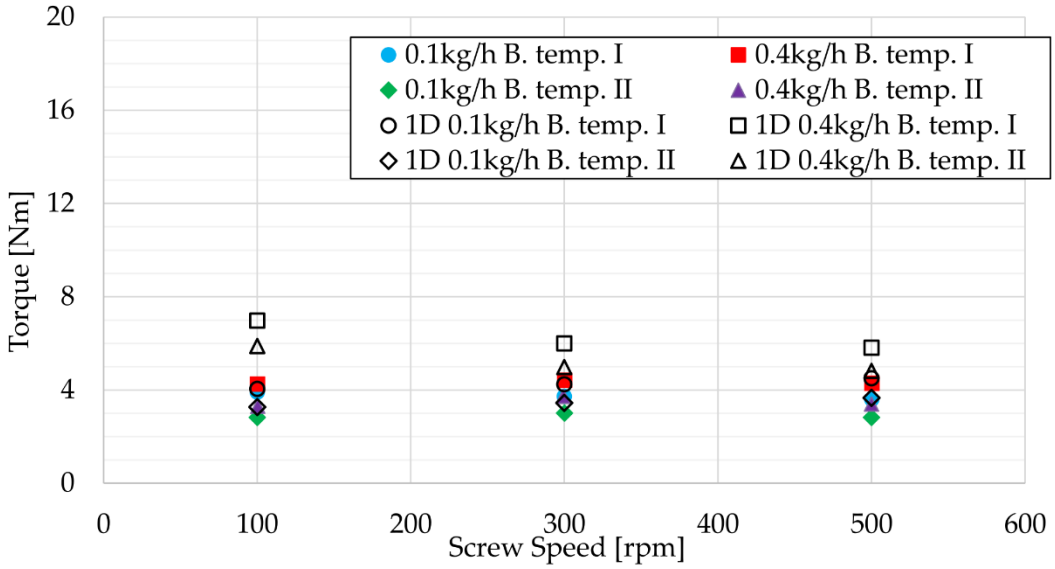

Figure 5.3. Influence of the process settings on the experimentally and *in silico* (1D) obtained extruder torque.

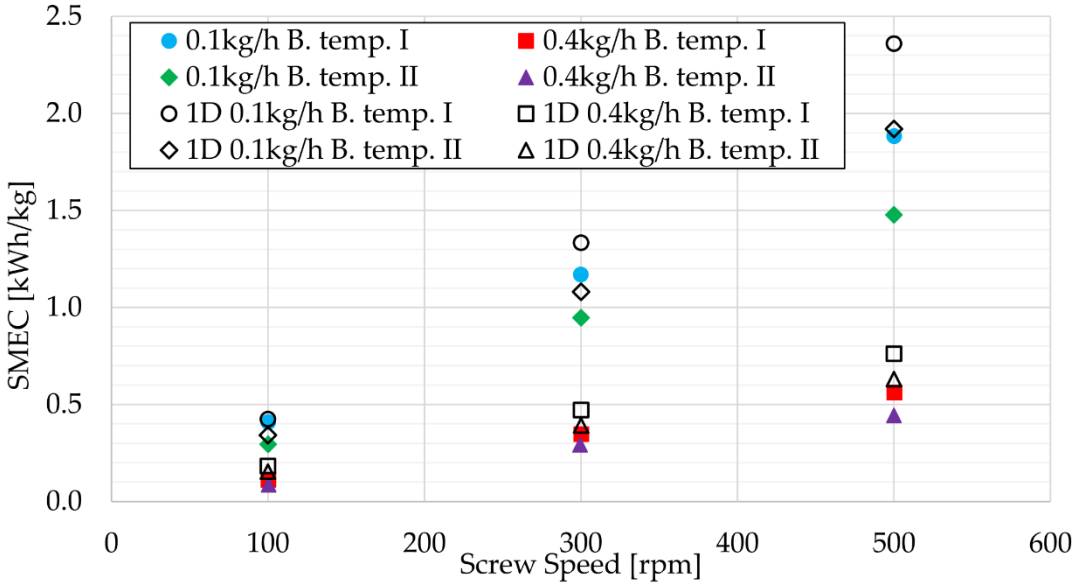

Figure 5.4. Influence of the process settings on the experimentally and *in* silico (1D) obtained process SMEC.

Although the model does not capture the torque exactly, it captures the torque and SMEC trends well. The ZSE12 extruder has a maximal available torque of 20Nm. An increase in the throughput results in an increase in the torque needed for the rotation of the shaft. This is expected since there is more material in the system to be processed. In contrast, an increase in the barrel temperature results in a decrease of the torque needed for processing. This can be attributed to overall higher melt temperature that is achieved due to an equilibrium between the heat dissipation and the higher barrel temperature settings. Higher melt temperature also means a reduced overall melt viscosity and since it lowers the resistance of the processed melt to deformation, it also reduces the torque needed for the screw rotations.

A change in screw speed does not seem to change the process torque in this example, most likely due to relatively low throughputs, i.e., low overall filling degree of the extruder. The torque and SMEC $[kWh/kg]$ are functionally connected as:

$$SMEC = \frac{2 \cdot \pi \cdot n \cdot \tau}{60000 \cdot \dot{m}} \tag{11}$$

Here, n is the rotation rate in [rpm] and τ the torque in [Nm] and $\dot{m}[kg/h]$. SMEC represents the energy the screws provide to process the material per kilogram of material. Therefore, an increase in the screw speed directly translates into more energy per kilogram of processed material. Similarly, an increase in the throughput or the barrel temperature reduces the energy consumed from the screws since the amount of material increases (increased throughput) or energy is provided by the increased barrel heat.

In addition to the torque and SMEC, experimental and *in silico* mRT values were obtained and analyzed. Experiments determining the mRT were performed using only pure Eudragit RL. Due to excessive clogging of the material in the powder intake zone it was impossible to run extrusions in the high-throughput-low-screw-speed setting (0.4kg/h and 100rpm). Thus, for both barrel temperatures and 0.4kg/h throughput settings, experiments were run at higher screw speeds, i.e., 250rpm instead of 100rpm. The results are summarized in Figure 5.5.

The 1D HME model captures well the measured mRT and the influence of the throughput, screw speed and barrel temperature on the mRT. A reduction in the mRT can be expected in response to an increase in the screw speed, at least in this screw configuration. A more drastic change in the mRT can be expected due to a change in the throughput. In contrast, a change in the barrel temperature has a minor effect on the mRT. The reason is could be that the mRT is also a measure of extruder filling, i.e., a higher screw speed empties the extruder until the lowest possible fill level is reached at a given throughput, after which it remains constant. On the other hand, an increase in the throughput forces the material to move faster at a given screw speed.

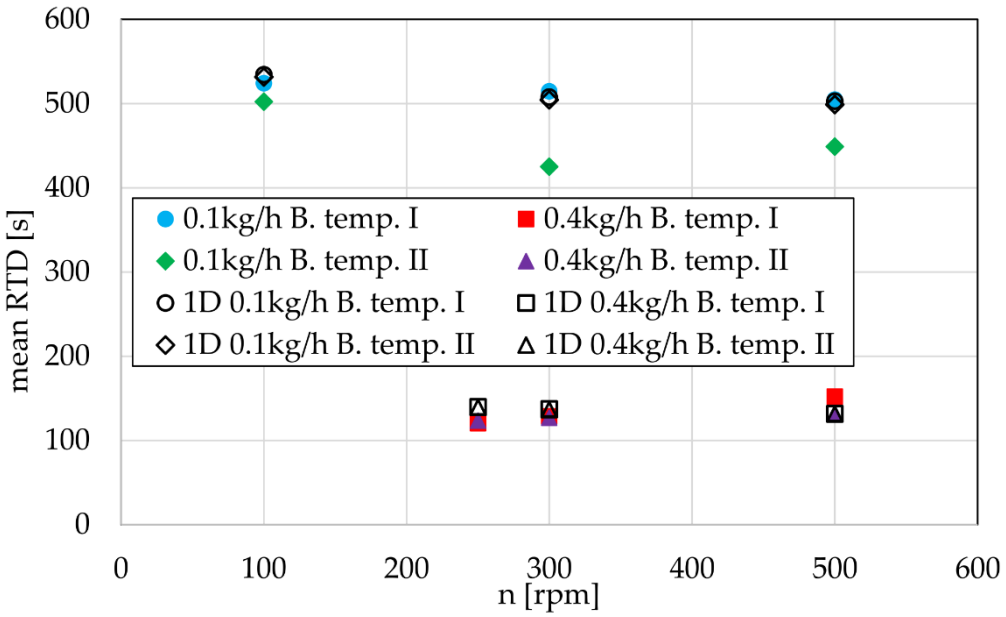

Figure 5.5. Influence of the process settings on the experimentally and *in silico* (1D) mean RTD (mRT).

In one setting (0.1kg/h @ 300rpm and Barrel temp. II), the difference between the experimental and *in silico* mRT values was more pronounced. It was most likely an outlier caused by an error in the RTD measurement since it does not follow the expected mRT behavior, i.e., the difference between the mRT obtained at barrel temperatures I and II in otherwise identical settings (0.1kg/h @ 300rpm) was higher than expected and higher than observed in any other settings. Moreover, it is implausible that the mRT is lower at 0.1kg/h @ 300rpm than at a screw speed of 500rpm in the same setting.

5.3.2 The effect of process settings on the degradation

As stated before, the HME process settings were chosen such that in some settings the API degradation would be observed. To that end, API degradation was analyzed as a function of the independent process variables: the screw speed, the throughput and the barrel temperature.

The influence of screw speed, throughput and barrel temperature on the API degradation is shown in Figure 5.6. With other process variables constant, an increase in the screw speed clearly leads to an increase in the API degradation. Since the shear rates in the extruder increase linearly with the screw speed, the viscous dissipation and the melt temperature are higher. Hence, the increase in degradation is linear to the screw speed. An increase in the throughput has the opposite effect on the API degradation due to a decrease in the residence time of the melt inside the extruder. Moreover, increasing the barrel temperature increases the API

degradation. Since the melt temperature is simply a balance between the viscous dissipation and the barrel's cooling power, it is clear that, with all other process variables constant, an increase in the barrel temperature will result in higher melt temperatures and a higher API degradation.

Interestingly, the 0.4kg/h-Barrel temp. II setting results in an equal or lower API degradation compared to the 0.1kg/h-Barrel temp. I setting, i.e., an increase in the API degradation that is only due to the barrel temperature increase (from Barrel temp. I to II) is lower than that due to a reduction in throughput (from 0.4kg/h to 0.1kg/h) in the studied system. Although it is possible to establish the limits within which the process variables can vary to yield an acceptable product quality (DS), the throughput and the barrel temperature cannot be used as a unique descriptor of the expected product quality (in our case, quantified as the extent of API degradation). This is an important result of this work.

In order to identify a unique descriptor of API degradation, the process state variables that can be measured during the process, e.g., mRT and SMEC, were investigated. The contribution of mRT to understanding the effect of process settings on the API degradation is illustrated in Figure 5.7. Since two throughputs are considered, the mRT results are clustered around 150s for 0.4kg/h throughput and around 500s for 0.1kg/h throughput at 3 screw speeds. The results suggest that the API degradation cannot be sufficiently explained based on the overall process mRT alone since relatively similar mRT values result in drastic variations in the API degradation. Hence, relying on the mRT as a sole process descriptor for setup and scale-up does not seem to be a good approach if consistent product quality is the goal.

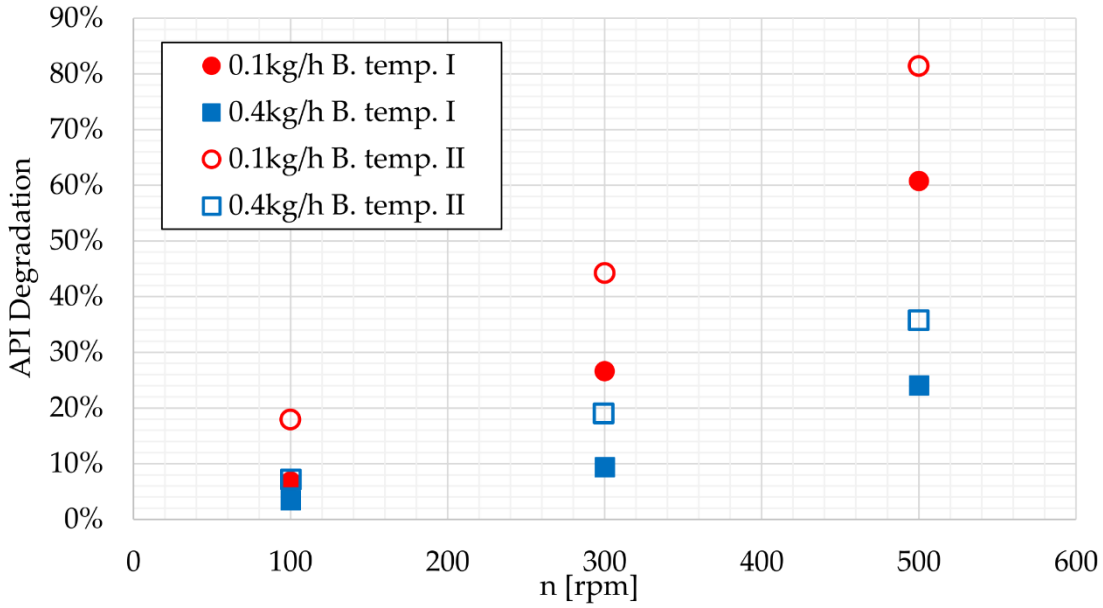

Figure 5.6. API degradation versus the process screw speed, throughput and barrel temperature.

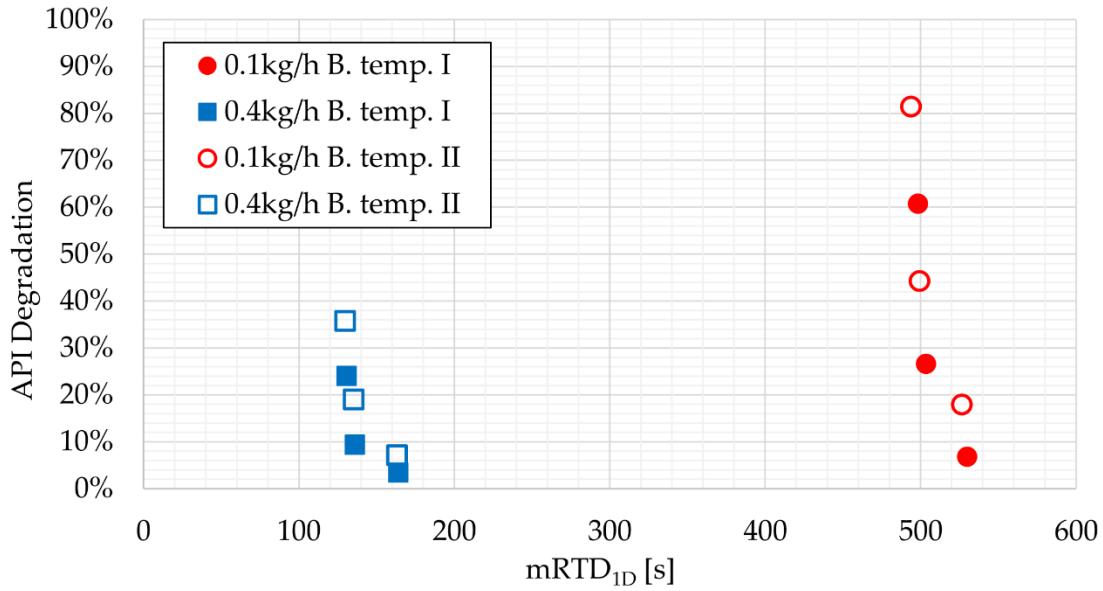

Figure 5.7 API Degradation as a function of process mRT_{1D}, throughput and barrel temperature.

Another dependent variable often used as a setup and scale-up criteria is the SMEC consumed during the process. Figure 5.8 shows the obtained API degradation as a function of the process SMEC. SMEC increases with an increase in the screw speed, but decreases with increased throughput and barrel temperature, provided that all other process variables are constant.

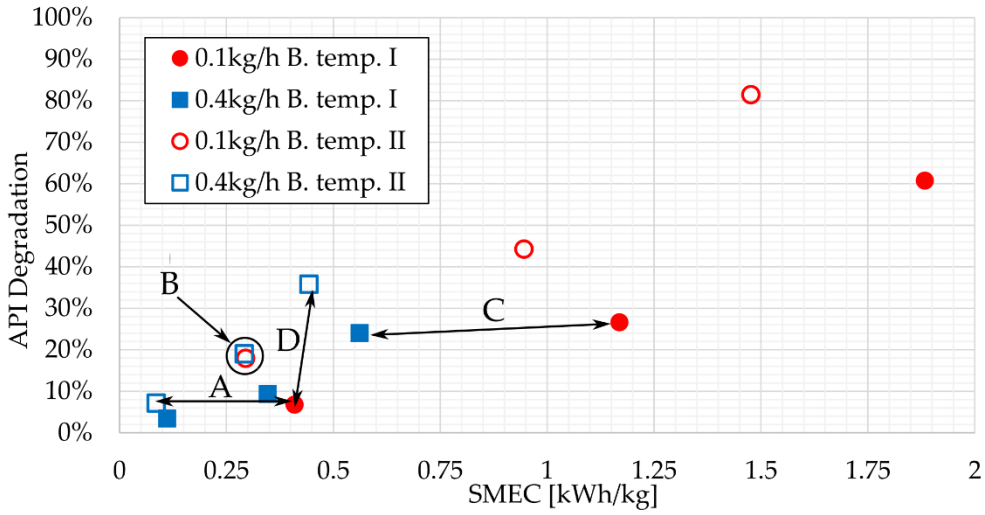

Figure 5.8. API Degradation versus process SMEC, with the cases A, B, C and D that either show similar API degradation for different SMEC values or different API degradation for similar SMEC values.

This was expected since, as discussed above, an increase in the barrel temperature leads to an increase in the melt temperature, lowering the melt viscosity and the viscous dissipation. Moreover, the throughput is in the denominator in the SMEC equation (Eq. 11).

At first glance, SMEC seems to be a good predictor/descriptor of API degradation, which rises steadily together with the rising SMEC. In processes with a throughput of 0.4kg/h, the SMEC and the API degradation do not exceed ~0.6 kWh/kg and 40%, respectively. At 0.1kg/h, a maximal SMEC of around 1.88kWh/kg and an API degradation of above 80% are achieved. It should be noted that this SMEC input is exceptionally high and most likely would not be considered a viable process setup in the traditional sense. Figure 5.8 shows that multiple process settings can result in different SMEC values but similar API degradation levels, and vice versa. In our case, it is possible to form at least three pairs of settings that result in a similar degradation:

A. PN 1 (0.1kg/h, 100rpm, temp I, 0.410kWh/kg) and PN 4 (0.4kg/h, 100rpm, temp. II, 0.087kWh/kg) with an API degradation of 7%

B. PN 3 (0.1kg/h, 100rpm, temp. II, 0.295kWh/kg) and PN 8 (0.4kg/h, 300rpm, temp. II, 0.292kWh/kg) with API degradations of 18% - 19%
C. PN 5 (0.1kg/h, 300rpm, temp. I, 1.170kWh/kg) and PN 10 (0.4kg/h, 500rpm, temp. I, 0.562kWh/kg) with API degradations of 27% and 24%, respectively

In addition to case B, there is one more case with a similar SMEC, yet a different API degradation:

D. PN 1 (0.1kg/h, 100rpm, temp. I, 0.410kWh/kg) and PN 12 (0.4kg/h, 500rpm, temp. II, 0.444kWh/kg) with API degradations of 7% and 36%, respectively

Clearly, similar API degradation and similar SMEC values are only achieved in case B. In the others cases, although the corresponding SMEC values are similar, the resulting API degradations vary significantly (e.g., settings A and C) or the SMEC values are similar but the API degradations are significantly different (e.g., case D).

This is an important result: although higher SMEC values generally result in higher API degradations, SMEC does not seem to be a good descriptor of the process and product quality equivalence. Therefore, it is not advisable to use it for scale-up, as suggested by many authors and discussed in one of our previous papers [52]. Moreover, even in case C with the same barrel temperature profile (profile I), the resulting SMEC values differ by a factor of two while the API degradation is similar. However, assuming that the maximal throughput is desirable, this is a good example of achieving the same product quality at two throughputs on the same machine.

In light of the above, rather than SMEC, the process mRT and the SMEC divided by the process mRT were considered as possible descriptors of API degradation, using integral process values (Figure 5.9). The SMEC is divided by the process mRT in order to eliminate the time variable from the SMEC values since the SMEC value indirectly contains the mRT.

Figure 5.9 shows that at a constant exposure time (mRT), an increase in the SMEC/mRT value results in an increased API degradation at constant barrel temperature. Furthermore, the results for the same barrel temperature settings indicate that similar SMEC/mRT values with a higher mRT result in a higher API degradation (i.e., if the formulation is exposed to the amount of power per kilogram for a longer time period, the API degradation is likely to increase). Since increasing the barrel temperature decreases the SMEC of the process while having no significant impact on the mRT, the comparability between the settings with different barrel temperatures is not provided. The example above indicates that same SMEC and mRT values can be obtained in different process settings (screw speed, throughput and barrel temperature settings) while similar SMEC and mRT values can be achieved using different screw

configurations. This implies that the product quality (in this case, API degradation) is not uniquely correlated with any of the independent or state variables that can be easily obtained and controlled during the process. Hence, process setup and scale-up methods whose goal is to maintain similar values of SMEC and mRT are fundamentally flawed and will inevitably result in extensive process optimization efforts.

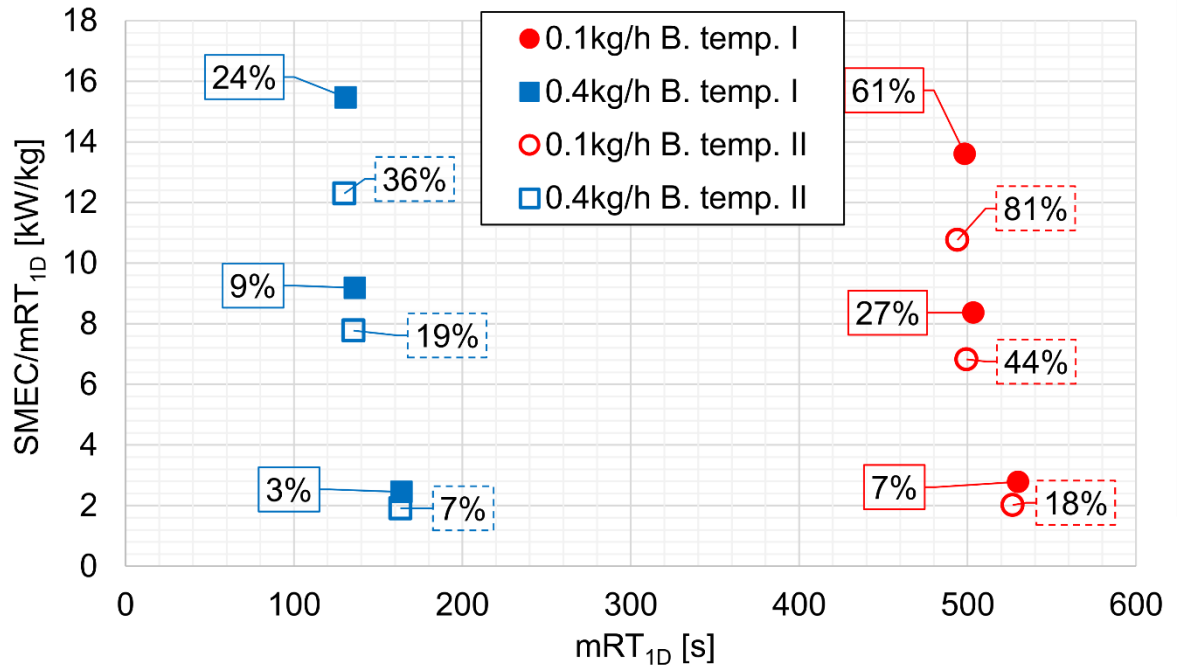

Figure 5.9. API degradation as a function of process SMEC/mRT_{1D} and mRT_{1D}

To find more suitable product quality descriptors results from the 1D HME simulations were analyzed in more detail. The distribution of filling degree and melt temperature of one exemplary setting obtained in 1D HME reduced-order simulations is shown in Figure 5.10. The shown setting is the 0.1kg/h throughput at 100rpm screw speed with the two barrel temperature settings. The filling degree of the extruder is a function of screw configuration (location and combination of screw elements with different melt conveying capacities), throughput and screw speed. A screw configuration with kneading elements that typically have lower conveying capacities than conveying elements [37], [52] will result in a higher filling degree or a fully filled section. This can be observed in the location of 90° kneading element (location 2 in Figure 5.10).

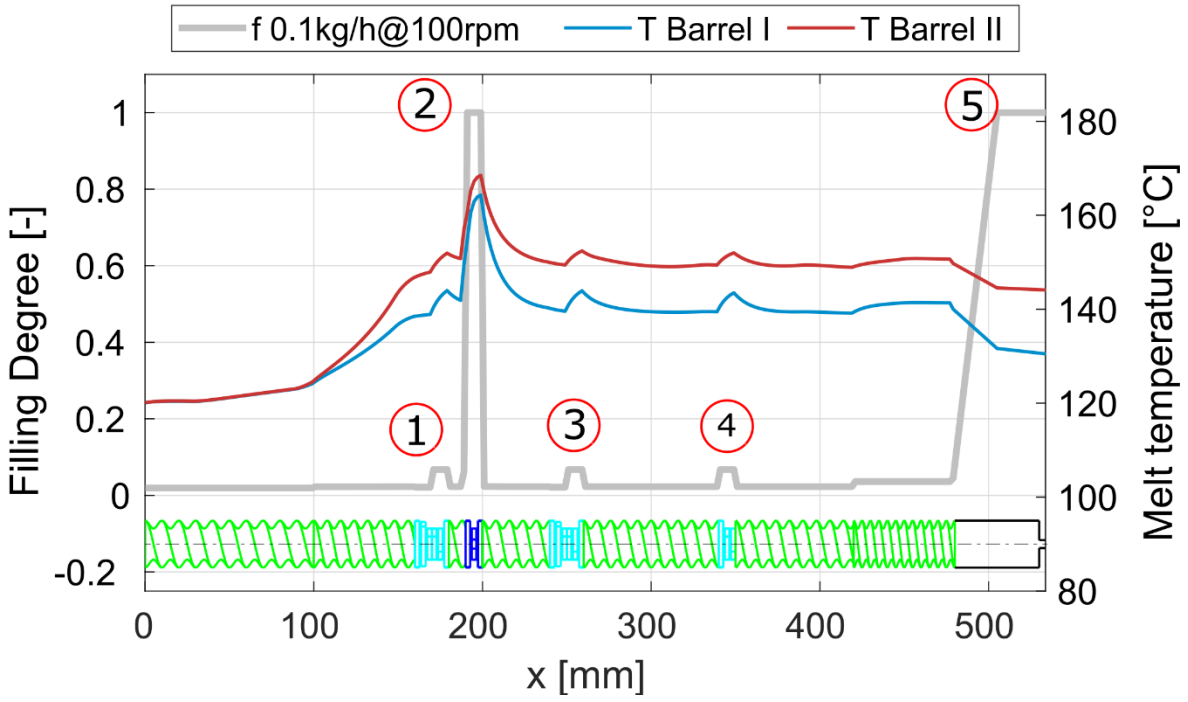

Figure 5.10. Melt temperature and filling degree obtained in the 1D HME simulations for the 0.1kg/h throughput at 100rpm screw speed and both barrel temperature settings.

An increase in the screw speed leads to a decrease in the overall filling degree, and an increase in the throughput has the opposite effect on the overall filling degree. It is important to note that a change in the barrel temperature generally does not result in a change in the extruder's filling degree. Examining the effect of increasing the barrel temperature on the melt temperature indicates that, when all other parameters are constant, the melt temperature also increases by the same degree (about 20°C in our example). The location of high temperature peaks does not change since it is primarily a function of screw configuration. Fully filled sections with kneading elements tend to create melt temperature peaks due to higher energy inputs and longer residence times in these regions, as illustrated below. Based on the melt temperature distribution, it was possible to investigate the (cross section-averaged) melt temperature and the local mRT (lmRT) values in various zones along the extruder screw configuration. To calculate the lmRT values, the lengths of individual kneading zones were taken as the representative lengths. Given the used screw configuration (Figure 5.2) and the location of melt temperature peaks, five possible zones of interest were defined: four kneading sections (from 1 to 4 in Figure 5.10) and the die section (5 in Figure 5.10). In Figure 5.11 to Figure 5.14, the relative API degradation (i.e., relative to the initial amount of API) is shown as a function of average melt temperature and lmRT in particular zones.

The first and the third kneading zone have the same configuration, the same lmRT values of ~0.5s- 2.8s and the same average melt temperatures of ~140°C - ~155°C (Figure 5.11). The second kneading zone is the most 'aggressive' kneading zone with 90° kneading elements, lmRT values of ~8s - ~33s and average melt temperatures of ~159°C-185°C (Figure 5.12). The fourth kneading zone section consisting of one 60° kneading element has lmRT values of ~0.4s-~2.9s and average temperatures of ~140°C - ~158°C (Figure 5.13). As stated above, the die section has the longest lmRT (~145s - ~460s), accounting for most of the overall lmRT, with temperatures ranging from ~139°C to ~157°C (Figure 5.14). Although the die section has the highest lmRT of all, the melt temperature is relatively low, with a low energy input (no dissipation from the screw). Note that there are different lmRTs in different locations along the screw. Whereas the fully filled sections in the location of 90° kneading element and the die section have two distinct lmRT values (~8s and ~33s for the 90° element and ~145s and ~460s for the die section), the partially filled kneading element section has three distinct lmRT values. This is due to the different forces driving the residence time in the fully and partially filled zones. In the former, the dominant RTD driving force is the throughput of the system (two distinct lmRT values resulting from two throughput settings), whereas in the latter the screw speed drives the transport of material and the RTD (three distinct lmRT values resulting from three screw speed settings).

Analyzing the lmRT and average melt temperature plots in terms of API degradation predictability shows that the average melt temperature and lmRT in the 90° kneading element zone correlate closely with the API degradation (Figure 5.12). Note that the residence time in this kneading zone is not a function of rpm since the screw is fully filled. All other zones do not provide a clear link between the API degradation and the melt temperature and lmRT. Figure 5.11, Figure 5.13 and Figure 5.14 indicate that a lower melt temperature results in a higher degradation despite a constant exposure time (constant lmRT) and that at constant melt temperature a shorter exposure time will result in a higher API degradation, which cannot be true.

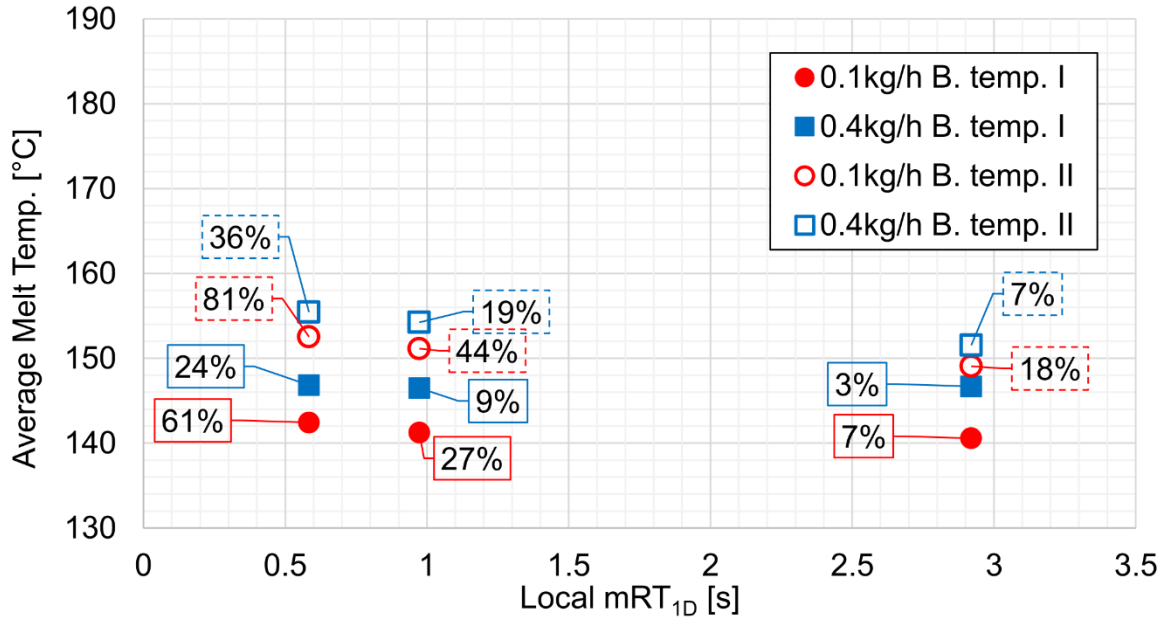

Figure 5.11. API degradation as a function of local mRT_{1D} and average melt temperature in the 1st and in the 3rd kneading zones, (assembled from 30° and 60° kneading elements). The amount of API degradation is shown in the boxes for every combination of local mRT_{1D} and averaged local melt temperature.

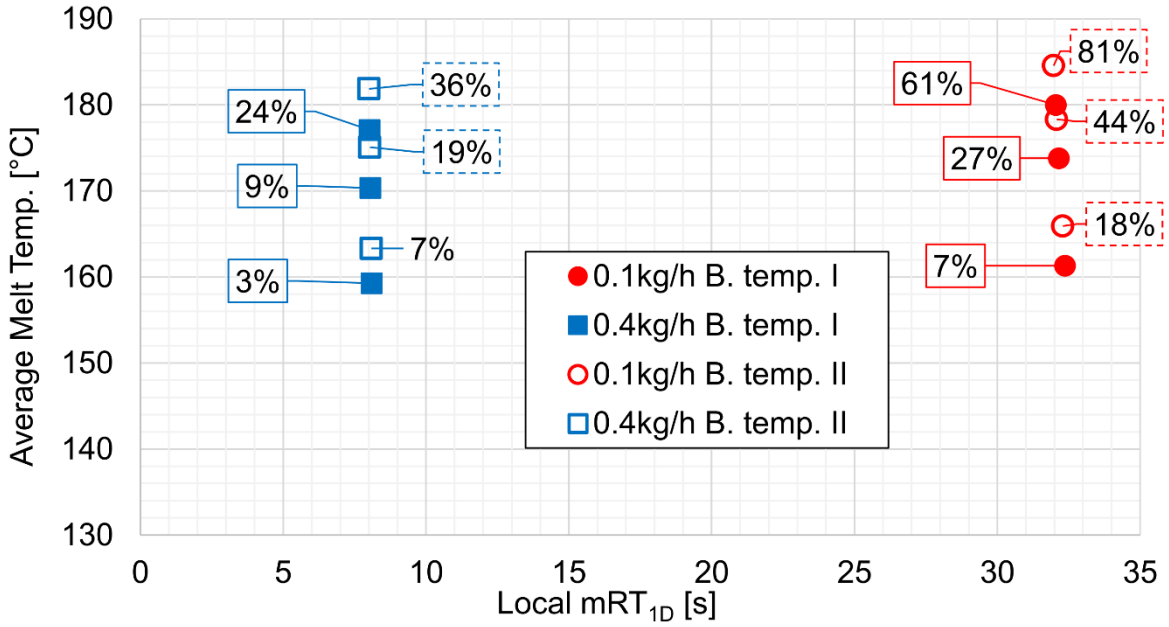

Figure 5.12. API degradation as a function of local mRT_{1D} and average melt temperature in the second kneading zone with a 90° (K90) kneading element. The amount of API degradation is shown in the boxes for every combination of local mRT_{1D} and averaged local melt temperature.

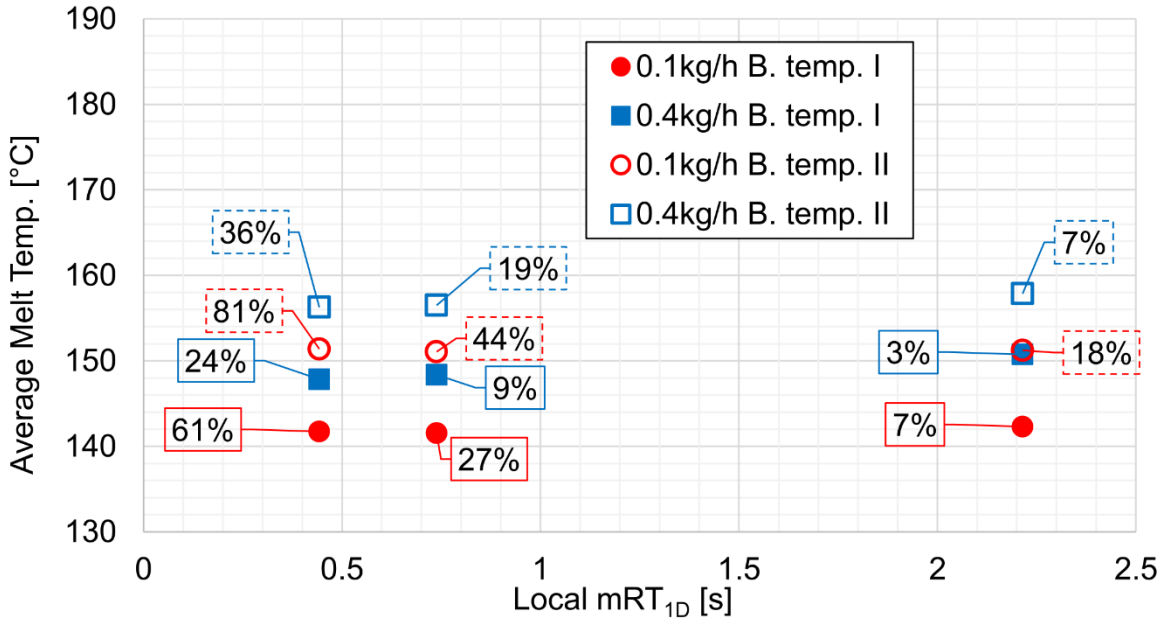

Figure 5.13. API degradation as a function of local mRT_{1D} and average melt temperature at the 4rd kneading zone, assembled from one 60° kneading element. The amount of API degradation is shown in the boxes for every combination of local mRT_{1D} and averaged local melt temperature.

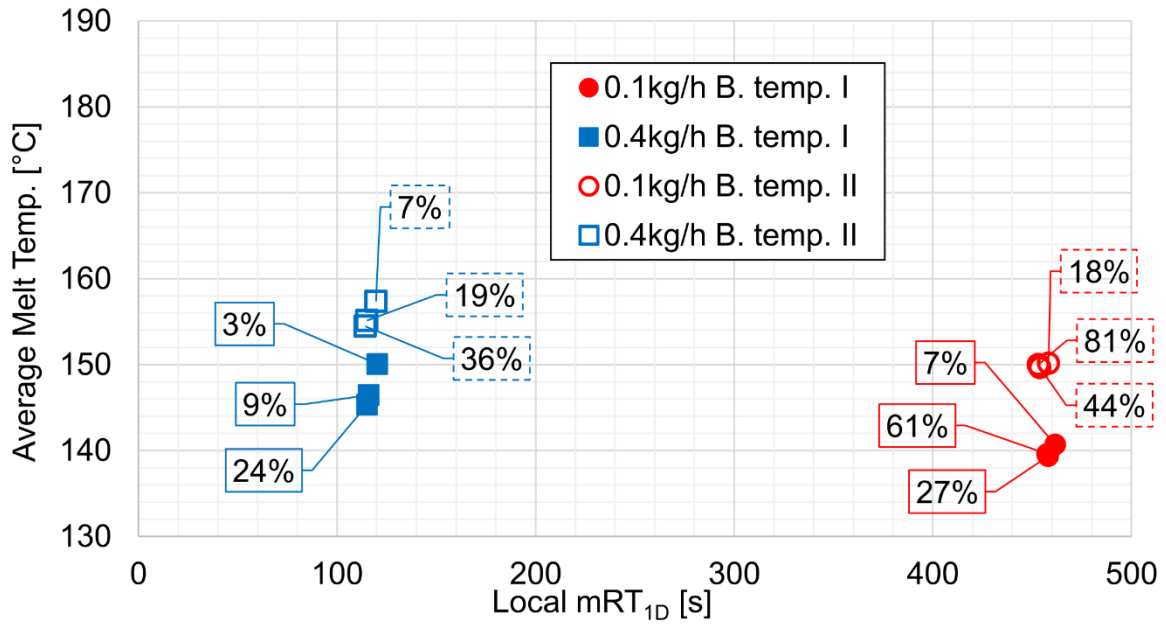

Figure 5.14. API degradation as a function of local mRT1D and average melt temperature in the die zone. The degree of API degradation is shown in boxes for every combination of local mRT1D and averaged local melt temperature.

Thus, at least in the presented case, the average melt temperatures and lmRT in the die and other kneading sections (except of the 90° kneading element zone) cannot be key drivers of the API degradation. Nevertheless, Figure 5.12 clearly shows the API degradation as a function of local mRT and average melt temperature. At a constant exposure time (constant lmRT), a higher

average temperature will always result in a higher API degradation. The effect of barrel temperature is also inherently included. In the case of constant (or similar) average melt temperature, longer exposure time at a certain temperature will result in a higher API degradation. Moreover, Famotidine has been reported to be a thermolabile drug substance that degrades at or slightly above the melting point of ~165°C [47], which is the temperature expected in the 90° kneading element zone, according to the simulation results. Hence, the temperature and time of exposure in certain zones along the screw configuration could be used a predictor of API degradation.

5.4 Summary and Conclusions

Developing roadmaps and tools for quick, safe and efficient pharmaceutical process setup and scale-up of continuous pharmaceutical processes is crucial for cost-efficient drug production. HME is especially interesting since it provides solubility enhancement to poorly soluble pharmaceutical APIs. What is more, it is a modular process with a variety of screw elements to choose from while designing the screw configuration. However, modularity can hinder the process design (e.g., the process may have to be developed from scratch for a new API and/or carrier combination), and, in addition to being poorly soluble, APIs are often temperature-sensitive and available in low quantities during the initial development phase. Hence, the HME process development and scale-up for pharmaceutical purposes has to be accomplished in a manner that is different from traditional pharma manufacturing. Process simulations and investigations of process-product relationships are essential for achieving a quick and reliable process setup.

In this work the degradation of Famotidine (in the 20% Famotidine and 80% Eudragit RL formulation) as a function of extruder settings was examined. A Leistritz ZSE12 12mm extruder was used, representing a small-scale extruder typically applied in product development. The API degradation was chosen as the relevant product response. The process settings selected assured a wide process window to elicit a significant degradation and reduce the product quality. The resulting API degradation was evaluated as a function of process SMEC and SMEC/mRT ratio. SMEC alone was not a good descriptor of process adequacy in terms of API degradation since a similar degradation was achieved at different SMEC values and similar SMEC values lead to different API degradation levels. Analyzing the API degradation as a function of mRT and SMEC/mRT was a better process descriptor in one barrel temperature

setting. At similar SMEC/mRT values, a higher API degradation was achieved with higher mRT. Assuming that the combination of melt temperature and mRT is responsible for the API degradation, zones of interest (zones of high stress) were defined along the screw. The most relevant zones are zones in kneading elements and the die section where overall higher residence times are expected. The API degradation was investigated as a function of local mRT and local average melt temperature obtained in the 1D HME simulations for all the relevant zones. It was established that the 90° kneading element zone has the highest average melt temperature peaks and correlates with the API degradation best, i.e., a higher API degradation is achieved at higher averaged melt temperature in this zone and a higher local mRT. The influence of screw speed, throughput and barrel temperature was taken into account. The above insights can be used in the HME process development according to the QbD framework prior to any actual extrusion trials. By analyzing the API degradation as a function of time and temperature, various screw configurations, screw speeds, throughputs, barrel temperatures and die designs can be evaluated in terms of resulting SMEC values, mRT values , local mRT values and melt temperatures in order to predict the product response. This can greatly simplify the pharmaceutical HME process setup and scale-up and eliminate a number of assumptions in the process design.

In summary, it means that future formulation quality charts could be developed that show the formulation quality as a function of temperature and exposure time. This way, the process could first be designed *in silico* to remain within the desired temperature and exposure time boundaries (i.e., the design space) along the entire screw configuration to guarantee adequate product quality. In the end of the process design phase, the *in silico* design space could be experimentally validated, significantly reducing empiricism, waste and energy demand during process and product development.

5.6 Abbreviations

A1	Inherent Conveying Capacity
A2	Inherent Pressure Build-Up Capacity
API	Active Pharmaceutical Ingredient
ACN	Acentonitrile
DS	Design Space
HME	Hot-Melt Extrusion
mRT	mean Residence Time
lmRT	local mean Residence Time
PAT	Process Analytical Technology
PC1	1st Principal Components
PVT	Pressure Volume Temperature
QbD	Quality by Design
RTD	Residence Time Distribution
SMEC	Specific Mechanical Energy Consumption
SPH	Smoothed Particle Hydrodynamics
TFA	Trifluoroacetic Acid
TSE	co-rotating Twin-Screw Extruder
ZSE12	Leistritz 12mm co-rotating twin-screw extruder

5.7 Nomenclature

Latin symbols

a_T [-]	Williams-Landel-Ferry temperature shift factor
$c_{p,s}$, $c_{p,m}$ [J/kgK]	Heat capacity of solid and melt, respectively
c_v [J/m³K]	Specific heat capacity at constant volume
c_0, $c_{extrudate}$	Initial API content and API content in the Extrudate, respectively
C_1, C_2 [–,°C]	Fitting parameters for the WLF temperature shift factor
D [m]	Barrel diameter
D_i [m]	Inner screw diameter
D_o [m]	Outer screw diameter
f [%]	Percentage of degradation
K_1, K_2, K_3, K_4, K_8, K_9 [bar cm³/g, bar cm³/g°C, bar, bar, °C, °C/bar]	Menges density factors

$\dot{m}$ [kg/h]	Throughput
n [rpm]	Screw speed
p [bar]	Pressure
Pe [-]	Peclet number
T, T_r, T_{tr} [°C]	Melt temperature, reference temperature and transition temperature
t [s]	Time

Greek symbols

α [°]	Cross section/kneading block tilt angle
$\dot{\gamma}$, $\dot{\gamma}_{crit}$ [s^{-1}]	Shear rate and critical shear rate, respectively
H, η_0 [Pas]	Fluid viscosity and zero-shear-viscosity, respectively
Θ [s]	mRT
λ [W/mK]	Thermal conductivity
ν [cm^3/g]	Specific volume
τ [s]	Dimensionless time
$\omega, \psi, \varepsilon, \chi, \kappa, \xi$ [-]	Exponents of the Menges and Feistkorn scale-up method

5.8 References

[1] H. McFall *et al.*, "Formulation of aripiprazole-loaded pH-modulated solid dispersions via hot-melt extrusion technology: In vitro and in vivo studies," *Int. J. Pharm.*, vol. 554, pp. 302–311, Jan. 2019.

[2] J. M. Vasoya *et al.*, "Development of Solid Dispersion by Hot Melt Extrusion Using Mixtures of Polyoxylglycerides With Polymers as Carriers for Increasing Dissolution Rate of a Poorly Soluble Drug Model," *J. Pharm. Sci.*, vol. 108, no. 2, pp. 888–896, Feb. 2019.

[3] A. Schittny, H. Ogawa, J. Huwyler, and M. Puchkov, "A combined mathematical model linking the formation of amorphous solid dispersions with hot-melt-extrusion process parameters," *Eur. J. Pharm. Biopharm.*, vol. 132, pp. 127–145, Nov. 2018.

[4] M. Monschke, K. Kayser, and K. G. Wagner, "Processing of Polyvinyl Acetate Phthalate in Hot-Melt Extrusion—Preparation of Amorphous Solid Dispersions," *Pharmaceutics*, vol. 12, no. 4, p. 337, Apr. 2020.

[5] K. E. Steffens and K. G. Wagner, "Dissolution enhancement of carbamazepine using twin-screw melt granulation," *Eur. J. Pharm. Biopharm.*, vol. 148, no. October 2019, pp. 77–87, Mar. 2020.

[6] Y. Zhu, N. H. Shah, A. Waseem Malick, M. H. Infeld, and J. W. McGinity, "Controlled Release of a Poorly Water-Soluble Drug from Hot-Melt Extrudates Containing Acrylic Polymers," *Drug Dev. Ind. Pharm.*, vol. 32, no. 5, pp. 569–583, Jan. 2006.

[7] A. Q. Vo *et al.*, "A novel floating controlled release drug delivery system prepared by hot-melt extrusion," *Eur. J. Pharm. Biopharm.*, vol. 98, pp. 108–121, Jan. 2016.

[8] M. Fukuda, N. A. Peppas, and J. W. McGinity, "Floating hot-melt extruded tablets for gastroretentive controlled drug release system," *J. Control. Release*, vol. 115, no. 2, pp. 121–129, Oct. 2006.

[9] R. Baumgartner, A. Eitzlmayr, N. Matsko, C. Tetyczka, J. G. Khinast, and E. Roblegg, "Nano-extrusion: A promising tool for continuous manufacturing of solid nano-formulations," *Int. J. Pharm.*, vol. 477, no. 1–2, pp. 1–11, Dec. 2014.

[10] R. Baumgartner, J. Matić, S. Schrank, S. Laske, J. G. J. Khinast, and E. Roblegg, "NANEX: Process design and optimization," *Int. J. Pharm.*, vol. 506, no. 1–2, pp. 35–45, Jun. 2016.

[11] A. M. Bhagurkar, M. A. Repka, and S. N. Murthy, "A Novel Approach for the

Development of a Nanostructured Lipid Carrier Formulation by Hot-Melt Extrusion Technology," *J. Pharm. Sci.*, vol. 106, no. 4, pp. 1085–1091, Apr. 2017.

[12] L. A. D. Silva *et al.*, "Preparation of a solid self-microemulsifying drug delivery system by hot-melt extrusion," *Int. J. Pharm.*, vol. 541, no. 1–2, pp. 1–10, Apr. 2018.

[13] H. Patil, X. Feng, X. Ye, S. Majumdar, and M. A. Repka, "Continuous Production of Fenofibrate Solid Lipid Nanoparticles by Hot-Melt Extrusion Technology: a Systematic Study Based on a Quality by Design Approach," *AAPS J.*, vol. 17, no. 1, pp. 194–205, Jan. 2015.

[14] C. Bode, H. Kranz, A. Fivez, F. Siepmann, and J. Siepmann, "Often neglected: PLGA/PLA swelling orchestrates drug release: HME implants," *J. Control. Release*, vol. 306, no. May, pp. 97–107, Jul. 2019.

[15] A. Cossé, C. König, A. Lamprecht, and K. G. Wagner, "Hot Melt Extrusion for Sustained Protein Release: Matrix Erosion and In Vitro Release of PLGA-Based Implants," *AAPS PharmSciTech*, vol. 18, no. 1, pp. 15–26, Jan. 2017.

[16] S. Eder *et al.*, "Establishment of a Molding Procedure to Facilitate Formulation Development for Co-extrudates," *AAPS PharmSciTech*, vol. 18, no. 8, pp. 2971–2976, Nov. 2017.

[17] I. Koutsamanis *et al.*, "Formulation and processability screening for the rational design of ethylene-vinyl acetate based intra-vaginal rings," *Int. J. Pharm.*, vol. 564, no. April, pp. 90–97, Jun. 2019.

[18] K. Kohlgrüber, *Co-Rotating Twin-Screw Extruder*. München: Carl Hanser Verlag GmbH & Co. KG, 2007.

[19] C. Rauwendaal, *Polymer extrusion: Fifth edition*, Fifth Edit. München: Carl Hanser Verlag GmbH & Co. KG, 2014.

[20] L. Saerens, C. Vervaet, J.-P. Remon, and T. De Beer, "Visualization and Process Understanding of Material Behavior in the Extrusion Barrel during a Hot-Melt Extrusion Process Using Raman Spectroscopy," *Anal. Chem.*, vol. 85, no. 11, pp. 5420–5429, Jun. 2013.

[21] J. Breitenbach, "Melt extrusion: from process to drug delivery technology," *Eur. J. Pharm. Biopharm.*, vol. 54, no. 2, pp. 107–117, Sep. 2002.

[22] M. M. Crowley *et al.*, "Pharmaceutical Applications of Hot-Melt Extrusion: Part I," *Drug Dev. Ind. Pharm.*, vol. 33, no. 9, pp. 909–926, Jan. 2007.

[23] M. A. Repka *et al.*, "Pharmaceutical Applications of Hot-Melt Extrusion: Part II," *Drug Dev. Ind. Pharm.*, vol. 33, no. 10, pp. 1043–1057, Jan. 2007.

[24] H. Patil, R. V. Tiwari, and M. A. Repka, "Hot-Melt Extrusion: from Theory to Application in Pharmaceutical Formulation," *AAPS PharmSciTech*, vol. 17, no. 1, pp. 20–42, Feb. 2016.

[25] R. C. Evans, S. O. Kyerematen, L. Asmus, M. Degenhardt, J. Rosenberg, and K. G. Wagner, "Development and Performance of a Highly Sensitive Model Formulation Based on Torasemide to Enhance Hot-Melt Extrusion Process Understanding and Process Development," *AAPS PharmSciTech*, vol. 19, no. 4, pp. 1592–1605, May 2018.

[26] J. Matić, A. Paudel, H. Bauer, R. A. L. Garcia, K. Biedrzycka, and J. G. Khinast, "Developing HME-Based Drug Products Using Emerging Science: a Fast-Track Roadmap from Concept to Clinical Batch," *AAPS PharmSciTech*, vol. 21, no. 5, p. 176, Jul. 2020.

[27] S. Huang, K. P. O'Donnell, S. M. Delpon de Vaux, J. O'Brien, J. Stutzman, and R. O. Williams, "Processing thermally labile drugs by hot-melt extrusion: The lesson with gliclazide," *Eur. J. Pharm. Biopharm.*, vol. 119, pp. 56–67, Oct. 2017.

[28] S. M. Dadou *et al.*, "The development and validation of a quality by design based process analytical tool for the inline quantification of Ramipril during hot-melt extrusion," *Int. J. Pharm.*, vol. 584, p. 119382, Jun. 2020.

[29] L. X. Yu *et al.*, "Understanding pharmaceutical quality by design," *AAPS J.*, vol. 16, no. 4, pp. 771–783, Jul. 2014.

[30] V. P. Kumar and N. V. Gupta, "A Review on quality by design (QBD) for Pharmaceuticals," *Int. J. Drug Dev. Res.*, vol. 7, no. 1, pp. 35–44, 2015.

[31] V. Mishra, S. Thakur, A. Patil, and A. Shukla, "Quality by design (QbD) approaches in current pharmaceutical set-up," *Expert Opin. Drug Deliv.*, vol. 15, no. 8, pp. 737–758, Aug. 2018.

[32] A. Gupta and M. A. Khan, "Hot-Melt Extrusion: An FDA Perspective on Product and Process Understanding," in *Hot-Melt Extrusion: Pharmaceutical Applications*, Chichester, UK: John Wiley & Sons, Ltd, 2012, pp. 323–331.

[33] ICH Q8, "EMEA/CHMP, 2009, ICH Topic Q 8 (R2) Pharmaceutical Development, Step 5: Note for Guidance on Pharmaceutical Development," vol. 8, no. June, 2017.

[34] M. T. Islam, M. Maniruzzaman, S. A. Halsey, B. Z. Chowdhry, and D. Douroumis, "Development of sustained-release formulations processed by hot-melt extrusion by using a quality-by-design approach," *Drug Deliv. Transl. Res.*, vol. 4, no. 4, pp. 377–387, Aug. 2014.

[35] D. Treffer, A. Troiss, and J. G. Khinast, "A novel tool to standardize rheology testing of

molten polymers for pharmaceutical applications," *Int. J. Pharm.*, vol. 495, no. 1, pp. 474–481, Nov. 2015.

[36] A. Eitzlmayr *et al.*, "Experimental characterization and modeling of twin-screw extruder elements for pharmaceutical hot melt extrusion," *AIChE J.*, vol. 59, no. 11, pp. 4440–4450, Nov. 2013.

[37] A. Eitzlmayr, J. Matić, and J. G. Khinast, "Analysis of flow and mixing in screw elements of corotating twin-screw extruders via SPH," *AIChE J.*, vol. 63, no. 6, pp. 2451–2463, Jun. 2017.

[38] A. Eitzlmayr and J. G. Khinast, "Co-rotating twin-screw extruders: Detailed analysis of conveying elements based on smoothed particle hydrodynamics. Part 1: Hydrodynamics," *Chem. Eng. Sci.*, vol. 134, pp. 861–879, Sep. 2015.

[39] A. Eitzlmayr and J. Khinast, "Co-rotating twin-screw extruders: Detailed analysis of conveying elements based on smoothed particle hydrodynamics. Part 2: Mixing," *Chem. Eng. Sci.*, vol. 134, pp. 880–886, Sep. 2015.

[40] A. Eitzlmayr *et al.*, "Mechanistic modeling of modular co-rotating twin-screw extruders," *Int. J. Pharm.*, vol. 474, no. 1–2, pp. 157–176, Oct. 2014.

[41] J. Pawlowski, *Die Ähnlichkeitstheorie in der physikalisch-technischen Forschung*. Berlin, Heidelberg: Springer Berlin Heidelberg, 1971.

[42] G. L. Perpétuo *et al.*, "Thermal behavior of some antihistamines," *J. Therm. Anal. Calorim.*, vol. 111, no. 3, pp. 2019–2028, Mar. 2013.

[43] R. I. Mustafin, "Interpolymer combinations of chemically complementary grades of Eudragit copolymers: a new direction in the design of peroral solid dosage forms of drug delivery systems with controlled release (review)," *Pharm. Chem. J.*, vol. 45, no. 5, pp. 285–295, Aug. 2011.

[44] M. Maniruzzaman, M. M. Rana, J. S. Boateng, J. C. Mitchell, and D. Douroumis, "Dissolution enhancement of poorly water-soluble APIs processed by hot-melt extrusion using hydrophilic polymers," *Drug Dev. Ind. Pharm.*, vol. 39, no. 2, pp. 218–227, Feb. 2013.

[45] M. Chordiya, H. Gangurde, K. Senthilkumaran, and L. Kothari, "Formulation development and in vitro evaluation of gastroretentive hollow microspheres of famotidine," *Int. J. Pharm. Investig.*, vol. 1, no. 2, p. 105, 2011.

[46] T. Parikh, S. S. Gupta, A. Meena, and A. T. M. Serajuddin, "Investigation of thermal and viscoelastic properties of polymers relevant to hot melt extrusion - III: Polymethacrylates and polymethacrylic acid based polymers," *J. Excipients Food Chem.*, vol. 5, no. 1, pp.

56–64, Mar. 2014.

[47] M. T. Viciosa, J. J. Moura Ramos, and H. P. Diogo, “The Slow Relaxation Dynamics in the Amorphous Pharmaceutical Drugs Cimetidine, Nizatidine, and Famotidine,” *J. Pharm. Sci.*, vol. 105, no. 12, pp. 3573–3584, Dec. 2016.

[48] T. W. Schmidt, “Zur Abschätzung der Schwindung,” Aachen, 1986.

[49] P. R. Wahl *et al.*, “In-line measurement of residence time distribution in melt extrusion via video analysis,” *Polym. Eng. Sci.*, vol. 58, no. 2, pp. 170–179, Feb. 2018.

[50] J. Kruisz, J. Rehrl, S. Sacher, I. Aigner, M. Horn, and J. G. Khinast, “RTD modeling of a continuous dry granulation process for process control and materials diversion,” *Int. J. Pharm.*, vol. 528, no. 1–2, pp. 334–344, Aug. 2017.

[51] J. Kruisz, J. Rehrl, E. Faulhammer, A. Witschnigg, and J. G. Khinast, “Material tracking in a continuous direct capsule-filling process via residence time distribution measurements,” *Int. J. Pharm.*, vol. 550, no. 1–2, pp. 347–358, Oct. 2018.

[52] J. Matić, A. Witschnigg, M. Zagler, S. Eder, and J. Khinast, “A novel in silico scale-up approach for hot melt extrusion processes,” *Chem. Eng. Sci.*, vol. 204, pp. 257–269, Aug. 2019.

6

Towards Predicting the Product Quality in Hot Melt Extrusion: Pilot Plant Scale Extrusion*

Following our study on the impact of hot melt extrusion (HME) process conditions on the product quality, we expanded our investigation to assessing the effect of scale-up on the product quality. To this end, we studied the influence of process settings and different scale-up variants on the active pharmaceutical ingredient (API) degradation in a pilot plant scale extruder. Six scale-up variants were investigated and none of them could replicate the product quality from the original process setup on a lab-scale extruder. By analyzing several process-dependent and -independent variables and cross referencing them to the experiments in the lab-scale extruder, we identified certain patterns. The results of the reduced order mechanistic 1D HME simulation of various process states made it possible to establish a correlation between the achieved API degradation and the local melt temperature and the exposure time in specific zones along the screw configuration. Since the same melt temperature and exposure time correlations were also valid for the lab scale-extruder, such an approach could be used in the future to predict the product quality as a function of processing conditions fully *in silico* prior to the first extrusion trials.

---

* This chapter is based on: J. Matić, C. Alva, S. Eder, K. Nickel, A. Paudel and J. Khinast, "Towards Predicting Product Quality in Hot Melt Extrusion: Pilot Plant Scale" *In Preparation.*

6.1 Introduction

Turning continuous manufacturing into the main production route of pharmaceuticals is one of the tasks that the Food Drug Administration (FDA) and the European Medicines Agency (EMA) are pursuing in an effort to increase both the production efficiency and the product quality. The Quality by Design (QbD) guidelines [1]–[6] emphasize understanding the product's ingredients, formulation and production steps to intrinsically guaranty a certain product quality.

Used in the polymer and food industries for decades, hot-melt extrusion (HME) is a continuous manufacturing process, which often utilizes closely intermeshing (self-wiping) co-rotation twin-screw extruders (TSE) as the platform of choice [7]–[9]. It is known for its flexibility in terms of process setup, allowing a formulation-specific process tailored by adjusting the screw configuration and speed, the barrel temperature profile, as well as feeding, venting and strand-shaping. Importantly, the process is solvent-free and ensures both distributive and dispersive mixing, guarantying a good content uniformity. HME is often used for enhancing the solubility of poorly soluble active pharmaceutical ingredients (APIs) [10]–[15] by creating amorphous solid dispersions or solutions of the APIs in a polymeric carrier. Alternately, the solubility enhancement can be achieved by creating nanoparticles that are then incorporated into a polymeric carrier via HME [16]–[21]. In such cases, HME is a one-step solidification process that transforms the liquid solid solution and/or dispersion into a solid dosage form, with the API being embedded in a polymer matrix, while guaranteeing the redispersion of nanoparticles once administered. Moreover, HME has been applied in the production of more traditional embedding of crystalline APIs and peptides in various polymer matrixes as well [22]–[25]. Depending on the polymer matrix and the HME process setup, immediate- or extended-release drug product can be manufactured [26]–[29]. As a production step, HME can significantly alter the critical quality attributes (CQAs) of the produced drug, depending on the used process settings. Even a few degrees of temperature difference the formulation experiences during production due to differences in the process setup or extruder scale can have a significant impact on the morphology of the polymer-API-additive mixture, be it amorphous or semi-crystalline, and thus, on the biopharmaceutics. Unfortunately, the impact certain changes in the process setup or equipment scale can have on the final product are often not known a priory. These effects and their impact on the final product during production have to be taken into account. Hence, to ensure rapid, cost-efficient and low-risk drug development, a holistic approach has to be established, including defining the intended biopharmaceutical profile and understanding

formulation development, production technologies, drug release mechanisms and pharmacokinetics. In this study we focus on the process setup, control and scale-up, using a combination of QbD and *in silico* tools.

In the past, we have worked on the development of rapid formulation screening tools via vacuum compression molding [24], [30], high-fidelity simulations based on Smoothed Particle Hydrodynamics (SPH) [31]–[41] and 1D HME mechanistic models [42], [43] for HME process analysis, design and scale-up [17], [44]–[46]. The current study is a follow up of the experiments, simulations and analysis performed using the Leistritz 12mm ZSE12 HP-PH extruder [46]. To assess various scale-up methods reported in the literature, six scale-up approaches were analyzed by determining the resulting product quality, comparing the outcomes to the desired product quality and creating detailed 1D HME process simulations. The target extruder chosen for this study was the Leistritz 18mm ZSE18 HP-PH pilot-plant-scale pharma extruder. In addition to the six scale-up attempts, a quasi-DoE setup of nine extrusions (three throughput and screw speed settings) was performed and analyzed in detail to fully understand the process space.

6.2 Materials and Methods

6.2.1 Equipment and Scale-up rules

The Leistritz ZSE18 pharma extruder is the next bigger extruder after the ZSE12 in the Leistritz pharma extruder lineup. It is often used in pilot plants or even in production settings, depending on the production size needed. The general data for ZSE18 is shown in Table 6.1 with a direct size comparison to the smaller ZSE12 extruder, whereas Figure 6.1 shows the general twin screw extruder cross section. Both extruders have the same ratio of 1.51 between their outer and inner screw diameters, making the screw transfer and scale-up easier. At the time of our investigation, the ZSE12 extruder had a fixed screw configuration consisting of three conveying elements with pitches of 10mm, 16mm and 20mm ($C10_{12}$, $C16_{12}$ and $C20_{12}$, respectively) and three kneading elements with angles between the kneading discs of 30°, 60° and 90° ($K30_{12}$, $K60_{12}$ and $K90_{12}$, respectively).

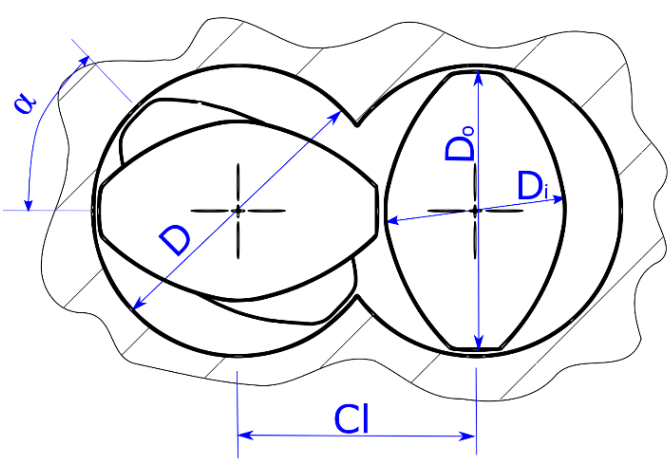

Figure 6.1. Details of the twin-screw extruder screw cross section showing the barrel diameter (D), screw outer and inner diameters (Do and Di, respectively), screw centerline distance (Cl) and the angle between the kneading discs for kneading elements (α).

Table 6.1. General characteristics of Leistritz lab-scale 12mm ZSE12 HP-PH extruder and the pilot plant scale 18mm ZSE18 HP-PH extruder.

	ZSE12 HP-PH	ZSE18 HP-PH
D – Barrel diameter	12mm	18mm
D_o – Outer screw diameter	11.85mm	17.8mm
D_i – Inner screw diameter	7.85mm	11.8mm
Cl – centerline distance	10mm	15mm
τ_{max} – Maximal available torque	20Nm	71Nm

A broader portfolio of screw elements is available for the ZSE18 extruder, including four conveying elements with pitches of 10mm, 15mm, 20mm and 30mm ($C10_{18}$, $C15_{18}$, $C20_{18}$ and $C30_{18}$, respectively), one mixing element with a pitch of 15mm ($M15_{18}$) and six kneading elements with three kneading disc angles of 30°, 60° and 90° ($K30_{18}$, $K60_{18}$ and $K90_{18}$, respectively) with two disc thicknesses of 4mm and 6.5mm (a kneading element with the thick kneading discs is marked with the letter L, i.e., $K30L_{18}$).

The first step in scaling up the HME process is to transfer the screw configuration. With that regard, the screw configuration was scaled with some guidelines in mind:

- The original screw configuration used during the extrusion with the ZSE12 extruder was divided into eleven functional sections;
- The sections were created with different processing tasks and screw groups in mind, with the goal to directly replicate the screw sections to the target extruder;

- The section length was scaled with the ration of 1.5, which is the ration between the nominal screw diameters between the target and original extruder. This ensured proper section lengths;
- The kneading sections were replaced taking into account the kneading section length and the kneading element disc thickness;
- Some conveying element parts of the screw configuration had to be adjusted due an insufficient number of screw element available. As some locations a 20mm pitches conveying elements was replaced with a 30mm pitched element. The changes were not significant and should not critically impact the performance of the screw.

Both the original and target screw configurations are shown in Figure 6.2, Table 6.2 and Table 6.3. Both screws have the same processing zones and nominal zone lengths, with a relatively complex screw configuration setup. The powder intake zone is designed to with long conveying element section with a pitch of 30mm, and a pitch reduction towards the first kneading zone to 20mm. The use of high pitched conveying elements in the powder intake zone is advantageous as it allows a high free volume for the intake of different powders, or powder mixtures, with various densities. The pitch reduction of the conveying element towards the first kneading zone has the task to density the powder, eliminating any air pockets, and to increase the filling degree before the firs kneading zone. The first kneading zone, also known as the melting zone, is designed as a combination of a kneading element with a stagger angle of 30° between individual kneading discs, followed by a 60° kneading element. Such an arrangement results in a soft stagnant zone since the 60° kneading element has a lower conveying capacity than the 30° kneading element. The second kneading section is created using an aggressive 90° kneading element that guarantees a fully-filled zone. The next two kneading sections feature a combination of 30° and 60° kneading elements and a single 60° kneading element. This type of setup is typically used to process more complex formulations and involves additional powder or liquid feeding between the kneading sections. Towards the die section an assembly of different conveying elements is used, with a descending pitch from 30mm to 20mm and finally 15mm towards the die.

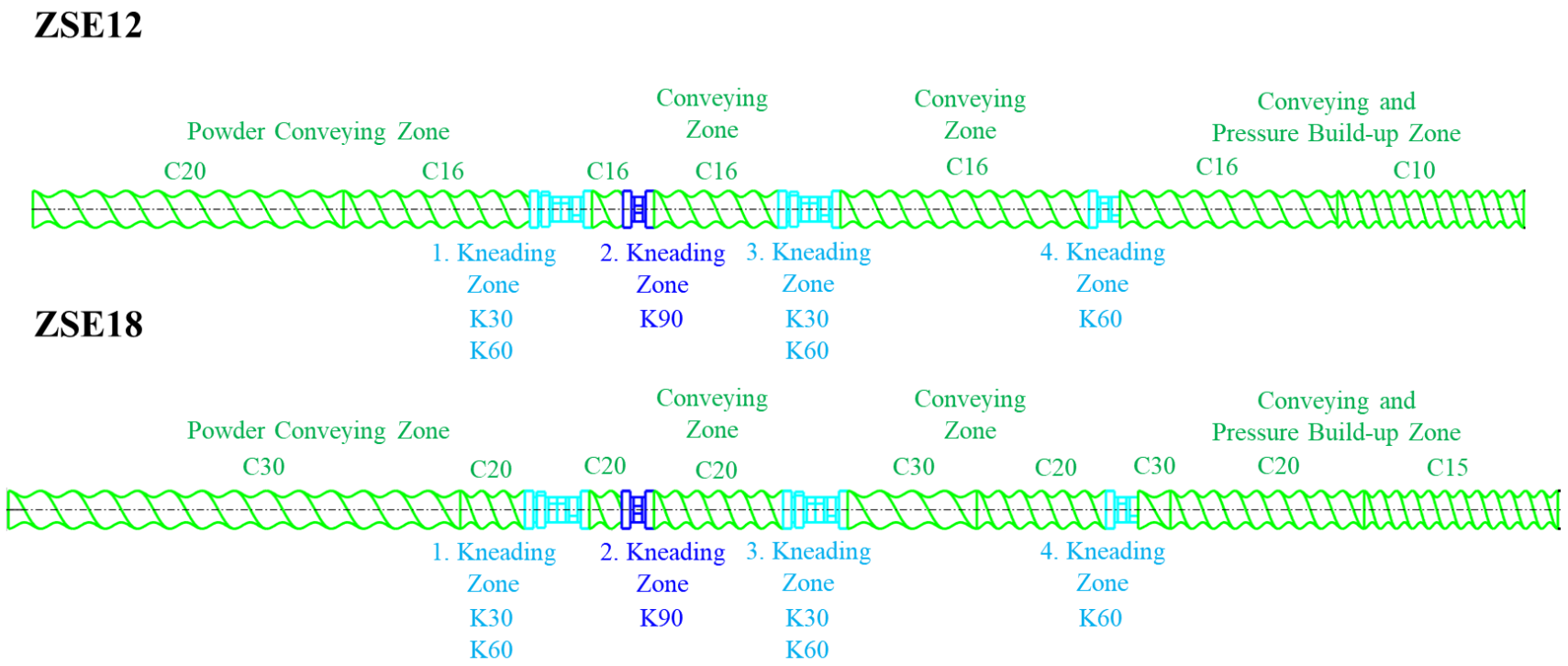

Figure 6.2. Prototype screw configuration used for the ZSE12 extruder experiments and 1D HME simulations for the first part of this paper and the corresponding transferred screw configuration on the ZSE18 extruder used for the experimental and 1D HME simulation setups.

Table 6.2. The screw configuration used during the ZSE12 extrusions discussed in detail in the first part of this paper [46].

Name	Screw Pitch/ Stagger Angle	Cumulative Length	Length Norm.	Length Norm. Sum	Section
GFF-2-20-30	20	30	2.50	2.50	1
GFA-2-20-30	20	60	2.50	5.00	
GFA-2-20-30	20	90	2.50	7.50	
GFA-2-20-10	20	100	0.83	8.33	
GFA-2-16-20	16	120	1.67	10.00	2
GFA-2-16-20	16	140	1.67	11.67	
GFA-2-16-20	16	160	1.67	13.33	
KB4-2-10-30°-Re	30°	170	0.83	14.17	3
KB4-2-10-60°-Re	60°	180	0.83	15.00	
GFA-2-16-10	16	190	0.83	15.83	4
KB4-2-10-90°	90°	200	0.83	16.67	5
GFA-2-16-20	16	220	1.67	18.33	6
GFA-2-16-20	16	240	1.67	20.00	
KB4-2-10-30°-Re	30°	250	0.83	20.83	7
KB4-2-10-60°-Re	60°	260	0.83	21.67	
GFA-2-16-20	16	280	1.67	23.33	8
GFA-2-16-20	16	300	1.67	25.00	
GFA-2-16-20	16	320	1.67	26.67	
GFA-2-16-20	16	340	1.67	28.33	
KB4-2-10-60°-Re	60°	350	0.83	29.17	9
GFA-2-16-20	16	370	1.67	30.83	10
GFA-2-16-20	16	390	1.67	32.50	
GFA-2-16-20	16	410	1.67	34.17	
GFA-2-16-10	16	420	0.83	35.00	
GFA-2-10-20	10	440	1.67	36.67	11
GFA-2-10-20	10	460	1.67	38.33	
GFA-2-10-20	10	480	1.67	40.00	

Table 6.3. The screw configuration used for the ZSE18 extrusions. The screw configuration was transferred from the one used during the ZSE12.

Name	Screw Pitch/ Stagger Angle	Cumulative Length	Length Norm.	Length Norm. Sum	Section
GFF-2-30-90	30	90	5.00	5.00	1
GFA-2-30-60	30	150	3.33	8.33	
GFA-2-30-60	20	210	3.33	11.67	2
GFA-2-20-30	20	240	1.67	13.33	
KB-4-2-15-30°-Re	30°	255	0.83	14.17	3
KB-4-2-15-60°-Re	60°	270	0.83	15.00	
GFA-2-20-15	20	285	0.83	15.83	4
KB-4-2-15-90°	90°	300	0.83	16.67	5
GFA-2-20-60	20	360	3.33	20.00	6
KB-4-2-15-30°-Re	30°	375	0.83	20.83	7
KB-4-2-15-60°-Re	60°	390	0.83	21.67	
GFA-2-30-30	20	450	3.33	25.00	8
GFA-2-30-30	20	480	1.67	26.67	
GFA-2-20-60	20	510	1.67	28.33	
KB-4-2-15-60°-Re	60°	525	0.83	29.17	9
GFA-2-30-15	20	555	1.67	30.83	10
GFA-2-20-30	20	585	1.67	32.50	
GFA-2-20-30	20	615	1.67	34.17	
GFA-2-20-30	20	630	0.83	35.00	
GFA-2-15-30	15	660	1.67	36.67	11
GFA-2-15-30	15	690	1.67	38.33	
GFA-2-15-30	15	720	1.67	40.00	

In contrast to the extrusions performed in the ZSE12 extruder, in the case of ZSE18, only one barrel temperature profile setup was chosen, with a maximal barrel temperature of 120°C in the processing zone. This will reduce the number of experiments since the effect of barrel temperature on the product quality was well addressed in our previous study [46]. Two settings from the previous ZSE12 extrusions were chosen for the scale-up tests: the PN 2 setting (0.4kg/h@100rpm with 3.4% API degradation) and the PN 9 setting (0.1kg/h@500rpm with 60.7% API degradation), both with a maximal barrel temperature of 120°C. These two settings represent the lowest and highest API degradations in the previous study of the ZSE12 extruder with the barrel temperature of 120°C. In the scale-up trials, six scale-up suggestions were investigated with nine additional extrusions acting as a quasi-DoE setup [7], [8], [47]. The scale-up variants are based on two principles:

- On geometric similarity with some kind of proportionality factor (five of the scale-up setups, e.g., to keeping mixing or heat-transfer times constant); and
- On π number dimensionless theory (one scale-up setup).

The setups relaying on geometric similarity all have the same basic form:

$$\frac{Y_2}{Y_1} = \left(\frac{D_2}{D_1}\right)^x \quad (1)$$

where x is the scale exponent, D_1 and D_2 are the nominal diameters of the original and target extruders (the ratio in brackets being 1.51), respectively. Y_1 and Y_2 are the transferred variables, such as screw speed, throughput or torque, of the original and target extruders, respectively. Scale exponent x is used as a scaling factor between the original and target extruders, as shown in Table 6.4.

Table 6.4. Values of the x scaling exponent used for the different scale-up rules based of geometry similarity between the ZSE12 and ZSE18 extruders.

	Common scale-up	Scale-up for heat transfer	Scale-up for mixing	Rauwendaal 1	Rauwendaal 2
n [rpm]	-0.5	-1	0	-0.769	-1
m [kg/h]	2	1.5	3	0	0.5

Scale-up based on the π-theorem approach by Menges and Feistkorn was reported in one of our previous papers [44]. The process settings are shown in Table 6.5. In comparison to the original settings, a combination of same or higher throughputs and same or lower screw speeds were calculated from the different scale-up laws. All scale-up variations shown in Table 6.5 span only a limited design space. Hence, in addition to the obtained process settings, nine additional DoE runs were performed to cover a range of 0.5kg/h to 1kg/h and 1.5kg/h and a screw speed of 100rpm, 200rpm and 300rpm. The goal of these additional settings was to explore a wider operating space. Varying the screw configuration to potentially obtain a better equivalent product quality at higher yield is another option, yet was not done in this study.

Table 6.5. Process parameters used for the scale-up trials and DoE on the ZSE18 target extruder. The original settings on the ZSE12 extruder were 0.4kg/h with a screw speed of 100rpm (resulting API degradation of 3.4%) and 0.1kg/h with a screw speed of 500rpm (resulting API degradation of 60.7%)..

	Process settings		m [kg/h]	n [rpm]	API Deg.
Literature Scale-up	Rauwendaal 1	R1-1	0.4	73	10.6%
		R1-2	0.1	366	100.0%
	Rauwendaal 2	R2-1	0.5	67	9.0%
		R2-2	0.1	333	100.0%
	Common scale-up	C1	0.9	82	5.2%
		C2	0.2	408	100.0%
	Scale-up for HT	HT-1	0.7	67	7.8%
		HT-2	0.2	333	100.0%
	Scale-up for Mixing	M-1	1.4	100	5.5%
		M-2	0.3	500	100.0%
	Menges & Feistkorn	Meng1	0.8	100	8.1%
		Meng2	0.2	500	100.0%
DoE Settings	DoE-1.1		0.5	100	9.5%
	DoE-1.2		0.5	200	39.4%
	DoE-1.3		0.5	300	60.0%
	DoE-2.1		1	100	7.8%
	DoE-2.2		1	200	17.1%
	DoE-2.3		1	300	28.8%
	DoE-3.1		1.5	100	5.3%
	DoE-3.2		1.5	200	11.5%
	DoE-3.3		1.5	300	19.4%

6.2.2 Formulation, API degradation and residence time distribution measurements

The formulation investigated was the same one used in our previous study (ZSE12 [46]): a simple two-component system with a 80% mass loading of Eudragit RL PO and a 20% mass loading of Famotidine as the API of choice for the preparation of a solid dispersion. Importantly, Famotidine is known to be prone to degradation right after melting [48]–[53]. Hence, the API degradation during extrusion was expected and used as a quality attribute. Degradation was measured offline with UPLC of samples collected during the extrusion. For more details of the approach to quantifying the API degradation, please refer to our previous publication [46]. For other details regarding (i) analysis and parametrization of the formulation, (ii) parametrization of the 1D HME simulation model and (iii) the measurement and analysis

method of the process residence time distribution (RTD) can also be found in our previous publications [44], [46], [54], [55].

6.3 Results and Discussion

During the experimental runs, the dependent process values, such as the torque, the specific mechanical energy consumption (SMEC) and the RTD, were monitored and characterized. The obtained results were compared to in silico obtained results of the same process settings using our 1D HME software developed in-house. These are in good agreement, as shown in Figure 6.3 to Figure 6.5. In the context of scale-up, it is interesting to compare the change of the dependent process variables as a function of the scale-up (i.e., the expected change in the values for a given extruder size difference). These results are summarized in Table 6.6. The obtained torque values from the ZSE18 experiments are all clustered around 30Nm. Considering that for process settings PN 2 (0.4kg/h@100rpm) and PN 9 (0.1kg/h@500rpm) of the original ZSE12 extruder 4.3Nm and 3.6Nm of torque were needed for processing, the torque required for equivalent processing on ZSE18 is around 7 times higher, while the screw diameter is only a 1.5 times larger. This is an important result with regard to choosing proper equipment to scale to and taking into account its torque limitations. In addition to the process torque, the process SMEC was evaluated and compared to the values obtained in silico (Figure 6.4). The SMEC is calculated based on the process torque, throughput and screw speed as follow:

$$SMEC\ [kWh/kg] = \frac{2 \cdot \pi \cdot n[rpm] \cdot \tau[Nm]}{60000 \cdot \dot{m}[kg/h]} \quad (2)$$

The resulting SMEC values show a higher overall achieved SMEC with a wider range of 0.25-0.54kWh/kg compared to the original 0.11kWh/kg (PN2 case) and of 4.1-10.6kWh/kg compared to the original 1.88kWh/kg (PN9 case). This indicates that similarly to the torque, after scale-up, the SMEC increases by a factor of 2 to 5. This is significant since SMEC mostly contributes to the viscous dissipation and an increase in melt temperature. If then the extruder size change is also considered, knowing that the increase in the available surface area for efficient cooling of the melt (scales with square power of the size) scales slower to the available material in a certain location that requires cooling (scales cubically), higher overall melt temperatures can be expected when processing the material in the ZSE18 extruder compared to the ZSE12, for the investigated scale-up rules.

In addition, the mean residence time (mRT) was evaluated and compared to the values obtained *in silico*, showing good agreement, Figure 6.5. Similarly to the torque and the SMEC, the mRT

changed as a result of scale-up. Having mRT of 164s at small scale (in PN2 case), the mRT values in the target extruder were about 140s to 420s, resulting in a difference of 0.85 to 2.6 compared to the small scale. Similar differences were observed in the second setup (PN9 case). At the small scale an mRT of 498s was observed and mRT values of about 495s to 475s were achieved at the large scale, resulting in 1 to 3 times longer mRTs. In line with the analysis of the SMEC values, this indicates that in addition to higher expected melt temperatures the formulation is subjected to an, on average, longer process time. Taking all of the above into consideration, the achieved API degradations can be analyzed as a function of process settings and dependent process variables, which can be compared to the originally achieved API degradations on the smaller extruder. Table 6.5 and Figure 6.6 show the small-scale process settings and the original API degradation points of the ZSE12 extruder, the process settings obtained using the various scale-up approaches and the DoE settings of the target ZSE18 extruder with the corresponding API degradations.

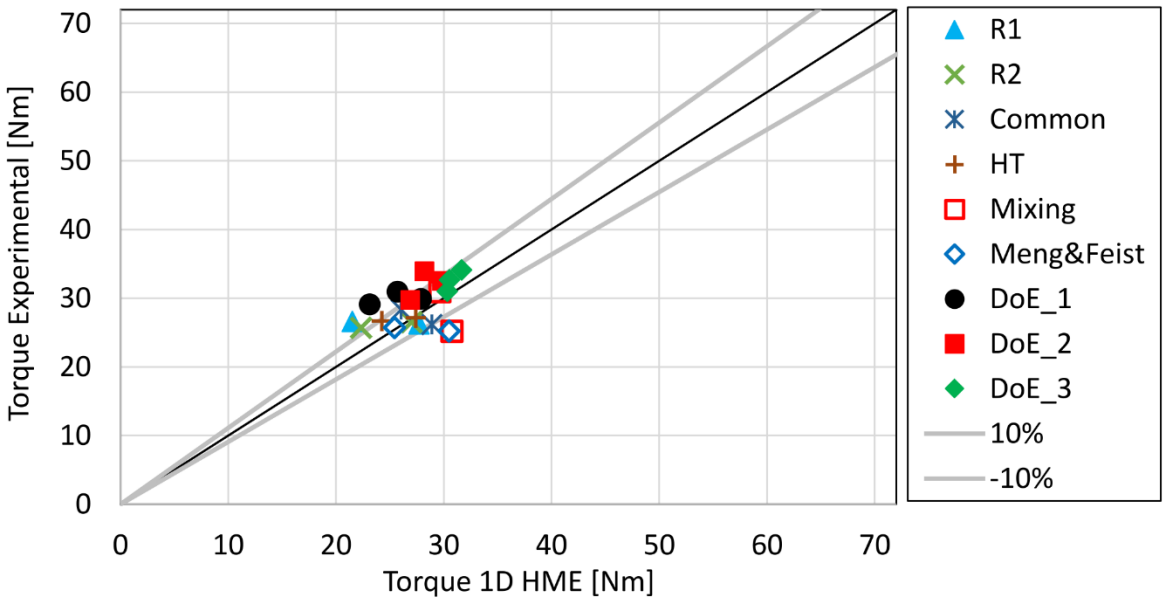

Figure 6.3. Comparison between the *in silico* and experimentally obtained torque values from the scale-up and DoE extrusion in the ZSE18 extruder.

Table 6.6. Comparison between the torque, SMEC and mRT values for two process settings of the original extruder (PN 2 and PN 9 of ZSE12) and their corresponding scale-up settings of the target ZSE18 extruder, with calculated relative change values.

ZSE12	ZSE18	n [rpm]	m [kg/h]	Torque ZSE12 [Nm]	Torque ZSE18 [Nm]	Relative Change [-]	SMEC ZSE12 [kWh/kg]	SMEC ZSE18 [kWh/kg]	Relative Change [-]	mRT ZSE12 [s]	mRT ZSE18 [s]	Relative Change [-]
PN 2 (0.4kg/h@100rpm)	R1-1	73	0.4	4.3	28.1	6.6	0.11	0.54	4.8	164	425	2.6
	R2-1	67	0.5		27.1	6.4		0.39	3.5		346	2.1
	C1	82	0.9		29.9	7.0		0.28	2.5		230	1.4
	HT-1	67	0.7		28.1	6.6		0.27	2.4		284	1.7
	M-1	100	1.4		32.6	7.7		0.25	2.3		143	0.9
	Meng1	100	0.8		27.2	6.4		0.36	3.2		215	1.3
PN 9 (0.1kg/h@500rpm)	R1-2	366	0.1	3.6	27.7	7.7	1.88	10.61	5.6	498	1475*	3.0
	R2-2	333	0.1		28.0	7.8		7.95	4.2		1476*	3.0
	C2	408	0.2		27.6	7.7		5.23	2.8		741*	1.5
	HT-2	333	0.2		28.6	8.0		5.42	2.9		743*	1.5
	M-2	500	0.3		26.5	7.4		4.10	2.2		495*	1.0
	Meng2	500	0.2		26.6	7.4		6.96	3.7		739*	1.5

*Obtained via 1D HME simulations

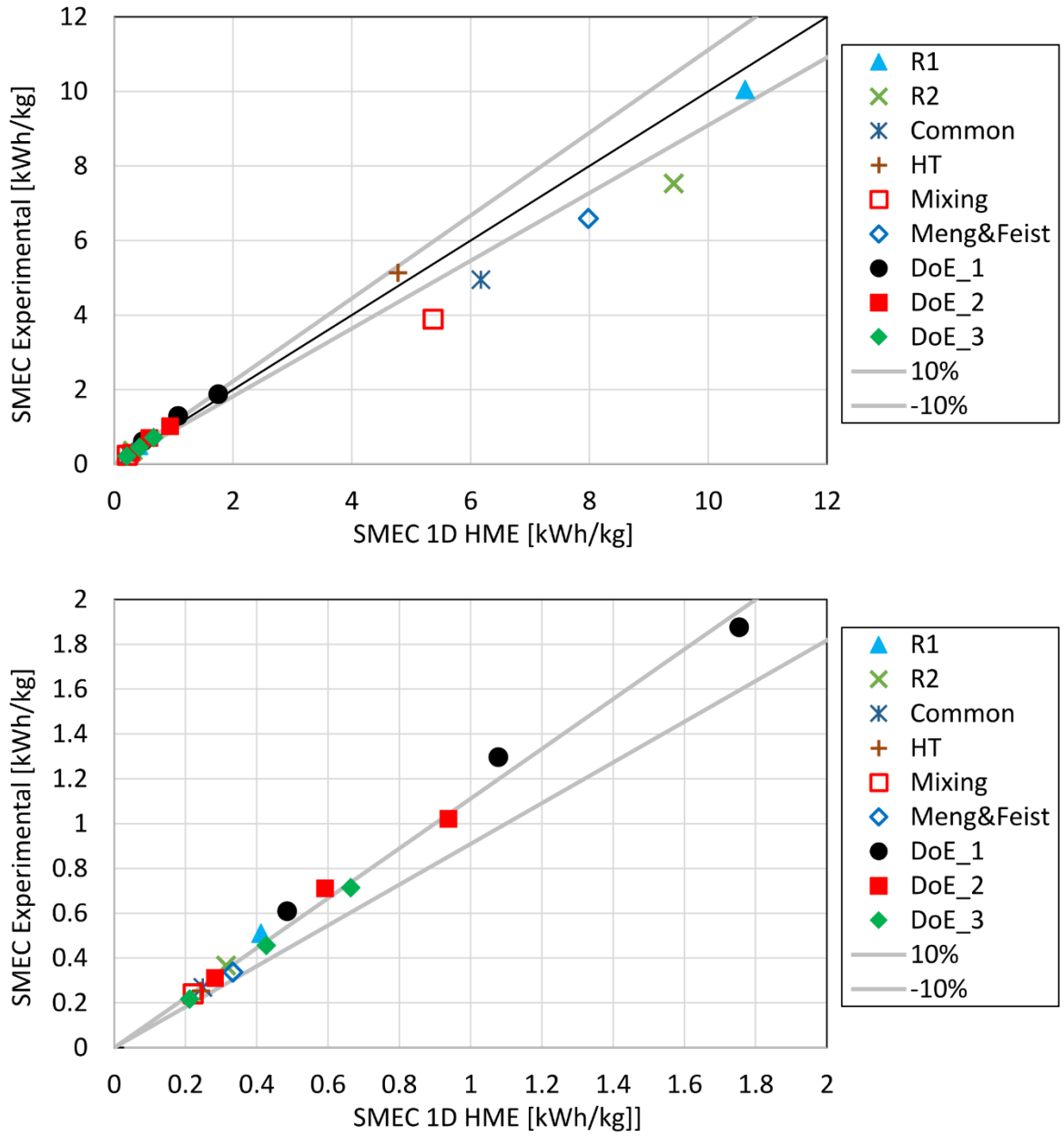

Figure 6.4. Comparison between the *in silico* and experimentally obtained SMEC values from the scale-up and DoE extrusion in the ZSE18 extruder. Top figure shows the SMEC values from 0 to 12kWh/kg, and bottom figure shows a zoomed in view with SMEC values from 0 to 2kWh/kg.

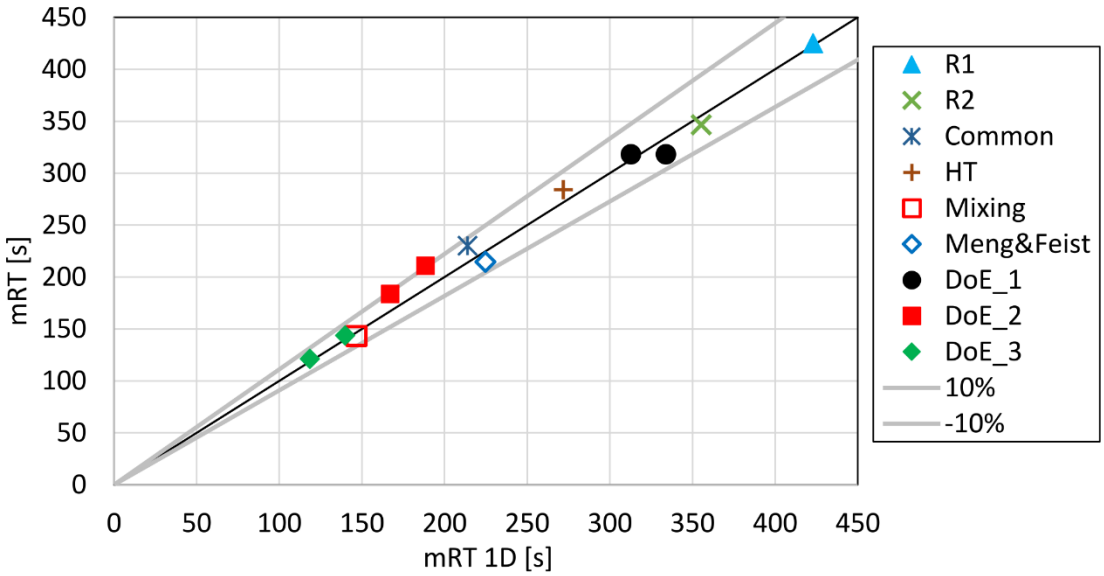

Figure 6.5. Comparison between the *in silico* and experimentally obtained mean RTD values from the scale-up and DoE extrusion in the ZSE18 extruder.

As can be seen from the Figure 6.6 and Table 6.5, none of the scale-up options resulted in the same API degradations. The API degradations range from 5.2% to 10.6% for the scale-up settings based on 3.4% API degradation settings (PN2, 0.4kg/h@100rpm, ZSE12), and the scale-up settings with 60.7% API degradation as a basis (i.e., PN9, 0.1kg/h@500rpm, ZSE12) resulted in a complete API degradation in the large-scale extruder. The DoE settings result in API degradations of 9.5% to 60% at 0.5kg/h throughput, 7.8% to 28.8% at 1kg/h throughput and 5.3% to 19.4% at 1.5kg/h throughput. As the ZSK18 settings derived from the PN9 setup from the small scale extruder, all resulting in complete API degradation, they will not be analyzed further. The Figure 6.6 bottom shows the process settings versus the API degradation derived from the PN2 setup and the nine DoE settings. If only the DoE settings are analyzed, it is clear that for a constant screw speed, barrel temperature and screw configuration an increase in the throughput directly decreases the API degradation. Given that everything except the throughput is kept constant, it can be argued that the prevailing stress state induced on the formulation is also constant since the stress acting on the formulation is a function of screw and barrel geometry parameters and the screw speed. Hence, an increase in the throughput reduces the API degradation due to the reduction in the mRT.

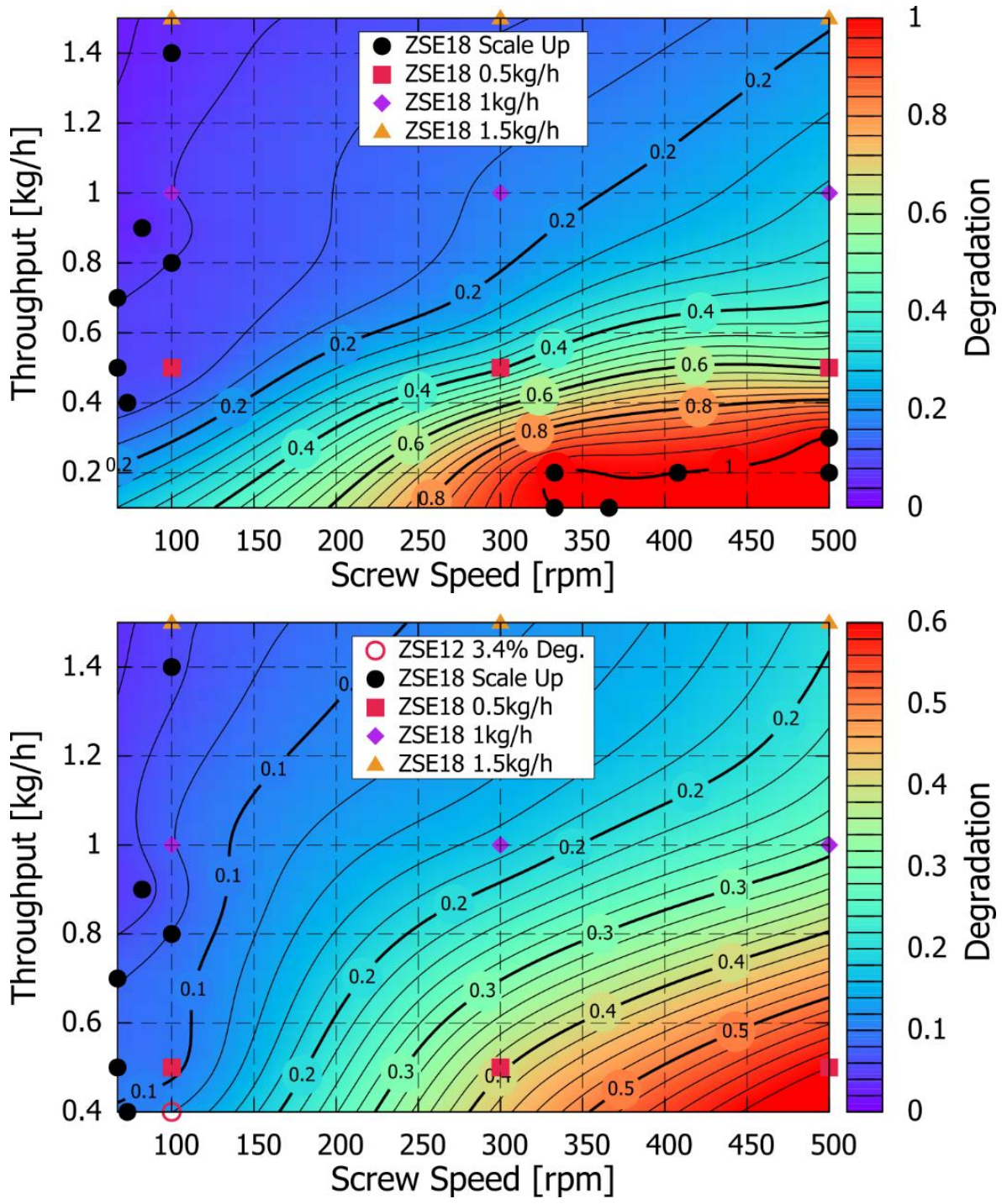

Figure 6.6. Process settings and product quality (extent of API degradation in the extrudate) related to various scale-up scenarios in the ZSE18 extruder. Top: Scale-up and DoE settings on the ZSE18 extruder; Bottom: Scale-up and DoE settings on the ZSE18 extruder, only based on the ZSE18 0.4kg/h@100rpm-3.4% API Degradation (this figure excludes the settings that resulted with 100% API Degradation)

This is demonstrated in Figure 6.7, which shows the achieved API degradation as a function of the overall process mRT_{1D}. Clearly, a reduction in the process throughput results in an increase of the processing time of the formulation (longer mean residence time) and higher overall

degradation and spread of achieved API degradations when varying the screw speed. Increasing the process throughput reduces the API degradation levels and the spread of achieved API degradations. Still, as suggested by the results of the scale-up settings, the mean residence time is not an unambiguous process descriptor and cannot be directly connected to the API degradation. Similar API degradations can be achieved at various mean residence times. For example, ~10% API degradation can be achieved with mRT_{1D} values of around 110s, 330s and 425s.

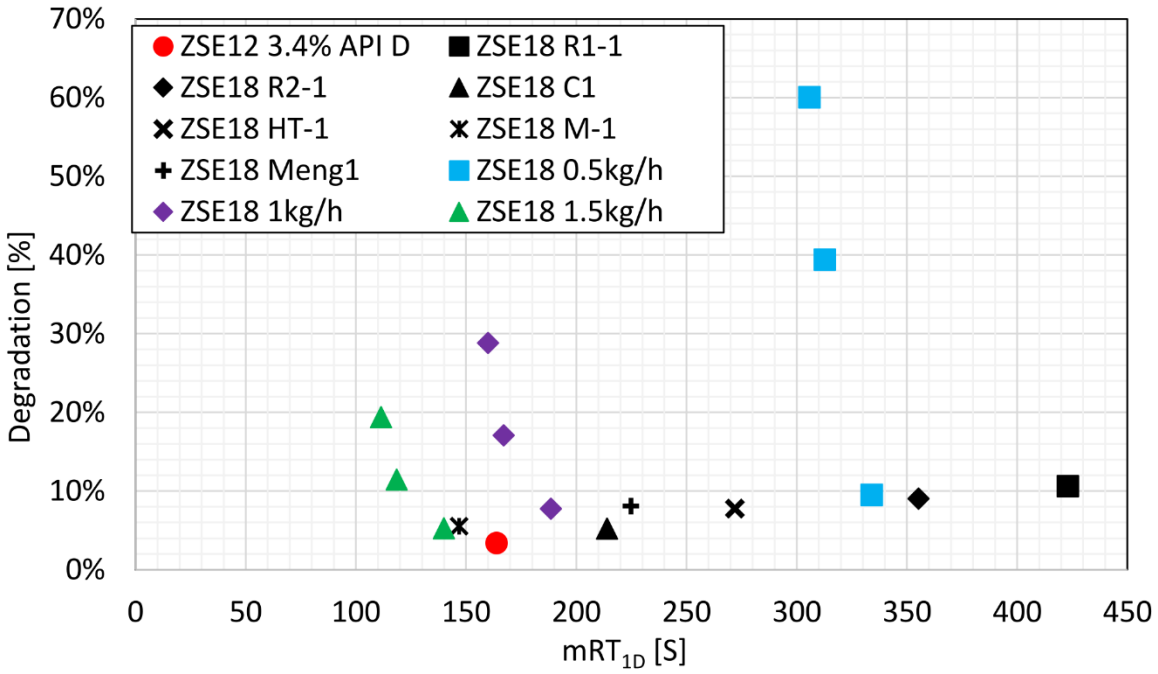

Figure 6.7. Achieved API degradation as a function of process mRT_{1D}. Comparison between 0.4kg/h@100rpm settings of the original extruder, resulting in a degradation of 3.4%, and the scaled and DoE settings of the target ZSE18 extruder.

Going back to Figure 6.6 and the DoE settings, any increase in the screw speed corresponds to an increase in the API degradation. Although an increase in the screw speed also leads to some reduction in the mRT, the mRT does not play the key role in such a scenario. Here the direct increase in the viscous dissipation caused by a higher screw speed directly results in an increase in the observed API degradation. Comparing the ZSE18 settings to the original setting on the ZSE12 extruder, the data suggest that a one to one process transfer (keeping the screw speed and throughput constant regardless of the extruder size change) would result likely result in an API degradation close to 12%, in comparison to the original 3.4%.

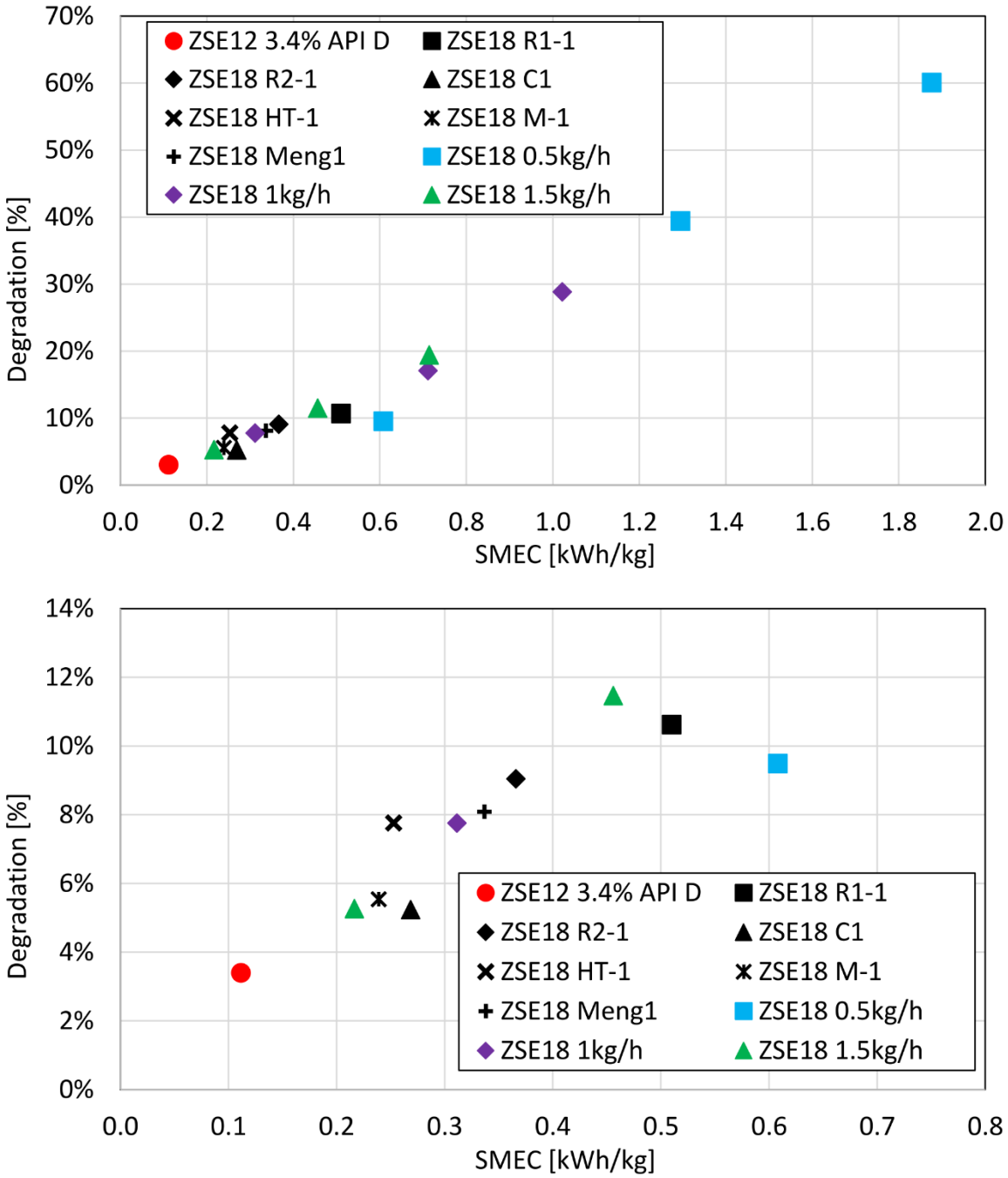

Figure 6.8. Achieved API degradation as a function of process SMEC for the small-scale extruder (PN2 case) and the large-scale ZSE18 extruder. Top figure in the full SMEC range from 0kWh/kg to 2kWh/kg, bottom figure in the SMEC range from 0kWh/kg to 0.8kWh/kg.

Trying to connect the achieved process SMEC to the achieved API degradation yields similar results as in the case of the mRT, Figure 6.8. At first glance, the SMEC linearly correlates with the API degradation, i.e., a higher process SMEC generally resulting in a higher API degradation. However, the correlation is not as clear when most of the available data for API degradations below ~12% is examined in detail. Again, multiple points can be found with either

a similar SMEC but different resulting API degradations or a similar API degradation achieved at different process SMEC values.

Please note that the above results only cover a limited range of process settings, one barrel temperature setting and, more importantly, only one screw configuration. Varying the screw configuration could lead to even bigger issues when trying to connect the API degradation or any other product specific quality attribute to the process dependent or independent variables. Therefore, the SMEC and the mRT cannot be considered unambiguous indicators of expected product quality. This also means that the use of statistics based analysis, such as those used in typical DoE setups, is limited.

Assuming that the API degradation directly correlates with the melt temperature and the mean residence time in the screw zones, heat maps were created for the different processing zones along the screw configuration. These heat maps show the API degradation as a function of the averaged melt temperature in the analyzed zone and the local mRT_{1D} (i.e. exposure time). The calculated values of the local melt temperature correspond to the melt temperature averaged over the section length and the screw cross section. From the DoE data it is clear that an increase in screw speed, for everything else left constant, leads to a direct melt temperature increase in the fully filled zones, in this case in the location of the 90° kneading element. On the other hand, and increase in throughput reduces the local exposure time (lmRT) the processed formulation in subjected to a certain temperature, in the fully filled screw zone. The combination of the exposure time and temperature have a good correlation to the achieved API degradation. Extrusions performed in the ZSE12 [46] extruder showed that the local melt temperature and the local mRT_{1D} of the harshest kneading element zone with 90° kneading elements correlates best with the achieved API degradation values. The same is true in the case of ZSE18 extrusions, as demonstrated in Figure 6.9. On the left side of the Figure, the starting point of the ZSE12 extruder is shown with a local mRT of about 8 seconds and an average melt temperature of about 158°C, which resulted in an API degradation of 3.4% in the extrudate. The remaining points in the plot are a result of the scale-up including the DoE settings. Similar to the results of the ZSE12 extrusions, an increase in the exposure time or exposure to a higher melt temperature inevitably leads to an increase in API degradation in the extrudate. This provides a very direct and intuitive link to the expected product quality and offers new possibilities for the process design and scale-up. Such a correlation could be very significant in the process design and scale-up phases.

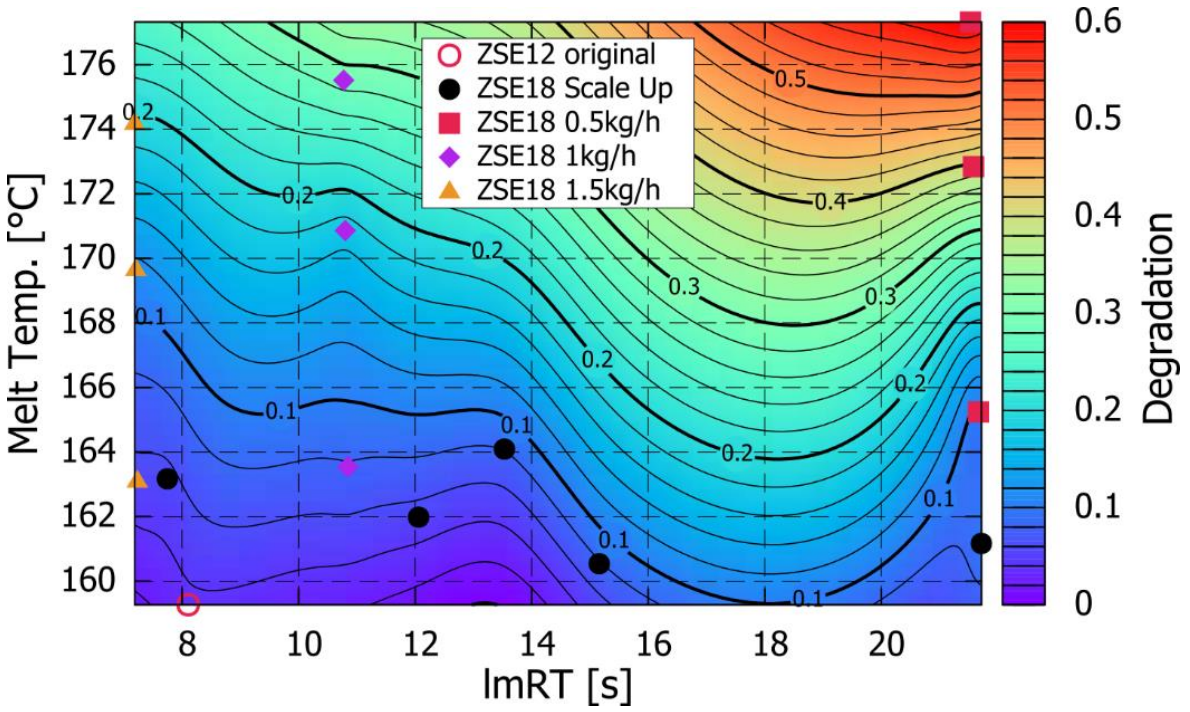

Figure 6.9. API degradation as a function of local average melt temperature and local mRT in the 90° kneading element section (at 90° kneading element). Only scale-up results for the small-scale case (PN2 with 3.4% API degradation at 0.4kg/h and100rpm) as a basis are shown.

By designing the formulation's heat map (exposure time vs. temperature vs. chosen quality attribute) before the first extrusion experiments, various extruder setups and settings could be investigated fully *in silico* to provide a first estimate of the expected product quality before any extrusion trials commence. Moreover, based on knowledge obtained from the formulation heat map, smaller-scale extrusions and mechanistic process simulations could be performed, greatly reducing the risk during the process scale-up since various process variants. Following this, potential process setups could be tested and evaluated fully *in silico* without the waste, facilities and costs associated with non-GMP and GMP process setups. It should be noted that, although promising, this approach should be tested and further improved using a variety of formulations, product quality attributes, extruders and process setups.

6.4 Summary and Conclusions

This study is a continuation of the previously reported analysis of experiments and simulations for small-scale ZSE12 twin screw extruder. Our work focuses on correlations between the process settings and the product quality (in this case degradation), as well as on the effect of the extruder size on the product quality. As part of the process transfer from ZSE12 to the ZSE18 extruder, the transfer of the screw configuration was addressed and several scale-up laws were applied. The resulting API degradation was compared to the original one from the previous study.

No scale-up law applied resulted in the same API degradation as the original one: all of the resulting API degradations were higher than those of the original ones. As part of the analysis, the influence of process independent and dependent variables was analyzed with the goal of finding correlations with the resulting process quality. In line with the previous study, it was established that the API degradation correlates well with the local average melt temperature and the local mean residence time in a certain zone along the screw configuration. In the case of the formulation and screw configuration studied, the 90° kneading element zone was the most significant one. Note that local values of the melt temperature along the screw configuration and local mean residence times for different sections along the screw configuration are not readily available with current experimental approaches, but are relatively simple to compute with help of different simulation approaches shown here. The above correlation seems to be scale-independent since it was established in both ZSE12 and ZSE18 extrusion studies. The results indicate the possibility of predicting the product quality *in silico* prior to any extrusion experiments, provided that a heat map of the formulation can be created showing correlations between the formulation's quality attributes, melt temperature and exposure time. The process scale-up could also be reduced to a simple *in silico* DoE study on various extruder scales. The next steps will be to evaluate this approach and refine it using a variety of formulations, product quality attributes, extruder and process conditions.

6.5 Abbreviations

1D	One Dimensional
API	Active Pharmaceutical Ingredient
CQA	Critical Quality Attributes
DoE	Design of Experiments
EMA	European Medicines Agency
FDA	Food Drug Administration
HME	Hot Melt Extrusion
QbD	Quality by Design
RTD	Residence Time Distribution
SPH	Smoothed Particle Hydrodynamics
TSE	Co-rotating twin-screw extruders
Y1, Y2, D1, D2	Original and target values for the scale-up transfer between extruder of two different diameters (D1 and D2)
ZSE12 HP-PH	12mm Leistritz Co-rotating Twin Screw Extruder
ZSE18 HP-PH	18mm Leistritz Co-rotating Twin Screw Extruder

6.6 Nomenclature

Latin symbols

Cl [mm]	Centerline distance
D, Do, Di [mm]	Barrel diameter, Outer Screw diameter, Inner screw diameter, respectively
lmRT [s]	local mean residence time or exposure time
m [kg/h]	Throughput
mRT [s]	mean Residence Time
n [rpm]	Screw speed
SMEC [kWh/kg]	specific mechanical energy consumption

Greek symbols

α [°]	Angle between the kneading discs
τ, τ_{max} [Nm]	Extruder torque and maximal available extruder torque, respectively

6.7 References

[1] ICH Q8, "EMEA/CHMP, 2009, ICH Topic Q 8 (R2) Pharmaceutical Development, Step 5: Note for Guidance on Pharmaceutical Development," vol. 8, no. June, 2017.

[2] L. X. Yu *et al.*, "Understanding Pharmaceutical Quality by Design," *AAPS J.*, vol. 16, no. 4, pp. 771–783, Jul. 2014.

[3] V. P. Kumar and N. V. Gupta, "A Review on quality by design (QBD) for Pharmaceuticals," *Int. J. Drug Dev. Res.*, vol. 7, no. 1, pp. 35–44, 2015.

[4] V. Mishra, S. Thakur, A. Patil, and A. Shukla, "Quality by design (QbD) approaches in current pharmaceutical set-up," *Expert Opin. Drug Deliv.*, vol. 15, no. 8, pp. 737–758, Aug. 2018.

[5] A. Gupta and M. A. Khan, "Hot-Melt Extrusion: An FDA Perspective on Product and Process Understanding," in *Hot-Melt Extrusion: Pharmaceutical Applications*, Chichester, UK: John Wiley & Sons, Ltd, 2012, pp. 323–331.

[6] M. T. Islam, M. Maniruzzaman, S. A. Halsey, B. Z. Chowdhry, and D. Douroumis, "Development of sustained-release formulations processed by hot-melt extrusion by using a quality-by-design approach," *Drug Deliv. Transl. Res.*, vol. 4, no. 4, pp. 377–387, Aug. 2014.

[7] K. Kohlgrüber *et al.*, *Co-Rotating Twin-Screw Extruder*. München: Carl Hanser Verlag GmbH & Co. KG, 2007.

[8] C. Rauwendaal, *Polymer extrusion: Fifth edition*, Fifth Edit. München: Carl Hanser Verlag GmbH & Co. KG, 2014.

[9] K. Kolter, M. Karl, and A. Gryczke, *Hot-Melt Extrusion with BASF polymers*, no. 2nd Revised and Enlarged. BASF, 2012.

[10] H. McFall *et al.*, "Formulation of aripiprazole-loaded pH-modulated solid dispersions via hot-melt extrusion technology: In vitro and in vivo studies," *Int. J. Pharm.*, vol. 554, pp. 302–311, Jan. 2019.

[11] M. A. Repka *et al.*, "Melt extrusion with poorly soluble drugs – An integrated review," *Int. J. Pharm.*, vol. 535, no. 1–2, pp. 68–85, 2018.

[12] J. M. Vasoya *et al.*, "Development of Solid Dispersion by Hot Melt Extrusion Using Mixtures of Polyoxylglycerides With Polymers as Carriers for Increasing Dissolution Rate of a Poorly Soluble Drug Model," *J. Pharm. Sci.*, vol. 108, no. 2, pp. 888–896, Feb. 2019.

[13] A. Schittny, H. Ogawa, J. Huwyler, and M. Puchkov, "A combined mathematical model linking the formation of amorphous solid dispersions with hot-melt-extrusion process parameters," *Eur. J. Pharm. Biopharm.*, vol. 132, pp. 127–145, Nov. 2018.

[14] M. M. Crowley *et al.*, "Pharmaceutical Applications of Hot-Melt Extrusion: Part I," *Drug Dev. Ind. Pharm.*, vol. 33, no. 9, pp. 909–926, Jan. 2007.

[15] M. A. Repka *et al.*, "Pharmaceutical Applications of Hot-Melt Extrusion: Part II," *Drug Dev. Ind. Pharm.*, vol. 33, no. 10, pp. 1043–1057, Jan. 2007.

[16] J. G. Khinast, R. Baumgartner, and E. Roblegg, "Nano-extrusion: a One-Step Process for Manufacturing of Solid Nanoparticle Formulations Directly from the Liquid Phase," *AAPS PharmSciTech*, vol. 14, no. 2, pp. 601–604, Jun. 2013.

[17] R. Baumgartner, J. Matić, S. Schrank, S. Laske, J. G. J. Khinast, and E. Roblegg, "NANEX: Process design and optimization," *Int. J. Pharm.*, vol. 506, no. 1–2, pp. 35–45, Jun. 2016.

[18] R. Baumgartner, A. Eitzlmayr, N. Matsko, C. Tetyczka, J. G. Khinast, and E. Roblegg, "Nano-extrusion: A promising tool for continuous manufacturing of solid nano-formulations," *Int. J. Pharm.*, vol. 477, no. 1–2, pp. 1–11, Dec. 2014.

[19] A. M. Bhagurkar, M. A. Repka, and S. N. Murthy, "A Novel Approach for the Development of a Nanostructured Lipid Carrier Formulation by Hot-Melt Extrusion Technology," *J. Pharm. Sci.*, vol. 106, no. 4, pp. 1085–1091, Apr. 2017.

[20] L. A. D. Silva *et al.*, "Preparation of a solid self-microemulsifying drug delivery system by hot-melt extrusion," *Int. J. Pharm.*, vol. 541, no. 1–2, pp. 1–10, Apr. 2018.

[21] H. Patil, X. Feng, X. Ye, S. Majumdar, and M. A. Repka, "Continuous Production of Fenofibrate Solid Lipid Nanoparticles by Hot-Melt Extrusion Technology: a Systematic Study Based on a Quality by Design Approach," *AAPS J.*, vol. 17, no. 1, pp. 194–205, Jan. 2015.

[22] C. Bode, H. Kranz, A. Fivez, F. Siepmann, and J. Siepmann, "Often neglected: PLGA/PLA swelling orchestrates drug release: HME implants," *J. Control. Release*, vol. 306, no. May, pp. 97–107, Jul. 2019.

[23] A. Cossé, C. König, A. Lamprecht, and K. G. Wagner, "Hot Melt Extrusion for Sustained Protein Release: Matrix Erosion and In Vitro Release of PLGA-Based Implants," *AAPS PharmSciTech*, vol. 18, no. 1, pp. 15–26, Jan. 2017.

[24] S. Eder *et al.*, "Establishment of a Molding Procedure to Facilitate Formulation Development for Co-extrudates," *AAPS PharmSciTech*, vol. 18, no. 8, pp. 2971–2976, Nov. 2017.

[25] I. Koutsamanis *et al.*, "Formulation and processability screening for the rational design of ethylene-vinyl acetate based intra-vaginal rings," *Int. J. Pharm.*, vol. 564, no. April, pp. 90–97, Jun. 2019.

[26] I. Koutsamanis, A. Paudel, K. Nickisch, K. Eggenreich, E. Roblegg, and S. Eder, "Controlled-Release from High-Loaded Reservoir-Type Systems—A Case Study of Ethylene-Vinyl Acetate and Progesterone," *Pharmaceutics*, vol. 12, no. 2, p. 103, Jan. 2020.

[27] Y. Zhu, N. H. Shah, A. Waseem Malick, M. H. Infeld, and J. W. McGinity, "Controlled Release of a Poorly Water-Soluble Drug from Hot-Melt Extrudates Containing Acrylic Polymers," *Drug Dev. Ind. Pharm.*, vol. 32, no. 5, pp. 569–583, Jan. 2006.

[28] A. Q. Vo *et al.*, "A novel floating controlled release drug delivery system prepared by hot-melt extrusion," *Eur. J. Pharm. Biopharm.*, vol. 98, pp. 108–121, Jan. 2016.

[29] M. Fukuda, N. A. Peppas, and J. W. McGinity, "Floating hot-melt extruded tablets for gastroretentive controlled drug release system," *J. Control. Release*, vol. 115, no. 2, pp. 121–129, Oct. 2006.

[30] D. Treffer, A. Troiss, and J. G. Khinast, "A novel tool to standardize rheology testing of molten polymers for pharmaceutical applications," *Int. J. Pharm.*, vol. 495, no. 1, pp. 474–481, Nov. 2015.

[31] R. A. Gingold and J. J. Monaghan, "Smoothed particle hydrodynamics: theory and application to non-spherical stars," *Mon. Not. R. Astron. Soc.*, vol. 181, no. 3, pp. 375–389, Dec. 1977.

[32] J. J. Monaghan, "Smoothed particle hydrodynamics," *Reports Prog. Phys.*, vol. 68, no. 8, pp. 1703–1759, Aug. 2005.

[33] H. Bauer, J. Matić, and J. Khinast, "Characteristic parameters and process maps for fully-filled twin-screw extruder elements," *Chem. Eng. Sci.*, p. 116202, Oct. 2020.

[34] J. J. Monaghan, "Smoothed Particle Hydrodynamics and Its Diverse Applications," *Annu. Rev. Fluid Mech.*, vol. 44, no. 1, pp. 323–346, Jan. 2012.

[35] R. A. Gingold and J. J. Monaghan, "Kernel Estimates as a Basis for General Particle Methods in Hydrodynamics," *J. Comput. Phys.*, vol. 46, pp. 429–453, 1982.

[36] M. Ellero and R. I. Tanner, "SPH simulations of transient viscoelastic flows at low Reynolds number," *J. Nonnewton. Fluid Mech.*, vol. 132, no. 1–3, pp. 61–72, Dec. 2005.

[37] J. P. Morris, P. J. Fox, and Y. Zhu, "Modeling Low Reynolds Number Incompressible Flows Using SPH," *J. Comput. Phys.*, vol. 136, no. 1, pp. 214–226, Sep. 1997.

[38] A. Eitzlmayr, J. Matić, and J. G. Khinast, "Analysis of flow and mixing in screw

elements of corotating twin-screw extruders via SPH," *AIChE J.*, vol. 63, no. 6, pp. 2451–2463, Jun. 2017.

[39] A. Eitzlmayr and J. G. Khinast, "Co-rotating twin-screw extruders: Detailed analysis of conveying elements based on smoothed particle hydrodynamics. Part 1: Hydrodynamics," *Chem. Eng. Sci.*, vol. 134, pp. 861–879, Sep. 2015.

[40] A. Eitzlmayr and J. G. Khinast, "Co-rotating twin-screw extruders: Detailed analysis of conveying elements based on smoothed particle hydrodynamics. Part 1: Hydrodynamics," *Chem. Eng. Sci.*, vol. 134, pp. 861–879, Sep. 2015.

[41] A. Eitzlmayr, G. Koscher, and J. G. Khinast, "A novel method for modeling of complex wall geometries in smoothed particle hydrodynamics," *Comput. Phys. Commun.*, vol. 185, no. 10, pp. 2436–2448, Oct. 2014.

[42] A. Eitzlmayr *et al.*, "Mechanistic modeling of modular co-rotating twin-screw extruders," *Int. J. Pharm.*, vol. 474, no. 1–2, pp. 157–176, Oct. 2014.

[43] A. Eitzlmayr *et al.*, "Experimental characterization and modeling of twin-screw extruder elements for pharmaceutical hot melt extrusion," *AIChE J.*, vol. 59, no. 11, pp. 4440–4450, Nov. 2013.

[44] J. Matić, A. Witschnigg, M. Zagler, S. Eder, and J. Khinast, "A novel in silico scale-up approach for hot melt extrusion processes," *Chem. Eng. Sci.*, vol. 204, pp. 257–269, Aug. 2019.

[45] J. Matić, A. Paudel, H. Bauer, R. A. L. Garcia, K. Biedrzycka, and J. G. Khinast, "Developing HME-Based Drug Products Using Emerging Science: a Fast-Track Roadmap from Concept to Clinical Batch," *AAPS PharmSciTech*, vol. 21, no. 5, p. 176, Jul. 2020.

[46] J. Matić *et al.*, "Towards predicting the product quality in hot-melt extrusion: Small scale extrusion," *Int. J. Pharm. X*, vol. 2, p. 100062, Dec. 2020.

[47] D. Douroumis, *Hot-Melt Extrusion: Pharmaceutical Applications*. Chichester, UK: John Wiley & Sons, Ltd, 2012.

[48] G. L. Perpétuo *et al.*, "Thermal behavior of some antihistamines," *J. Therm. Anal. Calorim.*, vol. 111, no. 3, pp. 2019–2028, Mar. 2013.

[49] R. I. Mustafin, "Interpolymer combinations of chemically complementary grades of Eudragit copolymers: a new direction in the design of peroral solid dosage forms of drug delivery systems with controlled release (review)," *Pharm. Chem. J.*, vol. 45, no. 5, pp. 285–295, Aug. 2011.

[50] M. Maniruzzaman, M. M. Rana, J. S. Boateng, J. C. Mitchell, and D. Douroumis,

"Dissolution enhancement of poorly water-soluble APIs processed by hot-melt extrusion using hydrophilic polymers," *Drug Dev. Ind. Pharm.*, vol. 39, no. 2, pp. 218–227, Feb. 2013.

[51] M. Chordiya, H. Gangurde, K. Senthilkumaran, and L. Kothari, "Formulation development and in vitro evaluation of gastroretentive hollow microspheres of famotidine," *Int. J. Pharm. Investig.*, vol. 1, no. 2, p. 105, 2011.

[52] T. Parikh, S. S. Gupta, A. Meena, and A. T. M. Serajuddin, "Investigation of thermal and viscoelastic properties of polymers relevant to hot melt extrusion - III: Polymethacrylates and polymethacrylic acid based polymers," *J. Excipients Food Chem.*, vol. 5, no. 1, pp. 56–64, Mar. 2014.

[53] M. T. Viciosa, J. J. Moura Ramos, and H. P. Diogo, "The Slow Relaxation Dynamics in the Amorphous Pharmaceutical Drugs Cimetidine, Nizatidine, and Famotidine," *J. Pharm. Sci.*, vol. 105, no. 12, pp. 3573–3584, Dec. 2016.

[54] P. R. Wahl *et al.*, "In-line measurement of residence time distribution in melt extrusion via video analysis," *Polym. Eng. Sci.*, vol. 58, no. 2, pp. 170–179, Feb. 2018.

[55] J. Kruisz, J. Rehrl, S. Sacher, I. Aigner, M. Horn, and J. G. Khinast, "RTD modeling of a continuous dry granulation process for process control and materials diversion," *Int. J. Pharm.*, vol. 528, no. 1–2, pp. 334–344, Aug. 2017.

7

Developing HME Based Drug Products Using Emerging Science: A Fast-Track Roadmap from Concept to Clinical Batch*

This paper presents a rational workflow for developing enabling formulations, such as amorphous solid dispersions, via hot-melt extrusion in less than a year. First, our approach to an integrated product and process development framework is described, including state-of-the-art theoretical concepts, modeling and experimental characterization described in the literature. Next, lab-scale extruder setups are designed (processing conditions and screw design) based on a rational, model-based framework that takes into account the thermal load required, the mixing capabilities and the thermo-mechanical degradation. The predicted optimal process setup can be validated quickly in the pilot plant. Lastly, a transfer of the process to any GMP-certified manufacturing site can be performed *in silico* for any extruder based on our validated computational framework. In summary, the proposed workflow massively reduces the risk in product and process development and shortens the drug-to-market time for enabling formulations.

* This chapter is based on: J. Matić, A. Paudel, H. Bauer, R. A. L. Garcia, K. Biedrzycka, and J. G. Khinast, "Developing HME-Based Drug Products Using Emerging Science: a Fast-Track Roadmap from Concept to Clinical Batch," AAPS PharmSciTech, vol. 21, no. 5, p. 176, Jul. 2020.

7.1 Introduction

Active pharmaceutical ingredients (APIs) are becoming more potent and selective, resulting in increasingly complex formulations and drug delivery strategies that are precisely tailored to achieve the required Pharmacokinetics (PK) profile of a drug. Typical examples include poorly soluble APIs that require solubility enhancement [1]–[3]. Moreover, advanced formulation strategies lead to more complex manufacturing processes, which increases the risk of development failure. In general, bringing a new drug to the market involves multiple time-consuming stages, with a go or no-go decision made at each stage. Since the pressure to bring a new drug to the market is immense, originators shy away from risky formulation designs and prefer simple drug delivery systems (DDSs), such as immediate release tablets. In order to counter this trend, our past work focused on de-risking the development and manufacturing stage of new and advanced DDSs**.** Examples include the development of small-scale formulation screening tools, i.e., the vacuum compression molding (VCM) tool [4], advanced hot melt extrusion (HME) process models, mechanistic studies of biopharmaceutics and stability aspects of enabling formulations and more, as described in detail in the sections to follow. Hence, we created a toolbox for rapidly developing hot-melt extruded formulations in tandem with the associated manufacturing process.

One approach to designing advanced formulations is solubility enhancement via amorphous solid dispersions (ASDs) made via pharmaceutical hot-melt extrusion (HME). HME is a potent production method, which is mostly used for the manufacturing of amorphous solid solutions and dispersions, as well as for dispersing and controlling the particle size distribution (PSD) of (nano-)crystalline APIs in polymer matrices [5]–[9]. The resulting DDS can deliver both immediate and controlled releases [10]–[12], with or without biodegradable polymer matrices. Twin screw extruders (TSE) are most commonly used in HME, allowing flexibility during the process development. The process can be tailored by adapting the screw configuration and process parameters to match the critical quality attributes (CQA) of the drug. Several drugs produced via HME have been marketed to date, including Norvir® and Kaletra® (Abbott Laboratories), Onmel® (Merz), Noxafil® (Merck), Palladone® (Purdue Pharma), Viekirax®, Venclyxto® and Mavyret® (Abbvie), Eucreas® (Novartis), Zithromax® (Pfizer), Nucynta® (Janssen) and Nurofen Meltlets lemon® (Reckitt Benckiser Healthcare) and several implants and inserts, such as Zoladex® (AstraZeneca), Lacrisert® (Valeant Pharmaceuticals, USA), Depot-Profact® (Sanofi Aventis), Ozudrex® (Allergan, Ireland) and Implanon® (Merck, USA).

The polymers typically used include HPMC, PEG, EVA, Soluplus, PVP and Copovidone of various grades.

Besides HME, spray drying (SD) can be applied for manufacturing enabling formulations, e.g., amorphous solid dispersions [13]. In both HME and SD similar approaches are employed for formulation/excipient selection in terms of biopharmaceutics and stability performance in terms of polymeric ASD. However, the processability requirements for the selected formulation candidates vary vastly since in SD solvents are added, which can alter and control the physical structure of the product. Focusing on overall aspects of HME-based formulation development, this review includes SD when early screening of formulations is performed in order to obtain information about the processability of the formulations.

Despite the advantages of HME (i.e., formulation processing without solvents, a small footprint of the system, an intensified nature of process, a low energy consumption, a continuous nature and manufacturing complex products with predefined release profiles in a single step) the vast majority of drugs on the market is made using other technologies. Moreover, several downstream options exist that enable companies to make tablets (calendering), powders (strand milling) and pellets for capsule filling of both spherical and cylindrical pellets (hot-die-face cutting or strand cutting).

There are several reasons why the adoption of HME is not much wider. First, HME does not have a long-standing history in the pharmaceutical industry and, as such, there is a lack of experienced formulators and process engineers. Second, the development of HME-based formulation is considered risky and requires a significant expertise. Since despite the added benefit to the formulations (e.g., solubility enhancement and defined release profile) HME may be too risky for the originators, such traditional approaches as micronization and functional coating are preferred. Third, the design of screws and the necessary scale-up is still performed mainly empirically for lack of sound design and scale-up framework. Lastly, the process flexibility poses significant challenges when dealing with new formulations and scale-up since the process window is not known *a priori* and has to be defined for every new formulation and extruder. Under the traditional approach, the formulation development is more or less detached from the process, i.e., the biopharmaceutical requirements are met from the formulation standpoint while the processability and the influence of process scale on the final product are not known. As a result, lengthy product development process is common, with multiple failed attempts leading to an unfavorable risk profile. Hence, integrated research, which takes into account formulation development from the pharmacological and processability standpoint, is needed for a “right-first-time” drug-to-market path.

To that end, for many years our group and some others have focused on developing scientific tools that allow a fast and minimum-risk development of HME-based formulations using several advanced tools. A good recent review of these efforts is provided in [14]. These include (1) advanced material science and screening, (2) small-scale test beds for formulations, (3) the design of small-scale processes and (4) the scale-up to GMP production of clinical batches. Since most of the scale-up are performed empirically, one of the goals of our group was to create *in silico* tools for a rational, science-based scale- up, while addressing other important aspects, such as an API degradation. Our multi-step approach is shown in Figure 7.1 together with the amount of materials required and the corresponding timelines.

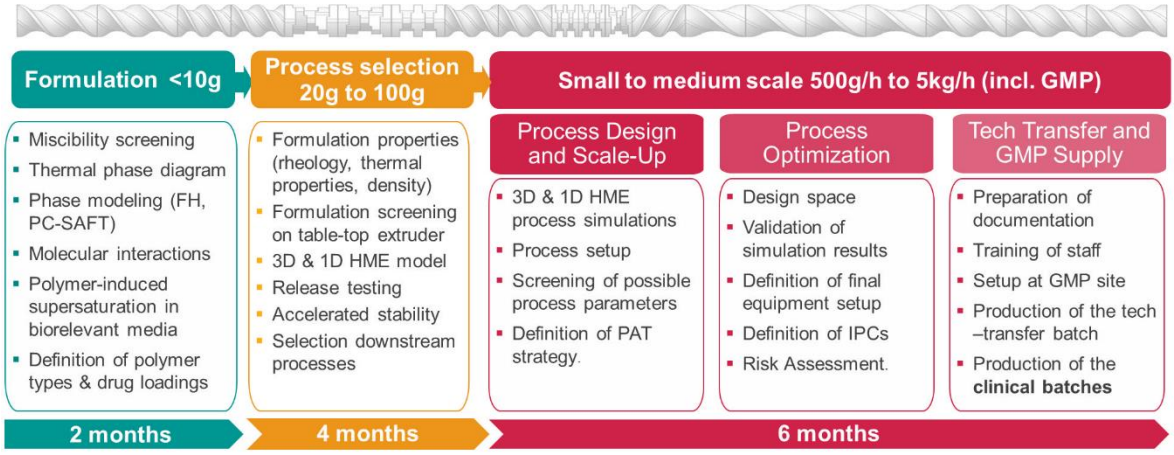

Figure 7.1. Integrated HME product development scheme.

All this is embedded in a quality-by-design (QbD) framework, including the definitions of quality target product profile (QTPP) and critical quality attributes (CQAs) of the drug product, a rational risk-based product and process development process, stability assessment and stability prediction, design space determination based on *in silico* and experimental tools, a control strategy based on risk assessment that includes specifications for the drug substance(s), excipient(s) and drug product and process capability and continual improvement [15]–[18]. Ultimately, clinical batches are manufactured according to GMP.

As Figure 7.1 illustrates, the formulation development requires a few weeks using less than 10g of API. The process selection, including stability assessment and biopharmaceutics, takes a few months and less than 100g of API. Finally, the process development can be performed rapidly using our advanced process design and scale-up framework. After about 6 months, the first clinical batch can be released. Details of the development process are provided below.

7.2 Product Development Guided by Quality by Design Principles

According to the ICH, Quality by Design (QbD) is a systematic approach to the development of pharmaceuticals that is based on sound science and quality risk management, with an emphasis on predefined objectives, product and process understanding and process control [15], [16], [19]–[24]. In the language of QbD, predefined objectives are reflected in the definition of the Quality Target Product Profile (QTPP) with the goal of achieving the intended therapeutic outcome and in the identification of Critical Quality Attributes (CQAs). The importance of this first step cannot be overstated since all of the following product development efforts aim to satisfy the predefined route of administration, delivery system, dosage form and strength, targeted in vivo drug release and pharmacokinetic profile as part of the QTPP requirements. Moreover, to ensure the desired product quality measured via the CQAs physical, chemical, biological and microbiological properties should be within the appropriate limits. Preformulation studies, formulation design and in vitro characterization focus on matching the final product's QTPP. However, various process-related technological parameters of API and excipients need to be specifically considered as well.

Figure 7.2 provides an overview of important parameters for developing bioavailability-enhancing formulations of a poorly-soluble drug molecule via HME and SD. For example, pH-solubility profile and intestinal membrane permeability of a drug molecule define the class of the drug in biopharmaceutics classification system (BCS) [25]. The molecules belonging to BCS class 2 and class 4 are poorly-soluble and their gastro-intestinal (GI) absorption can require solubilizing formulation concepts, such as ASD, lipid-based or nano-crystals formulations [26]. The BCS parameters need to be normalized by the intended dose of the given molecule, leading to the developability classification system (DCS) [27]. The absorption of orally administered DCS IIa drugs is limited by the dissolution rate and that of DCS IIb is limited by the solubility. In some cases, poor solubility originates from the surface wettability of drug crystals.

Besides biopharmaceutics properties, the basic physicochemical properties for designing ASD of a drug molecule are the glass transition temperature, glass formation propensity, hydrogen bond donor/acceptor in the structure, melting temperature and thermo-chemical stability. With regard to the ASD carrier selection, it is equally important to consider the properties of excipients. In the context of HME as a prospective technology, the drug and the polymers must have inherent thermal stability within the expected processing temperature. Since most pharmaceutical polymeric excipients are chemically stable at up to 200°C, high melting point

drugs require either a higher intrinsic solubility in the selected polymer or adding plasticizers to enhance their solubility in the polymer. Thermal rheology of polymers or selected formulations is decisive for processability via HME. For example, higher intrinsic viscosity and glass transition temperature of such cellulosic polymers as HPMC necessitate the use of plasticizer for extrusion.

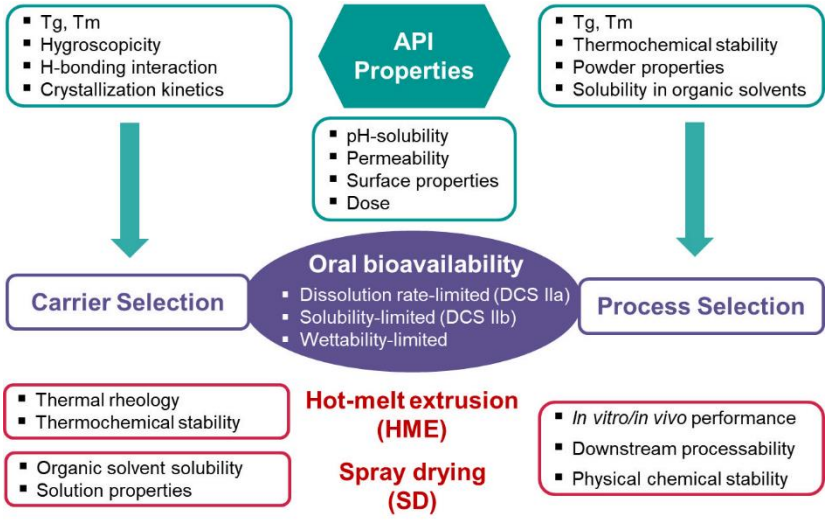

Figure 7.2. Basic physicochemical requirements for developing polymeric amorphous solid dispersions (ASDs) of poorly soluble drugs via HME and/or SD.

The next step under the QbD approach is achieving a scientific understanding of the interplay between the product quality (CQA) and the process characteristics, i.e., identifying the Critical Material Attributes (CMAs) and Critical Process Parameters (CPPs) and, most importantly, establishing the functional relationships between the CPPs, CMAs and CQAs, which may be a scientifically most demanding and most vulnerable part of the product development. Traditionally, the assessment of product quality relies on complying with the product's release specification criteria rather than designing the product by performing an appropriate risk assessment and defining a proper control strategy [19], [20], [28], [29]. The reason is often insufficient process understanding, especially with regard to complex processes that are borrowed from other industries and require a different formulation and process development approach than more traditional routes, as in the case of HME.

For HME purposes, the CPP-CMA-CQA relationship is typically established via extensive experimentation (currently performed based on DoEs), with a change in the CQA evaluated in terms of a change in the process settings, accompanied by elaborate statistical models that define the process windows. This approach, although widely applied, has a number of

disadvantages, e.g., poor predictability and impossibility of proper process transfer and scale-up since the process windows established are only valid for one formulation and one extruder under the exact conditions tested. Any departure from the formulation, equipment or process setting impairs the predictability and often requires a new set of experimental studies. This might be the single most important reason why HME is still not commonly used in the pharmaceutical industry.

The key to solving this problem is a proper definition of CPPs. In the case of HME, the list of process parameters currently considered to be critical is limited to the screw speed, the throughput, the barrel temperature, the screw configuration and the die design. Although these process settings are good candidates for the CPP list, they affect the product quality only indirectly. Thus, establishing a control strategy for these settings alone cannot be a sufficient guarantee of the product's quality. This is most evident during an HME process scale-up. The methodology traditionally has aimed to directly transfer the processes settings (mainly the screw speed and the throughput) from the original to the target scale using a geometrical factor that represents the change in the scale (typically the ratio between the outer screw diameters in some weighted form). However, this approach is not always successful. In the case of HME, the product CQAs, such as the degradation profile, are a result of the thermomechanical load cycle that the formulation experiences during the production. Hence, the proper CPP definition for HME must take into account the process states resulting from the process settings, e.g., the axial distribution of average and peak melt temperatures, the overall and local RTDs and the axial SMEC distribution [30]. Only mechanistically-based extruder models yield this kind of information. Machine-learning algorithms cannot be applied since they are based on data for one setting and formulation, which makes extrapolation and scale-up arbitrary.

It is important to note that in the event that proper CPP/CMA/CQA connections are established, it is comparably easy to go back to the product development if, for example, the required long-term stability of the amorphous form is not given. In this case the manufacturing process or formulation can be adapted. Moreover, process control and quality risk management are significantly simplified as well.

An overview of HME-based product design is provided in the next Section, covering the formulation development, the process screening and the stability assessment. Process development and scale-up as well as the GMP production of clinical batches are covered in Section 4.

7.3 Formulation Development

Our approach to developing an enabling ASD formulation for a poorly-soluble drug candidate via HME consists of (A) formulation and processability screening, (B) predictive computational and experimental methodologies for assessing biopharmaceutics and stability, and (C) advanced scale-up methods. This includes state-of-the art practices currently applied in industries in combination with emerging knowledge from academia. It should be emphasized that most of the workflow is equally applicable to the ASD development for manufacturing routes other than HME, such as spray drying (SD), milling, congealing or supercritical fluid technology (Figure 7.3).

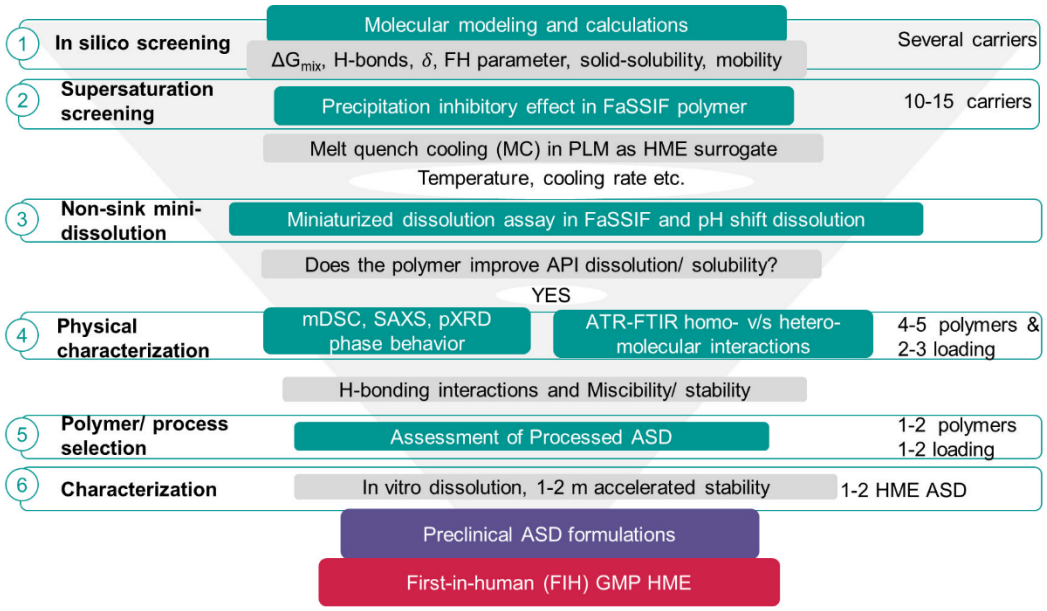

Figure 7.3. A systematic approach to potential carrier (polymer, surfactant and combinations) selection for HME-based amorphous solid dispersions.

7.3.1 Integrated Product Development and Process Screening

Early-phase product development is expected to balance the biopharmaceutics and stability targets and the manufacturability requirement for a given drug molecule. More precisely, the formulation candidates that are transferable from preclinical *in vivo* studies to first-in-human (FIH) dosing require systematic and thorough preformulation studies, screening and small-scale prototype preparation, which take into account the limited availability of drug candidate and the stringent development timeline. The preformulation screening is intended to provide the relevant information on biopharmaceutics, stability and processability as early as possible.

We applied an integrated product and process screening framework that connects the formulation design (e.g., carrier selection, drug loading) and the process screening (e.g., HME, spray drying). Figure 7.3 shows the flowchart with a systematic 6-steps approach, combining theoretical calculations with the experimental screening of preformulation. First, a thorough theoretical calculation is performed using the molecular and intrinsic structural properties of the drug molecule selected. The goal at this stage is to set up an *in-silico* formulation screening such that the experimental screening in terms of carrier types, their combinations and drug loading can be rationally narrowed down in order to minimize lengthy experimental evaluations. The excipients included in these theoretical calculations comprise diverse ASD polymers and surfactants and their combinations. At this stage, molecular miscibility between the selected drug and polymer pairs or in the ternary system, including surfactant/plasticizer, is estimated using the solubility parameters of individual components. The total or partial components (dispersive, polar and H-bonding) of Hansen´s solubility parameters (δ) of the selected drugs and carriers are estimated via group contribution methods. With the values of δ for different functional groups available in classical polymer chemistry text books, these calculations can be simply made manually using Excel spreadsheet. Alternatively, commercial tools such as MMP (www.norgwyn.com/mmpplus.html) can be used for this purpose. These values are further applied to assess the extent of drug-polymer miscibility. To that end, a simple and traditional approach, such as Greenhalgh classification, is employed with the purpose of obtaining qualitative values of miscibility [31]. For the miscible pairs and ternary systems, Flory-Huggins (FH) interaction parameters are calculated using solubility parameters of individual components. For ternary systems containing a drug and a polymer and a second polymer or surfactant, ternary miscibility can be obtained via the vector distance among mixing components in the Bagley plots of partial solubility parameters [32], [33]. If the glass transition temperature of the selected drug molecule is already available at this stage, a theoretical composition-versus-glass-transition temperature profile is created based on ideal mixing theories, such as the Gordon-Taylor approach. The outcome of this stage will guide the selection of carrier combinations for the next stage. These theoretical inputs are periodically updated as the work progresses further. For example, other descriptors (e.g., mixing energy, molecular mobility) are estimated *in silico* for promising systems using more advanced calculations, (e.g. molecular dynamics simulations).

In step 2 high-to-medium throughput screening is performed to evaluate the excipients' solubilization and supersaturation potential for a poorly soluble drug molecule with given physicochemical properties. The excipients include a range of polymeric carriers (PVP series,

HPMC series, methacrylate series, etc.) and surfactants/plasticizers (SLS, tween, polysorbate, etc.) that are commonly used for ASDs and are broadly/qualitatively found to be miscible *in silico* from step one. Based on the experimental and/or predicted equilibrium solubility of the drug in the simulated physiological media selected (such as fasted state intestinal fluid, FaSSIF), a certain degree of supersaturation of the dissolved drug is induced in the medium containing pre-dissolved polymer of a given concentration. Supersaturation can be created via solvent shift (e.g., introducing the drug solution into DMSO into FaSSIF), pH shift, temperature shift, etc. [34]. The depletion kinetics of supersaturation in the biorelevant medium is monitored using the time-dependent turbidity measurements. The dissolved concertation is analysed via chromatography. The data generated enable rank-ordering of excipients based on their supersaturation maintenance capacity for a given drug molecule.

Once a set of biopharmaceutically promising excipients is selected, in step three the miniaturized formulations are prepared via melt quench cooling to represent HME formulations. Alternatively, solution casting can be used to represent spray dried formulations [35]. The cast film formulation can be prepared at a milligram scale for each drug loading using either glass well plates at a high/medium throughput temperature-controlled stages or DSC pans. Given sufficient time and resources, such screening can be performed in more process-mimicking setups: for example, levitated single droplet drying, oven evaporation at varying temperatures or spin coating can be used to mimic spray drying [13]. In addition, for HME formulation screening, vacuum compression moulding (VCM) [4], thermal rheometers [36] or heated glass syringes with bent needles [37] can be employed to prepare mini-formulation samples to account for the extent of shear forces during HME. Varying drug loads are used until trace crystallinity is detected via polarized light microscopy. *In vitro* drug dissolution in these mini-formulations is assessed in a miniaturized way by directly introducing a biorelevant medium into the surface of films and periodically sampling and analyzing the dissolved drug. This test can verify the results obtained from the supersaturation experiments and swiftly establish the effect of drug loading on the dissolution performance.

In step four, the mini-formulations containing a range of drug loads that resulted in a promising dissolution performance are further characterized in terms of their solid-state properties as follows: the glass transition and the degree of molecular mixing (one T_g versus multiple T_g's) via calorimetric analysis (DSC); the drug miscibility and the lack of crystallinity via X-ray amorphous halo (XRPD); the presence and strength of stabilizing molecular interactions between the drug and the excipient in the formulation (e.g., hydrogen bonding, dipolar and ionic interaction etc.) via spectroscopy (infrared and/or Raman) and wettability via contact angle

methods. In addition, the rheological measurements, the specific volume, the heat capacity and the thermal conductivity are used to parametrize the models for the *in silico* assessment of the formulations' processability, as discussed in more detail below. This systematically guides the selection of excipient and drug loading that maximize the dissolution performance and the drug-excipient miscibility to ensure the physical stability and processability in terms of thermal rheological profiles of the formulations selected.

In step five, based on the ranking of biopharmaceutics and the solid-state outcome, ASDs with the drug loading selected are prepared on the laboratory-scale HME using the carrier(s) selected. The information on thermal transitions (glass transition, heat capacity, melting, recrystallization, dehydration. etc.) obtained via DSC and thermal rheology allows to rapidly select the optimal process parameters (e.g., the temperature profile of the extruder's elements). Typically, a few dozen of grams of ASD powders are prepared at this stage. The ASD extrudates generated are milled using a laboratory scale ball mill or other impaction mills with a capacity to handle the lower batch size. Depending on the mechanical properties of the extrudate, either cryogenic or room temperature milling is performed. Some basic process parameters (e.g., the milling intensity and time, the sieve size, etc.) can be varied to obtain ASDs of various particle sizes. Based on the information on the physical properties of the formulations selected, including the moisture sensitivity (which depends on the polymer/surfactant types), the processing operations may have to be performed under the reduced/controlled RH conditions.

The HME ASD formulations prepared in step five are thoroughly characterized in terms of solid-state, *in vitro* dissolution and short-term accelerated stability (typically 1-2 months) in step six. Depending on the intention and the development stage, milled HME ASD powders or powders compressed in tablets or filled into hard capsules are used. For example, if the dosing in the preclinical animal species is planned as an ASD suspension, the test also includes dissolution/supersaturation in the suspended state. The dissolution test at this stage includes the biorelevant media and transfer methods (pH/media shift from mimicking the gastric to intestinal environment), typically under the non-sink conditions. In addition to the milled powder and tablet/capsules of ASD, a physical characterization of the solid state is performed for the unmilled extrudate to ascertain the physical structure integrity during milling. The purpose of accelerated stability test at this stage is exploration rather than the prediction of actual shelf life. The propensity of crystallization/phase separation in the ASD candidates with promising *in vitro* performance is tested by storing them in an accelerated environment at elevated temperatures and RH, e.g., 40°C/75%RH. The test is performed under both open and closed

conditions, with samples periodically withdrawn and tested via physical characterization and *in vitro* dissolution.

Based on the results of the small-scale formulation analysis, including the accelerated stability in step six, the formulations are selected for preclinical *in vivo* studies and/or FIH dosing for clinical programs. In [38] we provided a summary of a case study of a drug candidate screened for HME ASD using the aforementioned approach. In this case, for a poorly soluble new chemical entity (NCE), an *in silico* formulation screening for the carrier selection was performed based on the chemical structure. Following the results, supersaturation kinetics in FaSSIF were studied in about 16 combinations of polymer and surfactant carriers. The outcome of this study led to the selection of 4 formulation systems, i.e., HPMC, Soluplus®, HPMC-AS and HPMC-AS/HPC combinations. Subsequently, mini-formulation surrogates containing several drug loadings were prepared via solvent casting (SC) and melt casting (MC). The solid state characterization of these MC and SC formulations was performed focusing on miscibility and crystallinity; a non-sink dissolution study of intact films was performed as well. The ranking of performance based on the data led to the selection of two formulations, one with HPMC and a second one with Soluplus® and two drug loadings each. Finally, these formulations were produced as powders using laboratory scale HME (and SD) for the characterization of biorelevant *in vitro* dissolution and short-term accelerated stability. Based on the data, the system with HPMC with a given drug loading was selected as FIH formulation candidate with the Soluplus®-based system as backup. A similar step-by-step approach that is less rigorous in terms of bio-predictive and stability aspects was recently published by Simões et al. for etravirine HME ASD [39].

The adoption of such a systematic approach makes it possible to meet the development timelines using limited API amounts at the early stage. The entire screening stage can be accomplished within four months or less and using fewer than 100g of API, depending on the complexity of physicochemical portfolio of the given drug. A thorough solid-state and biopharmaceutics characterization during the screening stage de-risks the development program. Rationally selected stabilizing carrier types and drug loading ranges that account for biopharmaceutics and processability provide a robust basis for interchanging drug loads (from low to high dosage strengths and vice versa), processing routes (HME to SD and vice versa) and iterating downstream processes and final dosage presentations (e.g., powders or pellets filled in capsules versus tablets). The results of the screening phase provide the material properties and the formulation-specific data as an input for the model-based HME process development during the process setup, transfer and scale-up. Moreover, the formulation

properties data, such as the dissolution and stability performance determined using mini-formulations, can guide the parameter selection when developing predictive process models for the product performance. The industrial use of ASD preformulation and formulation development generates an enormous amount of data using identical approach for several NCEs. To this end, application of machine learning and artificial intelligence can further assist reducing future experimental efforts for the decision making [40].

7.3.2 Stability Assessment and Prediction

As one of the key quality attributes, stability of pharmaceutical products has to be ensured for the patient safety and efficacy. Being able to predict stability by combining the experiments and *in silico* modeling can drastically shorten the development timeline, while reducing the risk of re-formulation. Although empirical models based on Arrhenius kinetics are widely applied in practice for theoretical shelf-life prediction, they are limited to simple formulations and to cases in which instability can be readily conjectured based on the functional groups involved (e.g., Milliard reaction between lactose and amine-containing drugs). In particular, with regard to ASDs the typical routes of instability are of both physical and chemical nature. On the one hand, amorphous phase separation and nucleation/crystal growth of active components of ASDs eliminate the expected solubility advantages. On the other hand, higher energetics and mobility of amorphous drug molecules in ASD prompt faster drug degradation and drug-excipient chemical interaction. Thus, an accurate prediction of stability in the final dosage forms is still challenging.

Ensuring physical stability of ASD requires a knowledge of both thermodynamic and kinetic factors governing (in)stability [41]–[47]. From a thermodynamic standpoint, it is imperative to estimate the equilibrium solubility as accurately as possible, as well as the kinetic miscibility of a drug molecule in a given polymeric carrier as a function of temperature. Experimentally, solid solubility of a drug molecule in the polymer is obtained via thermal methods (e.g., melting point depression in DSC, T_g versus composition diagram, moisture sorption experiments in a dynamic vapor sorption system (DVS)) and is based on the solubility in low molecular weight liquid analogues of the polymers [48]–[53]. As the fluid-state properties of polymers acting as the API solvent are challenging to establish, experimentally-determined solid-solubility are often severely over- or underestimated. Therefore, a high resolution characterization using solid-state NMR spectroscopy/relaxometry and/or X-ray diffuse scattering analysis is necessary to verify the accuracy of the estimated solubility/miscibility [54]. Moreover, experimental drug-

polymer miscibility studies can generally be complemented by theoretical modeling, e.g., Flory-Huggins lattice theory and perturbed-chain statistical associating fluid theory (PC-SAFT) [44]. Despite certain assumptions and limitations, these models can provide working thermal-phase diagrams of a given drug and polymer that are equally important for the processing temperature selection in HME. For example, the group of Sadowski has shown the applicability of PC-SAFT-derived thermal-phase diagrams to determining the drug-polymer solubility curves and miscibility gaps, even in the presence of moisture, and verified it using the experimental stability data for the ASDs containing physico-chemically diverse APIs and polymers [55]–[60].

A simpler, less accurate and faster approach to estimating miscibility is via the total or fractional solubility parameters of the mixing components based on the "like dissolves like" concept. Since the solubility parameter is the square root of the cohesion energy density, the proximity of these values for a given drug-polymer pair indicates miscibility. The solubility parameters can be decomposed into the partial parameters to represent dispersive, polar and hydrogen bonding contributions. These solubility parameter values can be estimated using group-contribution methods or, if the molecular structure is known, a molecular dynamics (MD) simulation. Besides thermodynamics, various modes of molecular mobility (global and local motions) can contribute as a kinetic factor for triggering the phase separation and the drug crystallization. Global molecular mobility can be estimated via structural relaxation experiments using DSC, NMR relaxometry, dielectric spectroscopy (DES) and dynamic mechanical analysis (DMA), while local mobility is determined via DES and DMA. Since the average time scale for global molecular motion can be empirically related to the onset of crystallization for the given systems as a function of temperature and humidity, it can be used to predict the physical stability [61].

Molecular dynamics (MD) simulations and first principle methods are increasingly applied to rationally develop a stability ranking based on both thermodynamic and kinetic factors [62]. For example, we recently employed MD simulations to investigate the relative contribution of thermodynamic factors (Gibbs free energy of mixing and hydrogen bonding interactions) and kinetic factors (diffusion coefficient and roto-vibrational mobility) to the physical stability of ASDs [63]. Comparing the outcome of MD simulations to the experimental stability data made it possible to define the prominent effect of molecular mobility on the stability in systems with a lower intrinsic molecular miscibility. Initially, the MD simulation-based approach appears to be slower and more costly. However, once the necessary force fields are created for common ASD polymers, they can be used repeatedly for ASDs of new drug molecules with a minimum

effort required for obtaining a rational stability ranking. Such a prediction framework has been applied to various NCEs and ASD candidates undergoing clinical developments.

In terms of chemical stability of ASDs, the predictive methods are still limited to empirical extended Arrhenius kinetics or statistical approaches, mainly due to the complexity and insufficient understanding of the mechanisms involved. However, to accurately predict the ASD stability, models that combine both physical and chemical transformations are required. On the experimental side, drug-excipient compatibility studies for developing HME-based ASDs need special attention so that any process- induced incompatibility can be ruled out as early as possible. A typical concern with this regard is reactive impurities (e.g., free radicals, oxidizing species and aldehydes) as a consequence of thermal treatment of polymers during extrusion and the drug's susceptibly to such reactive species during and/or after production of ASDs [64]. To that end, we recently applied the controlled pressurized oxygen heat space and temperature setup (RapidOxy) as a tool for rapid assessment of the chemical interaction between famotidine and PEG of different molecular weights and at different drug loads [65]. The temporal oxygen pressure drop was used to estimate the consumption of oxygen via polymer degradation. The formation of reactive radicals and formaldehyde was confirmed via ESR spectroscopy and IR spectroscopy, respectively. This method allows to assess the incompatibility within a day while other approaches may take months. Furthermore, we are working on developing a scientific insight with regard to the generation of reactive impurities, their solubilities and diffusion rates in polymeric excipient matrices with the ultimate goal of creating a predictive model for reactive-impurity- mediated drug degradation in ASDs.

7.3.3 Biopharmaceutical Assessment

Biopharmaceutics of pharmaceutical products contain the most important parameters for ascertaining the success of a given formulation and processing strategy, including the *in vivo* absorption of drug molecule and the systemic availability. The basis for establishing the biopharmaceutics of a drug product is the dissolution process (and possibly recrystallization due to supersaturation via ASD) in the GI milieu and permeation of the dissolved drug molecules through the GI membrane via active and/or passive transport. These parameters are tested *in vitro* via biorelevant dissolution testing and drug permeability through the artificial membrane or cell membrane. Biorelevant dissolution testing uses the gastric fluid simulated sequentially over time, followed by the simulated intestinal fluid. The *in vitro* results, together with *in vivo* pharmacokinetic data, are used to construct *in vitro-in vivo* correlations (IVIVC)

or to develop a predictive mechanistic physiologically-based pharmacokinetic (PBPK) model *in vivo*.

In the case of ASD formulation, predictive *in vitro* and *in silico* biopharmaceutics characterization can help to secure the *in vivo* success by considering the excipients' solubilization factors, supersaturation generation and maintenance potential, precipitation inhibitory capacity in the GI environment and contribution to accelerating or decelerating the drug permeation rate [66]. It is common practice to perform *in vitro* dissolution of ASD formulations under non-sink conditions, meaning that the total drug amount in a given medium volume is several times higher than the solubility of the crystalline counter-part [67]. The exact *in vitro*/*ex vivo* simulation of *in vivo* situations is challenging since disintegration, drug solubilization, ASD surface plasticization, supersaturation are connected events. However, the reasonable accuracy obtained by combining an advanced *in vitro* characterization with *in silico* models helps the formulators to choose and/or to modify the functional excipients, drug loading and processing parameters while scaling up the HME process for the production of clinical supplies [68], [69].

Recently we performed a systematic biopharmaceutics characterization of generic tacrolimus modified release ASDs (Envarsus® prepared by MeltDose®) in the form of tablets and compared these to the original ASD pellets in capsule formulation (Advagraf®) [70]. By employing the non-sink dynamic and the biorelevant *in vitro* dissolution in combination with the *in vitro* cell permeability as inputs for the compartment PK model, the *in silico* drug plasma concentration time profiles were generated using GastroPlus®. The *in silico* data obtained were compared to the *in vivo* clinical trial data to establish an IVIVC model, which enables a comparison of the two formulations with respect to the predicted *in vivo* population PK profiles.

There are several other aspects associated to the biopharmaceutics of ASDs that require a better scientific understanding. More precisely, the complex interplay between the formulation, the process and the performance of ASDs requires an integrated evaluation of the detailed solid-state and surface characterization and a thorough biopharmaceutics characterization of the products [71]. This way, *in vivo* predictive models can be developed to shorten the expensive clinical phases and replace bridging *in vivo* PK studies when either the formulation or the process is modified (e.g., different grades of polymer, HME vs. SD, or different production scales). Moreover, the *in vitro* assessment of food effects using appropriate biorelevant media can help to establish a virtual bioequivalence when developing a generic product [72]. Provided that there is sufficient *in vitro* data on dissolution and precipitation, the *in vivo* drug release profile of ASD can be described, combining drug dissolution and nucleation with crystal growth

models, which are yet to be incorporated into commercial PBPK models [73]. Clinical data of HME-based drug products, including ASDs, are still rarely reported in literature [74]. Currently process and product modeling are linked via *in vitro* data, i.e. the process modeling aims to cover the process behavior and aspires to predict the in vitro performance of the drug, whereas product modeling aim to link the *in vitro* data and predict the expected *in vivo* behavior. Increased accessibility of the *in vivo* data for the HME based product will enable improving as well as validating the end-to-end predictive solutions applied for the product development.

7.4 Process Development and Control

7.4.1 Process Setup and Scale-Up via Advanced Modelling

As mentioned above, HME has a number of advantages over traditional batch technologies in terms of process flexibility, footprint size, solvents requirements (or the lack thereof) and the possibility of single-step production [75]–[82]. One of its most important benefits is the continuous nature of process, allowing a seamless integration of upstream and downstream units into the drug production process. Yet challenges still remain, which are mainly due to the vast number of parameters and screw designs. For example, there are no readily available design tools for a process involving a novel drug (or even a generic drug for that matter) that do not require extensive experimental efforts of an experienced extrusion process scientist. This is a problem since experimental DoEs have in high material and facility costs and an unfavorable risk profile. To address this issue, we developed a rational design framework for twin screw extrusion HME processes and the corresponding downstream processing using novel *in silico* approaches. Specifically, we focused on:

- predicting performance of individual screw elements and their effect on the fluid flow and dispersive mixing via detailed 3D simulations [30], [83]–[85]**;**
- quantifying the effect of (complex) screw configurations and various process settings on the melt temperature, fill ratio, SMEC and RTD via advanced, fully-parametrized 1D HME simulations [5], [30], [86], [87]; and
- including material CMAs and product CQAs (e.g., crystallinity and degradation) into the modelling, allowing the process response prediction for an accurate process setup and scale-up.

Understanding the effect of screw geometry on the fluid flow, energy dissipation and distributive mixing is crucial for the design on new elements and the assembly of screw

configurations [75], [76]**.** A typical cross section of a TSE screw pair is shown in Figure 7.4-right. The cross section shows a pair of double-flighted conveying screw elements denoting their most important dimensions, like barrel diameter (D), outer (D_o) and inner (D_i) screw dimeter and the screw centerline distance (C). Our approach uses Smoothed Particle Hydrodynamics (SPH), a relatively new numerical method for simulating complex free surface flows occurring inside the rotating screws. SPH is a Lagrangian-based fluid dynamics model, with the fluid flow represented as a continuum of moving fluid parcels that can adjust naturally to the complex intermeshing movement of twin screw extruders without a numerical mesh [88]–[95]. The Lagrangian nature of the method also allows for a straightforward investigation of the flow in partially-filled screw elements, as well as a detailed investigation of the distributive mixing action of the screw geometry selected.

Using Newtonian fluids as a reference and assuming a creeping flow regime (low Reynolds number, i.e., high fluid viscosity), the flow data can be analyzed in a simple dimensionless manner, describing the performance of any screw element pair regardless of the material, screw speed and length of the screw element [30], [76], [83]–[85], [96]. Thus, the performance of any screw element pair can be described in terms of pressure and power characteristics. The pressure characteristics is a linear relationship (under the above- mentioned assumptions) between the dimensionless volumetric throughput and the pressure build-up capacity that a certain screw pair possesses [76], [83], [85]. Since the relationship is linear, the curve is sufficiently determined by the axial intersects termed inherent conveying A_1 and the pressure build-up capacities, A_2. The former represents the dimensionless volumetric throughput at zero backpressure, whereas the latter is the theoretical dimensionless backpressure where no overall mass flow occurs. Pressure characteristics are provided in Figure 7.4-left, with the x axis showing the dimensionless volumetric throughput and the y axis the dimensionless pressure build-up. The blue curve represents a typical pressure characteristics of a twin-screw extruder element pair, with its A_1 and A_2 axis intercepts. The non-Newtonian nature of fluids is accounted for separately as part of the 1D HME codes.

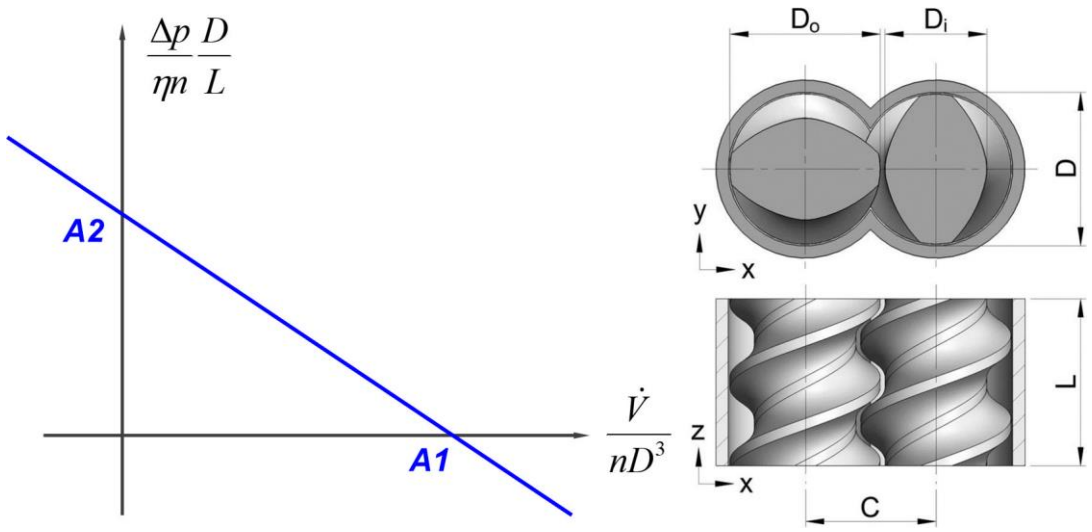

Figure 7.4. An exemplary plot of dimensionless pressure characteristic curve with A_1 and A_2 axis intercepts (left) and an example of a screw geometry for a conveying elements pair routinely used in the HME production (modified from [30]).

The power characteristics is a linear relationship between the dimensionless volumetric throughput and the power consumption, which can be described using axial intersects B_1 and B_2 (similarly to the pressure curve)[76], [96]. Over the past years, we have created a database of the most common twin-screw extruder elements of major pharma extruder manufacturers of various scales (12mm, 16mm, 18mm, and 27mm extruder sizes)[30], [83]–[85]. Since analyzing the flow and mixing behavior in such detail is computationally expensive, we developed an in-house software for accelerated simulations running on graphic cards (GPUs): the eXtended Particle Systems (XPS) software [97], [98], [107]–[109], [99]–[106]. It is a powerful simulation platform for simulating not only complex fluids via SPH, but also complex powders via the Discrete Element Method (DEM) with additional coupling to conventional CFD software.

Although the speedup and cost effectiveness offered by a GPU platform are significant in comparison to conventional software, the complexity of the flow and material behavior makes SPH unsuitable for simulating the full extruder for industrial settings. Thus, to design a process for our industrial partners, we developed a reduced-order 1D HME model on the basis of lessons learned from the detailed SPH analysis [5], [30], [86], [87]. Some results of such a reduced order simulation are shown in Figure 7.5, illustrating the fill ratio (top left), the pressure (bottom left), the melt temperature profiles (top right) and the residence time distribution (bottom right) at a certain rpm and throughput (starved feeding). This allows us to perform *in silico* DoEs using a variety of extruder setups, screw configurations, process settings and formulations.

From the process equipment standpoint, data acquired for the torque required for processing the formulation selected in the desired process settings make it possible to decide on the suitable extruder. Analyzing the thermal and mechanical loads (melt temperature, SMEC, local and overall RTD) to which the formulation is exposed to during the process can assist with the choice of formulation, process settings and screw configuration for obtaining the desired product CQAs [16], [30], [75]–[77].

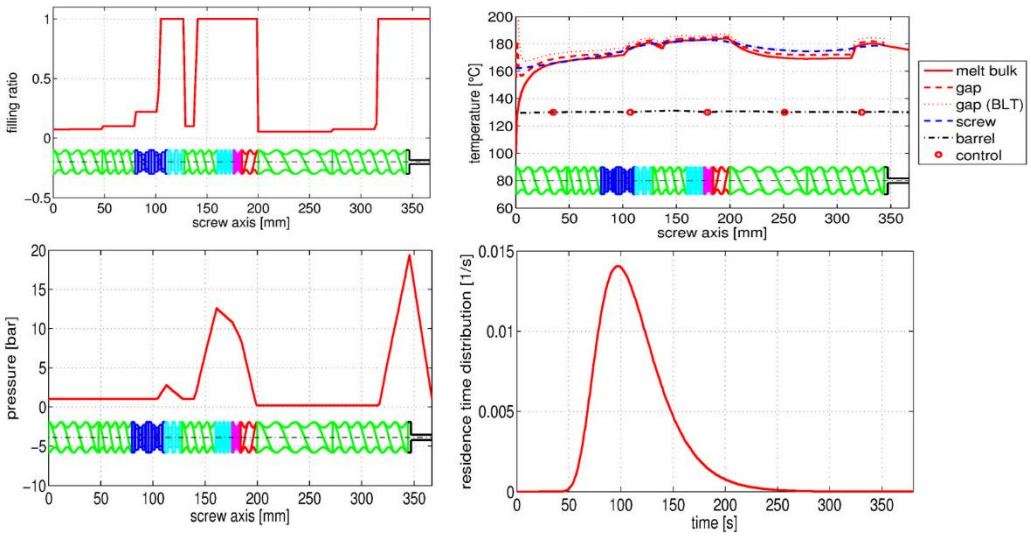

Figure 7.5. Example results showing the reduced order 1D HME simulation software showing the axial melt-filling ratio (top left), axial melt temperature distribution (top right), the axial melt pressure distribution (bottom left) and the residence time distribution (bottom right) [110]. The figures also show a color coded screw configuration. The green element are conveying elements, the blue elements kneading elements (dark blue being kneading elements with a 90° angle between the kneading discs), magenta represents mixing and red back-conveying elements.

This allows us, first, to choose the adequate formulation candidates in terms of formulation processability. In the second step, the suitable equipment, screw configuration and process settings can be selected. The product quality can be predicted even before transferring the process to the pilot plant scale. Our HME setup workflow consists of four steps:

1. Detailed analysis of the API and formulation candidates, including measurements of the formulation's rheology, heat capacity, thermal conductivity and specific volume, for the parametrization of 1D HME models.
2. A detailed analysis of the extruder's screw elements via SPH, determining the power, pressure and mixing characteristics of individual screw pairs, for a parametrization of 1D HME models.

3. An *in silico* DoE using the 1D HME model as a basis for determining the process response (torque, SMEC, melt temperature, RTD, etc.) as a function of the selected formulations, screw configuration variants and process settings, with the goal of determining the most promising formulation candidates and process settings.
4. Validation and fine tuning of the process setup in the pilot plant and prediction of the product's CQAs (including degradation and concentration).

The computational approach is highlighted in Figure 7.6. The characterization of the individual screw elements of the chosen extruder is done via the SPH simulation method (left top) [30], [83]–[85]. This includes the computation of the pressure and power characteristics, as well as the distributive mixing capabilities of the screw-element pair in a non-dimensional and formulation-independent manner, as discussed above. As such, the result reflects the geometrical capabilities of the screw element pairs and are in the next step used as descriptors in the 1D HME model (right top). In parallel to the SPH screw pair characterization, the API in question is analyzed and a suitable polymeric carrier is defined, according to the steps described in the formulation development section of this paper. Once the formulation is defined, the rheology, specific volume, heat capacity and thermal conductivity of the mixture are determined. The data are then used in the 1D HME model (left bottom). Once the screw element pairs and the formulation are parametrized, a variety of screw configuration and process conditions can be tested and evaluated *in silico* (right top) [30], [86], [87]. The obtained results range from axial distributions of the filling degree, melt temperature, pressure distribution, SMEC distribution to local and overall RTDs (local in the sense that RTD for only a certain screw section can be calculated, which is not possible to be done experimentally). In combination with experimental runs for the verification of the *in silico* results, it is possible to perform HME process setup and scale-up in an efficient and product-specific manner, taking into account the product CQAs (right bottom). Validation was performed on our fully-PAT equipped extruders on various scales.

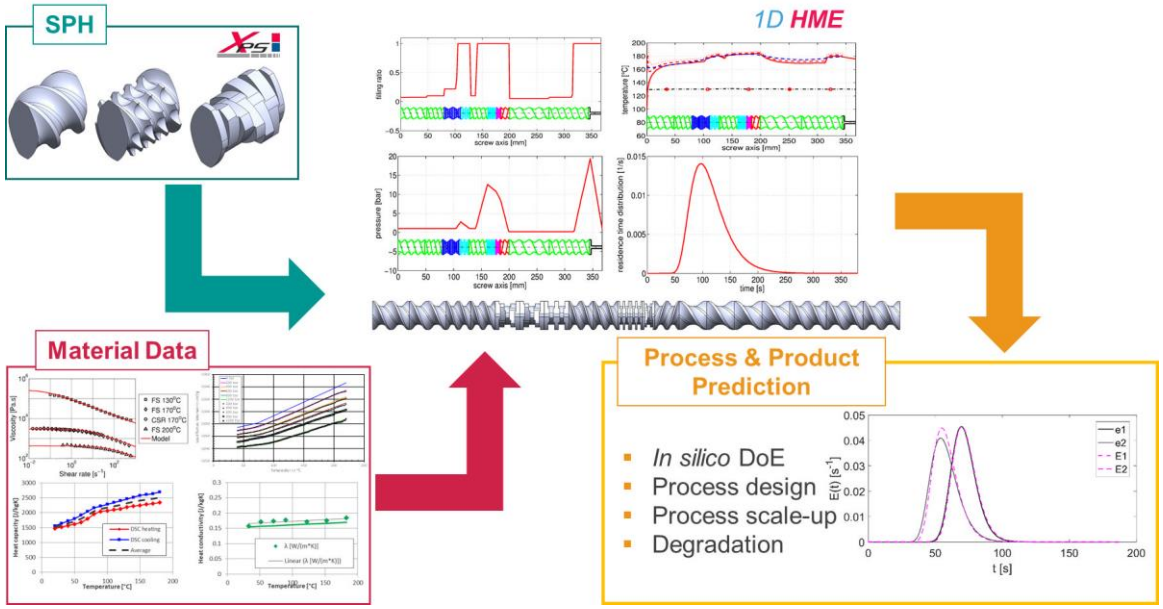

Figure 7.6. Steps for a quick and reliable HME process setup, including the investigation of material data (melt rheology, specific volume, heat capacity and thermal conductivity), detailed 3D SPH simulations of individual screw-pair elements; 1D HME validated process simulations and process & product prediction.

An essential part of product development from the first formulation screening efforts to the clinical batch manufacturing is the HME process scale-up and transfer. Knowing all the relevant product-process relationships makes it possible to scale-up the process from one scale to another in a rational manner. The guiding assumption for every process scale-up and/or transfer is that the product quality is the result of defined thermomechanical loads (i.e., SMEC, melt temperature distribution and RTD) that the formulation experiences during the production. Thus, keeping the thermomechanical loads constant across the various scales and types equipment is crucial for a consistent product quality.

By using our novel scale-up approach based on 1D HME models, we are able to adjust the screw configurations and process settings to match the thermomechanical load profile on the original extruder scale [30]. The great advantage of using *in silico* tools for process scale-up and transfer is that there are virtually no limitations in terms of screw configuration and process settings. Moreover, no material is wasted. Under traditional scale-up approaches, the prediction of process settings on the target scale is based on the process settings on the original scale multiplied by a geometrical factor representing the similarity between the scales. The thermomechanical load history is disregarded, which often necessitates significant additional experimental efforts with the goal of matching the product specifications. In addition, changing the extruder scale may require changing the extruder brand, which creates additional issues in

terms of matching the screw configuration and the extruder capabilities. In contrast to the traditional approaches, 1D HME model directly calculates the axial SMEC and the melt temperature distribution together with the local and overall RTDs, accounting for the thermomechanical load history.

Figure 7.7 shows an example of axial melt temperature profiles (black is small scale, pink is large scale) and mean RTDs in the various extruder zones. The scale-up was performed to keep the peak melt temperatures in the kneading and mixing zones similar to the peak temperatures that the formulation experienced in the original extrusion setup. In addition, the goal was to assure that the mean RTD of the formulation in the (high-temperature) kneading and mixing zones is equal or below the one in the original setup. This rules out any unexpected changes in the product quality (degradation). Hence, our approach directly aims to transfer the thermomechanical load history, regardless of the screw configuration, extruder scale and extruder manufacturer. This way, full flexibility in terms of extruder manufacturers is attained, allowing to test various extruders *in silico* before purchasing the actual equipment.

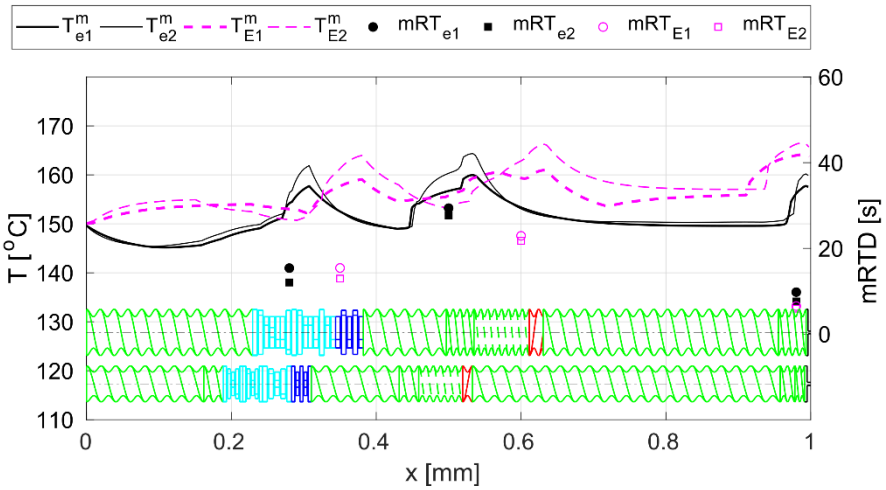

Figure 7.7. An example of axial melt temperature distributions and mean RTDs in various zones of screw configuration on two extruder scales. For more details refer to [30].

Specifically, our approach includes:

- precise assessment of extruder performance on different scales, from the formulation screening to pilot plant and production scales;
- design and optimization of HME process together with a control concept;
- rational scale-up procedures that are based on sound science, eliminating simplified rules;

- prediction of in-process degradation profiles.

7.4.2 Experimental Verification of Process Setup and Scale-Up

Validation is a critical part of every model development. To that end, model results were validated via multiple experimental investigations across various scales. Table 7.1 lists the equipment used. Beginning with the formulation screening on the 9mm ThreeTec table top extruder, moving to the pilot and clinical batch manufacturing scales using the 18mm Coperion extruder and finishing with the full-production scale process development on the 27mm Leistritz extruder, all the relevant pharma-scales were studied and the models were validated. In addition, several downstream options available (see Table 7.1) have been studied [110]–[113], including hot-die-face cutting, strand cutting, calendaring systems or mills, tableting or capsule filling equipment, allowing an initial manufacturing test of multiple dosage forms.

Table 7.1. Extruders, upstream and downstream equipment available at the RCPE pilot plant.

Upstream Equipment
Ktron K20 feeders (0.5 kg/h - 6kg/h)
Brabender feeder (0.1kg/h - 1kg/h)
RCPE's micro feeder (1-100g/h)
HNP liquid Pumps
Twin-Screw Extruders
Three Tec TT ZE9 9mm – table-top extruder
Coperion ZSK18 18mm – pilot plant scale extruder
Leistritz MIC27 27mm – pilot plant & production scale extruder
Thermo Fisher Pharma16 16mm – GMP pilot plant extruder
Single-Screw Extruder
Brabender Compactextruder KE 19 19mm – co-extrusion
Downstream Equipment
Maag Ex 22-4 melt pump
Maag Hot Die Face Pelletizer
Automatik P60E strand granulator
Gabler Engineering R-250 spheronizer
Colvistec UV-VIS inline spectrometer
Zumbach extrudate laser diameter measurement

Moreover, embedding of a nano-suspension in a polymeric matrix [5], [6] and co-extrusion using a twin- and single-screw extruder in combination can be modeled using this approach.
Lastly, we established a continuous HME-tableting line, with HME used to produce an ASD and nano-based formulation. The strand is cooled and cut into small pellets that are fed to a

continuous direct compaction line consisting of loss-in-weight feeders, a blender and a tablet press [114], [115]. Moreover, a sophisticated model-based control concept was developed that allows the continuous manufacturing process to remain in a state of control while combining various production steps. Figure 7.8 shows the flow sheet of the process, the control systems and the tools for dealing with the out-of-spec material.

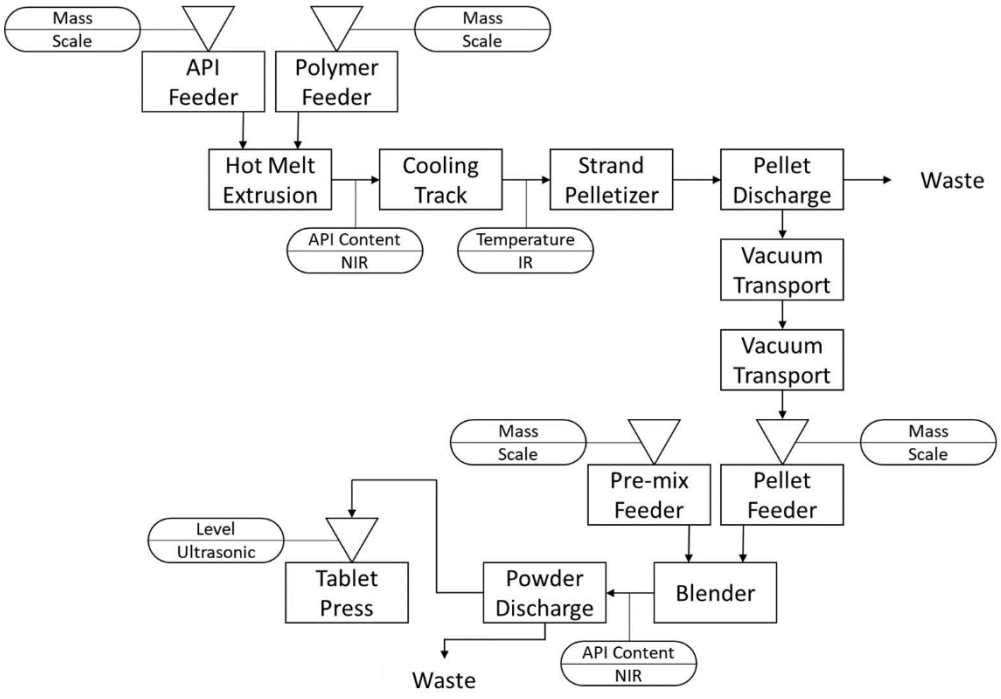

Figure 7.8. Process diagram and sensors for a continuous HME direct compaction manufacturing process [115].

7.5 GMP Production of Clinical Batch

After the formulation development, process setup and verification in a non-GMP environment, a transfer to a GMP facility can be made for clinical batch supply and product manufacturing. As mentioned above, properly establishing the CPP/CMA/CQA relationships greatly simplifies the subsequent process transfer to a GMP facility. Certain GMP activities, such as an evaluation and a qualification of source material, can actually begin before the manufacturing process development is completed. However, a deep understanding of CMAs and their link to CQAs should be achieved in order to control the source materials and especially the API.

Technology transfer is defined as a “logical procedure that controls the transfer of any process together with its documentation and professional expertise between development and manufacture or between manufacture site” [116]. Ideally, the location of the clinical batch and commercial product manufacturing is selected before or in parallel with the process

development. The reason for this is that the capabilities of the manufacturing facility (e.g., type of equipment, screw configuration availability, batch size and/or throughput, etc.) have to be considered when developing the product for the reason mentioned above. If the capabilities of the receiving site differ significantly from those used during the development, timelines may be affected and a greater effort on re-development can be expected [21]–[23], [116]. Determining the setup and the control strategy based on the process state rather than the equipment type/setting makes scale-up and transfer activities less dependent on the receiving site's particular equipment, hence following risk management approach. This way, extensive experimental runs can be avoided, saving material, time and use of GMP facilities. Even if the material specifications change during the transfer, a rational design model will be able to account for such a variability, eliminating trial and error. In addition, a more mechanistic understanding of the process can be a great tool for assessing and supporting the product's life cycle management.

Over the last years, RCPE has created a strategic partnership with AMS-Pharma in order to complement and support the development process up to clinical batch manufacturing under GMP. AMS-Pharma holds several GMP certifications for manufacturing operation and quality control activities of Human Investigational Medicinal Products and Human Medicinal Products. The facilities enable clinical batch manufacturing and commercial manufacturing supported by product and process development knowledge generated by RCPE's scientific expertise. The HME clinical batch manufacturing is performed using a TS extruder (PharmaLab 16 TSE) and upstream and downstream processing equipment (Table 7.2).

Table 7.2. GMP extruders available at AMS-Pharma

Upstream Equipment
Ktron K20 feeders (0.5kg/h - 6kg/h)
Twin-Screw Extruder
PharmaLab 16 TSE Thermo Scientific
Downstream equipment
1.2 m conveyor belt, air-cooled
Strand pelletizer, pellet length 1 - 3 mm

7.6 Summary and Conclusion

Drug product development is a complicated and risky endeavor, especially with regard to complex enabling formulations, such as ASDs made via hot-melt extrusion or spray drying. Here, a workflow for product development is presented that allow a rational design of formulations, process and scale-up/tech-transfer to GMP manufacturing within less than a year. The first step (Figure 7.1) is screening the suitable carriers and establishing a detailed understanding of API-carrier interactions, which allow an analysis of long-term stability and biopharmaceutics of the products. Both theoretical tools (e.g., MD simulation, PC-SAFT modeling, Flory Huggins model, Gordon-Taylor equation) and experimental screening methods (DSC, rheology, etc.) form a (semi-) predictive framework for a rational formulation development. Accelerated stability screening and detailed analysis of biopharmaceutical parameters (e.g., biorelevant supersaturation and in vitro dynamic dissolution) are the next logical step. The outcome of these efforts is the selection of suitable carriers for a specific API formulation (for example ASDs). In the past, it was demonstrated that such a rational formulation development workflow can be completed within a few months.

Once the formulation has been fixed, the carriers have been selected and the degradation profile has been established, the process development can be performed *in silico* based on detailed rheology data (Figure 7.6). Lab and pilot plant extruders are used to verify the model-based selection of processing conditions and screw design. If the screw parameters are available, simulations can proceed swiftly. If not, they have to be established via detailed SPH simulations. Altogether, this process can be completed within a few months.

The last step is the process transfer to the extruder at a GMP-certified site, with the goal of matching the thermo-mechanical load and the processing history. Once again modeling is the tool of choice, and a possible screw parameter for the GMP extruder has to be computed prior to the process transfer.

In summary, the proposed rational framework makes it possible to perform the product and process development for enabling formulations made via hot-melt extrusion within less than a year. Similar considerations can be applied to enabling formulation made via spray drying. This will be the focus of future research.

7.7 Abbreviations

API	Active Pharmaceutical Ingredient
ASD	Amorphous Solid Dispersion
BCS	Biopharmaceutical Classification System
CFD	Computational Fluid Dynamics
CMA	Critical Material Attributes
CPP	Critical Process Parameters
CQA	Critical Quality Attribute
CQA	Critical Quality Attributes
DCS	Developability Classification System
DDS	Drug Delivery System
DEM	Discrete Element Method
DES	Dielectric Spectroscopy
DMA	Dynamic Mechanical Analysis
DoE	Design of Experiments
DSC	Differential Scanning Calorimetry
ESR	Electron Spin Resonance
FH	Flory-Huggins
FIH	First-In-Human
GI	Gastro-Intestinal
GMP	Good Manufacturing Practice
GPU	Graphical Processing Unit
HME	Hot Melt Extrusion
ICH	International Council for Harmonisation of Technical Requirements for Pharmaceuticals for Human Use
IR	Infrared
IVIVC	In Vitro-In Vivo Correlations
MD	Molecular Dynamics
NCE	New Chemical Entities
NMR	Nuclear Magnetic Resonance
PAT	Process Analytical Technology
PBPK	Physiologically-Based Pharmacokinetics
PK	Pharmacokinetics

PSD	Particle Size Distribution
QTPP	Quality Target Product Profile
RH	Relative Humidity
RTD	Residence Time Distribution
SD	Spray Drying
SMEC	Specific Mechanical Energy Consumption
SPH	Smoothed Particle Hydrodynamics
TSE	Twin Screw Extruder
VCM	Vacuum Compression Molding
XPS	Extended Particle System
XRPD	X-Ray Powder Diffraction

7.8 References

[1] H. McFall *et al.*, "Formulation of aripiprazole-loaded pH-modulated solid dispersions via hot-melt extrusion technology: In vitro and in vivo studies," *Int. J. Pharm.*, vol. 554, pp. 302–311, Jan. 2019.

[2] J. M. Vasoya *et al.*, "Development of Solid Dispersion by Hot Melt Extrusion Using Mixtures of Polyoxylglycerides With Polymers as Carriers for Increasing Dissolution Rate of a Poorly Soluble Drug Model," *J. Pharm. Sci.*, vol. 108, no. 2, pp. 888–896, Feb. 2019.

[3] A. Schittny, H. Ogawa, J. Huwyler, and M. Puchkov, "A combined mathematical model linking the formation of amorphous solid dispersions with hot-melt-extrusion process parameters," *Eur. J. Pharm. Biopharm.*, vol. 132, pp. 127–145, Nov. 2018.

[4] D. Treffer, A. Troiss, and J. G. Khinast, "A novel tool to standardize rheology testing of molten polymers for pharmaceutical applications," *Int. J. Pharm.*, vol. 495, no. 1, pp. 474–481, Nov. 2015.

[5] R. Baumgartner, J. Matić, S. Schrank, S. Laske, J. G. Khinast, and E. Roblegg, "NANEX: Process design and optimization," *Int. J. Pharm.*, vol. 506, no. 1–2, pp. 35–45, Jun. 2016.

[6] R. Baumgartner, A. Eitzlmayr, N. Matsko, C. Tetyczka, J. G. Khinast, and E. Roblegg, "Nano-extrusion: A promising tool for continuous manufacturing of solid nano-formulations," *Int. J. Pharm.*, vol. 477, no. 1–2, pp. 1–11, Dec. 2014.

[7] A. M. Bhagurkar, M. A. Repka, and S. N. Murthy, "A Novel Approach for the Development of a Nanostructured Lipid Carrier Formulation by Hot-Melt Extrusion Technology," *J. Pharm. Sci.*, vol. 106, no. 4, pp. 1085–1091, Apr. 2017.

[8] L. A. D. Silva *et al.*, "Preparation of a solid self-microemulsifying drug delivery system by hot-melt extrusion," *Int. J. Pharm.*, vol. 541, no. 1–2, pp. 1–10, Apr. 2018.

[9] H. Patil, X. Feng, X. Ye, S. Majumdar, and M. A. Repka, "Continuous Production of Fenofibrate Solid Lipid Nanoparticles by Hot-Melt Extrusion Technology: a Systematic Study Based on a Quality by Design Approach," *AAPS J.*, vol. 17, no. 1, pp. 194–205, Jan. 2015.

[10] Y. Zhu, N. H. Shah, A. Waseem Malick, M. H. Infeld, and J. W. McGinity, "Controlled Release of a Poorly Water-Soluble Drug from Hot-Melt Extrudates Containing Acrylic Polymers," *Drug Dev. Ind. Pharm.*, vol. 32, no. 5, pp. 569–583, Jan. 2006.

[11] A. Q. Vo *et al.*, "A novel floating controlled release drug delivery system prepared by

hot-melt extrusion," *Eur. J. Pharm. Biopharm.*, vol. 98, pp. 108–121, Jan. 2016.

[12] M. Fukuda, N. A. Peppas, and J. W. McGinity, "Floating hot-melt extruded tablets for gastroretentive controlled drug release system," *J. Control. Release*, vol. 115, no. 2, pp. 121–129, Oct. 2006.

[13] A. Paudel, Z. A. Worku, J. Meeus, S. Guns, and G. Van den Mooter, "Manufacturing of solid dispersions of poorly water soluble drugs by spray drying: Formulation and process considerations," *Int. J. Pharm.*, vol. 453, no. 1, pp. 253–284, Aug. 2013.

[14] M. F. Simões, R. M. A. Pinto, and S. Simões, "Hot-melt extrusion in the pharmaceutical industry: toward filing a new drug application," *Drug Discov. Today*, vol. 24, no. 9, pp. 1749–1768, Sep. 2019.

[15] L. X. Yu *et al.*, "Understanding pharmaceutical quality by design," *AAPS J.*, vol. 16, no. 4, pp. 771–783, Jul. 2014.

[16] V. P. Kumar and N. V. Gupta, "A Review on quality by design (QBD) for Pharmaceuticals," *Int. J. Drug Dev. Res.*, vol. 7, no. 1, pp. 35–44, 2015.

[17] J. Rehrl, J. Kruisz, S. Sacher, J. G. Khinast, and M. Horn, "Optimized continuous pharmaceutical manufacturing via model-predictive control," *Int. J. Pharm.*, vol. 510, no. 1, pp. 100–115, Aug. 2016.

[18] J. Rehrl *et al.*, "Control of three different continuous pharmaceutical manufacturing processes: Use of soft sensors," *Int. J. Pharm.*, vol. 543, no. 1–2, pp. 60–72, May 2018.

[19] V. Mishra, S. Thakur, A. Patil, and A. Shukla, "Quality by design (QbD) approaches in current pharmaceutical set-up," *Expert Opin. Drug Deliv.*, vol. 15, no. 8, pp. 737–758, Aug. 2018.

[20] A. Gupta and M. A. Khan, "Hot-Melt Extrusion: An FDA Perspective on Product and Process Understanding," in *Hot-Melt Extrusion: Pharmaceutical Applications*, Chichester, UK: John Wiley & Sons, Ltd, 2012, pp. 323–331.

[21] ICH Q8, "INTERNATIONAL CONFERENCE ON HARMONISATION OF TECHNICAL REQUIREMENTS FOR REGISTRATION OF PHARMACEUTICALS FOR HUMAN USE PHARMACEUTICAL DEVELOPMENT Q8(R2)," 2009.

[22] ICH Q9, "INTERNATIONAL CONFERENCE ON HARMONISATION OF TECHNICAL REQUIREMENTS FOR REGISTRATION OF PHARMACEUTICALS FOR HUMAN USE ICH HARMONISED TRIPARTITE GUIDELINE QUALITY RISK MANAGEMENT Q9," 2005.

[23] ICH Q10, "INTERNATIONAL CONFERENCE ON HARMONISATION OF TECHNICAL REQUIREMENTS FOR REGISTRATION OF PHARMACEUTICALS

FOR HUMAN USE PHARMACEUTICAL QUALITY SYSTEM Q10," 2009.

[24] M. T. Islam, M. Maniruzzaman, S. A. Halsey, B. Z. Chowdhry, and D. Douroumis, "Development of sustained-release formulations processed by hot-melt extrusion by using a quality-by-design approach," *Drug Deliv. Transl. Res.*, vol. 4, no. 4, pp. 377–387, Aug. 2014.

[25] G. L. Amidon, H. Lennernäs, V. P. Shah, and J. R. Crison, "A Theoretical Basis for a Biopharmaceutic Drug Classification: The Correlation of in Vitro Drug Product Dissolution and in Vivo Bioavailability," *Pharm. Res.*, vol. 12, no. 3, pp. 413–420, Mar. 1995.

[26] H. D. Williams *et al.*, "Strategies to Address Low Drug Solubility in Discovery and Development," *Pharmacol. Rev.*, vol. 65, no. 1, pp. 315–499, Jan. 2013.

[27] J. M. Butler and J. B. Dressman, "The Developability Classification System: Application of Biopharmaceutics Concepts to Formulation Development," *J. Pharm. Sci.*, vol. 99, no. 12, pp. 4940–4954, Dec. 2010.

[28] L. Zhang and S. Mao, "Application of quality by design in the current drug development," *Asian J. Pharm. Sci.*, vol. 12, no. 1, pp. 1–8, 2017.

[29] J. Maguire and D. Peng, "How to Identify Critical Quality Attributes and Critical Process Parameters," *FDA/PQRI 2nd Conf.*, pp. 1–40, 2015.

[30] J. Matić, A. Witschnigg, M. Zagler, S. Eder, and J. Khinast, "A novel in silico scale-up approach for hot melt extrusion processes," *Chem. Eng. Sci.*, vol. 204, pp. 257–269, Aug. 2019.

[31] D. J. Greenhalgh, A. C. Williams, P. Timmins, and P. York, "Solubility parameters as predictors of miscibility in solid dispersions," *J. Pharm. Sci.*, vol. 88, no. 11, pp. 1182–1190, Nov. 1999.

[32] T. Kitak, A. Dumičić, O. Planinšek, R. Šibanc, and S. Srčič, "Determination of Solubility Parameters of Ibuprofen and Ibuprofen Lysinate," *Molecules*, vol. 20, no. 12, pp. 21549–21568, Dec. 2015.

[33] E. Meaurio, E. Sanchez-Rexach, E. Zuza, A. Lejardi, A. del P. Sanchez-Camargo, and J.-R. Sarasua, "Predicting miscibility in polymer blends using the Bagley plot: Blends with poly(ethylene oxide)," *Polymer (Guildf).*, vol. 113, pp. 295–309, Mar. 2017.

[34] L. S. Taylor and G. G. Z. Zhang, "Physical chemistry of supersaturated solutions and implications for oral absorption," *Adv. Drug Deliv. Rev.*, vol. 101, pp. 122–142, Jun. 2016.

[35] A. Paudel, E. Nies, and G. Van den Mooter, "Relating Hydrogen-Bonding Interactions

with the Phase Behavior of Naproxen/PVP K 25 Solid Dispersions: Evaluation of Solution-Cast and Quench-Cooled Films," *Mol. Pharm.*, vol. 9, no. 11, pp. 3301–3317, Nov. 2012.

[36] J. Aho, M. Edinger, J. Botker, S. Baldursdottir, and J. Rantanen, "Oscillatory Shear Rheology in Examining the Drug-Polymer Interactions Relevant in Hot Melt Extrusion," *J. Pharm. Sci.*, vol. 105, no. 1, pp. 160–167, Jan. 2016.

[37] S. P. O'Connell, "Hot-Melt Extrusion Through Syringes," 2014.

[38] A. Paudel, A. Mercuri, S. Mohr, M. Bresciani, and J. G. Khinast, "Abstract: Amorphous Solid Dispersion of Poorly Soluble API By Hot Melt Extrusion (HME) and Spray Drying (SD): A Rational Screening Approach," 2015.

[39] M. F. Simões *et al.*, "A 5-Stage Approach for a Systematic Screening and Development of Etravirine Amorphous Solid Dispersions by Hot-Melt Extrusion," *Mol. Pharm.*, p. acs.molpharmaceut.9b00996, Nov. 2019.

[40] R. Han *et al.*, "Predicting physical stability of solid dispersions by machine learning techniques," *J. Control. Release*, vol. 311–312, pp. 16–25, Oct. 2019.

[41] E. O. Kissi, H. Grohganz, K. Löbmann, M. T. Ruggiero, J. A. Zeitler, and T. Rades, "Glass-Transition Temperature of the β-Relaxation as the Major Predictive Parameter for Recrystallization of Neat Amorphous Drugs," *J. Phys. Chem. B*, vol. 122, no. 10, pp. 2803–2808, Mar. 2018.

[42] R. Laitinen, K. Löbmann, C. J. Strachan, H. Grohganz, and T. Rades, "Emerging trends in the stabilization of amorphous drugs," *Int. J. Pharm.*, vol. 453, no. 1, pp. 65–79, Aug. 2013.

[43] K. Chmiel, J. Knapik-Kowalczuk, and M. Paluch, "How does the high pressure affects the solubility of the drug within the polymer matrix in solid dispersion systems," *Eur. J. Pharm. Biopharm.*, vol. 143, pp. 8–17, Oct. 2019.

[44] A. Prudic, Y. Ji, C. Luebbert, and G. Sadowski, "Influence of humidity on the phase behavior of API/polymer formulations," *Eur. J. Pharm. Biopharm.*, vol. 94, pp. 352–362, Aug. 2015.

[45] A. Prudic, Y. Ji, and G. Sadowski, "Thermodynamic Phase Behavior of API/Polymer Solid Dispersions," *Mol. Pharm.*, vol. 11, no. 7, pp. 2294–2304, Jul. 2014.

[46] Y. Ji, R. Paus, A. Prudic, C. Lübbert, and G. Sadowski, "A Novel Approach for Analyzing the Dissolution Mechanism of Solid Dispersions," *Pharm. Res.*, vol. 32, no. 8, pp. 2559–2578, Feb. 2015.

[47] A. Prudic, A.-K. Lesniak, Y. Ji, and G. Sadowski, "Thermodynamic phase behaviour of

indomethacin/PLGA formulations," *Eur. J. Pharm. Biopharm.*, vol. 93, pp. 88–94, Jun. 2015.

[48] A. Paudel, J. Van Humbeeck, and G. Van Den Mooter, "Theoretical and experimental investigation on the solid solubility and miscibility of naproxen in poly(vinylpyrrolidone)," *Mol. Pharm.*, vol. 7, no. 4, pp. 1133–1148, Aug. 2010.

[49] D. Medarević, J. Djuriš, P. Barmpalexis, K. Kachrimanis, and S. Ibrić, "Analytical and Computational Methods for the Estimation of Drug-Polymer Solubility and Miscibility in Solid Dispersions Development," *Pharmaceutics*, vol. 11, no. 8, p. 372, Aug. 2019.

[50] M. M. Knopp *et al.*, "Comparative Study of Different Methods for the Prediction of Drug–Polymer Solubility," *Mol. Pharm.*, vol. 12, no. 9, pp. 3408–3419, Sep. 2015.

[51] M. M. Knopp, N. E. Olesen, P. Holm, P. Langguth, R. Holm, and T. Rades, "Influence of Polymer Molecular Weight on Drug–polymer Solubility: A Comparison between Experimentally Determined Solubility in PVP and Prediction Derived from Solubility in Monomer," *J. Pharm. Sci.*, vol. 104, no. 9, pp. 2905–2912, Sep. 2015.

[52] M. M. Knopp *et al.*, "Evaluation of Drug–Polymer Solubility Curves Through Formal Statistical Analysis: Comparison of Preparation Techniques," *J. Pharm. Sci.*, vol. 104, no. 1, pp. 44–51, Jan. 2015.

[53] M. B. Rask, M. M. Knopp, N. E. Olesen, R. Holm, and T. Rades, "Influence of PVP/VA copolymer composition on drug–polymer solubility," *Eur. J. Pharm. Sci.*, vol. 85, pp. 10–17, Mar. 2016.

[54] A. Paudel, J. Meeus, and G. Van den Mooter, "Structural Characterization of Amorphous Solid Dispersions," in *Amorphous Solid Dispersions*, 2014, pp. 421–485.

[55] C. Luebbert and G. Sadowski, "Moisture-induced phase separation and recrystallization in amorphous solid dispersions," *Int. J. Pharm.*, vol. 532, no. 1, pp. 635–646, Oct. 2017.

[56] C. Luebbert, F. Huxoll, and G. Sadowski, "Amorphous-Amorphous Phase Separation in API/Polymer Formulations," *Molecules*, vol. 22, no. 2, p. 296, Feb. 2017.

[57] C. Luebbert, C. Klanke, and G. Sadowski, "Investigating phase separation in amorphous solid dispersions via Raman mapping," *Int. J. Pharm.*, vol. 535, no. 1–2, pp. 245–252, Jan. 2018.

[58] C. Luebbert, M. Wessner, and G. Sadowski, "Mutual Impact of Phase Separation/Crystallization and Water Sorption in Amorphous Solid Dispersions," *Mol. Pharm.*, vol. 15, no. 2, pp. 669–678, Feb. 2018.

[59] C. Luebbert and G. Sadowski, "In-situ determination of crystallization kinetics in ASDs via water sorption experiments," *Eur. J. Pharm. Biopharm.*, vol. 127, pp. 183–193, Jun.

2018.

[60] K. Lehmkemper, S. O. Kyerematen, M. Degenhardt, and G. Sadowski, “Influence of Low-Molecular-Weight Excipients on the Phase Behavior of PVPVA64 Amorphous Solid Dispersions,” *Pharm. Res.*, vol. 35, no. 1, p. 25, Jan. 2018.

[61] S. Greco, J. R. Authelin, C. Leveder, and A. Segalini, “A practical method to predict physical stability of amorphous solid dispersions,” *Pharm. Res.*, vol. 29, no. 10, pp. 2792–2805, Oct. 2012.

[62] B. D. Anderson, “Predicting Solubility/Miscibility in Amorphous Dispersions: It Is Time to Move Beyond Regular Solution Theories,” *J. Pharm. Sci.*, vol. 107, no. 1, pp. 24–33, Jan. 2018.

[63] M. Brunsteiner, J. G. Khinast, and A. Paudel, “Relative contributions of solubility and mobility to the stability of amorphous solid dispersions of poorly soluble drugs: A molecular dynamics simulation study,” *Pharmaceutics*, vol. 10, no. 3, p. 101, Jul. 2018.

[64] K. Zhang, J. D. Pellett, A. S. Narang, Y. J. Wang, and Y. T. Zhang, “Reactive impurities in large and small molecule pharmaceutical excipients – A review,” *TrAC Trends Anal. Chem.*, vol. 101, pp. 34–42, Apr. 2018.

[65] I. Saraf *et al.*, “Feasibility of rapidly assessing reactive impurities mediated excipient incompatibility using a new method: A case study of famotidine-PEG system,” *J. Pharm. Biomed. Anal.*, vol. 178, p. 112893, Jan. 2020.

[66] B. J. Boyd *et al.*, “Successful oral delivery of poorly water-soluble drugs both depends on the intraluminal behavior of drugs and of appropriate advanced drug delivery systems,” *Eur. J. Pharm. Sci.*, vol. 137, p. 104967, Sep. 2019.

[67] C. A. S. Bergström *et al.*, “Biorelevant intrinsic dissolution profiling in early drug development: Fundamental, methodological, and industrial aspects,” *Eur. J. Pharm. Biopharm.*, vol. 139, pp. 101–114, Jun. 2019.

[68] A. Denninger, U. Westedt, J. Rosenberg, and K. G. Wagner, “A Rational Design of a Biphasic Dissolution Setup—Modelling of Biorelevant Kinetics for a Ritonavir Hot-Melt Extruded Amorphous Solid Dispersion,” *Pharmaceutics*, vol. 12, no. 3, p. 237, Mar. 2020.

[69] A. Schittny, S. Philipp-Bauer, P. Detampel, J. Huwyler, and M. Puchkov, “Mechanistic insights into effect of surfactants on oral bioavailability of amorphous solid dispersions,” *J. Control. Release*, vol. 320, pp. 214–225, Apr. 2020.

[70] A. Mitra, W. Zhu, and F. Kesisoglou, “Physiologically based absorption modeling for amorphous solid dispersion formulations,” *Mol. Pharm.*, vol. 13, no. 9, pp. 3206–3215,

Sep. 2016.

[71] V. Bhardwaj, N. S. Trasi, D. Y. Zemlyanov, and L. S. Taylor, “Surface area normalized dissolution to study differences in itraconazole-copovidone solid dispersions prepared by spray-drying and hot melt extrusion,” *Int. J. Pharm.*, vol. 540, no. 1–2, pp. 106–119, Apr. 2018.

[72] J. Rebeka *et al.*, “PBPK Absorption Modeling of Food Effect and Bioequivalence in Fed State for Two Formulations with Crystalline and Amorphous Forms of BCS 2 Class Drug in Generic Drug Development,” *AAPS PharmSciTech*, vol. 20, no. 2, p. 59, Feb. 2019.

[73] A. Kambayashi, T. Kiyota, M. Fujiwara, and J. B. Dressman, “PBPK modeling coupled with biorelevant dissolution to forecast the oral performance of amorphous solid dispersion formulations,” *Eur. J. Pharm. Sci.*, vol. 135, pp. 83–90, Jul. 2019.

[74] S. Guns and G. Van den Mooter, “Clinical and Preclinical Studies, Bioavailability and Pharmacokinetics of Hot-Melt Extruded Products,” in *Hot-Melt Extrusion: Pharmaceutical Applications*, Chichester, UK: John Wiley & Sons, Ltd, 2012, pp. 223–237.

[75] C. Rauwendaal, *Polymer extrusion: Fifth edition*, Fifth Edit. München: Carl Hanser Verlag GmbH & Co. KG, 2014.

[76] K. Kohlgrüber, *Co-Rotating Twin-Screw Extruder*. München: Carl Hanser Verlag GmbH & Co. KG, 2007.

[77] K. Kolter, M. Karl, and A. Gryczke, *Hot-Melt Extrusion with BASF polymers*, no. 2nd Revised and Enlarged. BASF, 2012.

[78] D. Douroumis, *Hot-Melt Extrusion: Pharmaceutical Applications*. Chichester, UK: John Wiley & Sons, Ltd, 2012.

[79] M. Maniruzzaman, J. S. Boateng, M. J. Snowden, and D. Douroumis, “A Review of Hot-Melt Extrusion: Process Technology to Pharmaceutical Products,” *ISRN Pharm.*, vol. 2012, pp. 1–9, 2012.

[80] M. M. Crowley *et al.*, “Pharmaceutical Applications of Hot-Melt Extrusion: Part I,” *Drug Dev. Ind. Pharm.*, vol. 33, no. 9, pp. 909–926, Jan. 2007.

[81] M. A. Repka *et al.*, “Pharmaceutical Applications of Hot-Melt Extrusion: Part II,” *Drug Dev. Ind. Pharm.*, vol. 33, no. 10, pp. 1043–1057, Jan. 2007.

[82] B. Lang, J. W. McGinity, and R. O. Williams, “Hot-melt extrusion – basic principles and pharmaceutical applications,” *Drug Dev. Ind. Pharm.*, vol. 40, no. 9, pp. 1133–1155, Sep. 2014.

[83] A. Eitzlmayr and J. G. Khinast, “Co-rotating twin-screw extruders: Detailed analysis of

conveying elements based on smoothed particle hydrodynamics. Part 1: Hydrodynamics," *Chem. Eng. Sci.*, vol. 134, pp. 861–879, Sep. 2015.

[84] A. Eitzlmayr and J. G. Khinast, "Co-rotating twin-screw extruders: Detailed analysis of conveying elements based on smoothed particle hydrodynamics. Part 1: Hydrodynamics," *Chem. Eng. Sci.*, vol. 134, pp. 861–879, Sep. 2015.

[85] A. Eitzlmayr, J. Matić, and J. G. Khinast, "Analysis of flow and mixing in screw elements of corotating twin-screw extruders via SPH," *AIChE J.*, vol. 63, no. 6, pp. 2451–2463, Jun. 2017.

[86] A. Eitzlmayr *et al.*, "Experimental characterization and modeling of twin-screw extruder elements for pharmaceutical hot melt extrusion," *AIChE J.*, vol. 59, no. 11, pp. 4440–4450, Nov. 2013.

[87] A. Eitzlmayr *et al.*, "Mechanistic modeling of modular co-rotating twin-screw extruders," *Int. J. Pharm.*, vol. 474, no. 1–2, pp. 157–176, Oct. 2014.

[88] H. Cheng and I. Manas-Zloczower, "Distributive mixing in conveying elements of a ZSK-53 co-rotating twin screw extruder," *Polym. Eng. Sci.*, vol. 38, no. 6, pp. 926–935, Jun. 1998.

[89] R. A. Gingold and J. J. Monaghan, "Smoothed particle hydrodynamics: theory and application to non-spherical stars," *Mon. Not. R. Astron. Soc.*, vol. 181, no. 3, pp. 375–389, Dec. 1977.

[90] J. J. Monaghan, "Simulationg free surface flows with SPH," *J. Comput. Phys.*, vol. 110, pp. 399–406, 1994.

[91] J. J. Monaghan, "SPH without a Tensile Instability," *J. Comput. Phys.*, vol. 159, pp. 290–311, Apr. 2000.

[92] R. A. Gingold and J. J. Monaghan, "Kernel Estimates as a Basis for General Particle Methods in Hydrodynamics," *J. Comput. Phys.*, vol. 46, pp. 429–453, 1982.

[93] J. J. Monaghan, "Smoothed Particle Hydrodynamics and Its Diverse Applications," *Annu. Rev. Fluid Mech.*, vol. 44, no. 1, pp. 323–346, Jan. 2012.

[94] P. Wittek, G. G. Pereira, M. A. Emin, V. Lemiale, and P. W. Cleary, "Accuracy analysis of SPH for flow in a model extruder with a kneading element," *Chem. Eng. Sci.*, vol. 187, pp. 256–268, Sep. 2018.

[95] M. Robinson and P. W. Cleary, "Effect of geometry and fill level on the transport and mixing behaviour of a co-rotating twin screw extruder," *Comput. Part. Mech.*, vol. 6, no. 2, pp. 227–247, Apr. 2019.

[96] J. Pawlowski, *Die Ähnlichkeitstheorie in der physikalisch-technischen Forschung*.

Berlin, Heidelberg: Springer Berlin Heidelberg, 1971.

[97] T. Forgber, P. Toson, S. Madlmeir, H. Kureck, J. G. Khinast, and D. Jajcevic, "Extended validation and verification of XPS/AVL-Fire™, a computational CFD-DEM software platform," *Powder Technol.*, vol. 361, pp. 880–893, Feb. 2020.

[98] P. Boehling *et al.*, "Analysis of large-scale tablet coating: Modeling, simulation and experiments," *Eur. J. Pharm. Sci.*, vol. 90, pp. 14–24, Jul. 2016.

[99] H. Kureck, N. Govender, E. Siegmann, P. Boehling, C. Radeke, and J. G. Khinast, "Industrial scale simulations of tablet coating using GPU based DEM: A validation study," *Chem. Eng. Sci.*, vol. 202, pp. 462–480, Jul. 2019.

[100] P. Boehling *et al.*, "Comparison of video analysis and simulations of a drum coating process," *Eur. J. Pharm. Sci.*, vol. 104, pp. 72–81, Jun. 2017.

[101] E. Siegmann *et al.*, "Powder flow and mixing in different tablet press feed frames," *Adv. Powder Technol.*, vol. 31, no. 2, pp. 770–781, Feb. 2020.

[102] P. Boehling *et al.*, "Simulation of a tablet coating process at different scales using DEM," *Eur. J. Pharm. Sci.*, vol. 93, pp. 74–83, Oct. 2016.

[103] P. Böhling *et al.*, "Computational Fluid Dynamics-Discrete Element Method Modeling of an Industrial-Scale Wurster Coater," *J. Pharm. Sci.*, vol. 108, no. 1, pp. 538–550, Jan. 2019.

[104] M. Ebrahimi, E. Siegmann, D. Prieling, B. J. Glasser, and J. G. Khinast, "An investigation of the hydrodynamic similarity of single-spout fluidized beds using CFD-DEM simulations," *Adv. Powder Technol.*, vol. 28, no. 10, pp. 2465–2481, Oct. 2017.

[105] S. Adam, D. Suzzi, C. Radeke, and J. G. Khinast, "An integrated Quality by Design (QbD) approach towards design space definition of a blending unit operation by Discrete Element Method (DEM) simulation," *Eur. J. Pharm. Sci.*, vol. 42, no. 1–2, pp. 106–115, Jan. 2011.

[106] P. Toson *et al.*, "Detailed modeling and process design of an advanced continuous powder mixer," *Int. J. Pharm.*, vol. 552, no. 1–2, pp. 288–300, Dec. 2018.

[107] M. Börner, M. Michaelis, E. Siegmann, C. Radeke, and U. Schmidt, "Impact of impeller design on high-shear wet granulation," *Powder Technol.*, vol. 295, pp. 261–271, Jul. 2016.

[108] E. Siegmann, D. Jajcevic, C. Radeke, D. Strube, K. Friedrich, and J. G. Khinast, "Efficient Discrete Element Method Simulation Strategy for Analyzing Large-Scale Agitated Powder Mixers," *Chemie Ing. Tech.*, vol. 89, no. 8, pp. 995–1005, Aug. 2017.

[109] D. Jajcevic, E. Siegmann, C. Radeke, and J. G. Khinast, "Large-scale CFD–DEM

simulations of fluidized granular systems," *Chem. Eng. Sci.*, vol. 98, pp. 298–310, Jul. 2013.

[110] J. G. Khinast and J. Rantanen, *Continuous Manufacturing of Pharmaceuticals*. Chichester, UK: John Wiley & Sons, Ltd, 2017.

[111] D. Treffer *et al.*, "In-line implementation of an image-based particle size measurement tool to monitor hot-melt extruded pellets," *Int. J. Pharm.*, vol. 466, no. 1–2, pp. 181–189, May 2014.

[112] A. Witschnigg, G. Koscher, D. Treffer, R. Mürb, S. Laske, and J. G. Khinast, "Micro-pelletizing of pharmaceutical HME formulations using a die face pelletizer," in *AIP Conference Proceedings*, 2016, vol. 1779, p. 130001.

[113] S. Schrank *et al.*, "The effect of the drying temperature on the properties of wet-extruded calcium stearate pellets: Pellet microstructure, drug distribution, solid state and drug dissolution," *Int. J. Pharm.*, vol. 478, no. 2, pp. 779–787, Jan. 2015.

[114] M. Kirchengast *et al.*, "Ensuring tablet quality via model-based control of a continuous direct compaction process," *Int. J. Pharm.*, vol. 567, p. 118457, Aug. 2019.

[115] S. Sacher *et al.*, "Towards a Novel Continuous HME-Tableting Line: Process Development and Control Concept," *Eur. J. Pharm. Sci.*, p. 105097, Oct. 2019.

[116] World Health Organization, "Annex 7 WHO guidelines on transfer of technology," *WHO Tech. Rep. Ser. No. 961, 2011*, no. 961, pp. 285–309, 2011.

8

Conclusions and Future Direction

The presented work shows the implementation of different *in silico* tools in the analysis, development and scale-up of pharmaceutical hot melt extrusion (HME) process in the pharmaceutical industry. The application of Smoothed Particle Hydrodynamics (SPH) for analyzing the performance of double- and triple flighted twin screw extruder elements was discussed and analyzed. This showed the impact the change in the cross section geometry has on the performance of the individual screw pairs. Further, the impact the change of extruder scale or vendor can have on the process state was analyzed, with guidelines on how to transfer the screw configuration from one extruder setup to another. Here the difference between scaling process parameters and scaling the overall process state was shown and discussed. Using reduced order 1D HME simulation a full pharmaceutical HME process setup was analyzed, discussing in detail the process transfer and scale-up. A number of different scale-up variants was evaluated, both *in silico* and experimentally. The differences in the thermomechanical load history the formulation experiences during processing and the differences in the load history arising from different setup and scale-up variants were analyzed in detail. Moreover, the product quality as a function of different process settings and process states was analyzed across two extruder scales, showing a correlation between the API degradation in the extrudates and the process state.

8.1 Conclusions

Three main conclusions can be drawn from this work:

i. The cross section geometry of the individual screw elements has a significant impact on the screw performance in terms of the conveying capacity of the screw, pressure build-up and power consumption. This is true both in cases with seemingly marginal differences in the cross section geometry (i.e. differences between the ratio of outer and inner screw diameters and gap distances) and with differences in the construction of the cross section (i.e. screw elements with a single flighted, double- or triple flighted screw cross sections). This comes in addition to the impact the screw pitch for conveying elements, the number, shape and arrangement of cut outs for mixing elements and number, angle and thickness of kneading blocks in kneading elements, have on the screw performance. Hence, assembly of the screw configuration should take into account all of the characteristics of the used screw element pairs to ensure proper assembling of the process functional zones along the screw configuration suitable for the processed formulation. Moreover, for the purpose of process transfer and scale-up, attention has to be payed to the transfer of the process functional zones from one extruder to another, taking into account the differences the individual screw element pairs have between different scales and potentially between different extruder vendors.

ii. The scale-up laws transferred from the food and polymer to the pharmaceutical industry do not work as intended for pharmaceutical products. The reasons for this vary from the individual characteristics of the used screw element pairs, as discussed above, to the specifics of the pharmaceutical formulations processed. The processed active pharmaceutical ingredients (APIs) often have a very limited processability window in comparison to the formulations typically processed in the polymer or food industries, i.e. small differences in the process setup on two different scales can have drastic impact on the product quality of HME processed pharmaceuticals. This can be easily seen when comparing the process states of the original and scaled-up process using different mechanistic *in silico* methods, as shown in this work. The reason why the more traditional scale-up rules do not result in the same process state is due to the basic assumptions used in the development of such rules. They rely mostly on integral process values like the overall process specific mechanical energy consumption (SMEC), overall residence time distribution (RTD), barrel temperature and cooling, local

pressure and melt temperature at the die and geometrical similarities of the extruder. In this work it was shown that the equivalence of integral process values does not guarantee that the process state in two HME setups is also equivalent. For example, a constant process SMEC across two different extruder scales does not guarantee that the local temperature peaks across the screw configuration are also equivalent, which can cause potential degradation (or some other response) of the processed formulation. The same is true for local residence times. This means that the focus should be shifted from the scale-up of process settings to the direct transfer of the process states. Equivalence of the process state, and consequently the resulting product, is not reached by ensuring that the integral process values stay constant. Rather, it is crucial to achieve the equivalence in the thermomechanical process cycle the formulation is experiencing across different extruder setups by ensuring that local values of temperature, residence time and energy input stay equivalent.

iii. Connecting the previous two points, taking into account the specifics of every screw element pair used in the screw configuration, the used process settings (screw speed, throughput, barrel temperature settings, die setup and so on) and the processed formulation, it is possible to link the achieved product quality to the process state. To show the relationship, the API degradation in the final product was compared to the achieved process state showing that the exposure time (local residence time at specific points along the screw configuration) and the local melt temperature correlate well with the resulting API degradation. This means that any increase in the peak temperature for a constant exposure time, and vice versa, results in an increase in the API degradation seen in the final product. This holds true also for different extruder scales regardless of the integral SMEC or RTD values. This is a significant result which shows that the achieved product quality is a function of the thermomechanical load history the formulation has been exposed to during processing regardless of the extruder scale. This makes it possible to screen different formulations under different temperature and exposure time conditions during the formulation development phase and to design the HME process *in silico* such as to keep the thermomechanical load history in a predefined processing window. Such an approach shifts from the currently prevailing trial-and-error approach in product development to a quality by design (QbD) approach that guaranties a certain outcome (product quality) if all the input variables are known (formulation characteristics, screw characteristics and so on) and the relations between

them (i.e. calculating the melt temperature from the screw characteristics, process setup and formulation characteristics).

8.2 Future Direction

The presented methodology can be further developed as a platform technology that would incorporate product definition, formulation development, automated process setup, scale-up and GMP transfer. From the simulation stand point the development should be tied to immediate needs of the pharmaceutical industry, which include quick and reliable process setup, product quality prediction and process transfer. All of these points have been touched upon in this work and to bring everything one more step closer to industrial application, the simulation and small scale experimental approaches should be further developed.

The developments should aim to eliminate some of the current shortcomings of the experimental drug development approach. For novel formulations, HME can be a significant hurdle. It is not obvious which polymers should be used as excipients, how those formulations are going to behave in the process and what is the expected product quality. For HME based products beyond amorphous solid dispersions, the issues are even more pronounced. If the API is crystalline and does not melt in the process it is not obvious how the loading and particle size distribution is going to affect the processability of the formulation and how the process setup is going to change the API particle size distribution and dispersion in the extrudate. Nanoparticle based extrusion face similar issues; it is not obvious what type of carrier polymer should be chosen, how to setup the process effectively to ensure high API loading and the stability of the nanoparticles. Further, for extended release formulation it is not obvious how the process setup is going to affect the API release.

Keeping in mind the final product attributes, the main goal should be to move the drug development from experimental to mainly virtual space. In order to achieve this, progress should be made in:

- Small scale formulation testing devices and procedures that are similar enough to the actual HME process and could be used to simulated the thermomechanical load history the formulation is experiencing during processing. After the formulation is experienced the thermomechanical load history associated with the HME process, the attributes of intended final product should be connected with the load history, resulting in the quality

heat map which would be used to guide the boundaries of the *in silico* process development.

- Further developments in capturing the accurate process state for different formulations and final product attributes. After moving from process settings oriented view to a process state view, it is clear that future efforts should aim to correctly capture the process state and the thermomechanical load history the formulation experiences for different types of formulations. The efforts should go beyond amorphous solid dispersion systems and include systems with crystalline immiscible APIs, nanoparticle based formulations and extended release formulations.

The accurate capturing of the process state is linked to the further development of high fidelity and reduced order simulation together with proper data analysis. The development should focus on:

- High fidelity screw simulations using SPH or some other CFD approach, with the focus on establishing more characterization features beyond the dimensionless power and pressure characteristics, of the individual screw element pairs used during extrusion. The SPH simulations presented in this work are all done with a Newtonian surrogate fluid which does not correspond to the actual fluid processed with extruders. Despite this shortcoming, the obtained results are still very useful in the context of dimensionless quantities and as they are only a function of the screw geometry (i.e. independent of the processed formulation) they can be used to parametrize reduced order models. Further development would include: detailed evaluation of the shear rate distribution characteristic for a certain screw element pair, residence time distribution in the whole element but also in different zones in the element pair cross section (in the channel region, screw intermeshing region and screw barrel gap region), further computational refinements of the different gap regions, multi-phase flow; but also the impact of non-Newtonian fluids on the dimensionless pressure and power characteristics and the melt temperature distribution as a function of the screw geometry and the processed formulation. Such a high fidelity simulation approach would generate a comprehensive data structure linked to the screw elements that could be used for parametrization of reduced order models. Adding to the more detailed characterization of the individual screw element pairs, resolving in detail the powder inflow, melting and degassing zones would also be of great interest.

- Further development of the 1D HME reduced order simulation approach should include the above mentioned results from the SPH/CFD simulations. In addition to representing the screw geometry by its dimensionless pressure and power curves, the addition of actual shear rate distributions, melt temperature distributions and residence time distribution would go a long way in further establishing the simulation method. The same approach should also be followed with representing different die geometry variants and increasing the accuracy of the pressure calculation in the location of the die. Further, taking into account the speed of the reduced order 1D HME simulations and automated *in silico* DoE framework could be integrated to represent different process variations (different screw speeds, throughputs, screw configurations, die setups and formulations) and to meaningfully compare them. The same approach could be used to perform different *in silico* scale-up variants and find the optimum. In addition to including more data from the high fidelity simulations and further automatization, efforts should be made to predict the product quality, making it possible to perform the process setup and scale-up fully *in silico*. A prerequisite for such development would also be the incorporation of formulation related properties beyond the viscosity, specific volume, heat capacity and thermal conductivity. In the case of formulations with crystalline immiscible API, introduction of the initial (as an input) and the final API particle size distribution and its dispersion in the final product (as an output) would be meaningful. Here, the API particle size distribution, loading and distribution in the melt would dynamically change the melt properties along the screw. The dynamic change of the melt properties would also be apparent when multiple feeding ports are used. A special case here is the processing of nanoparticles where a nanosuspension is feeded into the extrusion process and the process goal is to incorporate and distribute the nanoparticles in the polymeric carrier, without damaging them, but also making sure the watery phase is effectively degassed. A similar approach with two or more distinctly separate formulations could be used in capturing the process of co-extrusion, foaming and extrusion based API synthesis.

In the combination with current process and formulation knowledge, the above discussed improvements would lead to a truly Quality by Design driven product development. It would result in a virtual test bed for extrusion based products that would in turn lead to significantly reduced cost and environmental footprint, virtually no trial-and-error and faster time to market,.

Journal and Conference Contributions

9.1 Journal Contributions

Matić J, Alva C, Witschnigg A, et al. Towards predicting the product quality in hot-melt extrusion: Small scale extrusion. Int J Pharm X. 2020;2:100062. doi:10.1016/j.ijpx.2020.100062

Bauer H, Matić J, Khinast J. Characteristic parameters and process maps for fully-filled twin-screw extruder elements. Chem Eng Sci. October 2020:116202. doi:10.1016/j.ces.2020.116202

Matić J, Paudel A, Bauer H, Garcia RAL, Biedrzycka K, Khinast JG. Developing HME-Based Drug Products Using Emerging Science: a Fast-Track Roadmap from Concept to Clinical Batch. AAPS PharmSciTech. 2020;21(5):176. doi:10.1208/s12249-020-01713-0

Spoerk M, Koutsamanis I, Matić J, et al. Novel Cleaning-in-Place Strategies for Pharmaceutical Hot Melt Extrusion. Pharmaceutics. 2020;12(6):588. doi:10.3390/pharmaceutics12060588

Matić J, Witschnigg A, Zagler M, Eder S, Khinast J. A novel in silico scale-up approach for hot melt extrusion processes. Chem Eng Sci. 2019;204:257-269. doi:10.1016/j.ces.2019.04.016

Eitzlmayr A, Matić J, Khinast JG. Analysis of flow and mixing in screw elements of corotating twin-screw extruders via SPH. AIChE J. 2017;63(6):2451-2463. doi:10.1002/aic.15607

9.2 Conference Contributions

Matić J, Bauer H, Paudel A, Khinast J. Developing HME-Based Drug Products using QbD and Emerging Science. AIChE 2020 Annual Meeting, San Francisco, USA, November 16th - 20th, 2020

Bauer H, Matić J, Khinast J. New Insights into Local Residence Time Distributions of Twin Screw Extruder Elements Used in Hot Melt Extrusion via Smoothed Particle Hydrodynamics Simulations. AIChE 2020 Annual Meeting, San Francisco, USA, November 16th - 20th, 2020

Matić J, Khinast J. Simulation Aided Pharmaceutical Hot Melt Extrusion Process Understanding, Setup and Scale-Up. 16th Minisymposium Verfahrenstechnik and 7th Partikelforum, TU Wien, Austria, September 21st – 22nd, 2020

Matić J, Mostafa A, Alva C, Khinast J. Simulation Aided Pharmaceutical HME Scale-Up. AIChE 2019 Annual Meeting, Orlando, USA, November 10th – 15th, 2019

Bauer H, Matić J, Khinast J. Local Residence Time Distribution for Hot Melt Extrusion: Making a Black Box Concept Mechanistic. AIChE 2019 Annual Meeting, Orlando, USA, November 10th – 15th, 2019

Matić J, Alva C, Khinast J. Towards Predicting the Quality of HME Products. AIChE 2018 Annual Meeting, Pittsburg, USA, October 28th – November 2nd, 2018

Matić J, Paudel A, Khinast J. Modelling of Pharmaceutical HME Processes. AIChE 2017 Annual Meeting, Minneapolis, USA, October 29th – November 3rd, 2017

Matić J, Laske S, Paudel A, Pfefferlé F, Lovey-Martinetti J, Martel S, Khinast. Scale-up of HME Processes from a Trilobed 16mm to a Bilobed 27mm Extruder: SPH Simulations and 1D Mechanistic Modelling. AIChE 2016 Annual Meeting, San Francisco, USA, November 13th – 18th, 2016

Matić J, Eitzlmayr A, Kondor I, Koscher G, Khinast J. Particle-Based Modelling of Free-Surface Flow and Distributive Mixing in Modular Co-Rotating Twin-Screw Extruders. PARTEC 2016 International Congress on Particle Technology, Nürnberg, Germany, April 19th – 21st, 2016

Matić J, Eitzlmayr A, Khinast J. Scale-Up of an HME Process Supported by 3D SPH and 1D Mechanistic Modelling. Jahrestreffen Bingen 2016 - Fachgruppen Agglomerations- und Schüttguttechnik, Mehrphasenströmungen und Computational Fluid Dynamics (AGG, MPH, CFD), Bingen, Germany, February 29th – March 2nd, 2016

Matić J, Eitzlmayr A, Khinast J. Scale-Up of Pharmaceutical Hot Melt Extruders Supported by 3D Smoothed Particle Hydrodynamics and 1D Predictive Modelling. AIChE 2015 Annual Meeting, Salt Lake City, USA, November 8th – 13nd, 2015

Matić J, Eitzlmayr A, Kondor I, Koscher G, Khinast J. The Potential of SPH for Simulation of Fully and Partially Filled Co-Rotating Twin-Screw Extruder Elements. Polymer Processing Society Conference, Graz, Austria, September 21st – 25th, 2015

Kondor I, Eitzlmayr A, Matić J, Koscher G, Khinast J. SPH Simulations of Co-Rotating Twin-Screw Extruders, 10th SPHERIC International Workshop, Parma, Italy, June 15th – June 18th, 2015

Eitzlmayr A, Kondor I, Matić J, Koscher G, Khinast J. The Simulations of Mixing and Free Surface Flows in Co-Rotating Twin-Screw Extruders, AIChE 2014 Annual Meeting, Atlanta, USA, November 16th – 21st, 2014

Eitzlmayr E, Matić J, Koscher G, Khinast J. Novel Developments for the Simulations of Hot Metl Extrusion, Leistritz Pharma Workshop 2014, Nürnberg, Germany, Jun 11th – 12th, 2014

Eitzlmayr E, Matić J, Koscher G, Khinast J. A Novel Simulation Approach for Hot Melt Extrusion, 6th International Conference on Pharmaceutical Engineering, Graz, Austria, Jun 16th – 17th, 2014